SYNTHESIS AND CHARACTERIZATION OF HIGHLY BRANCHED, FUNCTIONAL POLY(ARYLENE ETHER SULFONE)S FOR WATER PURIFICATION MEMBRANES

by

Emine Billur SEVİNİŞ ÖZBULUT

Submitted to the Graduate School of Engineering and Natural Sciences
in partial fulfillment of the requirements for the degree of

Doctor of Philosophy

SABANCI UNIVERSITY

JUNE 2020

SYNTHESIS AND CHARACTERIZATION OF HIGHLY BRANCHED, FUNCTIONAL POLY(ARYLENE ETHER SULFONE)S FOR WATER PURIFICATION MEMBRANES

by

Emine Billur SEVİNİŞ ÖZBULUT

Submitted to the Graduate School of Engineering and Natural Sciences
in partial fulfillment of the requirements for the degree of

Doctor of Philosophy

Department of Material Science and Engineering Program

Thesis Advisor: Asst. Prof. Serkan ÜNAL

Thesis Co-Advisor: Prof. Dr. Yusuf Ziya MENCELOĞLU

SABANCI UNIVERSITY

25 JUNE 2020

Emine Billur Seviniş Özbulut, a Ph.D. student of Sabancı University Faculty of Engineering and Natural Sciences student ID 19935, successfully defended the dissertation entitled "SYNTHESIS AND CHARACTERIZATION OF HIGHLY BRANCHED, FUNCTIONAL POLY(ARYLENE ETHER SULFONE)S FOR WATER PURIFICATION MEMBRANES", which she prepared after fulfilling the requirements specified in the associated legislations, before the jury whose signatures are below.

APPROVED BY:

Thesis Advisor :   Asst. Prof. Dr. Serkan ÜNAL

Sabancı University

Co-advisor :   Prof. Dr. Yusuf Ziya MENCELOĞLU

Sabancı University

Jury Members :   Assoc. Prof. Dr. Fevzi Çakmak CEBECİ

Sabancı University

Prof. Dr. Bahattin KOÇ

Sabancı University

Assoc. Prof. Dr. Derya YÜKSEL İMER

Istanbul Technical University
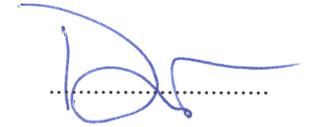
Prof. Dr. Metin Hayri ACAR

Istanbul Technical University

Date of Approval   : 25 June 2020

ABSTRACT

SYNTHESIS AND CHARACTERIZATION OF HIGHLY BRANCHED, FUNCTIONAL
POLY(ARYLENE ETHER SULFONE)S FOR WATER PURIFICATION MEMBRANES

Emine Billur SEVİNİŞ ÖZBULUT

Doctor of Philosophy, 2020

Material Science and Engineering

Thesis Advisor: Asst. Prof. Serkan ÜNAL

Thesis Co-Adviser: Prof. Dr. Yusuf Ziya MENCELOĞLU

Keywords: Highly branched polymer, A_2+B_3 polymerization, poly(arylene ether sulfone), oligomer synthesis, polymer blends, ultrafiltration membrane, nanofiltration membrane, thin film composite membrane, poly(arylate sulfone), ionic polymer, interfacial polymerization, sulfonated polymer, silane functional polymer, self-crosslinking polymer

Recovery of wastewater is a global and environmental matter on the sustainability of water sources. Pressure-driven membrane technology is one of the best options for wastewater treatment because of no need for chemicals. Poly(arylene ether sulfone)s (PAES) are widely used in membrane technology due to their unique chemical and thermal characteristics. Yet, the linear structure of PAESs limits their functionality, while branched polymers come with a multitude of terminal groups, which may be used to introduce unique functionalities to the polymer backbone. Highly branched polymers typically have a lower hydrodynamic volume; consequently, their solubility in organic solvents is higher than linear analogous. However, they have lower mechanical properties. Therefore, the terminal groups of branched polymers can be fully or partially designed to be cross-linkable end-groups, which can enhance their thermal and mechanical properties while retaining the functionality. The investigation of the

effect of degree of branching and the distance between branch points on the thermo-mechanical features and water purification performance of membranes fabricated from novel HBPAES synthesized via using the A_2+B_3 polymerization method forms the basis of this Ph.D. dissertation. These investigations have focused on three different types of materials, namely, (i) blend films of linear and highly branched PAES, (ii) UF membranes fabricated from linear and branched PAESs and (iii) TFC membranes prepared from sulfonated HBPAES (SHBPAES).

In the A_2+B_3 polymerization methodology employed in this study, A_2 species were difunctional reagents such as 4,4'-dichlorodiphenyl sulfone (DCDPS) or 3,3'-disulfonate-4,4'-dichlorodiphenyl sulfone (SDCDPS) type monomers or in-house synthesized PAES-based linear oligomers with varying degrees of polymerization (DP). 1,1,1-tris(4-hydroxyphenyl)ethane (THPE) was chosen as the B_3 monomer with three phenolic functionalities. The type of A_2 species, either a monomer or a difunctional oligomer with varying DPs enabled tailoring of the degree of branching and the average distance between branch points. Additionally, various strategies were developed to further introduce functional groups such as silane and phenolate on the chain ends of synthesized HBPAES products, which were characterized by Fourier Transform Infrared (FT-IR) and Nuclear Magnetic Resonance (NMR) spectroscopies, Size Exclusion Chromatography (SEC), Dynamic Mechanical Analysis (DMA), Differential Scanning Calorimetry (DSC) and stress-strain tests. Silane functionalities of HBPAESs offered the ability to crosslink final polymeric films or membranes in the presence of moisture and heat. These films and membranes were found to possess inorganic domains upon the crosslinking via the silane terminal groups of HBPAES, which generally have heat and chemical resistance. In order to enhance the thermal and mechanical properties of PAES-based UF membranes, the designed HBPAESs were proportionately blended with a commercially available linear PAES (LPAES). Lastly, the A_2+B_3 polymerization in the presence of SDCDPS as one of the A_2 reagents resulted in SHBPAES, which was observed to be soluble or dispersible in water depending on the SDCDPS content and allowed SHBPAESs in water-based applications such as the fabrication and characterization of novel TFC membranes having poly(arylate sulfone) active layer for the first time in the literature.

ÖZET

SU ARITMA MEMBRANLARI İÇİN YÜKSEK DALLANMIŞ, FONKSİYONEL POLİ(ARİLEN ETER SÜLFON)LARIN SENTEZİ VE KARAKTERİZASYONU

Emine Billur SEVİNİŞ ÖZBULUT

Doktora Tezi, 2020

Malzeme Bilimi ve Mühendisliği

Tez Danışması: Dr. Öğr. Üyesi Serkan ÜNAL

Eş Danışman: Prof. Dr. Yusuf Ziya MENCELOĞLU

Anahtar Kelimeler: Yüksek dallanmış polimer, $A_2 + B_3$ polimerizasyonu, poli (arilen eter sülfon), oligomer sentezi, polimer karışımları, ultrafiltrasyon membranı, nanofiltrasyon membranı, ince film kompozit membran, poli (arilat sülfon), iyonik polimer, arayüzey polimerizasyonu, sülfonatlı polimer, silan fonksiyonel polimer, kendiliğinden çapraz bağlanan polimer

Atık suyun geri kazanımı, su kaynaklarının sürdürülebilirliği konusunda küresel ve çevresel bir sorundur. Basınçla çalışan membran teknolojisi, elektrik enerjisine veya kimyasallara ihtiyaç duyulmamasından dolayı, atıksu arıtımı için en iyi seçeneklerden biridir. Poli (arilen eter sülfon) (PAES), benzersiz kimyasal ve termal özellikleri nedeniyle membran teknolojisinde yaygın olarak kullanılmaktadır. Yine de, PAES'lerin doğrusal yapıları işlevselliklerini sınırlamaktadır, diğer yandan dallı polimerler çok sayıda terminal gruplara sahiptir ve bu gruplar, polimer omurgasına benzersiz işlevsellik kazandırır. Yüksek dallanmış polimerler tipik olarak daha düşük hidrodinamik hacme sahiptir; bunun bir sonucu olarak, organik çözücüler içindeki çözünürlükleri lineer analoglarından daha fazladır. Fakat daha düşük mekanik özelliklere sahiptirler. Bu nedenle, dallı polimerlerin terminal grupları, termal

ve mekanik özelliklerini arttırabilmek için tamamen veya kısmen çapraz bağlanabilir uç gruplarla tasarlanabilir. Dallanma derecesinin ve dallanma noktaları arasındaki mesafenin $A_2 + B_3$ polimerizasyon yöntemi kullanılarak sentezlenen yüksek dallanmış poli (arilen eter sülfon) (HBPAES)'lerden üretilen membranların termo-mekanik özellikler ve su arıtma performansı üzerindeki etkisinin araştırılması bu doktoranın tezinin temelini oluşturmaktadır. Bu araştırmalar üç farklı malzeme türüne odaklanmıştır: (i) doğrusal ve çok dallı PAES karışım filmleri, (ii) doğrusal ve dallı PAES'lerden üretilen ultrafiltrasyon (UF) membranlar ve (iii) sülfonatlanmış HBPAES'den hazırlanan ince film kompozit (TFC) membranlar.

Bu çalışmada $A_2 + B_3$ polimerizasyon metodolojisiyle, A_2 türleri olarak iki fonksiyonel grubu olan ve klor uçlu, 4,4'-diklorodifenil sülfon (DCDPS) veya 3,3'-disülfonat-4,4'-diklorodifenil sülfon (SDCDPS) tipi monomerler veya kurum-içi sentezlenmiş değişik polimerizasyon derecesine (DP) sahip PAES bazlı lineer oligomerler kullanıldı. DİğEr yanfan, 1,1,1-tris (4-hidroksifenil) etan (THPE), üç fenolik işlevselliğe sahip B_3 monomeri olarak seçildi. İki işlevli bir monomer veya değişen DP'lere sahip bir oligomer olan A_2 reaktifleri, kullanılan türlerine göre, dallanma derecesini ve dallanma noktaları arasındaki ortalama mesafeyi değiştirmeyi sağlamaktadır. Ek olarak, Fourier Transform Infrared (FT-IR) ve Nükleer Manyetik Rezonans (NMR) spektroskopileri, Boyut Dışlama Kromatografisi (Boyut Dışlama Kromatografisi) (SEC), Dinamik Mekanik Analiz (DMA), Diferansiyel Taramalı Kalorimetre (DSC) ve gerilme-şekil değiştirme testleri ile karaterize edildiler. HBPAES'lerin silan işlevselliği, nihai polimerik filmlerin veya membranların nem ve ısı varlığında çapraz bağlama kabiliyeti sağladı. Böylece, bu silan işlevli filmler ve membranlar inorganik alanlara sahip hale gelerek, ısı ve kimyasal dirençleri iyileştirildi. PAES bazlı UF membranlarının termal ve mekanik özelliklerini arttırmak için, tasarlanan HBPAES'ler ticari olarak temin edilebilen doğrusal bir PAES ile orantılı olarak harmanlandı. Son olarak, $A_2 + B_3$ polimerizasyon metodu ile A_2 reaktiflerinden biri olan SDCDPS kullanılarak sülfonatlı HBPAES (SHBPAES)'ler elde edildi; literatürde ilk defa poli (arilat sülfon) aktif tabakaya sahip TFC membranları üretildi ve membran performansları incelendi.

To science workers,

ACKNOWLEDGEMENTS

I would like to state that having the degree of Ph.D. is an individual success made possible by the contributions of many people. Therefore, the most valuable part of my Ph.D. journey is to meet countless precious people, whom I will remember all with a sincere smile.

First of all, I would like to present my sincere and deep gratitude to my advisors Dr. Serkan Ünal and Prof. Yusuf Ziya Menceloğlu, for their encouraging and reassuring supports, their intellectual deepness, humility, tolerance, as well as their guidance and contributions at all stages of my Ph.D. study. I will sincerely and respectfully remember our academic and daily conversations with Dr. Ünal, which steer my scientific and professional personality. I feel appreciation to Prof. Menceloğlu, who always welcomes, listens with a great heartfelt and guides me on finding the root causes in the most challenging periods of my Ph.D. study. I would also like to state that it was a great opportunity for me to have worked with these two enthusiastic scientists who inspired me a lot along my long Ph.D. journey.

Besides my advisors, I would like to thank my thesis progress committee members Prof. Bahattin Koç and Dr. Fevzi Çakmak Cebeci, for their interest and help. I would also present my pleasure to Dr. Cebeci, who has given me consecutively four years the opportunity to be the teaching assistant of his polymer synthesis classes.

In addition, I would like to thank the rest of my thesis committee members Dr. Derya Yüksel İmer and Prof. Metin Hayri Acar, for their detailed thesis reviews and constructive criticisms, which enrich my Ph.D. thesis. I would also like to express my gratitude to Dr. Imer and Prof. Ismail Koyuncu, who sincerely convey their knowledge in the manufacturing methods of UF and NF membranes, which constitutes the main application area of my Ph.D. thesis. I would like to state that Prof. Acar has a different place in my life. Whenever I make a choice, I happily remember his statement: "People live with their preferences, Billur!". I am grateful to him that he always gave me his support and confidence.

to adulthood. I am grateful to Merve Özyaşar, Dr. Taylan Mercan, Dilay Serttan, Cağrı Kızıldağ and Dr. Ziya Saydam for their fruitful conversations.

A very special thanks to my beloved husband, Dr. Murat Özbulut, for his love, endless support and for the worldview and guidance, which has always fascinated me. Everything gets better with his presence.

Last but not least, I would like to present my sincerest thanks to my family, my mother and father Ülkü-Mustafa Seviniş, my sister Burcu Seviniş Hasbay and her daughter, my beloved niece, Güneş Lea Hasbay, my brother Mert Seviniş, family in law Nurcan-Eyüp Özbulut, and my aunt and uncle Taç-Orhan Düvencioğlu. I wistfully commemorate my family elders Nezihe-Saim Malkoç, Emine Seviniş, and Şükriye Birgin, who I know they would be very proud if they lived.

June 2020   Emine Billur SEVİNİŞ ÖZBULUT

TABLE OF CONTENT

ABBREVIATIONS

DB	**:**	Degree of branching
DLS	**:**	Dynamic Light Scattering
DMA	**:**	Dynamic Mechanical Analysis
DMAc	**:**	Dimethyl acetamide
DMSO	**:**	Dimethyl sulfoxide
DP	**:**	Degree of polymerization
DSC	**:**	Differential Scanning Calorimetry
FT-IR	**:**	Fourier Transform Infrared Spectroscopy
HB	**:**	Highly Branched
HBPAES	**:**	Highly Branched Poly(arylene ether sulfone)
HBPAES-Si	**:**	Ethoxysilane Functional Highly Branched Poly(arylene ether sulfone)
LPAES	**:**	Linear Poly(arylene ether sulfone)
NF	**:**	Nanofiltration
NMR	**:**	Nuclear Magnetic Resonance
PAES	**:**	Poly(arylene ether sulfone)
RO	**:**	Reverse Osmosis
SEC	**:**	Size Exclusion Chromatography
SEM	**:**	Scanning Electron Microscopy
SHBPAES	**:**	Sulfonated Highly Branched Poly(arylene ether sulfone)
SM0	**:**	HBPAES synthesized only with SDCDPS A_2 monomer

SMM0   **:** HBPAES synthesized with a 1:1 molar combination A_2 monomers:

                    SDCDPS:DCDPS

TFC   **:** Thin Film Composite

UF   **:** Ultrafiltration

UTM   **:** Universal Testing Machine

SYMBOLS

A_m : Membrane effective area

cm : Centimeter

C_f : The solution concentration of feed

C_p : The solution concentration of permeate

$°C$: Celsius degree

g : Gram

g_h : Branching structure indicator

h : Hour

J_w : Water flux

kDa : Kilo Dalton

L : Liter

M : Molar

mL : Milliliter

mM : Millimolar

M_w : Molecular weight

n : Mole

$[\eta]$: Intrinsic viscosity

Q_w : Flow rate of water

$R(\%)$: Rejection

R_h : Hydrodynamic radius

rpm   : Revolutions per minute

μm   : Micrometer

V_w : Volume (L) of permeated water

T_g : Glass Transition Temperature

w_e : Weight of polymer after extraction (g)

w_i : Weight of polymer before extraction (g)

LIST OF TABLES

LIST OF FIGURES

CHAPTER 1: Introduction

1.1. Dissertation overview

Although numerous studies have been reported in the literature on blending linear and highly branched polymers for a variety of applications, this dissertation reports the investigation of both films and ultrafiltration (UF) membranes fabricated from the blends of linear (LPAES) and highly branched (HBPAES) poly(arylene ether sulfone)s with a detailed investigation of the effect of the degree of branching on their mechanical, thermo-mechanical and morphological characteristics. For this purpose, novel HBPAESs bearing a multitude of phenolic end groups have been synthesized via the A_2+B_3 polymerization approach, and these phenolic end groups have been post-functionalized with an alkoxysilane group. Blends of these novel HBPAEs with LPAES have been prepared for the fabrication of films and UF membranes.

On the other hand, most nanofiltration (NF) membranes have polyamide-based structures fabricated by the interfacial polymerization of monomeric reagents such as amines and trimesoyl chloride (TMC); yet, there are a few examples of using functional oligomeric or polymeric reagents to form an active layer of thin film composite (TFC) membrane. These polyamide-based TFC membranes are widely used in water treatment and wastewater purification. Apart from polyamide-based active layers, polyarylate-based of active layers have been reported for the fabrication of NF membranes for organic solvent filtration and gas separation membranes. With the inspiration from these studies on the polyarylate-based NF membranes, a series of sulfonated, functional HBPAES (SHBPAES) have been synthesized in this study, which was utilized for the fabrication of NF membranes with a new generation of an active layer containing polyarylate sulfones for wastewater treatment. This dissertation reports the first-time fabrication of polyarylate sulfone-based NF membranes and their evaluation in wastewater treatment applications.

1.2. Objectives

This Ph.D. study focuses on the design of novel HBPAESs for UF and NF membranes and their synthesis via one-step A_2+B_3 copolymerization approach in an effort to introduce them as the new generation, functional oligomeric and polymeric raw materials for water purification membranes that can overcome low flux, high cost, and operational inefficiency issues in membrane processes.

Commercial UF membranes for water treatment and reuse are mostly produced from linear polymers, which yield high viscosity solutions and thus require the use of a high amount of organic solvents during the membrane manufacturing process by phase inversion. Highly branched polymers, which can be synthesized by varying degree of branching, naturally have lower hydrodynamic volumes compared to their linear analogues with similar molar masses and contain a multitude of terminal groups in comparison with only two terminal groups in linear analogues. As a result, highly branched polymers typically have higher solubility in organic solvents and offer significantly higher functionality at the terminal points for further chemistry compared to linear polymers. Yet, highly branched polymers show low mechanical properties due to a lack of entanglement. In this Ph.D. study, the effect of degree of branching, the distance between branched points, end-group functionalization, self-cross-linking ability, and incorporation of inorganic groups into the polymer backbone were investigated systematically on the final film and membrane properties. These various approaches were categorized in two depending on their application methods and summarized in Figure 1. The synthesized SHBPAESs bear pendant sodium sulfonate groups onto the branched polymer backbone, which enables tunability of the hydrophilicity of the TFC active layer fabricated from them. These ionic characters are expected to have a significant influence on critical membrane performances such as an increase in the water flux and ion rejection as well as enhanced anti-fouling properties. Therefore, a series of TFC NF membranes have been fabricated by reacting TMC in hexane with hydrophilic, phenolate functional SHBPAESs, dispersed or dissolved in water, to produce an active layer on a PAES based UF membrane as a support layer. Upon the fabrication of this fabricated layer made up of a poly(arylate sulfone) network, the study aims the evaluation of corresponding NF membranes in wastewater treatment applications, which is believed to offer endless potential applications for these new classes of raw materials and membranes in future studies.

Figure 1 A representative summary on synthesis of novel, highly branched, functional HBPAES by monomeric or oligomeric A_2 + B_3 polymerization for polymeric film, membrane applications: A. Approaches on blend thermoplastic films and UF membranes; B. Approaches on TFC NF membranes

1.3. Dissertation structure

This Ph.D. dissertation is comprised of seven chapters covering various synthetic approaches and three different applications to understand the structure-property relationship in HBPAES containing polymer blends and membranes. Chapter one describes an overview with objectives are and the dissertation structure (Figure 2). In chapter two, a literature review has been provided pertaining to membrane applications in water treatment and reuse, LPAES, and its applications, the synthesis of PAES based branched polymers via the A_2+B_3 polymerization approach and polymer blends.

Chapter three focuses on the experimental section containing materials used and detailed descriptions of experimental procedures on the syntheses of PAES based chlorine terminated oligomers, HBPAES-type branched polymers, post functionalization of HBPAES, fabrication techniques of blend films, UF and NF membranes, as well as their structural, mechanical, thermo-mechanical, and morphological characterizations.

Chapter four focuses on the synthesis of a series of HBPAESs synthesized with varying the distance between branch points by the one-step A_2+B_3 copolymerization, their blends with LPAES, and detailed characterizations to establish clear structure-property relationships. Chapter four also covers the post-functionalization of HBPAESs by converting phenol terminal groups into alkoxysilane groups. Chapter four presents the importance of structure-property relationships in thermoplastic and amorphous arylene ether sulfone-based polymer blend formations as a pioneering study on the potential applications of highly branched and linear polymer blends in the future.

Chapter five focuses on a series of HBPAESs with varying branching density and multifunctional or cross-linkable alkoxysilane end groups that have been utilized as additives to prepare polysulfone based UF membranes by the phase inversion technique. These blend UF membranes have been characterized performance-wise, morphologically, mechanically, and thermo-mechanically by water and dye permeation, scanning electron microscope (SEM), zeta potential, stress-strain tests and Dynamic Mechanical Analysis (DMA), respectively.

Chapter six presents the synthesis and characterization of a series of SHBPAES, which possess systematically varying ionic characters, synthesized by A_2+B_3 polymerization, from which, TFC active layers were fabricated and characterized in comparison with polyamide-based TFC membranes and a series of new TFC membranes fabricated by a combination of piperazine (PIP) and the B_3 monomer. These TFC membranes have been extensively characterized by performance tests, zeta potential, FT-IR spectroscopy, and contact angle measurements. These TFC membranes are a first attempt to produce poly(arylate sulfone)-based active layer. The effect of the ionic content of SHBPAES on the morphology and the performance of these novel membranes were discussed with morphological characterizations and permeability tests.

Chapter seven describes the overall conclusions of the dissertation on the studies focused on blend films and blend UF membranes containing novel HBPAES and HBPAES-Si synthesized in this study, as well as, TFC membranes made up of SHBPAES, THPE, and PIP for the first time in the literature.

CHAPTER 1
INTRODUCTION
1.1 Dissertation overview
1.2 Objectives
1.3 Thesis structure

CHAPTER 2
LITERATURE REVIEW
2.1: Importance of water reuse
2.2 -2.6 : Review on membrane applications
2.7: Poly(arylene ether sulfone)
2.8-2.9 Highly branched polymers
2.10 Post-functionalization
2.11 Blending linear and highly branched polymers

CHAPTER 3
EXPERIMENTAL
3.1 Materials
3.2 Synthesis
3.3 Blend film preparation
3.4 UF membrane preparation
3.5 NF membrane preparation
3.6 Characterization methods

CHAPTER 4
HIGHLY BRANCHED POLY(ARYLENE ETHER SULFONE)S AND THEIR BLENDS WITH LINEAR POLY(ARYLENE ETHER SULFONE)S

CHAPTER 5
FABRICATION AND CHARACTERIZATION OF UF MEMBRANES FROM HIGHLY BRANCHED AND LINEAR POLY(ARYLENE ETHER SULFONE) BLENDS

CHAPTER 6
FABRICATION AND CHARACTERIZATION OF TFC NF MEMBRANES FROM HIGHLY BRANCHED, SULFONATED, FUNCTIONAL POLY(ARYLENE ETHER SULFONE)S

CHAPTER 7
OVERALL CONCLUSIONS & FUTURE WORK

Figure 2 Overview of the dissertation structure

CHAPTER 2: Literature Review

2. 1. Importance of freshwater reuse

Although almost two-thirds of the Earth's surface is covered with water, only 0.3% is freshwater. The remaining 99.7% consists of seawater, glaciers, groundwater and water vapor. Water need has been escalating globally by about 1% per year since the 1980s due to population growth and socio-economic development and is expected to increase at a similar speed until 2050 [1]. The United Nations World Water Development Report (2019) warns about nearly a 25% increase in water usage in the 2050s mainly due to the climbing water use in industrial and energy sectors [2]. The climate change also contributes to the increased stress levels in freshwater sustainability.

Agriculture, industry (including power generation), and households are the three main water consumers. All agricultural practices, including irrigation, animal husbandry, and aquaculture, are the most significant water consumers worldwide, accounting for 69% of annual water expenditure. On the other hand, human consumption account for 12% and industrial usage for 19% [2]. In Figure 3, withdrawal and consumption amount of freshwater by various sectors are depicted. While water withdrawal describes the volume of freshwater removed from the source, water consumption expresses that the withdrawn water does not return to the source [3]. Overall, it can be deduced that the demand for water will gradually increase in years, and the usage of water sources will acquire more crucial status, which will, in turn, increase the importance of wastewater recovery in creating alternative water sources. Although the industrial usage of water is much less than agricultural usage, the contamination due to the discharge of industrial wastewaters to waterways generates long term risk to nature and human health [4].
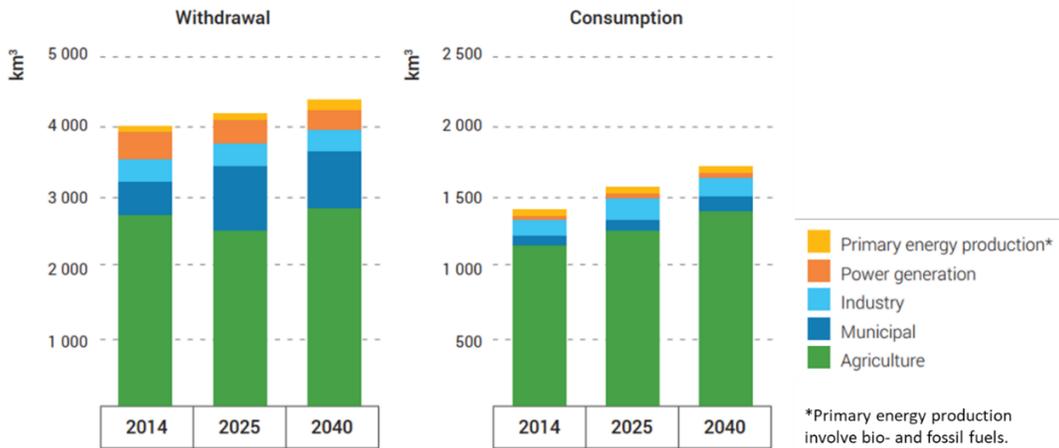
Figure 3 Global water demand by various sectors in 2014 and expectations for 2025 and 2040 [3]

In recent years, international regulations and policies govern countries to restrict the utilization of groundwater and discharge of industrial wastewater [2, 5]. The significant indications of the freshwater sustainability issues and legislation on the protection and management of water resources are driving forces for the studies on the industrial wastewater recovery.

2. 2.   Historical perspective on membrane applications

The first observation on the osmotic phenomenon was made almost three hundred years ago by Nollet [6]. After the discovery of the osmotic pressure, the first experiments were mostly performed with animal and plant originated membranes in the medical and biological fields [7]. The first artificial semipermeable membrane was prepared with the gelation of copper ferrocynadine on a porous clay by Traube [8]. This inorganic membrane was noticed to dilute electrolyte solutions with a notable property of a selective barrier. In the same period, synthetic membranes prepared from collodion were studied by Fick on dialysis of solutions [9]. Apart from this, Graham [10] also used this process to separate colloids from crystalloids in 1861 and described it as selective diffusion [7]. In 1866, he published a study on the diffusion of gases using different atmospheres and discovered that rubber behaves as a selectively permeable membrane to various gases [11].

In the late 1800s, physical chemists started to show interest in semipermeable membranes and investigate the phenomena of osmotic pressure, especially in gas kinetics. In 1877, Pfeffer examined the effect of osmotic pressure on cell mechanics [12]. Van't Hoff quantitatively displayed the similarity between the kinetic energy of the solute particles in a dilute solution and the kinetic energy of gas molecules in 1887 [13]. In 1888, Nernst [14] and Plank [15] developed flux equations for electrolytes under driven forces, which originated from the differences in concentration or electrical potential. Then, in 1911, a quantitative theory of membrane equilibria in the presence of non-dialyzing electrolytes was established by Donnan [16].

At the beginning of the 20th century, Bechold [17] developed membranes with graded porosity formed from the impregnation of acetic acid collodion on filter paper. They were pressure-driven membranes up to several atmospheric pressures, and Bechold used the term "ultrafiltration" to describe them. Except for Bakelite, which was developed in 1906; until the 1930s, a few polymeric materials such as celluloid, collodion, cellophane, and rayon, which were derived from cellulose, were used in membrane production [7]. In 1929, finely porous cellulose nitrate-cellulose acetate materials were commercialized as microfiltration (MF) membranes for practical applications by Sartorius, which was developed by Zsigmondy [18]. In 1937, Carothers [19] developed nylon which was the first synthetic polyamide. This milestone resulted in the development of many condensation polymers still used to produce high-performance membranes for NF and RO.

On the other hand, studies of Teorell [20], Meyer and Sievers [21] formed a basis for the current conception of modern electrodialysis membranes and membrane electrodes from the 1930s. In 1944 Kolff used membranes for the manufacturing of the first functional hemodialysis device for biomedical applications [22]. A summary of the breakthrough phenomena on membrane science is listed in Table 1.

Table 1 Historical breakthroughs in the membrane technology before 1950s [23]

Phenomenon	Year	Scientist
Osmosis	1748	Nollet [6]
Laws of diffusion	1855	Fick [9]
Dialysis, gas permeation	1861, 1866	Graham [10], [11]
Osmotic Pressure	1860-1887	Traube [8] , Pfeffer [12],Van't Hoff [13]
Microporous membrane	1907-1918	Zsigmondy [18]
Distribution law	1911	Donnan [16]
Membrane potential	1930s	Teorell [20], Meyer & Sievers [21]
Hemodialysis	1944	Kolff [22]

One of the significant advances in membrane science and technology has been the production of reverse osmosis (RO) membranes, which were based on cellulose acetate and required high salt retention and flux under moderate hydrostatic pressure, as reported by Reid [24] in 1959. This was the most remarkable development for obtaining fresh water from the sea. In 1963, a milestone, as far as industrial applications of membranes were concerned, was accomplished with asymmetric membranes which were developed by Loeb and Sourirajan [25]. The membranes had a dense surface, high selectivity, and higher flux than symmetric membranes, while the highly porous inner layer provided mechanical strength to the membrane. In the study, asymmetric cellulose acetate membranes were produced by the phase-inversion technique, in which the solvent was removed from the homogeneous polymer solution to obtain a porous polymeric membrane.

Since 1960s membrane technologies have been commonly applied in various industrial fields; for example, pharmaceutical industry [26, 27], food industry [28], fuel cell applications [29, 30], energy storage industry [31], potable water treatment [32, 33], industrial wastewater treatment and recovery especially in the textile industry [34, 35], etc. Although membranes show a significant performance in various applications, it has always had a driving force in the industry and academia to seek improvements in membrane performances and efficiencies via new membrane material chemistries and fabrication processes [36].

2. 3. Classification of membranes

An acceptable membrane performance depends on the combination of features like permeability, selectivity, thermal and chemical stability, fouling resistance, low cost, and easy production. Hence, improving at least one of the properties may enable the production of high-quality membranes. Membranes are classified according to various criteria such as their pore sizes, shapes, morphologies, raw materials, and separation processes.

2.3.1. Classification of membranes according to pore size

Membranes are mainly divided into four primary types as micro- (MF), ultra- (UF), nanofiltration (NF), and reverse osmosis (RO), according to their pore sizes. Properties of different types of membranes are summarized in Table 2.

Table 2 Main types and properties of pressure-driven membranes [37]

Membrane type	Main application	Polymeric Materials	Retention substances	Pore size (nm)	Pressure (bar)
MF	Clarification and sterilization	Cellulose nitrate, cellulose acetate, polyamide, polysulfone, poly(ether sulfone), polycarbonate, poly(ether imide), poly(vinylidene fluoride), polytetrafluoroethylene, polypropylene, polyacrylonitrile, regenerated cellulose	Particles, colloids, bacteria	10^3-10^2	0.5-2
UF	Macromolecular recovery and fractionation	Cellulose acetate, polyamide, polysulfone, poly(ether sulfone), polycarbonate, poly(ether imide), poly(vinylidene fluoride), polyacrylonitrile, poly(methyl methacrylate), regenerated cellulose	All the above plus viruses and macro-molecules	10^2-10	1-10
NF	Water softening	Polyamide	All the above plus divalent ions	10-1	3-30
RO	Desalination	Cellulose acetate	All the above plus monovalent ions	1>	10-100

MF membranes possess pore sizes in the 1000 to100 nm range, which enables the separation of suspended particles, colloids, turbidity, bacteria, macromolecules from fluids effectively. The pressure-driven separation mechanism in MF membranes is similar to physical sieving. Although there are various electrical charges and adsorption effects on the particles, the separation process is mainly size-dependent. The particles bigger than the pore size of the membranes are retained on the membrane surface. This property is a primary disadvantage due to fouling problems, which is the main focus of MF research. Therefore, they are commonly utilized in a pre-filtration step before UF, NF, or RO membranes. Hence, they ensure an extension of the lifetime of other type membranes, and as well provide a decrease in the cost of operation [38, 39]. Moreover, the homogeneity of pore size is the most critical property in MF membranes, which enables the retention of microbes or non-soluble particles, which, on the contrary, are extremely challenging to remove in coagulation-based water treatment membranes [40].

UF membranes are mainly fabricated from cellulose acetate, poly(sulfone) (PS), polyacrylonitrile (PAN), polyvinylidene fluoride (PVDF), polypropylene (PP), polyethylene (PE) and aromatic polyamides. The pore size of UF membranes is in the range of 100-10 nm. Rather than pore sizes, UF membranes are generally characterized by their molecular weight cut off values, which is defined on the basis of 90% rejection of a solute with a particular molecular weight. UF can only separate molecules that differ by at least an order of magnitude in size. Apart from MF membranes, UF membranes can usually separate viruses, bacteria, and particles higher than 1000 Da. The selectivity of the UF membrane depends on the size difference of materials to be separated, the surface load of components, membrane materials as well as the hydrodynamic operating conditions. It is not fully sensitive to dissolved substances and macromolecules that are smaller than 10 kDa [41]. During the operation, even if the mixture to be filtered creates osmotic pressure, this is only in the order of a few bars, and the actual filtering process is provided by hydrostatic pressure in the range of 1-10 bar. The most critical challenges in UF membranes are both internal and external fouling.

In Figure 4, Mehta *et al.* [42] compiled the selectivity-permeability trade-off (the analysis called Robeson Plot) of a wide range of UF membranes from the literature, which was tested using bovine serum albumin (BSA) as a model protein. All membranes showed the same

trend on the trade-off between permeability and separation factor. For instance, membranes with low separation factors exhibited high permeabilities, while the membranes with high separation factors exhibited low permeabilities.
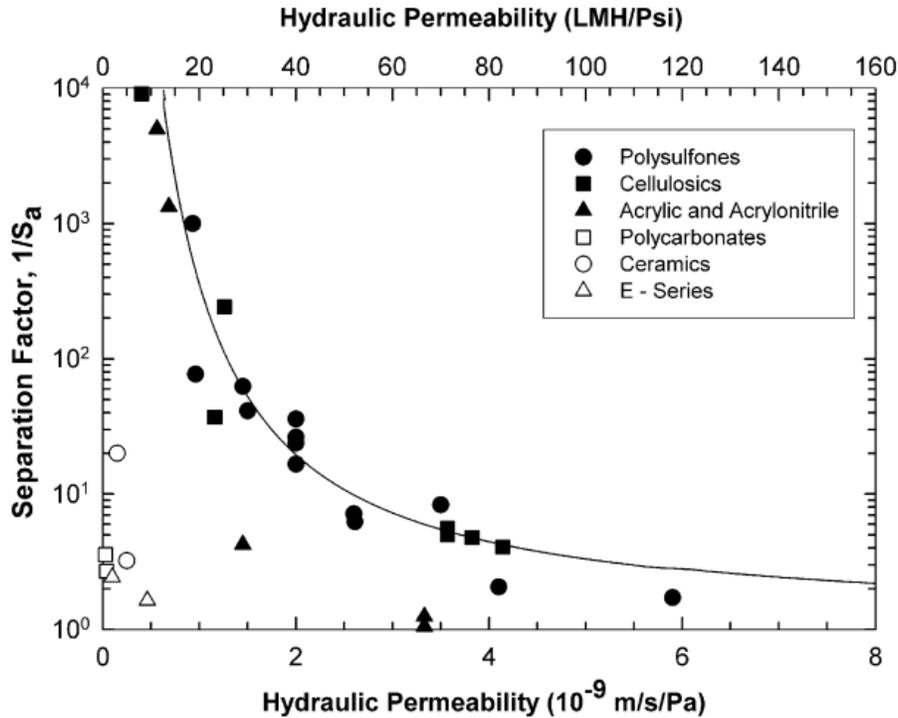
Figure 4 Selectivity–permeability trade-off of UF membranes using BSA as the model protein. Solid curve represents model calculations using a log–normal pore size distribution with $\sigma / \bar{r} = 0.2$ and $\varepsilon/\delta_m = 1 \ \mu m^{-1}$ [42]

Pore diameters of NF membranes vary between 1 and 10 nm. NF membranes have a charged surface that affects the features of selectivity and transport. Both the screening and diffusion transport mechanisms play a role in the NF membrane interface [41]. These membranes are highly effective in removing divalent salts, organic dyes, pesticides, and hardness.

RO membranes are mostly known as non-porous structures and they were initially prepared from cellulose acetate. The transport mechanism in the RO process is the dissolution/diffusion situation. The pure water passes along the RO membrane from a high concentration solution to a low concentration solution, and hydrostatic pressure should be applied higher than the osmotic pressure. RO membranes are capable of separating monovalent salts and metal ions [43].

2.3.2. Classification of membranes according to their configuration or geometry

There are four different fabrication methods and forms for membranes, which are flat-sheets (e.i. stacks of flat discs, spiral wound or as is), hollow fiber, tubular, and capillary. Flat-sheet membranes are plate-shaped, and one surface of the membranes is an active separation layer. The filtered water discharges through the other surface. Flat-sheet membranes are generally produced by coating the polymer on a support material that is a mostly nonwoven fabric. Thus, while the nonwoven fabric provides the mechanical strength of the membrane, the polymer layer achieves the separation and selection process.

Hollow fiber membranes are cylindrical and can operate either internally or externally. The layer on which the separation takes place can be produced on the inner surface or the outer surface. In processes where the concentration of suspended solids is high, hollow membranes with externally active internal layers are preferred. Besides, these membranes can be produced by a polymer coating method on the hollow rope to increase their mechanical strength. Such membranes are called reinforced hollow fiber membranes.

Tubular membranes are cylindrical and slightly larger in diameter. It is especially preferred for contaminated water containing high concentrations of suspended solids. Tubular membranes are produced by polymer coating of the inner surfaces of the cylindrical nonwoven fabric. These membranes, where the active layer is on the inner surface, work from the inside out.

Membranes, referred to as capillary, are defined as membranes containing a plurality of water flow channels in their module, and they work from the inside out principle. These membranes may be polymeric or ceramic, but generally, ceramic membranes are in this type. Figure 5 shows how the membranes are arranged according to their geometric structure. For example, flat plate membranes are configured as spiral wound modules, whereas tubular-shaped membranes cannot be used in the spiral-wound configuration [44]. Modules and process modes that can be used depending on the membrane geometry are limited and specific.
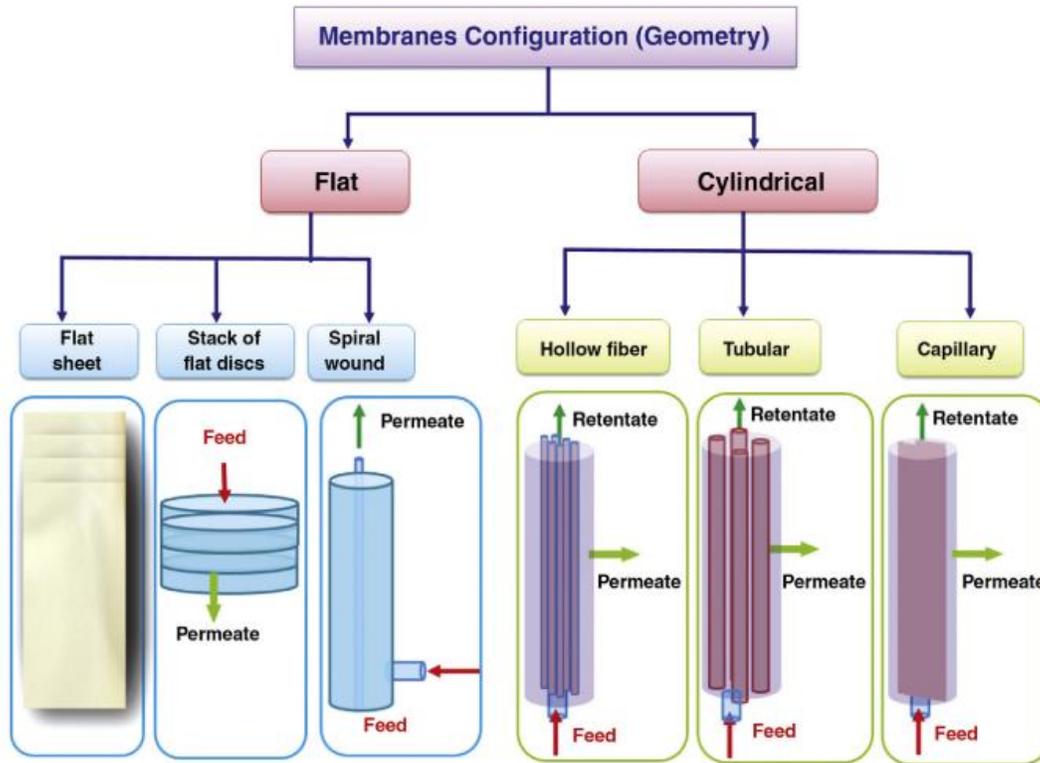
Figure 5 Classification of membranes according to their configuration [44]

2.3.3. Classifications of membranes according to their structure and morphology

Membranes are classified as dense, porous, and electrically charged barriers according to their morphological features. The classification of membranes by morphological features is schematically given in Figure 6. In dense membranes [45], water flow is naturally slow due to its nonporous structure. They are widely utilized as RO membranes and gas separation membranes. Unlike dense membranes, porous membranes contain pores on the surface or inside. Porous membranes are divided into two classes as symmetrical and asymmetric according to the size distribution of pores. In the symmetrical porous membrane, the pores in each region of the membrane are of equal size, and all pores have an almost constant diameter along the lateral cross-section of the membrane [46]. In asymmetric porous membranes, the diameters of the pores decrease as moved from the support layer to the surface. In asymmetric membranes, separation occurs by small pores on the surface, and the filtered water passes through the larger pores in the inner layer of the membrane [47].

15

Therefore, asymmetric membranes have lower hydrostatic resistance than symmetric membranes, and they also provide better separation performance and higher permeability values. Asymmetric structures, which are given in Figure 6 under the porous membrane type, have cross-sectional morphologies called finger-shaped or sponge-like. The finger-shaped (bottom-left) membranes have thin channels perpendicular to the surface, while the porous membranes (bottom-right) have small and dense hollow spaces with interconnected pores. Finger-shaped membranes are generally preferred in applications that do not require high pressure, such as MF and UF. When sponge-like and finger-shaped membranes are compared, it is observed that the hydraulic resistance is less, and accordingly the flux is higher in finger-shaped membranes. On the other hand, the finger-shaped membranes exhibit less mechanical strength than the sponge-like. Due to these properties, membranes of the sponge-like structure are widely utilized as support layers in membrane production. Notably, the sponge-like structures have been preferred as support layers in the commercial RO membranes and some membrane bioreactors (MBR).
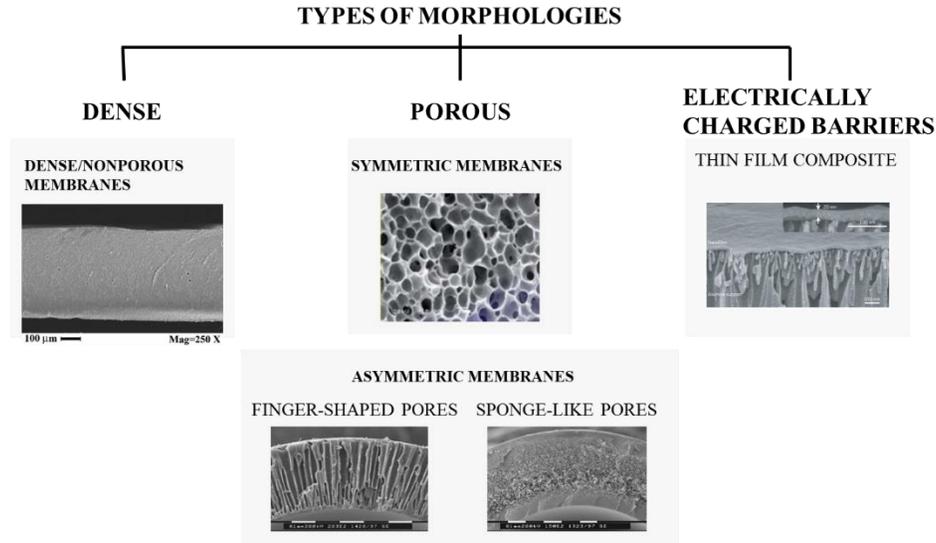
Figure 6 Classification of membranes according to their morphology (dense [45], symmetric membranes [46], finger-shaped & sponge like [47], TFC [48])

Morphologically, in the case of the composite membranes, the inner part has a porous structure, and the upper surface that comes into contact with water is dense [48]. In other words, one layer is porous and forms the backing layer while the other is a nonporous layer and forms the top layer. Thin-film composite (TFC) coated membranes are the most successful examples of membranes in this morphology. The support layer is not selective in contrary to the non-porous top layer due to the pore size differences. For example, in the desalination process, it is the top layer that has the separation ability and selectivity. The thickness of the dense polymeric non-porous layers showing active separation is about 5-10 micrometers, whereas, in TFC membranes, the thin porous polymers (mostly polyamide) in 50-500 nm thickness are coated on support membranes by interfacial polymerization. Both the dense structure and the thinness of the active layer in TFC membranes provide high removal efficiency.

2.3.4. Classification of membranes according to materials

Membranes are produced from a wide variety of materials with different structures and functionalities. Key properties of membranes such as chemical resistance, thermo-mechanical strength, membrane morphology, operating conditions, cost, and the separation rate mainly depend on which material is used in membrane fabrication. Membranes are generally divided into three main classes according to their material types utilized in their membrane manufacturing:

- Organic
  - Polymers
  - Elastomers
  - Modified natural products like cellulose-based materials
- Inorganic
  - Ceramics
  - Metals
- Composite
  - Organic-organic mixtures
  - Organic-inorganic mixtures
  - Inorganic-inorganic mixtures

The membrane material should ideally possess the listed properties below in order to provide an effective separation process [49]:

- High chemical resistance
- High mechanical strength
- High thermal resistance
- High permeability
- High selectivity or retention rate
- Low production and process cost
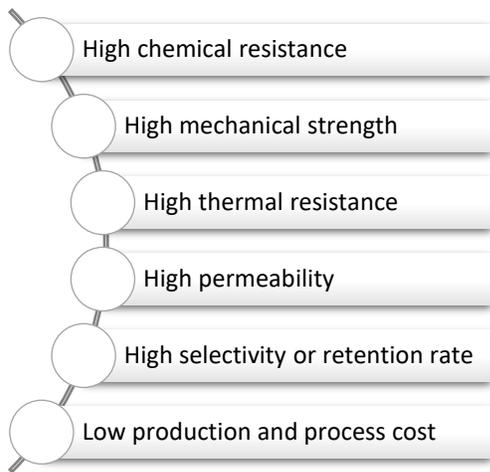
Organic membranes are produced from various polymeric materials such as polyethersulfone (PES), polysulfone (PSf), polyacrylonitrile (PAN), cellulose acetate (CA), polyamide (PA) and polyvinylidene fluoride (PVDF) and so on as listed below [44].

- **Polysulfones:** Polysulfone (PSf), Poly(ether sulfone), Poly(arylene ether sulfone) (PAES), Poly(phenyl sulfone) (PPSu)
- **Polyamides:** Aliphatic polyamides (Nylons), Aromatic polyamides and copolyamides
- **Polycarbonates:** Bisphenol A polycarbonate
- **Fluoropolymers:** Poly(tetrafluoroethylene) (PTFE), Poly(vinylidene fluoride) (PVDF)
- **Hydrocarbon-Based Polymers:** Polyethylene (PE), Polypropylene (PP)
- **Cellulosic Polymers:** Cellulose acetate (CA), Cellulose nitrate (CN)

Polymeric membranes are most preferred in water and wastewater treatment because of their ease of processability. However, they have some operational limitations associated with high pH, high temperature, and free chlorine as given in Table 3, in which the chemical resistance of different types of membrane are summarized. These limitations create a driving force to improve these features of polymeric materials.

Inorganic membranes have high thermal, thermo-mechanical properties, and mechanical strength; therefore, they can be utilized at temperatures higher than 200 °C in industrial chemical separation processes. In manufacturing inorganic membranes, ceramic, glass, zeolitic and metallic materials are commonly used as listed below.

Ceramic: Macroporous (50 nm <), Mesoporous (2 to 50 nm) and Microporous (< 2 nm)

Glass

Zeolitic

Metallic: Supported, unsupported
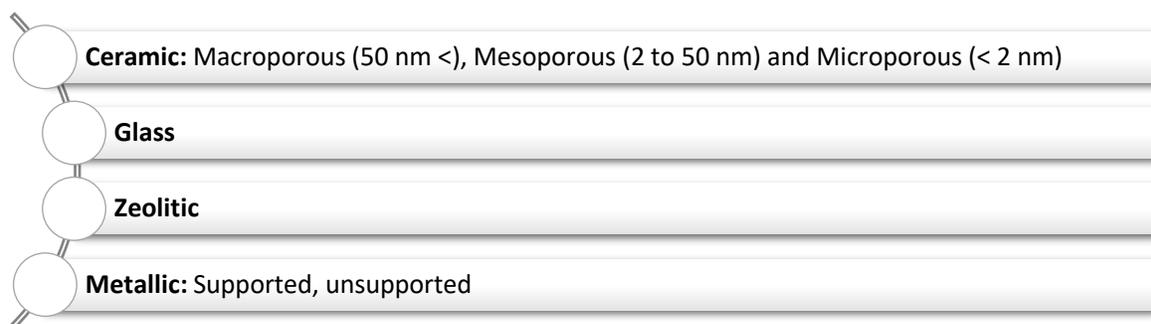
Inorganic membranes are intrinsically brittle, and their manufacturing costs are higher than polymeric membranes. Moreover, they are heavier than polymer-based membranes, and they have some limitations on reproducibility [44].

Table 3 Chemical resistance of membrane materials

Chemical Conditions	Composite	CA	PAES PSf PES	PVDF	PAN	Cellulose
3<pH<8	✓	✓	✓	✓	✓	✓
pH<3 or 8<pH	✓	✗	✓	✓	✓	✓
Temperature> 35°C	✓	✗	✓	✓	✓	✓
Humic acid	✓	✓	✗	✗	✓	✗
Proteins	✓	✓	✓	✓	✓	✓
Polysaccharides	✓	✗	✓	✗	✓	✗
Textile waste	✓	✗	✓	✓	✓	✗
Aliphatic hydrocarbons	✗	✗	✗	✓	✓	✓
Aromatic hydrocarbons	✗	✗	✗	✓	✗	✓
Oxidizers	✗	✓	✓	✓	✓	✓
Ketones and esters	✗	✗	✗	✓	✗	✓
Alcohol	✓	✗	✓	✓	✓	✓

2.3.5. Classification of membranes according to separation processes

In a separation process, a membrane is placed between the feed and filtrate phase currents. The mass flow should be directed from the feed side towards the filtrate side. The membrane separation process operates according to the principle of separating the feed stream into concentrate and filtrate streams. The driving force in the separation process of a membrane are the differences between pressure, temperature, concentration, or electrical potential (Figure 7).
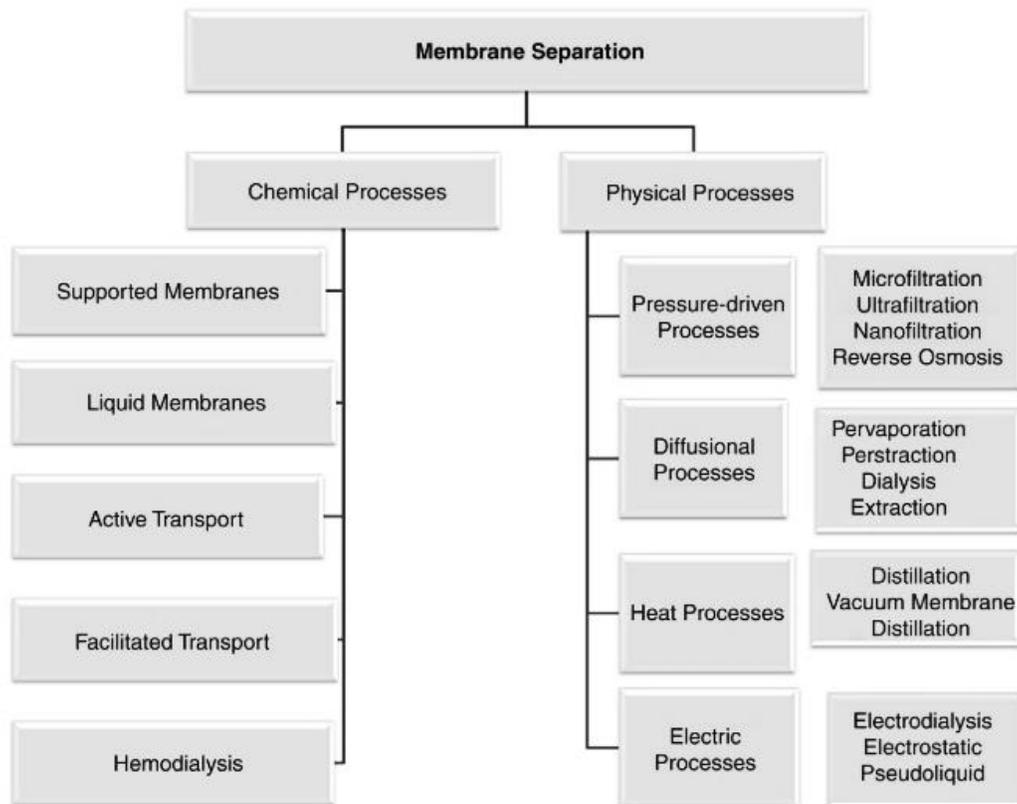
Figure 7 A classification of membrane separation according to physical and chemical processes [44]

MF and UF membranes can separate the feed by molecular filtration like sieving due to their microporous structure, whereas dense solution-diffusion membranes like NF and RO membranes can separate the feed not only by molecular filtration and but also diffusion (Figure 8).
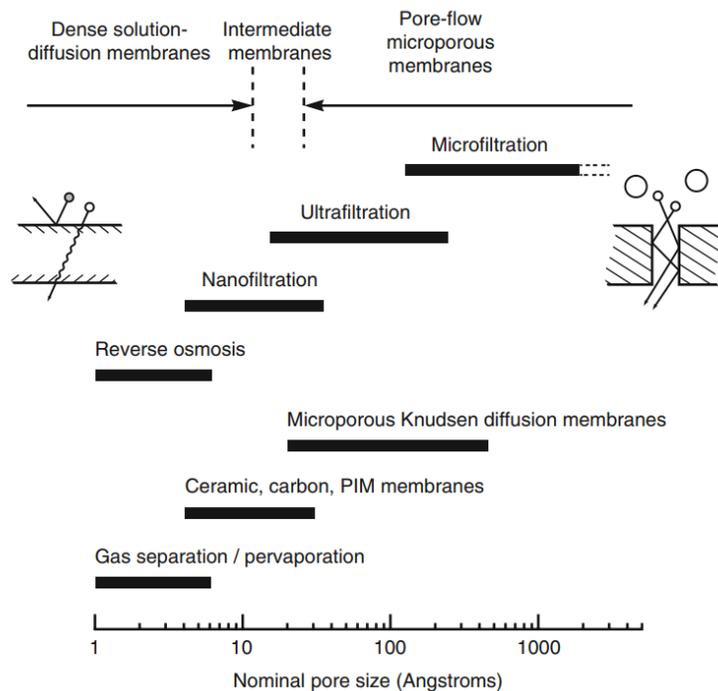
Figure 8 Schematic representation of the nominal pore size for the membrane separation mechanisms [50]

Examples of pressure-driven membrane separation processes are MF [51-53], UF [54-56], NF [57, 58], RO [58, 59], gas separation [60], and pervaporation [61, 62]. The release mechanism may be dependent on the size or affinity. Electrodialysis and membrane electrolysis are examples of membrane separation processes operated with an electrical potential difference. Examples of membrane separation processes performed by the concentration gradient are dialysis, diffusion dialysis, membrane contactors, osmosis, and liquid membranes. The separation mechanism may depend on the size, affinity, or chemical structure. Examples of membrane separation processes where the mass flux is regulated by both pressure and concentration gradient are membrane contactors. Their separation mechanism may depend on gravity. Examples of membrane separation processes driven by both pressure and temperature gradient are thermo-osmosis and membrane distillation. The separation mechanism depends on the vapor pressure. The structure and material of the membranes are critical in determining their application areas. In Table 4, the differences between the properties of some separation processes are shown. Driving force, concentrate and filtrate types are the factors that determine where the membrane can be used.

Table 4 Separation power of the membranes according to driving force, retentate and permeate [44]

Separation Process	Driving Force	Retentate	Permeate
RO	Pressure	Substances, water	Water
NF	Pressure	Water, bivalent ions, dissociated acids, molecules of low molecular weight	Monovalent ions, nondissociated acids, water
UF	Pressure	Particles, bacteria, water	Small molecules, water
MF	Pressure	Suspended solids, water	Substances dissolved in a solution, water
Dialysis	Concentration	Big molecules, water	Small molecules, water
Pervaporation	Partial Pressure	Nonvolatile Potential molecules, water	Volatile small molecules, water
Electrodialysis	Potential	Dissolved nonionogenic substances, water	Ionized substances dissolved in a solution, water

Physical properties of molecules such as the size, density, vapor pressure, and freezing point facilitate the membrane separation. Other factors include gravity and the electrical charge. Thus, the properties of the components to be separated are essential in the separation process and can be used in the selection of the most suitable separation process.

2. 4. Membrane applications for water recovery

Laboratory-scale applications of membranes with various possible types of processes have rapidly transformed into industrial processes of valuable technical and commercial importance since the early 1960s. Nowadays, the membrane technology in industrial wastewater recovery has been regarded as the most critical technology of purification technique in separating contaminant physically or physicochemically from a polluted water source [63].

Membranes act as semipermeable materials like cells, and separate two different media, allowing the passage of particular constituents while retaining others. For the transportation

of substances through the membrane, the driving force implements an inequality in a gradient of pressure, concentration, temperature, the electrical or chemical potential. In membrane processes, there is no chemical reaction or the annexing of chemicals in the feed flood, and it is solely based on physical separation. Hence, this separation technique becomes a great alternative to conventional methods such as coagulation-flocculation, precipitation, distillation, ion exchange, biological treatment, or adsorption by active carbon. The representation of the required filter media for industrial wastewater applications is given in Figure 9.
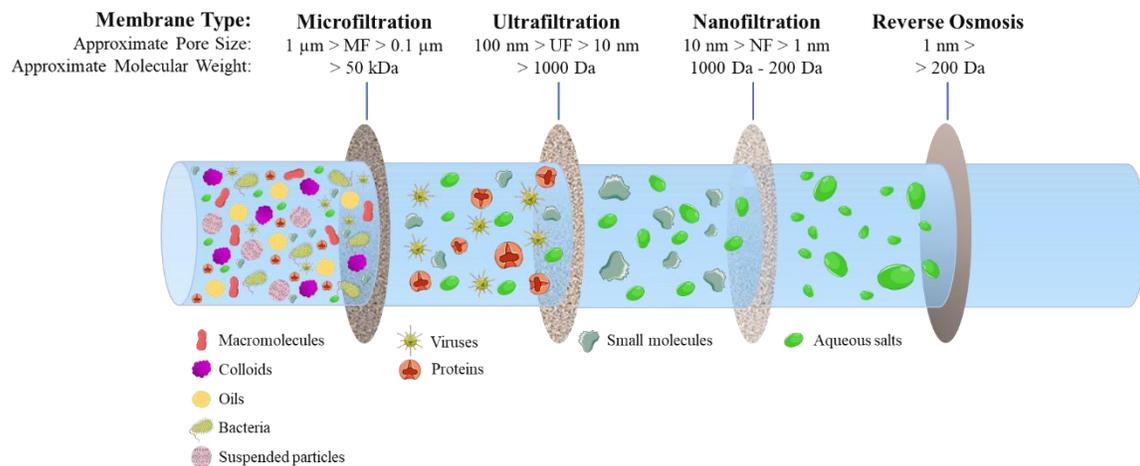
Figure 9 Required filter media according to the separation power used in industrial wastewater recovery

Membranes as a separation tool have been utilized in a wide range of applications to recover substantial amount of substances, enhance products, improve the visual/physical quality of the solutions, and also the efficiency of processes. MF, UF, RO, and NF membranes provide various opportunities in industrial wastewater recovery (Table 5).

Table 5 Industrial filtration processes via MF, UF, NF and RO membranes for various matrix

Industrial filtration process	MF	UF	NF	RO
Water recovery & reuse	✓	✓	✓	✓
Clarification	✓	✓		
Macromolecules		✓	✓	✓
Desalination			✓	✓
Softening			✓	
Dye removal			✓	✓
Organic substance removal			✓	✓
Process water feeding				✓
Salt removal				✓
Small compounds removal			✓	✓

2. 5. Ultrafiltration membranes

UF is a separation technique in membrane application to filtrate microorganisms, bacteria, viruses, dissolved macromolecules, and colloidal solid particles by the sieving mechanism larger than 0.1 µm due to the pore size of a UF membrane in the range 0.1 µm to 0.001 µm. The operational driving force is the pressure which is applied between 1 and 10 bar [64].

UF is sensitive to retain macromolecules, colloidal substances, low molecular weight species; however, low molecular weight organic molecules and ions such as sodium, magnesium chloride, calcium cannot be removed [65]. Therefore, the differences in osmotic pressure across the UF membrane surface count can be negligible. For high flux rates in a UF membrane application, low transmembrane pressures are adequate. Flux for a membrane can be defined as the amount of permeate solution generated per unit area of active membrane surface per unit time. Flux is stated as cubic meters per hour (LMH) or gallons per square foot per day (GFD) in general. Typically, the UF membranes can have high flux values, which vary in a range of 25 and 100 LMH at about one bar, on the contrary, RO membranes have flux values varying between 17 and 51 LMH at a pressure range of 4 to 28 bar.

UF membranes can concentrate the feed solutions to suspended and emulsified solutions, and do not allow them to pass through the transmembrane. During the separating process in UF membranes, the concentration gradient in the feed solution increases in the vicinity of the membrane surface. This phenomenon is called polarization of concentration. As a result, a boundary layer with high-concentration matters forms on the membrane surface, which

inhibits the feed flowing through the UF membranes and adversely affects the membrane performance. Polarization concentration can be prevented by a high-velocity fluid flow parallel to the membrane surface. Besides flow across the membrane surface, operating pressure and operating temperature also influence the membrane performance. Permeation rates directly increase as applied pressure escalates. A similar increment can be observed at higher operating temperatures. Operating pressures mostly do not surpass 7 bar due to limitations such as physical strength, increasing compaction, and fouling and the water flux in the porous medium of an UF membrane are directly proportional to the applied pressure, which is called Darcy's Law [50]. Also, the thermal properties of UF membranes may limit the performances of membranes at elevated operating temperatures.

Generally, polymeric materials are used to produce the UF membrane due to their operational flexibility [65]. Polymeric materials for UF membranes can be summarized as:

- Poly(arylene ether sulfone) (PAES),
- Poly(ether sulfone) (PES),
- Polyethylene (PE)
- Poly(methyl methacrylate) (PMMA)
- Polyamide (PA)
- Poly(tetrafluoro ethylene) (PTFE)

- Poly(phenyl sulfone) (PPS)
- Poly(vinylidene fluoride) (PVDF)
- Polypropylene (PP)
- Cellulose and Cellulose acetates (CA)
- Polyacrylonitrile (PAN)
- Polycarbonate (PC)

Although there is a variety of polymeric materials that can be used in the production of UF membranes, most commercial UF membranes are manufactured from cellulose acetate or polysulfone-based materials. Particularly, polysulfone is widely utilized in membrane applications because of its high-performance thermoplastic nature with superior thermal resistance, chemical tolerance, and mechanical properties than other polymeric materials. On the other hand, polysulfone has a hydrophobic character that negatively influences the performance of UF membranes. Moreover, the hydrophobicity can affect the mechanical properties during the preparation of polysulfone based UF membranes; in this step, macro voids may form that corrupt the homogeneity of pore distributions. To suppress the formation of the macro voids in the process of the membrane manufacture, the solution of polymeric

membrane materials can be modified with additives such as hydrophilic polymers, surfactants, salts, and mineral fillers. Hence, the usage of additives serves to well-distribute the pore, also, improving the hydrophilicity and interconnectivity of them.

Highly branched polymers can be used as additives because they indicate low viscosity and excellent solubility in solvents. They also possess multifunctional end groups [66, 67] in the backbone, which can be easily converted to customized functionalities. In the studies on proton-exchange membranes, there have been a few cases where highly branched polymers are used to improve membrane properties and performance. For example, using a mixture of sulfonated highly branched poly(arylene ether sulfone) and linear sulfonated poly(ether sulfone) (SPES), Zou and co-workers [68] prepared new proton exchange membranes, which showed temperature dependent proton conductivity, with better water uptake and mechanical properties than the membrane formed only with SPES. Another example of blending linear and hyperbranched polymers is the study reporting blend films prepared in N,N-dimethylacetamide (DMAc) that were crosslinked by using a Friedel–Craft acylation reaction in the presence of $FeCl_3$ between sulfonic acid end groups of hyperbranched poly(ether sulfone) (HBPES) and electron-rich aromatic rings of linear poly(ether ether ether sulfone) [69]. As a consequence, the mechanical properties of blend polymer were similar to that of the linear one. However, the proton conduction of crosslinked blend films improved, but spinodal decomposition into bicontinuous phases was observed in the morphology.

2.5.1. Ultrafiltration membrane preparation

The first method for the fabrication of a polymer-based asymmetric membrane was invented in 1960 by Loeb and Sourirajan [25], which is still the most common technique nowadays, known as the phase-inversion process to manufacture UF membranes. In general, there are two kinds of asymmetric UF membranes prepared via phase-inversion technique (Figure 6): Finger-shaped and sponge-liked. Both asymmetric membranes have a very thin and dense skin layer and porous sub-layer. In the phase-inversion process, a homogenous solution-cast polymer film is submerged into a coagulation bath in order to solidify polymer, and the exchange between the solvent of polymer film and the nonsolvent of coagulation bath forms the asymmetric porous membrane structure. During this process, liquid-liquid and solid-liquid phase separation occur which directly depends on parameters below [70, 71]:

- Type of polymeric material (molecular weight and molecular weight distribution)
- Type of organic solvent
- Type of additives
- The casting solution composition
- Temperature of the casting solution
- Type of quenching medium
- Temperature of quenching medium
- The casting atmosphere composition
- The casting atmosphere temperature
- Evaporation conditions
- Casting thickness
- Casting speed
- Type of membrane support material
- Drying conditions

Especially, coagulation bath conditions can directly influence the kinetic and thermodynamic factors of a phase inversion system [72-75]. In the preparation of a membrane using a phase inversion method, the casting-solution mostly includes, in addition to the polymer and the solvent, additives that work as a nonsolvent agent to suppress macro void formation by minimizing the solvent power in the solution. The schematic representation of a UF membrane preparation process by phase inversion technique is given in Figure 10. As the polymeric additive, poly(vinyl pyrrolidone) (PVP) has been widely utilized in casting solutions to fabricate polysulfone-based membranes due to its high miscibility in polysulfone and excellent solubility in water [76-79].
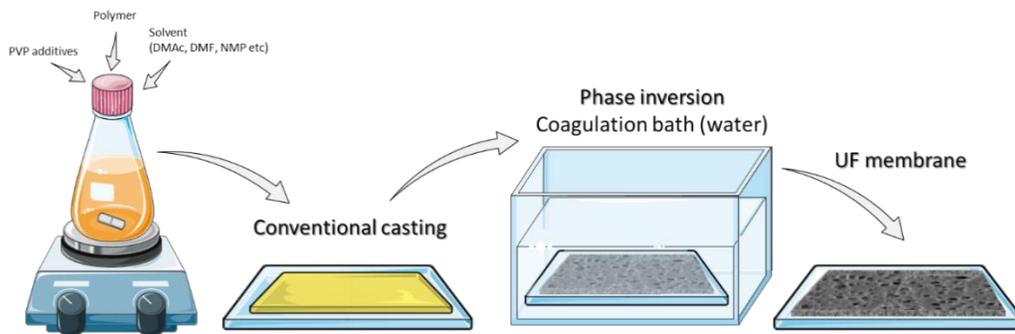
Figure 10 Schematic representation of the preparation of UF membranes by the phase inversion technique

2.5.2. Ultrafiltration membrane properties

An ideal UF membrane should have excellent mechanical strength and thermal stability within the operating pressure and temperature ranges, also high chemical and pH resistance, high permeability as well as high product retention. At the same time, it should also have anti-fouling properties in order to prevent the accumulating of the filtrate on the membrane skin. The top layer of membrane plays a critical role in the selectivity, separation factor, and permeability, which determine the overall UF membrane performance.

2. 6. Nanofiltration membranes

NF is a pressure-driven separation technique similar to MF, UF, and RO. The separation power of NF membranes is in between UF and RO membranes; UF membranes can reject dissolved macromolecules higher than 5000 Da, and RO membranes can retain almost all kinds of salts and small molecules greater than 100 Da with high rejection ratio [80].

In 1984, FilmTec Corporation coined the term "nanofiltration" for the first time that expressed loose RO membranes with pore sizes larger than one nm. This expression on the description of NF membranes can be extended such that; NF membranes have a pore size diameter smaller than 2 nm, which matches up with the molecular weight cut-off for organic matters in the range of 150-2000 Da [81]. NF membranes allow the passage of monovalent ions, but they have a high rejection ratio for divalent ions. In general, NF membranes can reject neutral and positively charged compounds according to their shape and size.

The active layer of NF membranes is usually fabricated via the interfacial polymerization reaction that occurs between monomer solutions, which are immiscible to each other. The interfacial polymerization reaction occurs mostly in the organic phase because of the low solubility of the organic reagent in the aqueous phase [82, 83]. The main reason for choosing the interfacial polymerization technique is the fact that an extremely thin active layer can be formed on a porous support layer. Also, the reaction rate is high wherever the monomers contact each other; however, as the formation of the active layer continues, the monomer transportation to the interface is limited. Thus, the reaction slows down, and the formation of the active layer is self-limited. To summarize, a very thin and uniform active layer can be produced via the interfacial polymerization technique, and as a consequence, NF membranes

with such active barrier layers typically have high rejection yields for polyvalent ions and small organic compounds at moderate pressures.

Mass transfer in NF membranes occurs by filtration, electrostatic forces, and diffusion taking place at the porous and non-porous membrane interface according to Fick's Law. NF membranes have moderate surface charges due to both the dissociation of functional groups on the surface and the adsorption of charged solutes. These surface charges intrinsically contribute to the rejection of the charged molecules like divalent or polyvalent ions and the selectivity of NF membranes. On the other hand, the RO membranes are successful in the removal of monovalent ions by diffusion transport mechanisms due to their non-porous structure. Yet, NF membranes can operate with higher water flux and higher water recovery at lower pressures than RO membranes because of their porous and non-porous structure, which also results in less energy consumption during the operation.

NF membranes reported in the literature often consist of polyamide networks, which form via the interfacial polymerization reaction between piperazine (PIP) or *m*-phenylenediamine (MPD) in the aqueous phase and trimesoyl chloride (TMC) in the organic phase. Besides polyamide-based NF membranes, ultra-thin polyarylate active layers formed via the interfacial polymerization reaction have drawn for the fabrication of novel thin-film composite (TFC) membranes, which have an outstanding performance in organic solvent nanofiltrations (OSN) [48, 84] and gas separation membranes [85]. Mainly, monomers containing hydroxyl functional groups, contorted- and spiro-centers have been utilized for the polyarylate based TFC membranes, as illustrated in Figure 11. The polyarylate network formed by these monomers shows inefficient packing due to the contortions of backbones. The contortions intrinsically create interconnected voids less than 2 nm which behave like micropores [48]. Before the interfacial polymerization reaction, phenol functional groups are converted to phenolate ions in alkaline conditions (by NaOH solution) to increase the nucleophilicity of organic monomer and the reaction rate.

5,5',6,6'-tetrahydroxy-3,3,3',3'-tetramethylspirobisindane (TTSBI)

cardo-structured 9,9-bis(4-hydroxyphenyl)fluorene (BHPF)

planar-structured 2,6-dihydroxyanthraquinone (DHAQ)

1,3-benzenediol (RES)
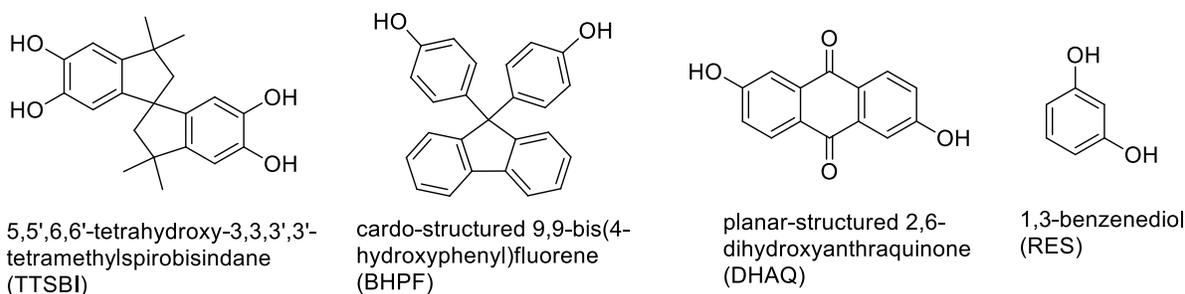
Figure 11 The monomers of polyarylate active layer formed by interfacial polymerization for NF [48]

In addition to the use of typical monomeric amines for the In addition to use of typical monomeric amines for the interfacial polymerization reaction, polymeric reactants such as polyethyleneimines were reported in the formation of an active layer (Figure 12), which is known as NS100 (North Star, USA), by the reaction with toluene diisocyanate [86-90]. There are other studies showing the use of polymeric amines such as poly(vinyl amine)s [91], polyepiamines [92, 93], poly(vinyl imidazoline)s [94, 95], poly(diallyl amine)s [95] in the formation of the active layer of NF membranes. Still, the monomeric amine-based NF membranes are the most common, commercial ones. In general, PIP and MPD are utilized as water-soluble amine monomers [83, 96]. The diffusions of polymeric reagents to the interface could be more difficult than the monomeric ones due to their macromolecular nature; in this respect, they cannot be as highly reactive as the monomeric ones. Wei *et al.* developed an active layer with the interfacial reaction between a hydroxy-functional aliphatic hyperbranched polyester (HPE) and terephtaloyl chloride or TMC [97-99]. It was shown that the surface roughness of membranes increased with an increase in the concentration of HPE. Also, a reduction of membrane flux and an improvement of salt rejection were reported with increasing TMC concentration.
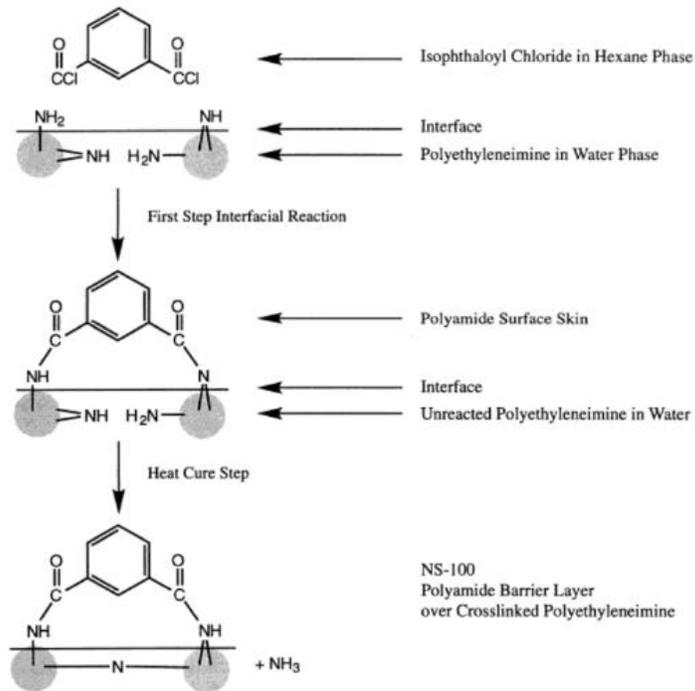
Figure 12 The mechanism of the active layer formation for NS100 membrane [90]

NF membranes are used for the treatment of salty cheese in the food industry, removal of color and organic matter in the textile industry, the concentration of organic substances, and the removal of salinity in the pharmaceutical industry. It can be used alone as well as together with UF and RO membranes in the purification systems. Moreover, they are utilized to reduce the hardness of surface water, removal of dissolved solids in well water, as well nitrate, pesticide, and micropollutant removal and demineralization. Especially in surface waters with low osmotic pressure, it is a superior process compared to RO systems due to low operating pressure. Typical flux values are in the 20-200 L/m^{2}h range. Various examples of the use of NF membranes are summarized in Table 6.

Table 6 General applications for NF membranes

Application Area	Industry	References
Water recovery for the boiler feed and cooling tower water, water treatments for power plants	Energy	[100-102]
Water generation and recovery for chemical process	Chemical process	[103]
Water/organic liquid separation and separation of organic liquid mixtures	Chemical process	[104, 105]
Treatment of mining wastes, recovery of coating rinse waters and recovery of metals	Metal and metal processing	[106, 107]
Milk processing, lactose separation, sweetener concentrate, fruit juice and beverage processing and wastewater treatment	Food processing	[108-110]
Wastewater treatment, recovery of dyeing and finishing chemical and water	Textile	[111-113]
Removal of heavy metals polluting the environment from surface and groundwater	Heavy metal treatment	[114-116]

2.6.1. Nanofiltration membrane preparation

Polymer-based NF membranes can be fabricated by various methods such as the interfacial polymerization reaction, phase inversion, post-treatment of a porous support layer by surface coating or grafting, layer-by-layer coatings, incorporation of aquaporins and utilization of glassy polymers [80]. The most common technique to fabricate NF membranes is the interfacial polymerization reaction approach that is a polycondensation reaction occurring between two or more monomers at the interphase of immiscible aqueous and organic solutions.

At first, the aqueous monomer solution is used to soak the porous support membrane, then, the excess monomer solution is removed by a roll from the support layer. Afterward, the organic monomer solution is poured onto the support layer, and a thin film as a barrier layer is instantaneously formed at the interface. The main steps for the fabrication of NF membranes by interfacial polymerization are illustrated in Figure 13.
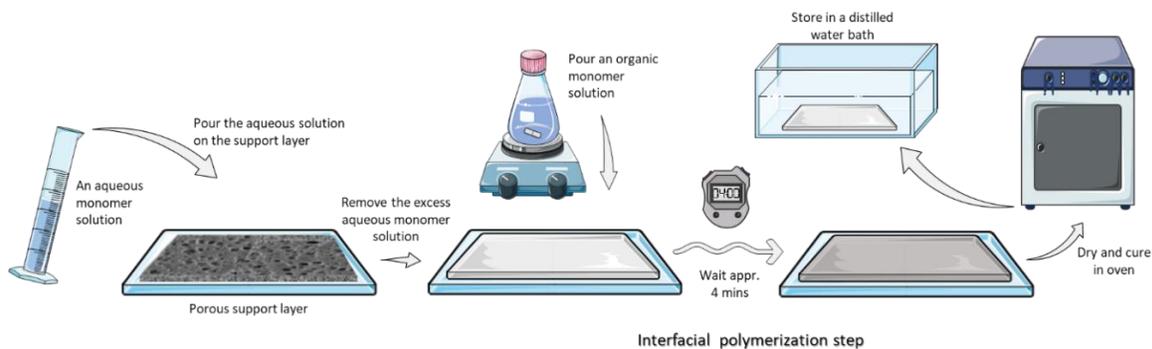
Figure 13 General steps for the fabrication of a TFC NF membrane by interfacial polymerization

2.6.2. Nanofiltration membrane properties

The main characteristics of NF membranes can be expressed as follows; NF membranes have a pore size diameter smaller than 2 nm, which matches up with the molecular weight cut-off for organic matters in the range of 150-2000 Da [81]. NF membranes allow the passage of monovalent ions significantly, while they have a high rejection ratio for divalent ions. NF membranes can reject neutral and positively charged compounds depending on their shape and size.

2. 7. Poly(arylene ether sulfone) (LPAES)

Partially Taken From:

Ozbulut, E. B. S.; Seven, S.; Bilge, K.; Akkas, T.; Tas, C. E.; Yildiz, B.; Atilgan, C., Menceloglu, Y. Z.; Unal, S. "Blends of highly branched and linear poly(arylene ether sulfone)s: Multiscale effect of the degree of branching on the morphology and mechanical properties", Polymer, 188 (2020), 122114.

Poly(arylene ether sulfone) (LPAES) is a commercial high-performance transparent amorphous thermoplastic engineering polymer that is oxidatively stable under service conditions at elevated temperatures because of its high glass transition temperature (T_g ~185°C) [117]. LPAESs are widely utilized in membrane applications such as hemodialysis,

gas separation, and UF membranes [118, 119], medical applications such as artificial organs due to its bio-compatibility [120, 121] and electronic applications such as automobile parts, circuit boards, connector, and switches [122]. One of the most frequent approaches for the post-functionalization for LPAES is the incorporation of sulfonic groups on phenylene rings to improve the conductivity but this results in the deterioration of mechanical properties [123]. On the other hand, there have been many investigations on miscible LPAES blends. For instance, blending LPAES with oligomeric poly(bisphenol-A)s decreased the solution viscosity and they acted as a plasticizer in the blend [124]. For a desalination application, zwitterionic PAES-co-SBAES copolymer was blended with LPAES to advance the fouling resistance [125]. There is miscible 1,4 arylene (1,4 phenylene or 1,4-biphenylene unit) based polymeric blends with single T_g, and they are suitable for electrical applications due to dimensional and hydrolytic stability and high heat and chemical resistance [126]. Another compatible blend example is the blends of sulfonated branched PAES with LPAES to decrease water uptake and increase conductivity for proton exchange membrane fuel cells (PEMFC) [127]. Blending a linear polymer with its branched analog can result in interesting final properties. Branched polymers do not have high-strength due to lack of entanglements, however, they may provide unique benefits in blends with their linear analog. For instance, PEMFCs that were prepared by blending sulfonated hyper branched poly(arylene ether sulfone)s (SHBPAES) with sulfonated poly(ether sulfone)s demonstrated promising mechanical properties in the non-crosslinked system [68].

2.7.1. Commercially available poly(sulfone)s

Polysulfones have been commercially available since 1965 [128] and they are utilized in a wide range of applications such as the membranes technology [121, 129-131], connectors and switches [132], circuit boards, dielectric parts in capacitors [133], structural foams [134], medical applications [135], automotive applications [136], household appliances (microwave ovens, coffeemakers, and humidifiers), and sensors [137]. Victrex®, Udel®, and Radel® are common examples for commercially available polysulfones with their chemical structures given in Figure 14.
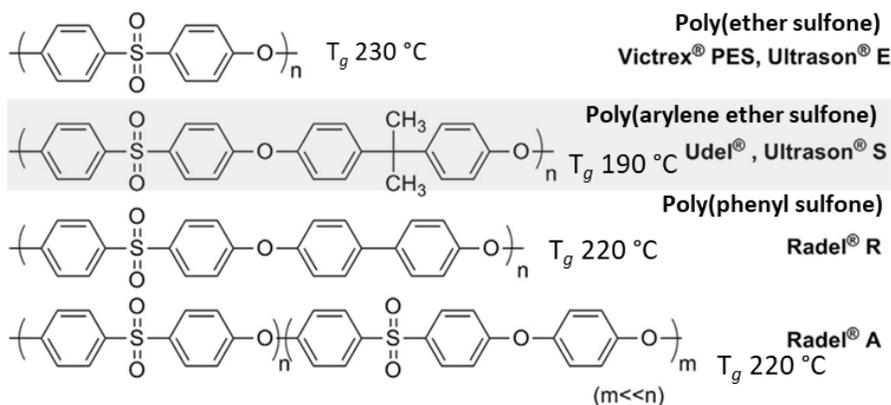
Figure 14 Commercially available polysulfones

2.7.2. Copolymerization routes for poly(sulfone)s

Polysulfones can be easily synthesized via the two most common methodologies such as nucleophilic aromatic substitution [138-140] and electrophilic aromatic substitution [141]. Nucleophilic aromatic substitution is widely utilized in the industry, for instance, commercial high-performance engineering thermoplastic polymers Udel® (bisphenol-A based PAES), Victrex® (polyethersulfone), Radel® (biphenol based poly(phenyl sulfone) have been manufactured with this synthetic route, which is a polycondensation reaction between a kind of bisphenol and bis(chlorophenyl)sulfone (Figure 15).
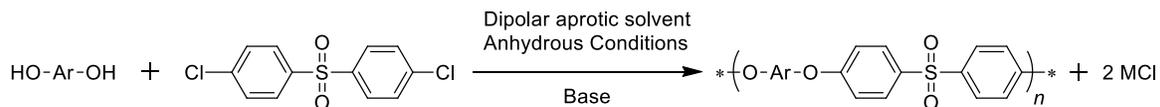
Figure 15 The generic nucleophilic aromatic substitution step growth polymerization of polysulfone (M: Metal counter ion)

Nucleophilic aromatic substitution takes place from two sequential reaction mechanisms: the first step is an addition reaction (S_NAr), and the second one is the elimination reaction. The first step starts with an attack of the nucleophile at the activated site of the aromatic ring to form arenium ion intermediate stabilized with resonance, which is called Meisenheimer

complex. The addition reaction has been generally accepted as the rate-determining step of the reaction. In the second step, the elimination reaction takes place much faster than S_NAr, and the leaving group departs from the phenyl ring, which is driven by the re-establishment of the aromaticity.
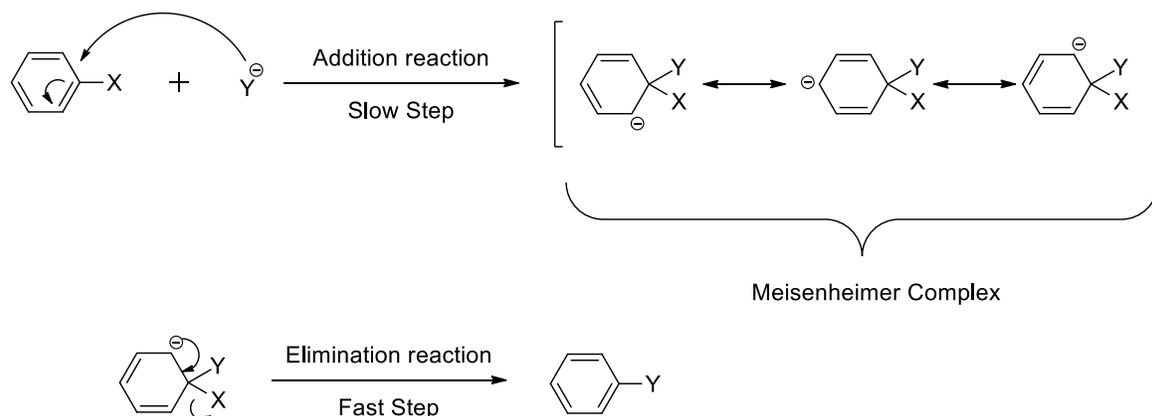
Figure 16 General addition-elimination reaction mechanism [142]

The leaving group type can influence the reaction rate in the S_NAr reaction mechanism. When the leaving group is a halogen, the reaction rate increases in the order of $F \gg Cl \geq Br \geq I$. On the other hand, the strength of the carbon-halogen bond decreases in the same order [143]. The strength of the carbon-halogen bond is ineffective in determining the reaction rate. However, the electronic effect of the leaving group on the attached carbon determines the rate of the S_NAr reaction. The fluorine atom has the strongest electronegativity in the series, which pulls the electron-density away from the adjacent carbon atom via the inductive effect, and the adjacent carbon atom becomes susceptible to nucleophilic attack. Moreover, these conditions make the Meisenheimer complex stable. The fluorine atom has the lowest steric hindrance in the series, which may allow the nucleophile to attack the adjacent carbon atom easier.

The strength of nucleophile can also influence the reaction rate in the order of $ArS^- > RO^- > R_2NH^- > ArO^- > OH^- > ArNH_2 > NH_3 > I^- > Br^- > Cl^- > H_2O > ROH$ [143]. In the copolymerization reaction of poly(arylene ether sulfone), the nucleophilicity of phenoxide ion (ArO^-) is stronger than hydroxide ion, halogen ions, water and phenol or alcohol groups.

Furthermore, the choice of the solvent is another critical parameter to achieve the copolymerization of poly(arylene ether sulfone)s. The solvent must not react with any other species during the nucleophilic aromatic substituent reaction. All species in the reaction medium must be fully soluble in the solvent in order to complete the copolymerization reaction. Moreover, the solvent should weaken the interaction between the pair of nucleophilic ion and metal counterion [144]. Polar aprotic solvents are chosen as media in nucleophilic aromatic substation reactions in order to prevent any interactions between solvent and nucleophile; otherwise, the strength of the nucleophile is influenced adversely. In other words, the capability of the nucleophile to attack the activated adjacent carbon is lost in the protic solvents because of their solvation effect on the nucleophile in S_NAr reactions [145]. Dimethyl sulfoxide (DMSO), 1,2-methyl pyrrolidone (NMP), DMAc, diphenyl sulfone, and sulfolane can be utilized as a polar aprotic solvent in S_NAr reactions after drying by distillation with a drying agent such as CaH_2.

During the phenoxide formation from bisphenol in the presence of potassium carbonate or sodium hydroxide, two moles of water per one mole of bisphenol are generated. Before the dihalide addition, water must be removed from the reaction medium by an azeotrope solvent such as toluene, xylene, or o-dichlorobenzene. Otherwise, water can hydrolyze the Meisenheimer complex, which can limit the molecular weight of the final polymer due to the limited conversion of monomers.

The synthesis of PAES can be accomplished by using a strong base as NaOH or a weak base as potassium carbonate (K_2CO_3). Using a strong base is the common route to synthesize bisphenol-A based polymers as illustrated in Figure 17; however, this type of reaction is more sensitive to the presence of water than the reactions with weak bases. The initial step is the hydroxyl ion attack on the proton of bisphenol to form phenoxide ion with the counterion. Before dihalide addition, the generated water must be removed from the reaction medium. The commercial product Udel is produced by this method, which is a swift reaction, but it is important to keep in mind that there are side-reaction possibilities in the presence of water.
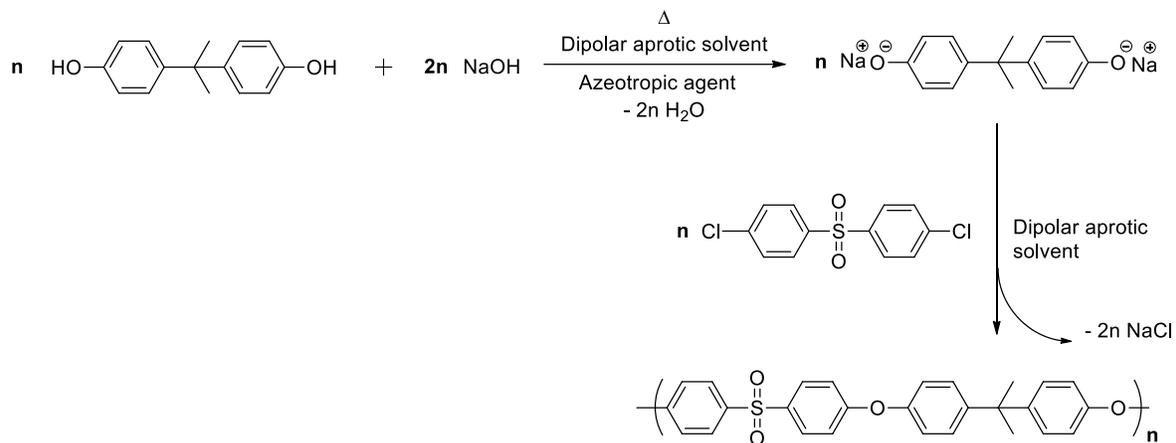
Figure 17 Poly(arylene ether sulfone) synthesis via the strong base method

In the weak base method to synthesize poly(arylene ether sulfone), anhydrous potassium carbonate as a weak base can react with bisphenol in a dipolar aprotic solvent to form phenolate as a product and water as a byproduct. The reaction between potassium carbonate and bisphenol is given in Figure 18. In the weak base approach, potassium carbonate should be used excessively, 10-20 mol% in excess, to obtain a high molecular weight poly(arylene ether sulfone) [140]. The disubstituted phenolate formation rate with potassium carbonate is much lower than the strong base method. However, the excess of potassium carbonate cannot hydrolyze 4,4'-dichlorodiphenylsulfone (DCDPS) and the polymer chain under copolymerization conditions, unlike the strong base reaction. The copolymerization reaction in a dipolar aprotic solvent with NaOH is a second-order reaction which directly depends on the concentration of functional groups, yet, the weak base reaction cannot follow the same kinetics due to the slower reaction rate of the disubstituted intermediate formation that can take about 300 minutes.
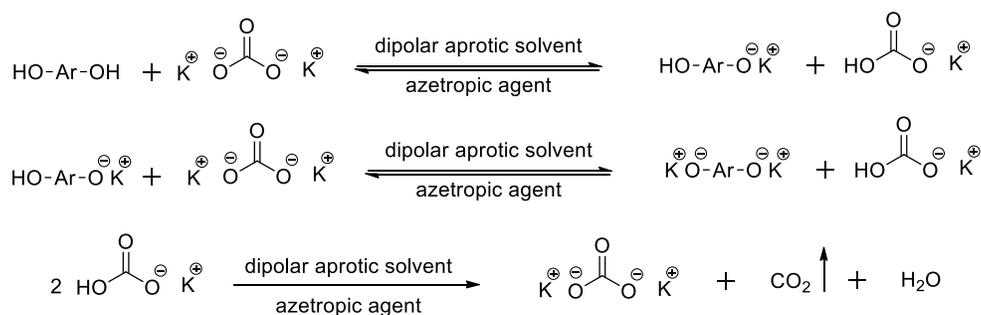
Figure 18 The reactions between potassium carbonate and bisphenol and formation of water [140]

38

Also, an azeotropic agent should be utilized to remove the water from the reaction medium prior to the addition of dihalide monomers. To get bisphenol terminated poly(arylene ether sulfone)s, the stoichiometry of the bisphenol monomer can be slightly excess; moreover, the molecular weight of copolymer could be controlled by this approach. The reaction mechanism between potassium phenolate and DCDPS is given in Figure 19.
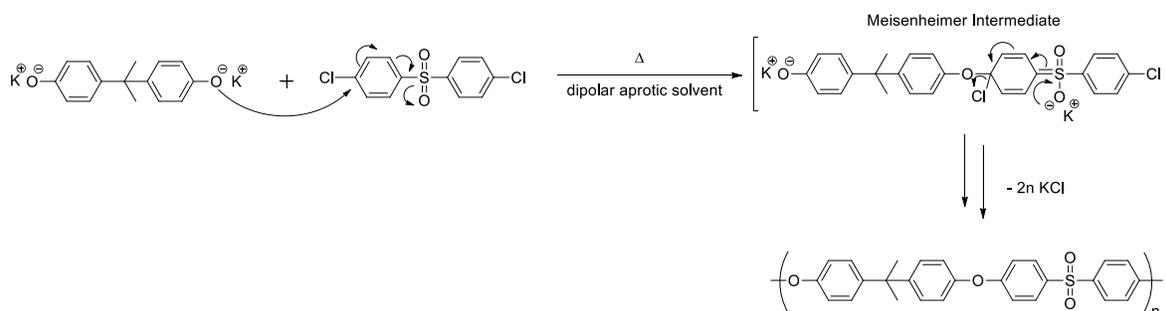
Figure 19 The mechanism of the nucleophilic aromatic substitution reaction of poly(arylene ether sulfone)

2. 8.   Highly branched polymers

Partially Taken From:

Ozbulut, E. B. S.; Seven, S.; Bilge, K.; Akkas, T.; Tas, C. E.; Yildiz, B.; Atilgan, C., Menceloglu, Y. Z.; Unal, S. "Blends of highly branched and linear poly(arylene ether sulfone)s: Multiscale effect of the degree of branching on the morphology and mechanical properties", Polymer 188 (2020) 122114.

Hyperbranched or highly branched (HB) polymers do not typically have high mechanical strength due to lack of entanglements and they resemble dendrimers in many aspects such as high branching density, the multitude of functional end groups, high solubility in organic solvents, and a compact structure [146]. The comparison of HB polymers with linear and dendrimers are tabulated in Table 7. Moreover, viscosity characteristics of dendrimers, linear, and HB polymers in organic solvents are plotted in Figure 20. The synthesis of HB polymers is usually easier than dendrimers because they can be effortlessly synthesized in

one-pot reactions [147-149]. Unlike monodisperse, perfect dendrimer structures, HB polymers are synthesized with polydisperse molecular weights and degrees of branching; however, they attract attention from the industry as they are suitable for low-cost production and large-scale applications. A_2+B_3 copolymerization is a unique alternative to AB_n type polymerization approach to synthesize HB polymers due to the vast availability of A_2 and B_3 type symmetric monomers commercially [150]. Even though A_2+B_3 reactions have a high risk of gelation, the determination of the critical point of conversion (p_c) for gelation and terminating the polymerization prior to this point are essential to prevent the gelation and obtain HB polymers with acceptable molecular weights and high degrees of branching [151, 152].

The critical conversion of A_2 and B_3 monomers for gelation has been investigated both theoretically and experimentally in previous studies [149, 153]. Hyperbranched poly(aryl ester)s were obtained without gelation by the slow addition of a dilute solution of 1,3,5-benzenetricarbonyl trichloride (B_3) into a dilute solution of bisphenol A (A_2) [154]. By changing the A_2:B_3 ratio to tune the final functionality of the branched polymer, the reaction between phenol terminated poly(arylene ether sulfone) oligomers having various molecular weights (A_2) and tris(4-fluorophenyl) phosphine oxide (TFPPO) as B_3 monomer has been reported as an example to control the distance between branch points in A_2+B_3 polymerizations [155]. In fact, the distance between branch points and the multitude of functional end groups in HB polymers may significantly influence their macromolecular features, such as thermal stability, solubility, hydrophobicity/hydrophilicity, and T_g [151, 156-158]. While such unique characteristics enable HB polymers to be utilized as additives in numerous formulations as multifunctional crosslinkers [159, 160], resins [161, 162], dispersants [163], catalysis [164] and additives [165-167], etc., a better understanding of the structure-property relationships in their miscible blends with thermoplastic linear polymers is of critical importance in terms of mechanical improvements and morphological changes.

Table 7 Comparison of highly branched polymers with linear polymers and dendrimers [146]

	Linear Polymers	**Highly Branched Polymers**	**Dendrimer**
Structure			
Topology	Linear, 1D	Irregular, 3D	Regular, 3D
Synthesis	One-step, facile	One-step, relatively facile	Multi-step, laborious
Purification	Precipitation	Precipitation or classification	Chromatography
Scaling-up	Common, easy	Common, easy	Difficult
Molecular weight distribution	Discrepant	Discrepant	Identical
Polydispersity index	1.1<	1.1<	1.0 (<1.05)
Degree of branching	0	0.4-0.6	1.0
Entanglement	Strong	Weak	Very weak or none
Viscosity	High	Low	Very low
Solubility	Low	High	High
Functional group	At two ends	At linear and terminal units	Periphery (terminal units)
Reactivity	Low	High	High
Strength	High	Low	Very low
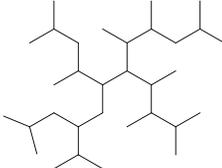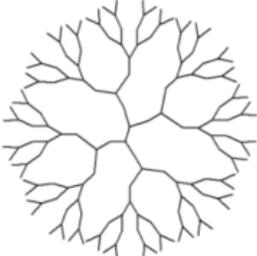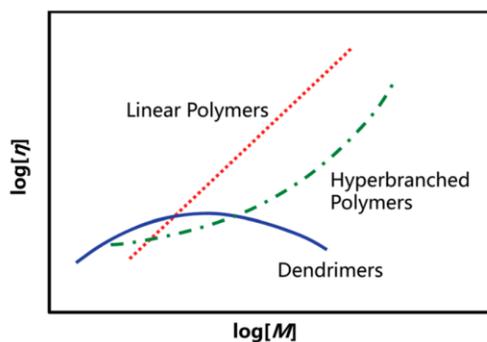
Figure 20 The analogy between log[M] and log [η] for linear, dendrimer and hyperbranched polymers [146]

2.8.1. General synthetic approaches and theoretical aspects of A₂+B₃ copolymerization methodology

The synthesis of HB polymers formed by the self-condensation reaction between AB_2 type monomers was firstly introduced by Flory in 1952 [168, 169]. The HB polymer has a three-dimensional structure due to the initial multifunctional monomers, which have the functionality more than two. Hence, the determination of the stoichiometric ratio of functional end groups and the monomer conversions are very critical to prevent the gelation phenomena in nonlinear polymerization such as A_2+B_3 methodology. The branching coefficient, α, is described as the probability which a functional group of the multifunctional monomer giving a reaction to another branching unit. In an A_2+B_3 methodology, α can be calculated using Equation 1:

$$\alpha = r \times p_A^2 = p_B^2/r \qquad\qquad \textbf{Equation 1}$$

where r is the ratio of A to B number of functional groups (A/B); and p_A and p_B are the fraction of A and B groups that have reacted.

The critical branching coefficient, α_c, which defines the gel point, is another important term. The gel point, abruptly changing the viscosity of the reaction mixture, it can be determined with the calculation of α_c that is calculated using Equation 2:

$$\alpha_c = {}^1\!/_{(f-1)} \qquad\qquad \textbf{Equation 2}$$

where f is the average functionality of multifunctional monomers in the reaction medium.

In A_2+B_3 methodology, f is three because there is one multifunctional monomer, which is B_3 reagent as the trifunctional monomer. Therefore, α_c is calculated as 0.5 according to Equation 2. During A_2+B_3 copolymerization, when $\alpha < 0.5$, a soluble polymer is obtained; whereas a sol-gel mixture of polymer is formed when $\alpha \geq 0.5$. The degree of branching and the α value of a polymer are directly proportional to each other; for example, when monomers converge fully, a crosslinked system forms; hence α value reaches one that is the maximum value

calculated from Equation 1. At the gel point, to calculate the critical conversion of A and B is essential; therefore, for various r values, the critical conversions of A_2 and B_3 monomers are summarized in Table 8 [170]. According to the calculations, it can be deduced that as the value of r increases, the gel point takes place at lower monomer conversion. For example, gelation can never happen when r is 0.37. On the other hand, it takes place at 50% of A_2 conversion when r is two.

Table 8 The critical monomer conversions at gel point in A_2+B_3 copolymerization methodology [170]

$A_2 : B_3$	$r = A/B$	p_{A_c}	p_{B_c}
0.55:1.00	0.37	1.16	0.43
0.75:1.00	0.50	1.00	0.50
0.85:1.00	0.57	0.94	0.53
1.00:1.00	0.67	0.86	0.58
1.25:1.00	0.83	0.78	0.64
1.50:1.00	1.00	0.71	0.71
2.00:1.00	1.33	0.61	0.81
3.00:1.00	2.00	0.50	1.00

Flory's theory on gelation is based on three assumptions such as:

  i.   During polymerization, the reactivity of the functional groups remains the same
 ii.   The reactions happen only between A and B type functional groups
iii.   The polymerization comprises no cyclization reactions

However, Hao et al. suggested that a macromolecular structure with low branching density formed in the early stage of polymerization, and further reactions of B_3 monomer with the rest of the A_2 monomer formed a three-dimensional hyperbranched structure [171, 172]. With this nonideal A_2+B_3 polymerization method, it could be possible to avoid gelation, and at the end of the reaction, a high molecular weight hyperbranched polymer is obtained, which can form a self-standing film.

In 2003, Schmaljohann and Voit studied the reaction kinetics of the A_2+B_3 system via numerical simulations that indicated how to influence the compactness of the final product by the slow addition and the different monomer addition methods [173]. They identified

seven different structural units shown in Figure 21, which are substructures of the terminal, linear, and dendritic units in the system. Also, they demonstrated in the plot given in Figure 22 that gelation occurs at lower p_A values, as the ratio of A_2 to B_3 monomer increases.
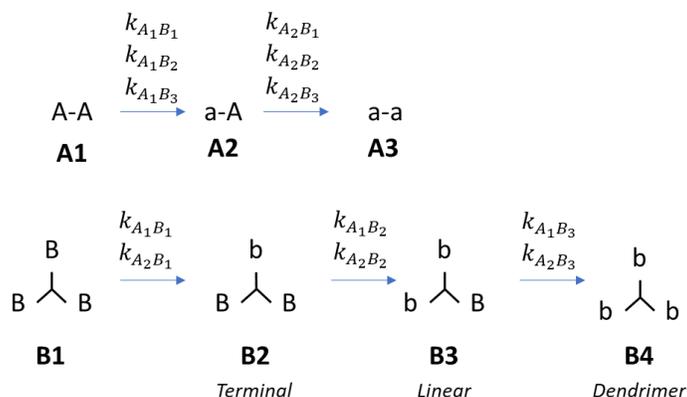
Figure 21 A_2+B_3 reaction pathways and notation of structural units [173]

The capital letters A and B indicate non-reacted functionalities and the lower-case letters a and b indicate reacted groups. An A_2 species can have a maximum of two, and a B_3 species maximum of three adjacent units.
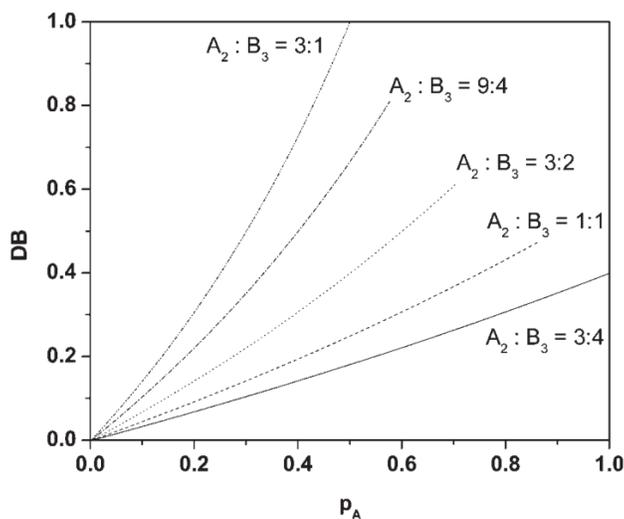
Figure 22 Degree of branching versus conversion of A functional group (p_A) for various monomer compositions in an $A_2 + B_3$ polymerization [173]

In 2003, Schmaljohann and Voit also revealed that the slow addition of both A_2 and B_3 type monomers directly affects the degree of branching of HB polymers [173]. For instance, the

slow addition of B_3 species to A_2 type ones provided to high conversions with no gelation, and the degree of branching of A_2+B_3 based copolymer reached 91%. On the other hand, the degree of branching of the HB polymers attained a maximum of 65% with the slow addition of A_2 species to B_3 monomers (Figure 23).
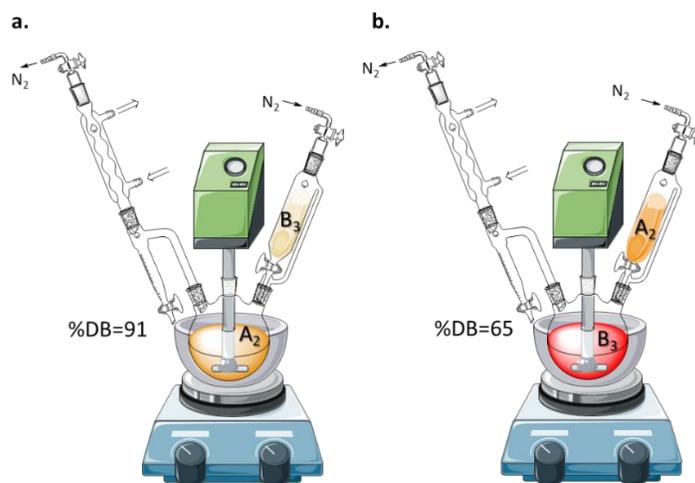
Figure 23 The reaction set-ups in accordance with monomer addition methods, which can directly influence the degree of branching of final products

Before the kinetic study by Schmaljohann and Voit, the monomer sequence of A_2+B_3 copolymerization was enlightened via NMR analysis by Komber et al [174], and the schematic representation of the reaction pathways and the structural units formed during A_2+B_3 polymerization is given in Figure 24.
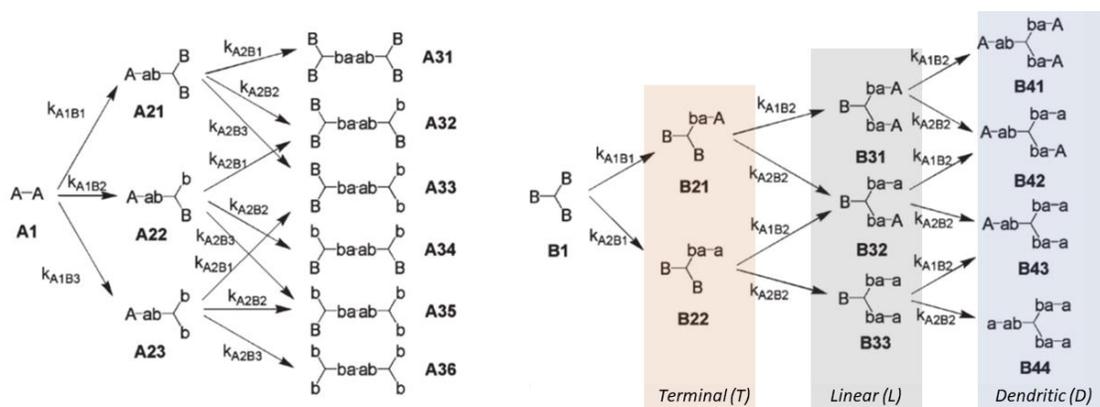
Figure 24 The reaction pathways and structural units for the A_2+B_3 polycondensation of polycondensation of *p*-phenylenediamine (A_2) and trimesic acid (B_3) [173, 174]

The degree of branching is one of the most critical parameters that can change the final properties of a polymer, such as solubility, topology, and mechanical behavior. In 1991, Hawker, Lee, and Fréchet [175] described the degree of branching for AB_2 condensation as the ratio of the sum of dendritic and terminal units to the sum of linear, dendritic and terminal units (Equation 3).

$$DB(Fréchet) = \frac{D+T}{D+T+L} \qquad \textbf{Equation 3}$$

where D, T, and L indicate dendritic, terminal, and linear units in high branched polymers, respectively, and D+T+L=1. Equation 3 is merely valid for high molecular weight HB polymers that arise from monomeric A_2 and B_3 species.

In 1997, Holter, Burgath, and Frey proposed a general expression (Equation 4) to determine the degree of branching of AB_2 based hyperbranched polymeric systems with both high and low molecular weights [176].

$$DB(Frey) = \frac{2D}{2D+L} \qquad \textbf{Equation 4}$$

On the other hand, Unal, Mourey, and Long modified the equation (Equation 5) for oligomeric $A_2 + B_3$ polymerizations because when DP of A_2 oligomers increases, the degree of branching of HB polymers decreases because of the contribution of A_2 oligomers to the linearity of the main chain [161].

$$DB(Long) = \frac{D+T}{D+T+L+n} \qquad \textbf{Equation 5}$$

where the value n is expressed as the number of linear repeat units of A_2 oligomer when D+T+L equals to 1.

2.8.2. Synthetic routes to highly branched polymers for A₂+B₃ approach

Highly branched polymers can be synthesized by various methodologies such as polycondensation [177-180], addition polymerizations [181-183], self-condensing by proton-transfer or ring-opening reactions [184-188], and chain-transfer polymerizations[189-192]. There are several kinds of highly branched polymers such as poly(arylene ether sulfone)s [180], poly(ether sulfone)s [193], poly(arylene ether)s [155, 194], poly(ether ester)s [149, 161], poly(ether ketone)s [195], polyesters [196], polyethers [181], polyamides [174], polyurethanes [197, 198], poly(urethane urea)s [199], polyimides [171], and polysiloxanes [200] synthesized using A₂+B₃ polycondensation approach.

The condensation reaction to form HBPAES via the A₂+B₃ approach is similar to the synthetic pathways of nucleophilic aromatic substitution of LPAES, as explained in 2.7.2. This reaction commonly occurs between halogenated aromatic and phenolic monomers, one of the reactive species has to have a functionality greater than two.

2. 9.   Highly branched poly(arylene ether sulfone)s

Lin and Long reported hyperbranched poly(aryl ester)s that were obtained without gelation by the slow addition of a dilute solution of 1,3,5-benzenetricarbonyl trichloride (B₃) into a dilute solution of bisphenol A (A₂) [154]. By changing the A₂:B₃ ratio to tune the final functionality of branched polymer, the reaction between phenol terminated poly(arylene ether sulfone) oligomers having various molecular weights (A₂) and tris(4-fluorophenyl) phosphine oxide (TFPPO) as B₃ monomer has been reported as an example to control the distance between branch points in A₂+B₃ polymerizations [155]. In fact, the distance between branch points and the multitude of functional end groups in HB polymers may significantly influence their macromolecular features, such as thermal stability, solubility, hydrophobicity/hydrophilicity, and T_g [151, 156-158]. While such unique characteristics enable HB polymers to be utilized as additives in numerous formulations as multifunctional crosslinkers [159, 160], resins [161, 162], dispersants [163], catalysis [164] and additives [165-167], etc., a better understanding of the structure-property relationships in their miscible blends with thermoplastic linear polymers is of critical importance in terms of mechanical

improvements and morphological changes. In Table 9, there are examples of A_2 and B_3 types of monomers for the synthesis of HBPAESs from the literature.

Table 9 A_2 and B_3 monomer examples from literature to synthesize HBPAESs

Application Area	A_2	B_3	References
Proton exchange membrane			[68]
-			[193]
-			[201]
Potential for dielectric coatings			[202]
-			[155]
Blend films			[180]
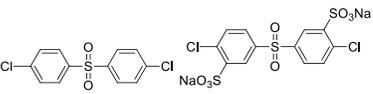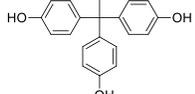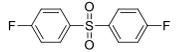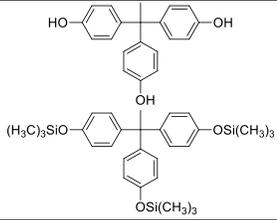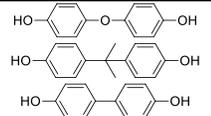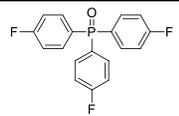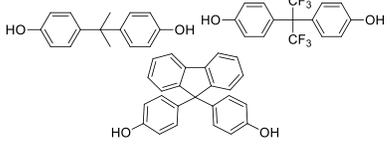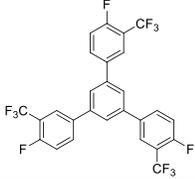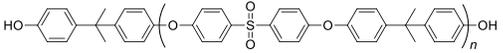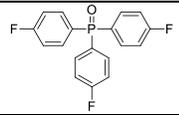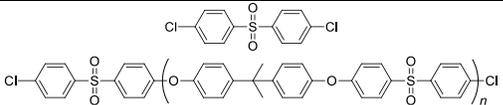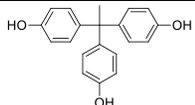
2. 10. End group functionalization of HBPAESs

Highly branched polymers intrinsically have a multitude of functional end groups, contrary to linear polymers that possess only two functional end groups. This multitude of functional end groups can be modified by post-functionalization approaches to enhance morphological, topological, mechanical, thermo-mechanical, and chemical properties; in other words, they allow redesigning of HB polymers according to desired features for the final material to be developed. For example, the incorporation of inorganic-organic moieties into a polymer backbone is typically reported to improve the heat resistance, mechanical and thermo-

mechanical properties, interface, and morphology [203-205]. The types of organic-inorganic hybrid materials are representatively given in Figure 25.
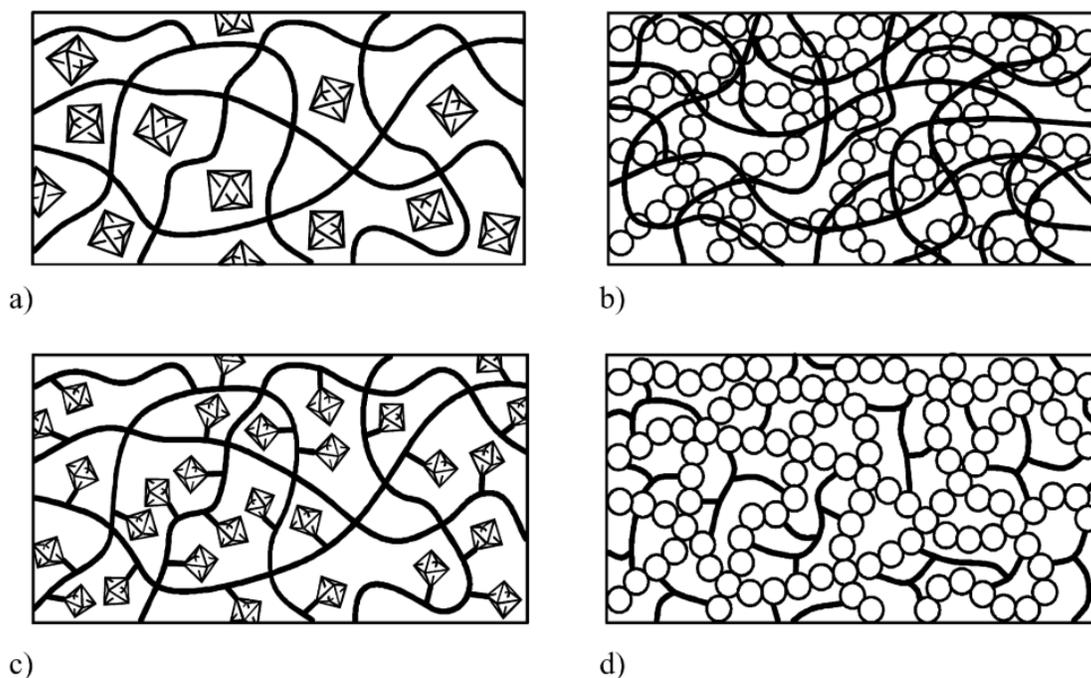
Figure 25 Various types of organic-inorganic composite materials; (a) embedment of inorganic moieties into the polymer, (b) interpenetrating networks (IPNs) with covalent bonds, (c) incorporation of inorganic species into the polymer backbone by covalently bonding, (d) dual organic-inorganic hybrid polymer [203]

The application of industrial water recovery requires membranes with excellent mechanical and thermo-mechanical performance at high alkaline conditions and working temperatures at or above 25 °C. In order to enhance these properties, incorporating self-crosslinkable inorganic functional end groups into the HB polymer backbone can be utilized is a good approach. During the membrane fabrication, these end groups may impart the sol-gel reaction to form dual organic-inorganic hybrid polymer blends. Organosilane coupling agents are quite appropriate for this purpose, and a wide variety of organosilane coupling agents can be easily accessed in the market.

2. 11. Blending linear and highly branched polymers

A linear polymer typically has limited post-functionalization capabilities, and the post-functionalization frequently leads to the deterioration of some of the original physical properties. Blending at least two different types of polymers is a conventional technique applied in the industry to enhance the chemical and physical properties of commercial polymers with low cost and effort. Polymer blends can be prepared by melt mixing or solution mixing in a suitable solvent. The final properties of miscible polymer blends are complemented by favorable attributes of each component. Particularly, properties such as modulus, toughness, viscoelastic and thermal behaviors, morphology, and chemical resistance of a polymer can be tailored by blending with another type of polymer [207]. For the combination of two or more polymers with amorphous morphologies, miscibility is a critical factor determining the final physical and mechanical properties. The negative free energy of mixing (ΔG_m) and the exothermic heat of mixing ($\Delta H_m < 0$) lead to a thermodynamically favorable mixture which originates from the intermolecular interactions between blended polymer chains. In brief, hydrogen bonding, dipole-dipole, and ionic interactions between energetically-suitable chain segments govern the miscibility in polymer blends [207]. Blending linear polymers with their branched analogues can be a feasible approach to achieve unique physical properties and enhance the melt viscosity and proton conductivity of linear polymers while ensuring the miscibility [127, 208]. Linear−hyperbranched multiblock copolymers of linear *p*-phenoxyphenylsulfone and sulfonated hyperbranched poly(ether sulfone) (SHBPES) have been prepared to utilize the multitude of sulfonic acid end-groups of SHBPES in ion-exchange membranes and the incorporation of a linear block resulted in higher mechanical properties for structural support as a membrane [69]. In another study, blending sulfonated hyperbranched poly(arylene ether sulfone)s (SHBPAES) with sulfonated poly(ether sulfone)s has resulted in enhanced proton conductivity with a low-temperature dependence without sacrificing their thermal and mechanical properties [68]. While the enhancement of the physical and chemical properties of linear polymers by combining with their branched analogues has been shown to be a very promising approach, limited studies have been reported on the investigation of mechanical and morphological properties of linear-branched polymer blends.

CHAPTER 3: Experimental

Partially Taken From:

Ozbulut, E. B. S.; Seven, S.; Bilge, K.; Akkas, T.; Tas, C. E.; Yildiz, B.; Atilgan, C., Menceloglu, Y. Z.; Unal, S. "Blends of highly branched and linear poly(arylene ether sulfone)s: Multiscale effect of the degree of branching on the morphology and mechanical properties", Polymer 188 (2020) 122114.

3. 1.   Materials

2,2-bis(4-hydroxyphenyl)propane (BisA, 99+%), 4,4'-dichlorodiphenyl sulfone (DCDPS, 98%), and 1,1,1-tris(4-hydroxyphenyl)ethane (THPE, 99%) were purchased from Aldrich. Potassium carbonate (K_2CO_3, 99+%), toluene (99.7+%), N,N-dimethylacetamide (DMAc, 99%), %), molecular sieves 4Å and poly(vinylpyrrolidone)s (PVP), which were PVP10 (av. M_w: 10 kDa) and PVP40 (av. M_w: 40 kDa), 1,3,5-benzenetricarbonyl trichloride (or trimesoyl chloride, TMC, 98%), anhydrous piperazine (PIP, 99+%), anhydrous n-hexane (99+%) and Reactive Orange 16 (RO16, 70+%) were purchased from Sigma-Aldrich, and Setazol Red (Reactive Red 120, RR120, 50+%) was kindly donated by Setas Chemicals. DMAc and toluene were stored over 4 Å molecular sieves until use. BisA, DCDPS, THPE, and K_2CO_3 were dried under vacuum at 125 °C overnight before use. 3,3'-Disulfonated-4,4'-dichlorodiphenyl sulfone (SDCDPS) was purchased from AKRON Polymer Systems. Dimethyl sulfoxide (DMSO, 99.9+%) and HPLC-grade N,N-dimethyl formamide (DMF, 99.9+%) were purchased from Carlo Erba. Calcium hydride (CaH_2, 95%), sodium hydroxide (NaOH, 97+%) and glacial acetic acid (99.7+%) were purchased from Merck. DMSO was dried over calcium hydride and freshly distilled before use. 3-(triethoxysilyl)propyl isocyanate (IPTES, 95%) was purchased from Momentive. Poly(arylene ether sulfone) was kindly donated by Solvay (Udel® P 3500 LCD MB, T_g= 190 °C, M_w=78-84 kDa). It was used after drying at 135°C overnight to desorb the ambient moisture on its surface. SnakeSkin®

Dialysis Tubing 3.5K MWCO (Cellulose Membrane) was purchased from Thermofisher Scientific. All solvents and chemicals were used as received unless otherwise noted. The structures and properties of chemicals used in this study are listed in Table 10.

Table 10 Chemical structures and properties of chemicals used in this study, and purification methods used before use.

Compound Name	Chemical structure	Properties & Purification methods applied
2,2-Bis(4-hydroxyphenyl)propane (BisA) **Cas# 80-05-7**		-Melting point: 158-159 °C -Molar Mass: 228.29 g/mol -Dried under vacuum at 125 °C overnight prior to use in condensation reactions.
4,4'-dichlorodiphenyl sulfone (DCDPS) **Cas# 80-07-9**		-Melting point: 143-146 °C -Molar Mass: 287.16 g/mol -Dried under vacuum at 125 °C overnight prior to use in condensation reactions.
3,3'-Disulfonated-4,4'-dichlorodiphenyl sulfone (SDCDPS) **Cas# 51698-33-0**		-Melting point: >300 °C -Molar Mass: 491.25 g/mol -Dried under vacuum at 125 °C for overnight prior to use in condensation reactions.
1,1,1-tris(4-hydroxyphenyl)ethane (THPE) **Cas# 27955-94-8**		-Melting point: 246-248 °C -Molar Mass: 306.36 g/mol -Dried under vacuum at 125 °C overnight prior to use in condensation reactions.
Potassium carbonate **Cas# 584-08-7**	K_2CO_3	-Melting point: 891 °C -Molar Mass: 138.21 g/mol -Dried under vacuum at 125 °C overnight prior to use in condensation reactions.
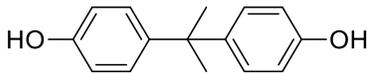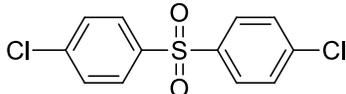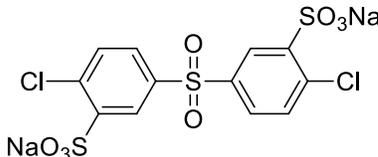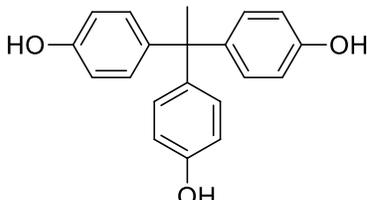
Compound Name	Chemical structure	Properties & Purification methods applied
Dimethyl sulfoxide (DMSO) **Cas# 67-68-5**		-Boiling point: 189.0 °C -Molar Mass: 78.16 g/mol -Density: 1.100 g/cm^3 at 25 °C -Dried over calcium hydride and freshly distilled prior to use in condensation reactions.
Toluene, Anhydrous **Cas# 108-88-3**		-Boiling point: 110-111 °C -Molar mass: 92.14 g/mol -Density: 0.865 g/cm^3 at 25 °C -Azeotropic solvent -Stored over molecular sieves.
N,N-dimethylacetamide (DMAc) **Cas# 127-19-5**		-Boiling point: 165.0 °C -Molar mass: 87.12 g/mol -Density: 0.937 g/cm^3 at 25 °C -Stored over molecular sieves.
Dimethylformamide (DMF) **Cas# 68-12-2**		-Boiling point: 153.0 °C -Molar mass: 73.09 g/mol -Density: 0.944 g/cm^3 at 25 °C -Stored over molecular sieves.
Poly(vinylpyrrolidone)s (PVP) **Cas# 9003-39-8**		-PVP10 (M_w: 10 kDa) -PVP40 (M_w: 40 kDa) -Oven-dried at 110 °C for 10 mins before use -Additive for the production of UF membranes
3-(triethoxysilyl)propyl isocyanate (IPTES) **Cas# 24801-88-5**		-Boiling point: 283 °C -Molar mass: 247.36 g/mol -Density: 0.999 g/cm^3 at 25 °C
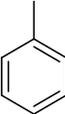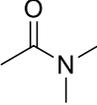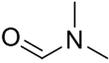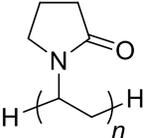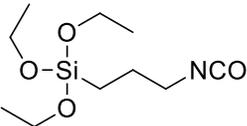
Compound Name	Chemical structure	Properties & Purification methods applied
		-Used as received from Momentive
Poly(arylene ether sulfone) (LPAES) Cas# 25135-51-7		-T_g: 190 °C -M_w: 75-84 kDa -Dried under vacuum at 135 °C overnight prior to use in blend film or UF membrane preparation.
Calcium hydride Cas# 7789-78-8	CaH_2	-Melting point: 816 °C -Molar Mass: 42.09 g/mol -Drying agent - Used as received from Merck.
Glacial acetic acid Cas# 64-19-7		-Boiling point: 117-118 °C -Molar Mass: 60.05 g/mol -Density: 1.049 g/cm^3 at 25 °C - pH adjustment - Used as received from Merck.
Sodium hydroxide Cas# 1310-73-2	$NaOH$	-Melting point: 318°C -Molar Mass: 40.00 g/mol -pH adjustment - Used as received from Merck.
Water	H_2O	-Boiling point: 100°C -Molar Mass: 18.00 g/mol -Density: 1.004 g/cm^3 at 25 °C .
Trimesoyl chloride Cas # 4422-95-1		-Melting point: 32-38 °C -Molar Mass: 265.48 g/mol -Density: 1.487 g/cm^3 at 25 °C
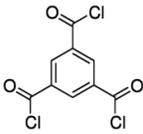
Compound Name	Chemical structure	Properties & Purification methods applied
Piperazine **Cas # 110-85-0**		-Melting point: 109-112 °C -Boilig point: 145-146 °C -Molar Mass: 86.14 g/mol -Density: 1.487 g/cm^3 at 25 °C
n-**hexane** **Cas # 110-54-3**		-Boiling point: 69 °C -Molar Mass: 86.18 g/mol -Density: 0.66 g/cm^3 at 20 °C - Used as received from Sigma-Aldrich.
Reactive Orange 16 **Cas # 12225-83-1**		-Melting Point: >300 °C -Molar Mass: 617.54 g/mol - Absorption: λmax 388 & 494 nm - Anionic monoazo reactive dye
Setazol Red **(Reactive Red 120)** **(Brilliant Red HE-3B)** **Cas # 61951-82-4**		-Melting Point: >300 °C -Molar Mass: 1463 g/mol - Absorption: λmax 530 nm - Anionic, bifunctional azo reactive dye
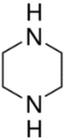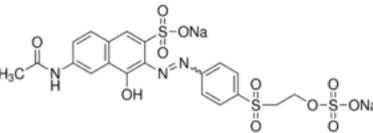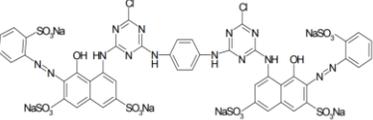
3. 2.   Synthesis

3.2.1.   Synthesis and characterization of chlorine-terminated A$_2$ oligomers

Chlorine-terminated telechelic poly (arylene ether sulfone) (PAES) oligomers with the varying degrees of polymerization (DP) from 3 to 19 were synthesized via nucleophilic aromatic substitution (Figure 26-a.). BisA (4.91 g, 21.50 mmol), DCDPS, and K$_2$CO$_3$ (6.83 g, 49.44 mmol) were dissolved in freshly distilled DMSO in a 150 mL 4-necked round-bottomed flask equipped with an overhead mechanical stirrer, thermocouple, N$_2$ gas inlet, and a Dean-Stark trap attached to a reflux condenser. The ratio of DMSO and toluene was 2:1 (v/v). The solid content of the reaction mixture in DMSO was adjusted to 35%. The molar feeding ratio of monomers is given in Table 12. The by-product H$_2$O was azeotropically removed with toluene from the reaction mixture upon the reaction of K$_2$CO$_3$ with phenolic end groups of BisA to convert to phenolate groups at 150 °C in ~4 h. After the dehydration step, the reaction temperature was gradually increased to 170 °C and the azeotropic mixture was collected from the Dean-Stark trap. At the end of 24 h, the reaction mixture was cooled to room temperature and filtered to remove the by-product KCl salt and the final polymer was precipitated in distilled water. The precipitate was filtered and washed with distilled water. The final product was dried under vacuum at 120 °C for 48 h. The yield of the synthesis was >92.

Moreover, chlorine-terminated telechelic sulfonated PAES oligomers with a DP of three were synthesized using SDCDPS instead of DCDPS by the same method above (Figure 26-b.).
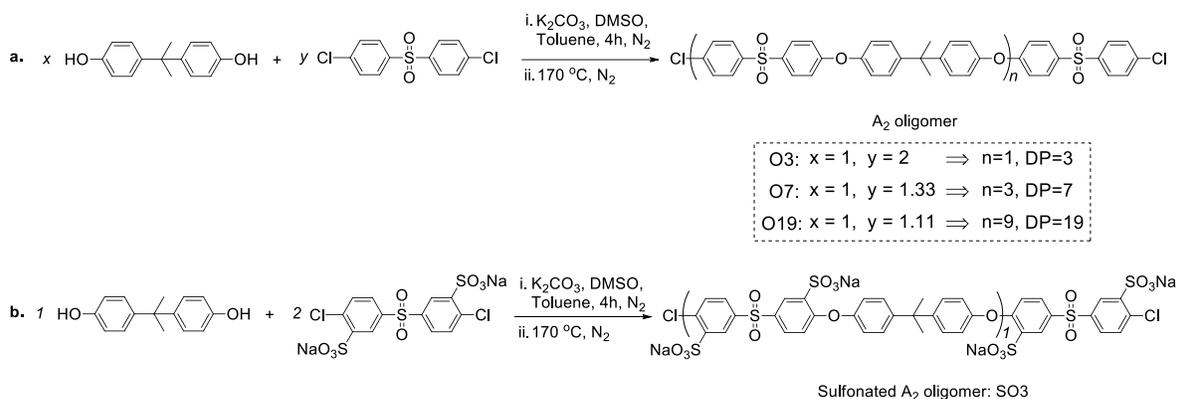
Figure 26 Schematic representation of the synthesis of chlorine terminated PAES A_2 oligomers: a. A_2 oligomers for HBPAES synthesis; b. the sulfonated A_2 oligomer (SO3) for the SHBPAES synthesis

<u>BisA</u>: ^{1}H NMR (500 MHz, DMSO) δ 9.14 (s, 2.00 H), 6.99 (m, 4.00 H), 6.65 (m, 4.00 H), 1.53 (s, 6.00 H).

<u>M0</u> (DCDPS): ^{1}H-NMR (500 MHz, DMSO-d6) δ 8.02-8.00 (m, 4.00 H), 7.74-7.72 (m, 4.00 H).

SM0 (SDCDPS): ^{1}H-NMR (500 MHz, D$_2$O) δ 8.40-8.38 (m, 2.00 H), 8.24-8.22 (m, 2.00 H), 7.94-7.92 (m, 2.00 H).

<u>O3</u>: ^{1}H-NMR (500 MHz, CDCl$_3$) δ 7.88-7.85 (m, 8.11 H), 7.50-7.46 (m, 4H), 7.26-7.24 (m, 4.23 H), 7.03-7.01 (m, 4.27 H), 6.96-6.94 (m, 4.27 H), 1.70 (s, 6.01 H).

<u>O7</u>: ^{1}H-NMR (500 MHz, CDCl$_3$) δ 7.87-7.85 (m, 15.99 H), 7.49-7.46 (m, 4H), 7.26-7.24 (m, 11.96 H), 7.03-7.00 (m, 11.97 H), 6.96-6.94 (m, 11.96 H), 1.70 (s, 18.02 H).

<u>O19</u>: ^{1}H-NMR (500 MHz, CDCl$_3$) δ 7.86-7.84 (d, J=8.8 Hz, 40.54 H), 7.47-7.46 (m, 4H), 7.25-7.23 (d, J=8.6 Hz, 34.57 H), 7.01-7.00 (d, J=8.8 Hz, 34.64 H), 6.95-6.93 (d, J=8.6 Hz, 36.47 H), 1.69 (s, 50.98 H).

<u>SO3</u>: ^{1}H-NMR (500 MHz, CDCl$_3$) δ 8.35-8.27 (m, 4.30 H), 7.89-7.84 (m, 4.57 H), 7.70-7.67 (m, 2.24 H), 7.28-7.26 (m, 4.28 H), 6.99-6.91 (m, 6.66 H), 1.65 (s, 6.01 H).

3.2.2. Synthesis and characterization of highly branched poly(arylene ether sulfone)s

HBPAESs were synthesized using monomeric and oligomeric A_2 with B_3 monomer via the A_2+B_3 polymerization (Figure 27). THPE (1.41 g, 4.61 mmol) and K_2CO_3 (2.20 g, 15.89 mmol) were dissolved in freshly distilled DMSO in a 150 mL 4-necked round-bottomed flask equipped with a dropping funnel containing A_2 species which were prepared according to $A_2:B_3$ ratio as 0.85. The conversion of phenolate ions and dehydration was allowed to take place in about ~4 hours at 150°C. After this step, the reaction temperature was gradually increased to 160 °C, and the azeotropic mixture was collected from the Dean-Stark trap. The total solid content of the reaction was set to 8% (w/w) in DMSO. A_2 species was drop-by-drop added into reaction mixture under N_2. After the A_2 addition, the reaction continued for 48 hours and then the reaction mixture was cooled to ambient conditions and filtered to remove the by-product KCl salt and precipitated in acetic acid-acidified deionized water (pH~3). The precipitated polymer was filtered, washed with deionized water, stirred in boiling deionized water for four hours, filtered again and washed with deionized water and finally dried under vacuum at 120 °C for 48 hours. (yield >90%)
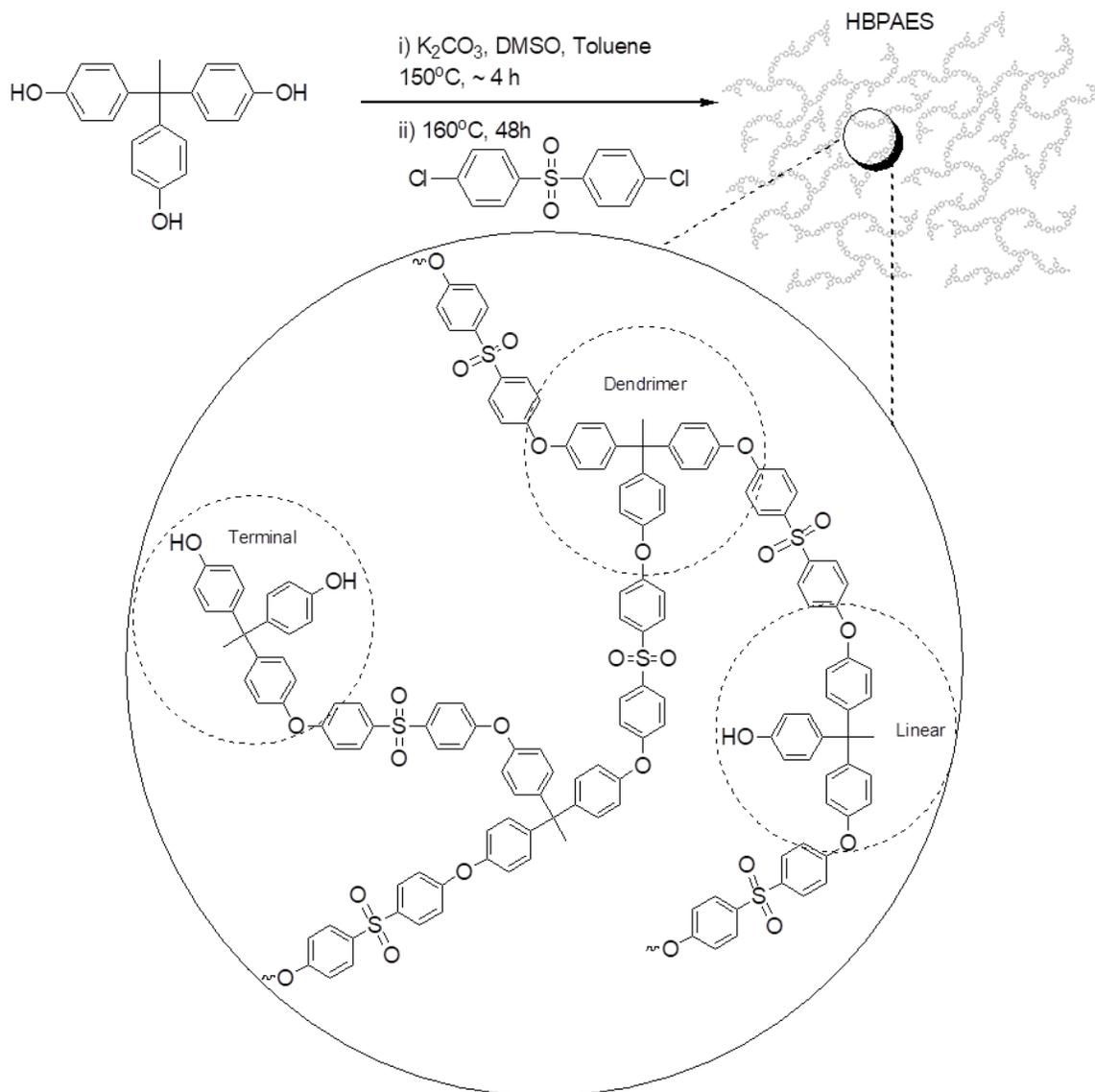
Figure 27 Schematic representation of A_2+B_3 polymerization for HBPAES synthesis [180]

<u>M0-0.55</u>: ^{1}H NMR (500 MHz, DMSO-d6) δ 9.35-9.15 (m, 10.55 H), 7.92-7.80 (m, 15.40 H), 7.43-7.42 (m, 6.00 H) 7.10-6.81 (m, 93.40 H), 2.16-1.89 (m, 21.00 H).

<u>M0-0.75</u>: ^{1}H NMR (500 MHz, DMSO-d6) δ 9.35-9.15 (m, 12.40 H), 7.92-7.82 (m, 27.00 H), 7.43-7.42 (m, 9.00 H) 7.10-6.66 (m, 123.00 H), 2.16-1.89 (m, 27.00 H).

<u>M0-0.85</u>: ^{1}H NMR (500 MHz, DMSO-d6) δ 9.34-9.14 (m, 28.00 H), 7.92-7.82 (m, 74.80 H), 7.43-7.42 (m, 18.00 H) 7.08-6.65 (m, 320.80 H), 2.16-1.88 (m, 66.00 H).

M0-1.00: ^{1}H NMR (500 MHz, DMSO-d6) δ 9.31 (bs, 33.00 H), 7.91-7.80 (m, 116.00 H), 7.43-7.41 (m, 30.00 H) 7.08-6.65 (m, 440.00 H), 2.16-1.89 (m, 87.00 H).

O3-0.85: ^{1}H NMR (500 MHz, DMSO-d6) δ 9.34-9.14 (m, 28.00 H), 7.92-7.82 (m, 149.60 H), 7.43-7.42 (m, 18.05 H) 7.30-6.62 (m, 533.20 H), 2.16-1.88 (m, 66.00 H).

O7-0.85: ^{1}H NMR (500 MHz, DMSO-d6) δ 9.34-9.14 (m, 28.00 H), 7.92-7.82 (m, 299.20 H), 7.43-7.42 (m, 18.00 H) 7.30-6.62 (m, 994.00 H), 2.16-1.88 (m, 66.00 H), 1.65-1.59 (m, 336.60 H).

O19-0.85: ^{1}H NMR (500 MHz, DMSO-d6) δ 9.34-9.14 (m, 28.00 H), 7.92-7.82 (m, 761.73 H), 7.43-7.42 (m, 19.05 H) 7.30-4.66 (m, 2368.67 H), 2.16-1.88 (m, 66.18 H), 1.65-1.58 (m, 1029.85 H).

3.2.3. Silane functionalization of phenolic end groups of HBPAES

To impart the self-crosslinking ability and for the incorporation of inorganic groups into HBPAES backbone, phenolic terminal groups of HBPAES polymers were reacted with IPTES at 80 °C in DMAc under N_2 atmosphere. The solid content of the synthesis was adjusted to 20% (w/w) and the reaction between the phenolic OH functional group and NCO bearing silane alkoxy group was followed by monitoring the isocyanate (NCO) stretching peak at 2268 cm^{-1} via FT-IR spectrometer. After the disappearance of the NCO peak on the spectrum, the silane-functional polymer solution was directly utilized in the production blend films and UF membranes without any purification.

3.2.4. Synthesis of sulfonated HBPAESs (SHBPAES)

SHBPAESs were synthesized via the same procedure used for the synthesis of HBPAESs as shown in Figure 28. SDCDPS or sulfonated A_2 oligomers were used to impart hydrophilicity to the main structure rather in place of DCDPS. The reaction temperature was kept at 170 °C. At the end of the reaction, the mixture was filtered to remove KCl salt and excess K_2CO_3. The reaction mixture was concentrated in the rotary evaporator and then the polymer was precipitated in isopropyl alcohol (IPA) and washed extensively with IPA. The branched polymer was then dialyzed by SnakeSkin® 3.5K MWCO in deionized water. The polymer solution was evaporated to remove the deionized water via the rotary evaporator and

dissolved in DMSO and precipitated again in IPA and washed with IPA. The final product was obtained by drying at 120 °C for 48 h at 1 mbar.
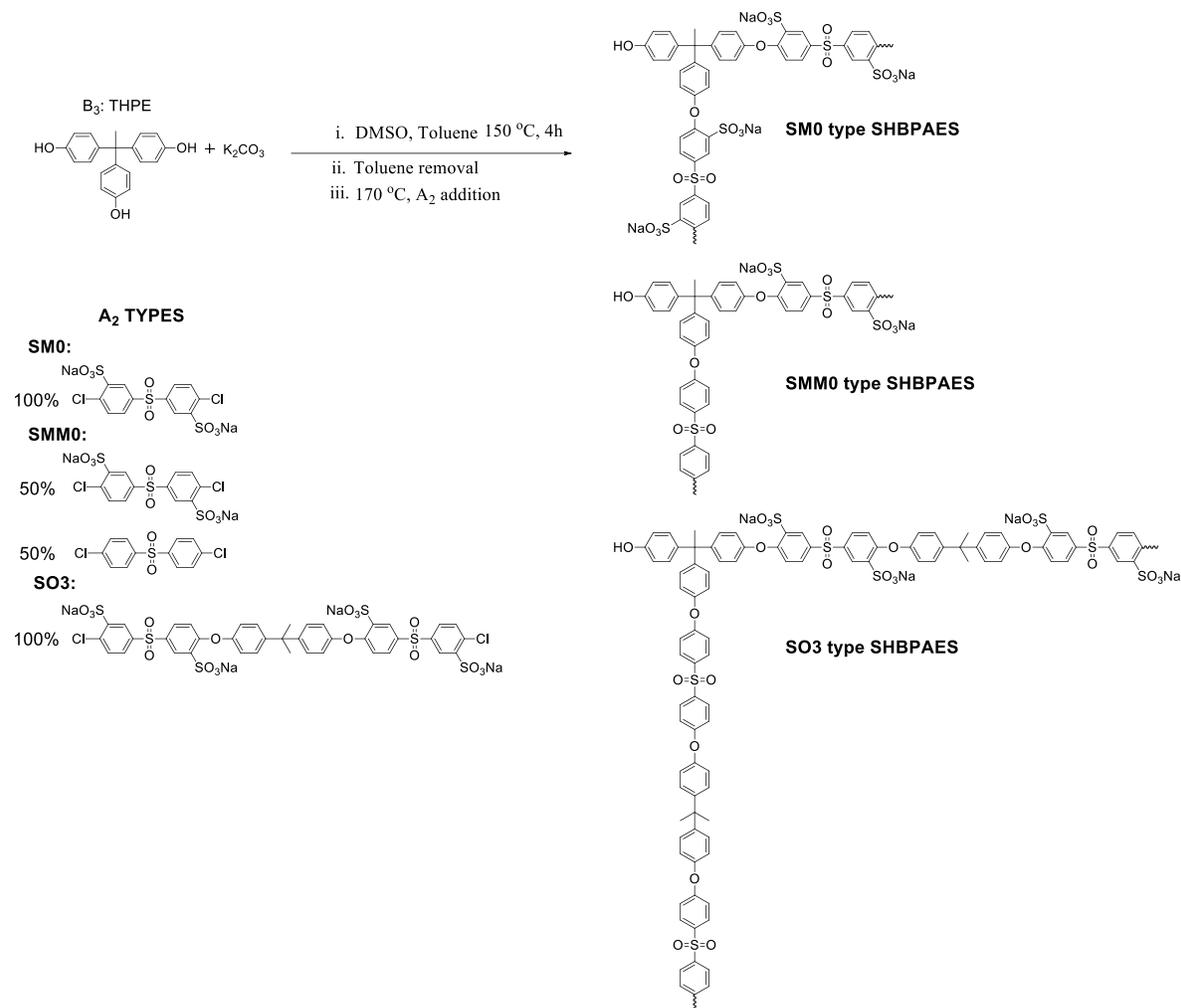
Figure 28 Schematic representation of SHBPAES synthesis with SM0, SMM0 and SO3 type A_2 species via A_2+B_3 copolymerization

SM0-0.55: ^{1}H NMR (500 MHz, DMSO-d6) δ 8.55-8.50 (m, 1.34 H), 8.25-8.16 (m, 10.75 H),7.95-7.74 (m, 10.78 H), 7.46-7.44 (m, 8.43 H) 7.03-6.60 (m, 42.90 H), 2.41 (s, 19.27 H), 2.17-1.90 (m, 21.00 H).

SM0-0.75: ^{1}H NMR (500 MHz, DMSO-d6) δ 9.27 (bs, 9.00 H), 8.54-8.52 (m, 1.15 H), 8.26-8.16 (m, 12.53 H), 7.93-7.74 (m, 12.53 H), 7.42-7.40 (m, 10.33 H), 7.10-6.66 (m, 82.12 H), 2.41 (s, 9.00 H), 2.17-1.90 (m, 27.00 H).

<u>SM0-0.85</u>: ^{1}H NMR (500 MHz, DMSO-d6) δ 8.54-8.52 (m, 6.03 H), 8.26-8.17 (m, 33.26 H), 7.84-7.74 (m, 32.75 H), 7.42-7.41 (m, 18.14 H), 7.05-6.59 (m, 169.05 H), 2.41 (s, 23.06 H), 2.17-1.89 (m, 66.00 H).

<u>SM0-1.00</u>: ^{1}H NMR (500 MHz, DMSO-d6) δ 9.98 (bs, 6.40 H), 8.54-8.50 (m, 1.38 H), 8.26-8.18 (m, 29.06 H), 7.82-7.74 (m, 28.95 H), 7.42-7.40 (m, 18.18 H) 7.04-6.41 (m, 174.00 H), 2.41 (s, 43.64 H), 2.21-1.88 (m, 87.00 H).

<u>SMM0-0.55</u>: ^{1}H NMR (500 MHz, DMSO-d6) δ 8.55-8.50 (m, 1.87 H), 8.26-8.15 (m, 8.42 H),7.95-7.73 (m, 8.47 H), 7.46-7.44 (m, 7.00 H) 6.91-6.40 (m, 61.87 H), 2.41 (s, 7.71 H), 2.17-1.96 (m, 21.00 H).

<u>SMM0-0.75</u>: ^{1}H NMR (500 MHz, DMSO-d6) δ 8.54-8.52 (m, 0.83 H), 8.27-8.16 (m, 8.94 H), 7.93-7.75 (m, 16.79 H), 7.44-7.40 (m, 6.18 H), 7.10-6.44 (m, 89.44 H), 2.41 (s, 4.62 H), 2.17-1.90 (m, 27.00 H).

<u>SMM0-0.85</u>: ^{1}H NMR (500 MHz, DMSO-d6) δ 8.55-8.52 (m, 2.61 H), 8.27-8.18 (m, 20.21 H), 7.93-7.75 (m, 40.66 H), 7.44-7.42 (m, 20.50 H), 7.03-6.46 (m, 174.19 H), 2.41 (s, 12.11 H), 2.17-1.89 (m, 66.00 H).

<u>SMM0-1.00</u>: ^{1}H NMR (500 MHz, DMSO-d6) δ 10.13 (bs, 7.36 H), 8.56-8.54 (m, 3.75 H), 8.27-8.17 (m, 38.68 H), 7.91-7.74 (m, 62.12 H), 7.44-7.41 (m, 31.80 H) 7.09-6.44 (m, 220.31 H), 2.41 (s, 28.13 H), 2.18-1.88 (m, 87.00 H).

<u>SO3-0.75</u>: ^{1}H NMR (500 MHz, DMSO-d6) δ 9.32-9.09 (m, 17.35 H), 8.54-8.52 (m, 0.77 H), 8.26-8.16 (m, 20.22 H), 7.95-7.73 (m, 22.21 H), 7.42-7.40 (m, 8.07 H), 7.26-7.20 (m, 8.07 H), 7.10-6.66 (m, 104.75 H), 2.41 (s, 16.09 H), 2.17-1.91 (m, 27.00 H), 1.64-1.42 (m, 29.01 H).

3. 3.   LPAES/HBPAES blend film preparation

Films of LPAES and HBPAES blends were fabricated from DMAc solutions in order to analyze their mechanical and thermomechanical properties (Section 4.1.4.). The ratio of HBPAES to LPAES were 10% (w/w) and the total polymer content in DMAc was 25% (w/w), which allowed the preparation of blend polymer solutions with viscosities in a range of 1400-1800 cP (25 °C) at 25 rpm. Each polymer solution was allowed to stir at 50 °C for

24h and mixed via planetary mixer prior to casting on a steel substrate using Doctor Blade with 25-mil thickness. The blend films were first dried in an oven at 60 °C for 24 h, and then further dried under vacuum at 60 °C for 24 h. Afterward, dry polymer films were kept in a water bath for 24 hours to extract any residual solvent, and then they were dried under vacuum at 120 °C for 24 h. The steps of blend film preparation are depicted in Figure 29.
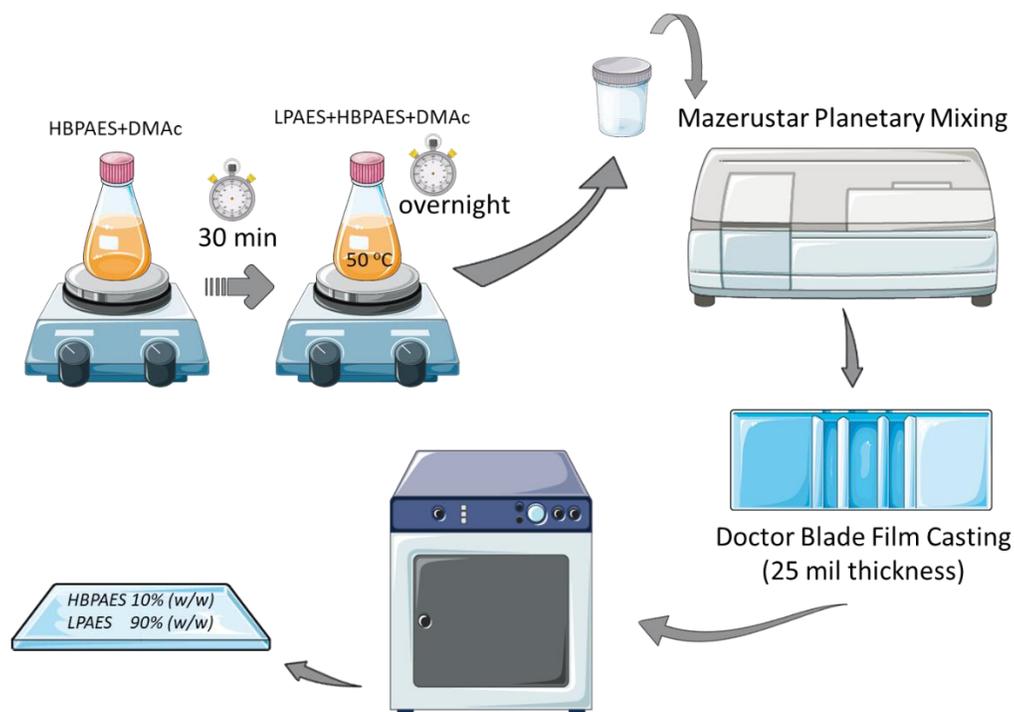
Figure 29 Schematic representation of the steps of blend film preparation

Furthermore, films of LPAES and HBPAES-Si blends were prepared to investigate their mechanical and thermo-mechanical characteristics (Section 4.1.5.), and the ratio of HBPAES-Si to LPAES was again 10% (w/w) to compare with HBPAES-BF. LPAES in DMAc was stirred at 50 °C for 24h, and then 20 wt.% HBPAES-Si solution in DMAc was added into LPAES solution and mixed via planetary mixer before casting on a steel substrate using Doctor Blade with 25-mil thickness. The total polymer content in DMAc was 25% (w/w). After drying the blend films as described earlier, they were annealed at 195 °C under 2.5 tons for two hours to form Si-O-Si bonds.

3. 4. Preparation of ultrafiltration membranes via phase inversion technique

UF membranes were prepared from LPAES and LPAES/HBPAES solution blends by using the nonsolvent induced phase separation technique (phase-immersion method) [79] applied on a nonwoven fabric. This UF membrane production technique is schematically represented in Figure 30. Ingredients of the UF membrane production and their percentage by weight were given in Table 11. HBPAES and LPAES were dried under vacuum at 120 °C for 72 h, whereas PVP10 and PVP40 were dried at 110 °C for 5 min before use. The viscosity of all-polymer mixtures was kept at 1650 cPs ± 9%.

Table 11 Ingredients of functional UF membrane preparation

Ingredients	Percentage by weight (%)	Mass (g)
DMAc	74.0 ± 1.0	18.500 ± 0.150
PVP10	4.5	1.125
PVP40	1.5	0.375
LPAES	18.0	4.500
HBPAES/-Si	2.0	0.500

At first, PVP10 and PVP40 were dissolved in DMAc at 4.5% and 1.5% by mass, respectively. After 30 min, 2% (w/w) HBPAES was added into the solution stirred at 50 °C for one hour. After obtaining a clear polymer solution, LPAES was weighed into the mixture which leads to a final concentration of 18% (w/w) LPAES and stirred again at 50 °C for 24 h. Before casting the polymer with a speed of 80 mm/s on a nonwoven surface at RT using Doctor Blade with 5-mil wet thickness, it was homogenized via Mazerustar Revolutionary Planetary Mixer. The polymer films were immediately immersed in a 17 °C coagulation bath and waited for one minute. Then, UF membranes were stored in a pure water bath at 4 °C for a week before performing any analysis.
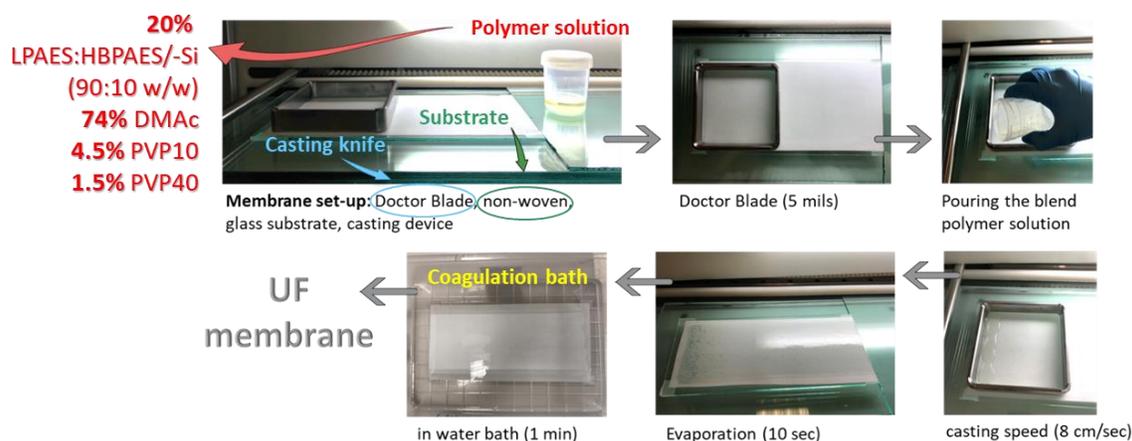
Figure 30 The phase inversion technique of blend polymer solution on a non-woven fabric

3. 5.   Thin film composite membrane preparation via interfacial polymerization

Phenolic end groups of HBPAESs were converted to sodium phenolate terminal groups in order to increase their nucleophilicity to react with TMC [209]. An aqueous solution was prepared to contain 2% HBPAES (w/w) and pH was adjusted to 13 using NaOH pellets. TMC solution was prepared as 0.1% (w/w) in the organic phase, hexane. Prior to the interfacial polymerization reaction, an LPAES-based UF membrane support layer was placed and sealed between three-piece auxiliary frames (25x25 cm x cm). The basic aqueous solution of HBPAES was poured onto the support layer surface to adsorb this aqueous phase and left for 5 min. Then, the excess polymer solution was poured out and removed from the UF membrane surface via a silicone roller. After this step, the TMC/hexane solution was poured onto the support layer to react with the phenolate ion of HBPAES. This interfacial polymerization reaction was allowed for 4 min at ambient temperature. The active layer, which is also termed as TFC, was then cured in an oven at 80°C for 10 min. At the end of this process, the final TFC NF membrane was stored in the distilled water bath at 4°C. The scheme of the reaction and TFC production steps were given below in Figure 31 and Figure 32, respectively.
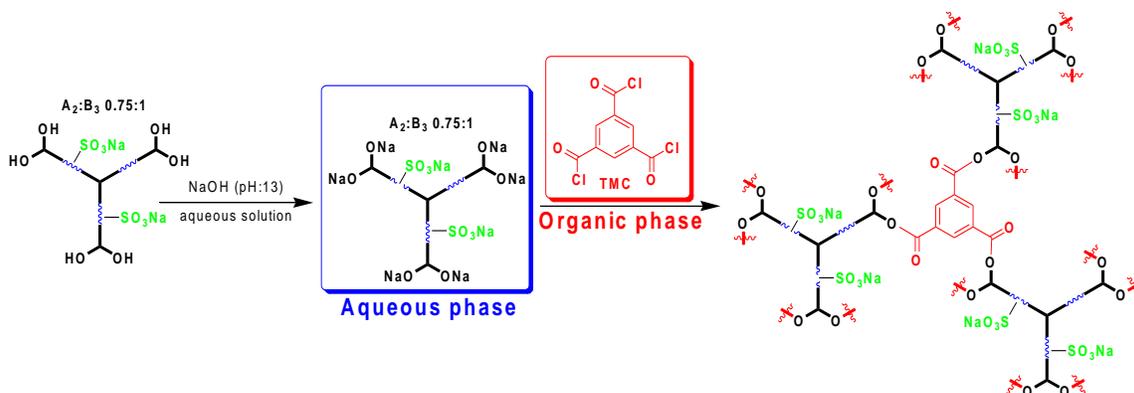
Figure 31 Schematic representative of active layer formation between HBPAES and TMC
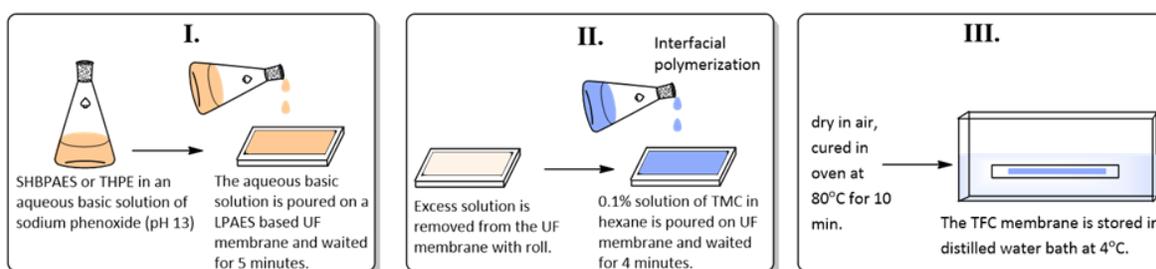
Figure 32 Steps of manufacturing TFC membrane

3. 6.   Characterization

3.6.1. Nuclear Magnetic Resonance (NMR)

The chemical structure of monomers, telechelic oligomers, polymers were identified via Proton (^{1}H) and Silicon (^{29}Si) Nuclear Magnetic Resonance (NMR). NMR specimens were prepared as 5% (w/v) 600 µL solution in DMSO-d_6 or CDCl$_3$ and the structural analyses were performed on Varian Inova NMR spectrometry operating at 500 MHz for ^{1}H NMR and 99 MHz for 29Si NMR. The chemical shifts of ^{1}H spectra were adjusted according to tetramethylsilane (TMS) at 0 ppm. ^{1}H-NMR spectra were used to calculate molecular weights of oligomers, OH equivalent weight and the degree of branching of HBPAES samples.

3.6.2. Fourier Transform Infrared (FT-IR) Spectroscopy

Monitoring functionalization reactions, as well as, functional group characterizations were performed by using Bruker Equinox 55IR Fourier Transform-Infrared Spectrophotometer equipped with diamond Smart ATR Attenuated Total Reflectance sampling accessory. The measurement range limits were 4000 to 550 cm^{-1} with a resolution of 0.5 cm^{-1}.

3.6.3. Size Exclusion Chromatography (SEC)

For the molecular weight determination, triple detection Viscotek GPCmax VE-2001 was used as SEC which was conducted in HPLC grade DMF at 55 °C, and the eluent flow rate was set to 1 mL/min. Mixed-D column system (D5000-D3000-D1000-DGuard or D5000-D3000-DGuard) was utilized with refractive index (RI), multiple angle laser light scattering (MALLS) and viscometer detectors. The molecular weights of polymers were calculated using the MALLS detector input, whereas, molecular weights of Cl-terminated oligomers were calculated from a conventional calibration made with 12 narrow PMMA standards in the range of 0.6 to 300 kDa. Intrinsic viscosities ([η]) of HBPAES samples were determined via the viscometer detector, which provided information on the relative size of polymer molecules in solution.

3.6.4. Gas Pycnometer

Specific densities of HBPAESs and their blend films were determined under helium atmosphere using Micromeritics AccuPyc II 1340 Gas Pycnometer.

3.6.5. Thermo-Gravimetric Analysis (TGA)

Thermal properties of polymer samples were investigated by Mettler Toledo STAR^e Thermo-Gravimetric Analyzer (TGA) with a heating rate of 10 °C/min between 30 °C and 1000 °C under nitrogen gas.

3.6.6. Differential Scanning Calorimetry (DSC)

The T_g of the polymer samples was determined using Mettler Toledo STAR^e Flash Differential Scanning Calorimetry (DSC) (Heating rate 10 °C/min between 50 °C and 300 °C, under N$_2$, 2nd cycles).

3.6.7. Dynamic Mechanical Analysis (DMA)

For the thermo-mechanical analysis of blend films of HBPAESs, tensile test measurements were performed using Mettler Toledo Dynamic Mechanical Analysis (DMA). The blend film specimens were prepared according to ASTM E 1640-13 at 1 Hz frequency; 5 μm amplitude, and at a temperature rate of 3 °C/min in a temperature range from 30 °C to 225 °C.

3.6.8. Stress-strain test

Mechanical tests specimens of blend films were prepared according to ASTM D 1708, and they were performed using INSTRON® 5982 Universal Testing Machine with 5 kN load cell. Young modulus, stress at break and strain at break were calculated as described in ASTM D 1708.

3.6.9. Scanning Electron Microscopy (SEM)

The morphologies of the fracture surfaces coated Au-Pd of films were examined with scanning electron microscope (SEM) Zeiss LEO Supra 35VP employing secondary electron detector at 5 kV.

3.6.10. Dynamic Light Scattering (DLS)

Particle size and distribution of SHBPAESs dispersions were performed using ZetaSizer, Malvern Instruments provided with laser diffraction and polarized light of three wavelengths detectors. Approximately 100 μL of SHBPAES dispersion was diluted with distilled water to an adequate concentration in the cell and measured at room temperature.

3.6.11. Contact Angle

Static contact angle measurements of a water droplet on membrane specimens in the air were performed with the sessile-drop method utilizing an optical tensiometer via Theta Lite Contact Angle Measurement System. The optical tensiometer records water drop images and automatically analyzes the drop shape from a high-quality image, which is guaranteed by a high-resolution digital camera, quality optics, and the accuracy of the drop fitting method. The measurements were taken from five different areas of each specimen, and then contact angles were determined from the average values.

3.6.12. Gel Content

The degree of crosslinking of alkoxysilane functional HBPAES (HBPAES-Si) was determined by measuring the gel content of crosslinked HBPAESs. This measurement was performed via Soxhlet extraction in DCM for 24 h and the residue was dried in vacuum oven at 120 °C for 24 h. The cured HBPAES were weighted before and after extraction. Then, the percentage of gel content was calculated with Equation 6.

$$\% \ gel \ content = \frac{w_e}{w_i} \times 100 \qquad \qquad \textbf{Equation 6}$$

where w_i is the initial weight of the polymer, and w_e is the weight of polymer after extraction process.

3.6.13. Zeta Potential measurements

Zeta Potential, also known as electrokinetic potential, measurements have been performed using Electrokinetic Analyzer for Solid Surface Analysis: SurPASS-Anton Paar equipped with an "Adjustable Gap Cell" (Figure 33). The zeta potential values of membrane surfaces have been measured in the function of pH in 1.0 mM KCl electrolyte solution and by varying the pH of electrolyte from 4 to 11 by the addition of 0.05 M HCl or NaOH via the automatic titration. The method applied in the experiments is the potential difference method of tangential fluid flows.

SurPASS detects the streaming potential and streaming current caused by the pressure-driven flow of an electrolyte solution, which passes through a thin slit channel arisen by two identical sample surfaces [210].
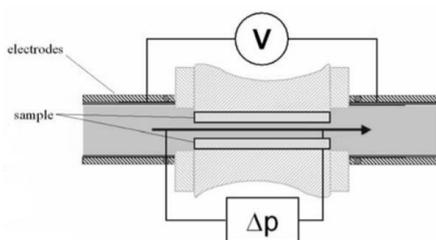
Figure 33 Representative schematic of tangential measuring technique in the "Adjustable Gap Cell" of SurPASS [210]

3.6.14. Ultrafiltration membrane performance

UF membranes fabricated from LPAES only, HBPAES/LPAES, or HBPAES-Si/LPAES (10/90 w/w) blends were investigated in terms of water flux and morphology. Permeation tests were performed via a dead-end stirred cell pressurized by nitrogen gas at room temperature, whose active area was 14.6 cm^2 (Sterlitech, HP4750). Before performance tests, all UF membranes were compressed under 5 bar for one hour. The performance tests of membranes were monitored gravimetrically at 1.0, 1.5, and 2.0 bar, each transmembrane pressure was applied for one hour. Water flux (J_w, L/(m^{2}h)) of the blend UF membranes was calculated using Equation 7.

$$J_w = \frac{Q_w}{A_m} = \frac{V_w}{A_m \times t}$$

Equation 7

where Q_w, V_w, A_m and t are flow rate of water, volume (L) of permeated deionized water, effective area (m^2) of UF membrane setup and time (h), respectively.

UF membranes were analyzed to determine specific permeate flux (J_{sp}, L/(m^{2}hbar)) of deionized water and J_{sp} is calculated by Equation 8.

$$J_{sp} = \frac{Q_w}{A_m \times P}$$

Equation 8

where P (bar) is the applied pressure.

Moreover, 100 ppm solution of Reactive Orange 16 and Reactive Red 120 were utilized as the feed for the analysis of the rejection (R, %) of dissolved macromolecules (Equation 9). The filtration performance of UF membranes at 25 °C and 40 °C was analyzed with model dye solutions with regards to permeation and rejection.

$$R(\%) = \frac{C_f - C_p}{C_f} \times 100$$

Equation 9

where C_f and C_p were the solution concentration of feed and permeated solution, respectively.

3.6.15. Thin Film Composite membrane performance

TFC membranes formed with SHBPAES and TMC were investigated in the aspect of water flux, the rejection of salt and organic dye, pH, and morphology. Permeation tests were performed via a dead-end stirred cell pressurized by nitrogen gas at room temperature, whose active area was 14.6 cm^2 (Sterlitech, HP4750). Prior to performance tests, all TFC membranes were compressed under 8 bar for one hour. The performance tests of membranes were monitored gravimetrically at 6, 9, 12, and 15 bar, each transmembrane pressure was applied for one hour. Deionized water, 2000 ppm solutions of MgSO$_4$ and NaCl were used as the feed to analyze the permeation of TFC membranes. Moreover, 100 ppm solution of Reactive Orange 16 and Reactive Red 120 (Setazol Red) were utilized as the feed for the analysis of the rejection of dissolved macromolecules.

3.6.16. Multi-criteria decision making by applying TOPSIS methodology for the determination of the best membrane performance

A proper membrane performance depends on the combination of a multitude of membrane features such as permeability, selectivity, flux, thermomechanical properties, thermal stability, chemical stability, fouling resistance, low cost, and easy production [211]. Because of these various features, it is never easy to make a decision on the best membrane. Within this scope, various multi-criteria decision-making methodologies have been developed [212-217], and one of them is a Technique for Order Preference by Similarity to an Ideal Solution (TOPSIS) that was introduced in 1981 by Hwang and Yoon [212]. Using the TOPSIS method, the best alternative can be chosen both by the shortest geometric distance from the positive ideal solution and the longest one from that of the negative.

This method has been applied in various field such as product design [218], quality control [219], manufacturing [220], location analysis [221], transportation [222], human resources [223], water management [224], multi-objective decision making [225], as well as, group decision making [226]. Also, this method has been frequently used to determine the best membrane performance in water purification membrane studies [227-229].

To determine the best membranes, Technique for Order Preference by Similarity to an Ideal Solution (TOPSIS) method was utilized as described in main steps as given below [213, 214, 230, 231].

1. Define the decision matrix and the weight of criteria

$$\text{Decision matrix} \qquad X = (x_{ij}) \qquad\qquad \text{Equation 10}$$

$$\text{Weight vector} \qquad W = [w_1, w_2, \ldots, w_n] \qquad\qquad \text{Equation 11}$$

Criteria of the functions can be positive or negative functions.

2. Calculate the normalized decision matrix

$$\text{The normalized decision matrix} \qquad n_{ij} = \frac{x_{ij}}{\sqrt{\sum_{i=1}^{m} x_{ij}^2}} \qquad\qquad \text{Equation 12}$$

$$n_{ij} = \begin{cases} \dfrac{x_{ij} - \min\limits_{i} x_{ij}}{\max\limits_{i} x_{ij} - \min\limits_{i} x_{ij}} & \text{if } C_i \text{ is a positive ideal solution} \\[2ex] \dfrac{x_{ij} - \min\limits_{i} x_{ij}}{\max\limits_{i} x_{ij} - \min\limits_{i} x_{ij}} & \text{if } C_i \text{ is a negative ideal solution} \end{cases} \qquad \text{Equation 13}$$

for $i = 1, 2, \ldots, m; j = 1, 2, \ldots, n$.

3. Calculate the weighted normalized decision matrix

$$\text{The weighted normalized decision matrix} \qquad v_{ij} = w_j n_{ij} \qquad\qquad \text{Equation 14}$$

for $i = 1, 2, \ldots, m; j = 1, 2, \ldots, n$.

4. Identification of positive and negative ideal solutions

$$\text{Positive ideal solution} \qquad A^+ = (v_1^+, v_2^+, \ldots, v_n^+) = \left(\left(\max_i v_{ij} \,\middle|\, j \in I \right), \left(\min_i v_{ij} \,\middle|\, j \in J \right) \right) \qquad \text{Equation 15}$$

$$\text{Negative ideal solution} \qquad A^- = (v_1^-, v_2^-, \ldots, v_n^-) = \left(\left(\min_i v_{ij} \,\middle|\, j \in I \right), \left(\max_i v_{ij} \,\middle|\, j \in J \right) \right) \qquad \text{Equation 16}$$

where I denotes positive criteria, J negative criteria.

5. Calculate Euclidean distance from positive and negative ideal solutions

$$d_i^+ = \sqrt{\sum_{j=1}^{n}\left(v_{ij} - v_j^+\right)^2} \ , \ i = 1, 2, \dots m \qquad\qquad \text{Equation 17}$$

$$d_i^- = \sqrt{\sum_{j=1}^{n}\left(v_{ij} - v_j^-\right)^2} \ , \ i = 1, 2, \dots m \qquad\qquad \text{Equation 18}$$

6. Calculate the relative closeness to the positive ideal solution

$$R_i = \frac{d_i^-}{d_i^- + d_i^+} \qquad\qquad \text{Equation 19}$$

where $0 \le R_i \le 1, i = 1,2, \dots, m$.

7. Select the best alternative closest to 1.

CHAPTER 4: Highly branched poly(arylene ether sulfone)s and their blends with linear poly(arylene ether sulfone)s

Partially Taken From:

Ozbulut, E. B. S.; Seven, S.; Bilge, K.; Akkas, T.; Tas, C. E.; Yildiz, B.; Atilgan, C., Menceloglu, Y. Z.; Unal, S. "Blends of highly branched and linear poly(arylene ether sulfone)s: Multiscale effect of the degree of branching on the morphology and mechanical properties", Polymer 188 (2020) 122114.

4.1. Introduction

A linear polymer typically offers limited post-functionalization capabilities, and the post-functionalization frequently leads to the deterioration of some of the original mechanical properties. The blending of at least two polymers is a conventional technique applied in the polymer industry to enhance the chemical and physical properties of commercial polymers with low cost and effort under relatively short periods. Particularly, it is an excellent alternative to multi-step, costly chemical synthesis to obtain new and advanced materials. The material properties that can be improved by blending polymers include modulus, toughness, viscoelastic behavior, thermal properties, morphology, and chemical resistance. The miscible physical combination of two or more polymers in amorphous morphology is necessary because the immiscible polymer mixtures have poor physical and mechanical properties due to phase separation. The negative free energy of mixing (ΔG_m) and exothermic heat of mixing ($\Delta H_m < 0$) lead to thermodynamically favorable mixtures. Hydrogen bonds, dipole-dipole, and ionic interactions between energetically-suitable chain segments govern the miscibility in polymer blends [207]. In amorphous thermoplastic polymeric systems, there are limited studies on using hyperbranched polymers as additives by blending with linear analogues to improve final mechanical properties. This study presents the importance of structure-morphology relationships in thermoplastic, functional, and amorphous arylene

ether sulfone-based linear and highly branched polymer blends as pioneering work to reveal their potential applications in the future. For this purpose, a series of HBPAESs with varying distances between branch points were synthesized by the A_2+B_3 copolymerization approach (Section 3.2.2). The synthesized HBPAESs were optionally post-functionalized with IPTES (Section 3.2.3). All samples were characterized via NMR spectroscopy (Section 3.6.1), SEC (Section 3.6.3), DSC (Section 3.6.6), Gas Pycnometer (Section 3.6.4), and FT-IR Spectrometry (Section 3.6.2). Then, blend films of HBPAES and LPAES were prepared in DMAc (Section 3. 3). The effect of the branching density and the content of HB branched polymer on the thermal, mechanical and viscoelastic properties of prepared polymer blends were systematically investigated using DSC, DMA (Section 3.6.7), SEM (Section 3.6.9) and stress-strain tests (Section 3.6.8).

4.2. Results & Discussion

4.2.1. Synthesis and characterization of chlorine terminated A_2 oligomers

A series of chlorine terminated A_2 oligomers with controlled molecular weights were synthesized from BisA and DCDPS via the nucleophilic aromatic substitution copolymerization (Figure 26). The molecular weights of oligomers were adjusted by balancing the stoichiometry between the number of equivalents of phenol and chlorine groups. The stoichiometric ratios and intrinsic properties of synthesized linear oligomers are tabulated in Table 12.

BisA was used as the limiting reagent during the synthesis to endcap oligomers with aromatic halides from DCDPS. The DPs of A_2 oligomers were calculated from the modified Carothers equation for linear polymerizations. If one monomer is present in excess, the DP is calculated according to Equation 20 [232-235], and the repeating unit (n), as well as the average molecular weights of oligomers, can be theoretically determined using Equation 21 and Equation 22, respectively.

$$DP = \frac{1 + \dfrac{n_{DCDPS}}{n_{BisA}}}{1 - \dfrac{n_{DCDPS}}{n_{BisA}}} \qquad \textbf{Equation 20}$$

$$n = \frac{DP - 1}{2} \qquad \textbf{Equation 21}$$

$$Mn\ (theoretical) = n \times 442.53 g/mol + 287.16\ g/mol \qquad \textbf{Equation 22}$$

where DP, n_{DCDPS}, n_{BisA}, n, and Mn represent DP, the number of moles of DCDPS, the number of moles of BisA, repeating unit, and molar mass, respectively. In Equation 22, the average molar mass of each repeating unit is 442.53 g and the molar mass of chlorine end group from excess DCDPS is 287.16 g.

The A_2 oligomers were structurally characterized with ^{1}H-NMR spectroscopy, and their molecular weights were determined from the spectra shown in Figure 34. Oligomers with DPs of 3, 7, and 19, were denoted by O3, O7, and O19, respectively, and M0 denoted DCDPS. After each reaction, specific peaks of DCDPS completely shifted downfield in oligomers. For example, peak-a protons moved from 7.74-7.72 ppm to 7.50-7.46 ppm (peak-c) and 7.03-7.01 ppm (peak-h). When DCDPS was used in excess, all oligomer chains naturally bore two chlorine end groups, and there existed four protons at the ortho position of chlorine through the oligomer chain. These protons were monitored between 7.50-7.46 ppm (peak-c) and used as an identifier to calculate the molecular weight of each oligomer sample. As DPs of oligomers increased, their molecular weights increased, and hence, the values of T_g, hydrodynamic radius (R_h), and intrinsic viscosity ($[\eta]$) gradually increased as expected [236, 237]. Furthermore, the increases in the molecular weights of oligomers were also confirmed by SEC analysis given in Table 12. Approximate extended lengths of A_2 oligomers (Figure 35) were calculated using specific bond angles and distances of the repeating unit of PAES, using the calculations of Bersted [238].
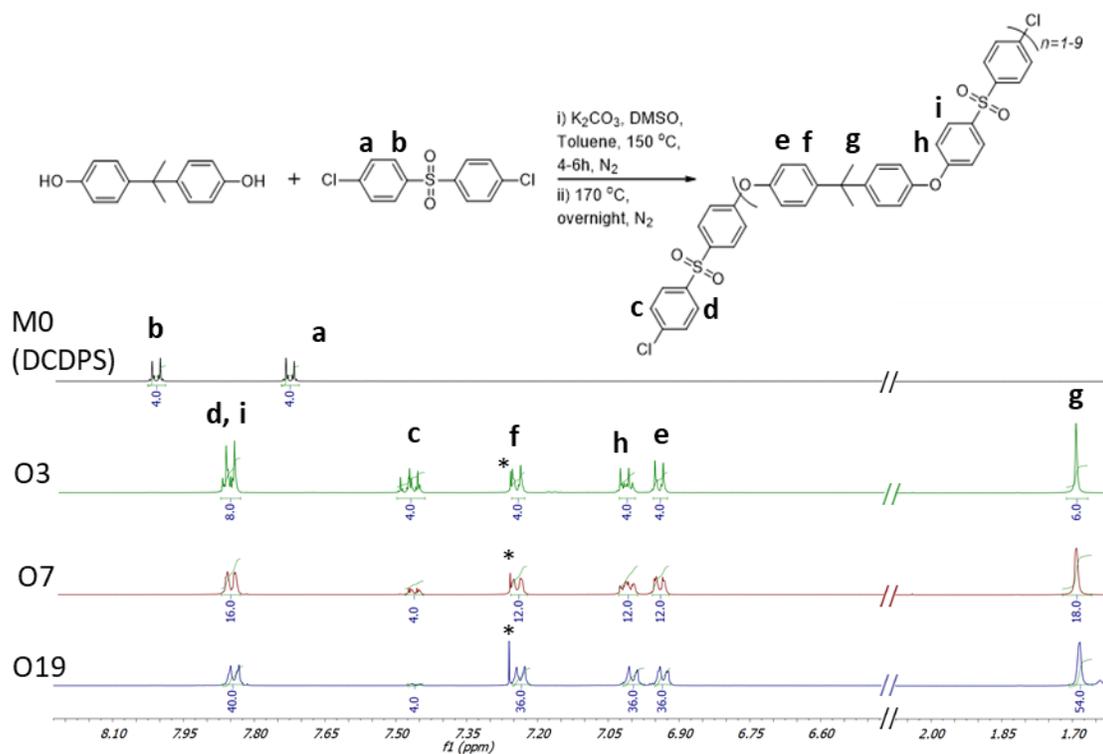
Figure 34 Synthesis scheme of chlorine-terminated linear oligomers and ^{1}H-NMR spectra of Cl-terminated A_2 reactants. *CDCl$_3$ [180]

Table 12 Characterization of chlorine terminated A_2 monomer and oligomers [180]

	M0 (DCDPS)	**O3**	**O7**	**O19**
n_{BisA}/n_{DCDPS}	-	1.00/2.00	1.00/1.33	1.00/1.11
n [a]	-	1.00	3.00	9.18
T_g (°C) [b]	-	71.99	104.23	159.49
M_n (theo.) (kDa)	0.29	0.73	1.61	4.27
M_n (^{1}H NMR) (kDa) [a]	0.29	0.74	1.63	4.27
M_n (SEC) (kDa) [c]	-	1.81	3.78	8.41
PDI	-	1.06	1.08	1.77
R_h (nm)	-	1.04	1.94	2.70
[η] (dL/g)	-	0.04	0.09	0.12
App. extended length (Å)	7.54	28.01	64.20	172.70

[a] Calculated from ^{1}H NMR spectra;
[b] Determined from DSC 2nd cycle analysis;
[c] Calculated from SEC analysis
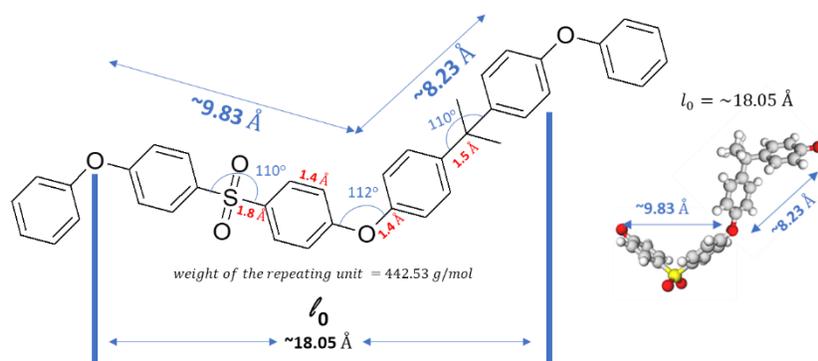
Figure 35 Specific bond angles and bond distances of the repeating unit of PAES [180]

4.2.2. Synthesis and characterization of HBPAES

HBPAESs with designed architectures were synthesized utilizing the A_2+B_3 strategy, which involved a step-growth polymerization between difunctional DCDPS monomer or chlorine terminated oligomers as A_2 species and trifunctional THPE monomer as B_3 species. B_3 monomer was activated with K_2CO_3 at 150 °C for four hours before the addition of A_2 species into B_3 solution. A_2 is slowly added into the B_3 solution 48 hours after the completion of the addition, the color of reaction mixture turned bright dark green with a significant increase in the solution viscosity, which typically indicated the completion of the reaction. The terminal, linear and dendritic units of HB polymer are shown in Figure 27.

As previously reported in the literature, A_2+B_3 polymerization reactions pose a high risk of gelation because of the possible crosslinking reactions which may occur depending on the A_2:B_3 molar ratio and the conversion of functional groups [151, 237]. To synthesize gel-free HB polymers, the determination of the critical conversion at the gel point is essential, which is dependent on the branching coefficient (α) and the critical branching coefficient ($α_c$) as defined in Equation 23 and Equation 24, respectively [149, 151, 237].

$$\alpha = r \times p_A^2 = p_B^2/r \qquad\qquad \text{Equation 23}$$

where r denotes the ratio of A type to B type functional groups, and p_A and p_B are the fractions of A type to B type functional groups that have reacted.

$$\alpha_c = \frac{1}{f - 1}$$
<div align="right">Equation 24</div>

where f is the average functionality of multifunctional monomers in the system (f=3 for A_2+B_3 copolymerization).

When α is smaller than α_c, soluble, branched polymers can be obtained, and gelation is expected to occur when α is equal to or greater than α_c. Therefore, the critical conversion values of monomers, which can be determined when α is equal to α_c, are important to know for the specific $A_2:B_3$ ratio used during the synthesis. For instance, in systems where $A_2:B_3$ ratio is equal to one, critical conversion values are ~87% for A species and ~58% for B species [149, 151, 237]. Apart from the partial conversion of functional groups [181, 193], the slow addition of one species to another species [154] or dilute reaction conditions that promote cyclization reactions [193] are the two other approaches that can be followed to prevent gelation in the A_2+B_3 methodology. According to Flory's description, A_2+B_3 reaction occurs with constant reactivity of functional end-groups during the polymerization [169, 237], and cyclization reactions are omitted; however, the reactivity of functional end-groups is significantly reduced due to created steric hindrance in proceeding polymer chains at adjacencies of functional groups [155, 239, 240]. In our study, HBPAESs were synthesized in 8 wt% solutions using an $A_2:B_3$ ratio of 0.85, at which the critical conversion values were calculated as ~94% for A species and ~53% for B species. In addition, A_2 species were slowly added into B_3 solution to further avoid gelation. During the slow addition of A_2 into B_3, B_2AB_2 type intermediate oligomers are expected to form initially, which then generate short linear polymer chains and transform into highly branched polymer chains through the formation of dendritic units as the A_2 addition proceeds [158]. The synthetic scheme for the HBPAESs by the reaction of THPE and DCDPS and the final structure of the HB polymer with terminal, linear, and dendritic units are shown in detail in Figure 27. In addition to the reaction with DCDPS as the A_2 monomer, THPE was reacted with chlorine-terminated A_2 oligomers with varying DPs to control the distance between branch points as structurally demonstrated in Figure 38. The completion of the reactions was verified by both the color change of the reaction mixture to bright dark green with a significant increase in the viscosity

within 48 h after the A_2 addition into B_3, and ^{1}H-NMR spectroscopy through the complete shifting of protons adjacent to the chlorine end-groups of DCDPS or A_2 oligomers. It should be noted that although the critical conversion values were ~94% for A species and ~53% for B species for the A_2:B_3 ratio of 0.85, no gelation was observed upon 100% conversion of A species during the syntheses of HBPAESs, which was presumed to be due to dilute solution polymerization conditions and the slow addition of A_2 into B_3.

In this study, two approaches have been utilized to synthesize HBPAESs: (i) changing degree of branching by gradually adjusting A_2:B_3 ratio from 0.55 to 1.00; (ii) tuning the distance between branch points by modifying the DP of A_2 oligomers. Figure 36.a-d schematically illustrates how the topology of these HB polymers changes with A_2:B_3 ratio. When the A_2:B_3 ratio is 0.85, the final topology of the HB polymer has a moderately branched structure, and the possibility of gelation is much less than the HB polymer with the ratio 1:1 of A_2:B_3. For the second strategy mentioned above, the linear A_2 oligomers with the controlled DP have been utilized to tune the distance between branch points of HB polymers. In this case, the ratio of A_2:B_3 was taken as 0.85 as a safe region without premature crosslinking, as the oligomers could significantly increase the solution viscosity of the A_2+B_3 reaction mixture and lead to gelation at higher ratios.
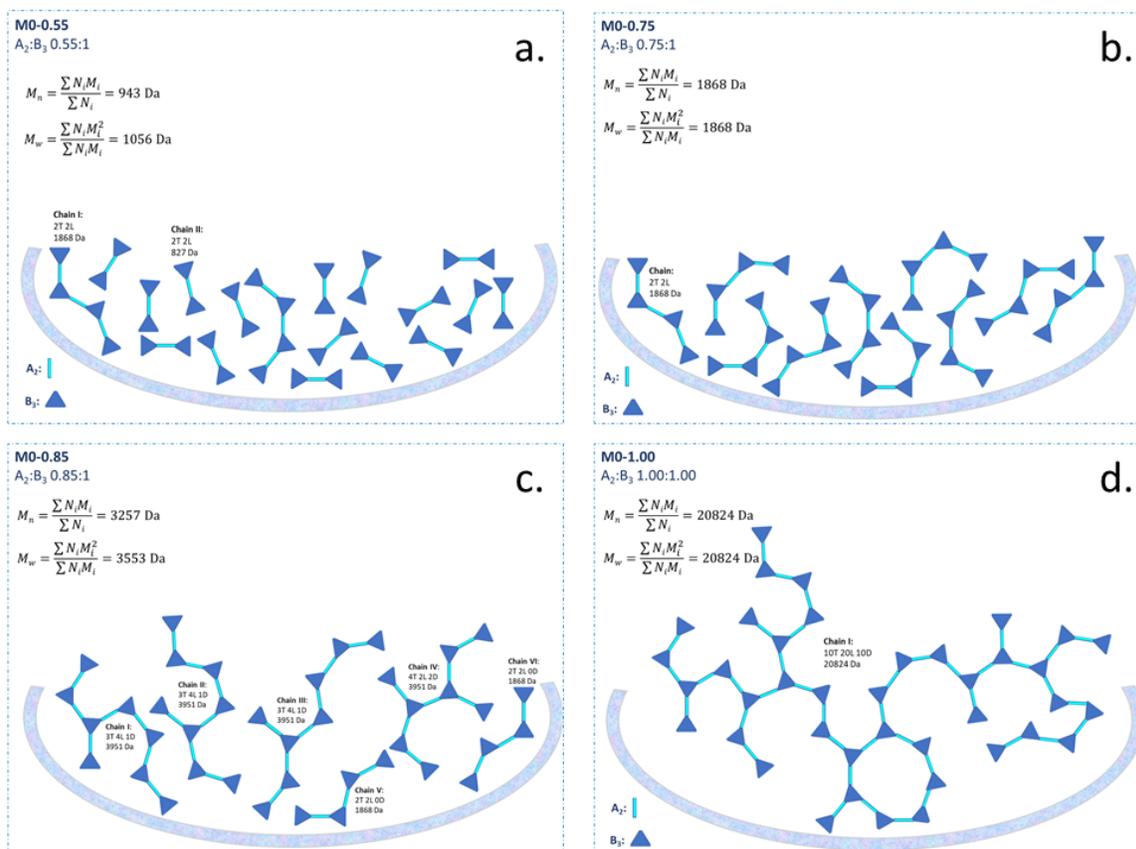
Figure 36 Effect of A_2:B_3 ratio on the final structure of highly branched polymers. **a**. A_2:B_3 ratio: 0.55; **b.** A_2:B_3 ratio: 0.75; **c.** A_2:B_3 ratio: 0.85; **d.** A_2:B_3 ratio: 1.00.

The ratio of the HB polymer's R_h to the R_h of its linear analogue gives critical information on the branching topology, which is referred to as branching structure indicator (g_h) (Equation 25) [241]. As the g_h value approaches one, it indicates a linear structure, whereas degree of branching increases with decreasing g_h value.

The determined R_h values of M0-0.55,-0.75, -0.85, and -1.00 from the SEC analyses (Figure 37.a) and the results of g_h calculations for HBPAESs are given in Table 14. As the mole content of A_2 species increases (as A_2:B_3 increases), their M_w values increase, thus, their R_h and g_h values tend to increase. From the analogy of degree of branching with various methodologies in Figure 37.b, the results are at the same trend with the functionality of the polymers calculated from Equation 29, which helps to determine the average number of

unreacted phenol end groups (f_{final}) on HB polymer backbone, in case of the number of moles of B₃ (n_{B_3}) higher than the number of moles of A₂ (n_{A_2}).

Branching structure indicator

$$g_h \cong \frac{R_{hb}}{R_{hl}}$$

Equation 25

where g_h is the branching structure indicator, R_{hb} and R_{hl} are the hydrodynamic radius of branched and linear polymers, respectively.
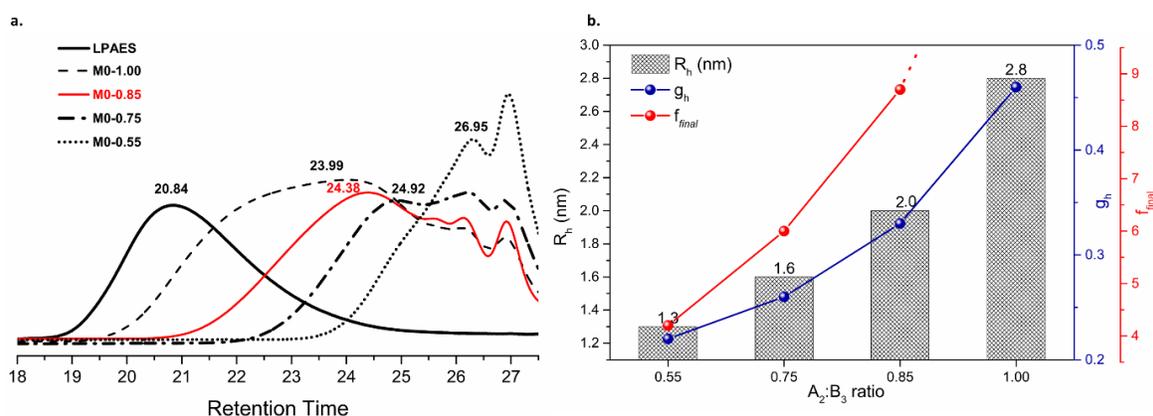
Figure 37 a. SEC chromatogram of HBPAESs with changing A₂:B₃ ratio. b. Comparison of $\boldsymbol{g_h}$ and R_h (obtained from SEC analysis) with f_{final}.
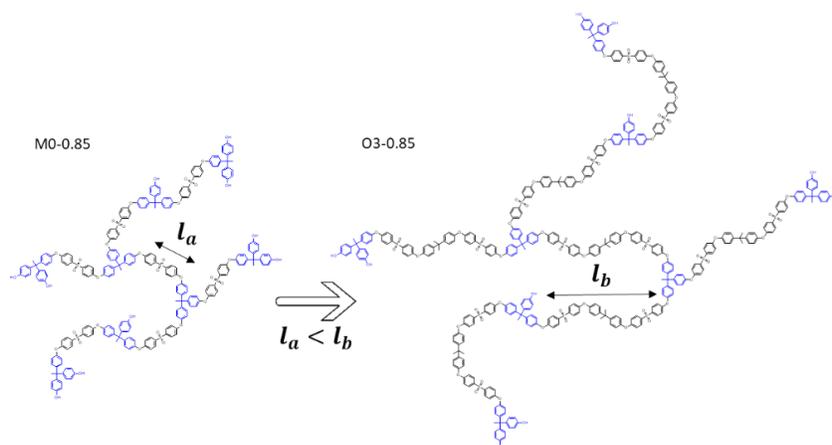
Figure 38. Control of the distance between branch point by changing oligomer length [180]

For all HBPAES samples synthesized, OH-equivalent weights and the degrees of branching were determined from ¹H NMR spectra. Beforehand, the ¹H-NMR spectrum of the commercial monomer THPE (Figure 40) was analyzed in order to ensure that its phenol end

groups in DMSO-d_6 do not participate in any hydrogen bonding, which can change the integrated area under the curve for corresponding peaks [242-245]. The degree of branching of HBPAESs were then calculated from the content of terminal, linear and dendritic units in each HBPAES sample, which were determined from ^{1}H-NMR spectra using Equation 26, Equation 27, and Equation 28. All HBPAESs possess aliphatic C-H peaks from B_3 (THPE) denoted as peak-8 between 2.16-1.88 ppm and for calculations, 66 protons were assigned for the integral of peak-8, which would correspond to the assumption that HB polymers contain 22 THPEs as T, L, D units. The A_2:B_3 ratio of the M0-0.85 sample was then verified by the integral of aromatic C-H protons at meta positions of sulfone group (peak-1&1') between 7.90-7.80 ppm. On the other hand, C-H protons at the ortho positions of quaternary carbon (peak-7') in dendritic units were monitored between 7.43-7.41 ppm and the integral value of peak 7' showed how many dendritic units (D) are present in each HBPAES sample. The protons of phenolic end groups (peak-11&12) were observed in the range of 9.36 and 9.10 ppm, and the integral is equal to the sum of two-terminal units and one linear unit, (2T+L). Thus, the content of terminal, linear, and dendritic units in the M0-0.85 sample (Figure 39.a) can be practically determined. On the other hand, O3-0.85, O7-0.85 and O19-0.85 samples possess BisA groups arising from the linear A_2 oligomer species, in contrary to M0-0.85 (Figure 38), therefore aliphatic C-H as peak-5 was observed between 1.65-1.52 ppm in Figure 39.b. The M_w of used A_2 oligomer can be evaluated by the integral of peak-5, and so the integral of peak-1&1' was used for the verification of the A_2:B_3 ratio.

$$D = \frac{\int Peak7' / 6H}{\int Peak8 / 3H} \qquad \text{Equation 26}$$

$$2T + L = \left(\int Peak11 \right) + \left(\int Peak12 \right) \qquad \text{Equation 27}$$

$$T + L + D = \frac{\int Peak8}{3H} \qquad \text{Equation 28}$$
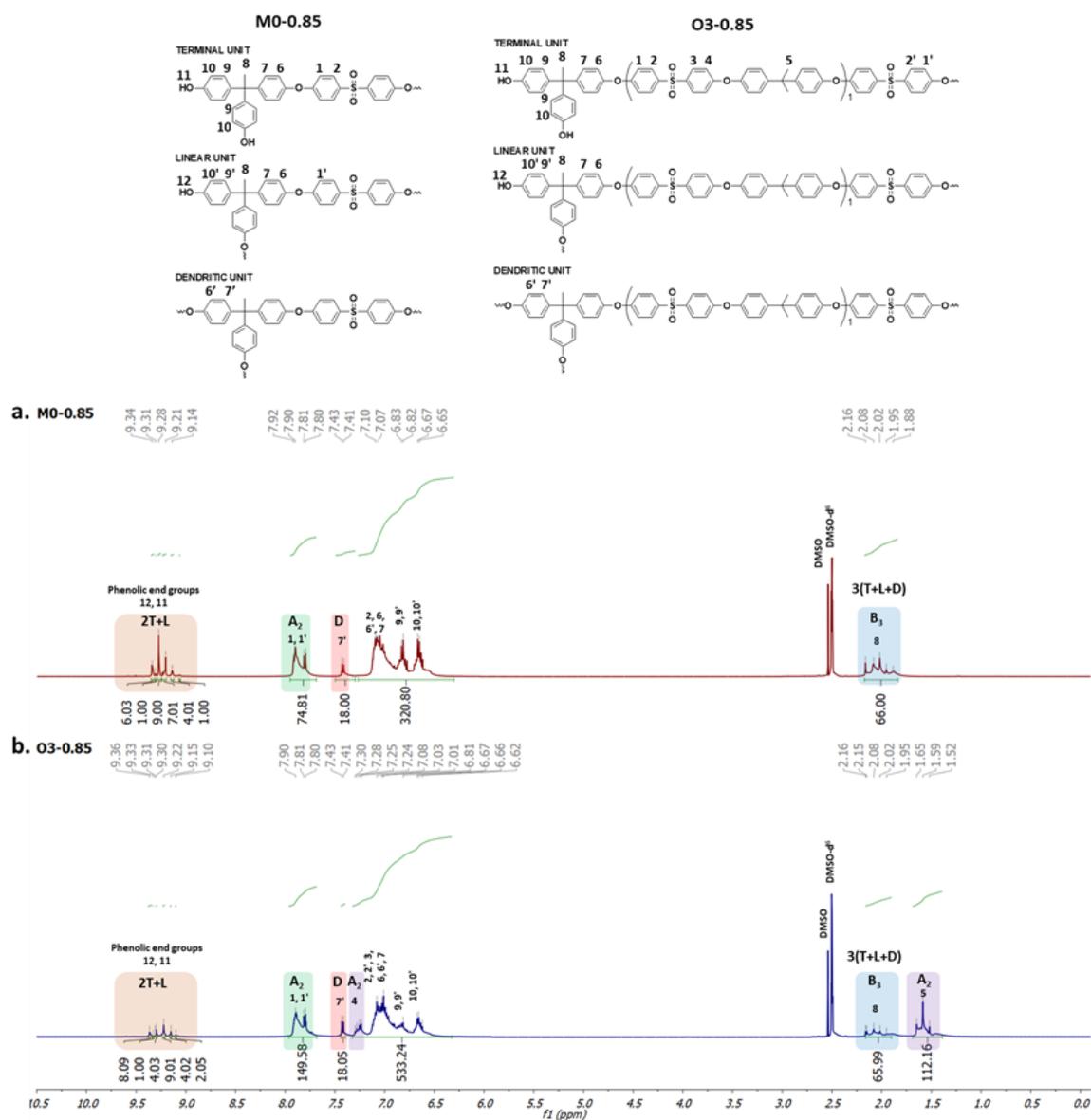
Figure 39. ^{1}H NMR spectra of M0-0.85. and O3-0.85 [180]

For the HBPAES product synthesized using a ratio of A_2:B_3 as 0.85, f_{final} was determined as 8.67 according to Equation 29, and this value is independent from a change in the structures or molecular weights of monomers or final HB polymers. For the rest of HB polymers, the calculated f_{final} values are tabulated in Table 13. The possible formation of HBPAES's chains with A_2:B_3 0.85 are depicted in Figure 36.c. According to this demonstration, M_n's are theoretically calculated as 3.26 kDa, 5.79 kDa, 10.66 kDa, and 25.70 kDa for M0-0.85, O3-0.85, O7-0.85 and O19-0.85, respectively. Hence, the OH-equivalent

weights of HBPAESs were defined by their M_n's divided by f_{final} in Table 14. On the other hand, the experimental OH-equivalent weights were determined from ^{1}H-NMR analysis. The experimental and theoretical OH-equivalent weights of HBPAESs were found to be very close and show a consistent trend as a function of the A_2 length as shown in Figure 41.
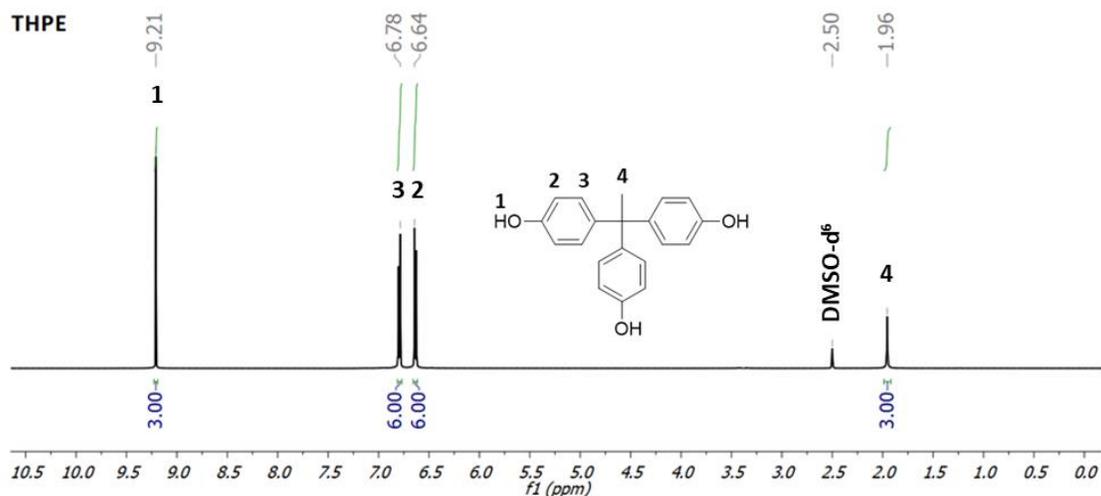
Figure 40 ^{1}H-NMR spectrum of THPE in DMSO-d^6

$$f_{final} = \frac{(N_B)-(N_A)}{(n_{B_3}-n_{A_2})} , \qquad \qquad \textbf{Equation 29}$$

where N_B, N_A, n_{B_3} and n_{A_2} denotes moles of B equivalent, moles of A equivalent, moles of B$_3$ and moles of A$_2$, respectively. n_{B_3} value shall be a higher number than n_{A_2} value.

Table 13 The number of unreacted phenol end groups (final functionalities) of HB polymers with varying A_2:B_3 ratios

HBPAES	A₂:B₃ ratio	f_{final}
M0-0.55	0.55	4.22
M0-0.75	0.75	6.00
M0-0.85	0.85	8.67
M0-1.00	1.00	-
O3-0.85	0.85	8.67
O7-0.85	0.85	8.67
O19-0.85	0.85	8.67
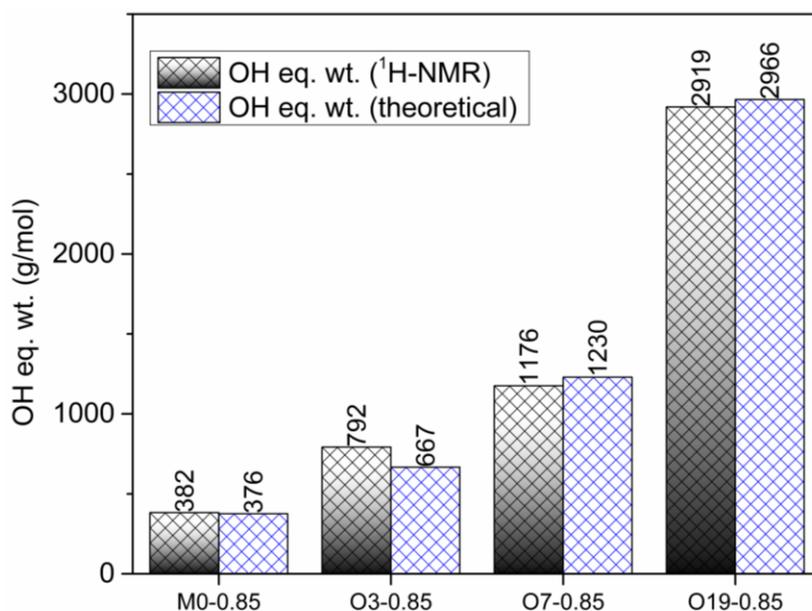
Figure 41 A comparison of theoretical results of OH equivalent weights of HBPAESs with those obtained from ^{1}H-NMR spectra

Upon the determination of terminal, linear, and dendritic unit contents from ^{1}H-NMR spectra, the degree of branching value of each HBPAES could be readily calculated as described in the literature [173, 198]. For example, the calculation of the degree of branching from the Fréchet equation (Equation 30) is simply valid for high molecular weight HB polymers. On the other hand, Long modified the equation for oligomeric species are used in $A_2 + B_3$ polymerizations (Equation 31) because when DP thus the extended length of A_2 oligomers increase, degree of branching of corresponding HB polymers decreases because of the contribution of the linear A_2 segment to the overall linearity of the main chain [198]. The calculated degree of branching values are given in Table 14 for synthesized HBPAES samples. A decreasing trend in the degree of branching of HBPAES calculated from Equation 31 could be noticed, whereas degree of branching values from Equation 30 remained nearly constant. It should be noted linear, terminal, and dendritic units were found to be present in descending order in synthesized HB polymers. Besides, according to the Kuhn-Mark-Houwink-Sakurada (KMHS) equation [147, 246], the KMHS-α exponents of M0-0.85 and O3-0.85 were calculated in between 0.3 and 0.5 for HB polymers, while the values of O7-0.85 and O19-0.85 were in the linear polymer range (0.5< KMHS-α<1.0). As listed in Table

14, g_h values of HBPAESs obtained from the SEC analysis also supported that the overall linearity of the whole polymer backbone increases and the density of branching decreases as the A$_2$ oligomer length is increased.

$$\%DB(Fréchet)\!:DB = \frac{D+T}{D+T+L} \times 100 \qquad \textbf{Equation 30}$$

$$\%DB(Long)\!:DB = \frac{D+T}{D+T+L+n} \times 100 \qquad \textbf{Equation 31}$$

where D, T, and L indicated dendritic, terminal, and linear units in HBPAES, respectively, and n represented the repeating unit of the telechelic poly(arylene ether sulfone) oligomers.

The chain mobility of HB polymers is greatly influenced by the branching density, degree of branching and end group interactions, which may cause a considerable change in T_g [247]. In this dissertation, both synthesized HBPAESs and commercial LPAES were amorphous polymers. Typically, no crystallinity was observed in these polymers due to the tetrahedral gem-dimethyl and sulfone groups in HBPAES and LPAES backbones [248]. The T_g of HBPAES with monomeric A$_2$, M0-0.85 sample, was 157.0 °C by DSC measurement and when the distance between branch points is increased with an A$_2$ oligomer having a DP of three, O3-0.85, the T_g decreased by 10 °C to 146.9 °C due to increased mobility arising from the aryl-ether bond rotation in HB polymer backbone. Moreover, the T_gs of O7-0.85 and O19-0.85 samples that have higher linearity as depicted by degree of branching values and KMHS-α exponents get closer to the T_g value of LPAES (190.3 °C) due to the addition of longer linear chains in between branch points, which also induces a rise in their M_w. As a result, the linearity observed in HB polymers possessing A$_2$ oligomers with DP of seven or higher in between branch points has become more significant in dominating the chain behavior of HBPAESs than the branched topology [249].

Table 14 Intrinsic properties of HBPAES [180]

Polymer:	LPAES	M0-0.55	M0-0.75	M0-0.85	M0-1.00	O3-0.85	O7-0.85	O19-0.85
A_2:B_3 ratio	-	0.55	0.75	0.85	1.00	0.85	0.85	0.85
M_n (kDa)[a]	36.3	1.9	4.7	3.5	8.9	33.1	94.9	83.6
M_w (kDa)[a]	75.1	6.2	8.8	13.5	34.9	46.8	130.2	137.8
$[\eta](10^{-3}dL/g)$[a]	210.0	29.0	32.0	50.1	57.0	77.8	64.5	145.7
R_h (nm)[a]	6.00	1.3	1.6	2.00	2.80	3.80	5.00	6.50
g_h	1.00	0.22	0.26	0.33	0.46	0.62	0.83	1.01
KMHS–α[a]	0.564	0.380	0.460	0.497	0.390	0.434	0.641	0.625
KMHS–logK[a]	-3.376	-3.030	-3.261	-3.334	-2.940	-3.131	-4.483	-4.030
T_g (ºC)[b]	190.30	-	127.0	157.00	171.2	146.90	178.30	183.60
%Terminal[c]	-	65.2	54.4	40.9	31.1	40.9	40.9	42.2
%Linear[c]	-	20.3	28.9	45.5	51.7	45.5	45. 5	44.3
%Dendritic[c]	-	14.50	16.7	13.6	17.2	13.6	13.6	13.6
%DB (Frèchet)	-	79.7	71.1	54.5	48.3	54.5	54.5	55.8
%DB (Long)	-	79.7	71.1	54.5	48.3	27.2	13.6	5.6
OH eq. wt. (g)[c]	-	285.3	338.9	382.1	457.6	792.4	1175.7	2919.2
OH eq. wt (g) (theoretical)[d]	-	223.5	311.3	375.7	-	667.7	1229.9	2965.5

[a]*Calculated from MALS detector;* [b]*Calculated from DSC 2nd cycle;* [c]*Calculated from 1H NMR spectra,* [d]*Calculation from the estimated configuration of Figure 36.*

4.2.3. Synthesis and characterization of HBPAES-Si

For the HBPAES to attain self-crosslinking ability and to incorporate inorganic groups into the HB polymer backbone, phenolic end groups of HBPAES were post-functionalized with 3-isocynatopropyltriethoxysilane (IPTES) in DMAc at 80 °C (Figure 42). The solid content of the reaction mixture was 20% (w/w). The post-functionalization reaction was followed by FT-IR spectrometer. Within six hours, the isocyanate (-N=C=O) asymmetric stretching peak at 2267 cm^{-1} was observed to completely vanish in the FT-IR spectrum (Figure 43). Upon the completion of the reaction, the solution containing HBPAES-Si was immediately used to prepare films or UF membranes from their blends with LPAES.
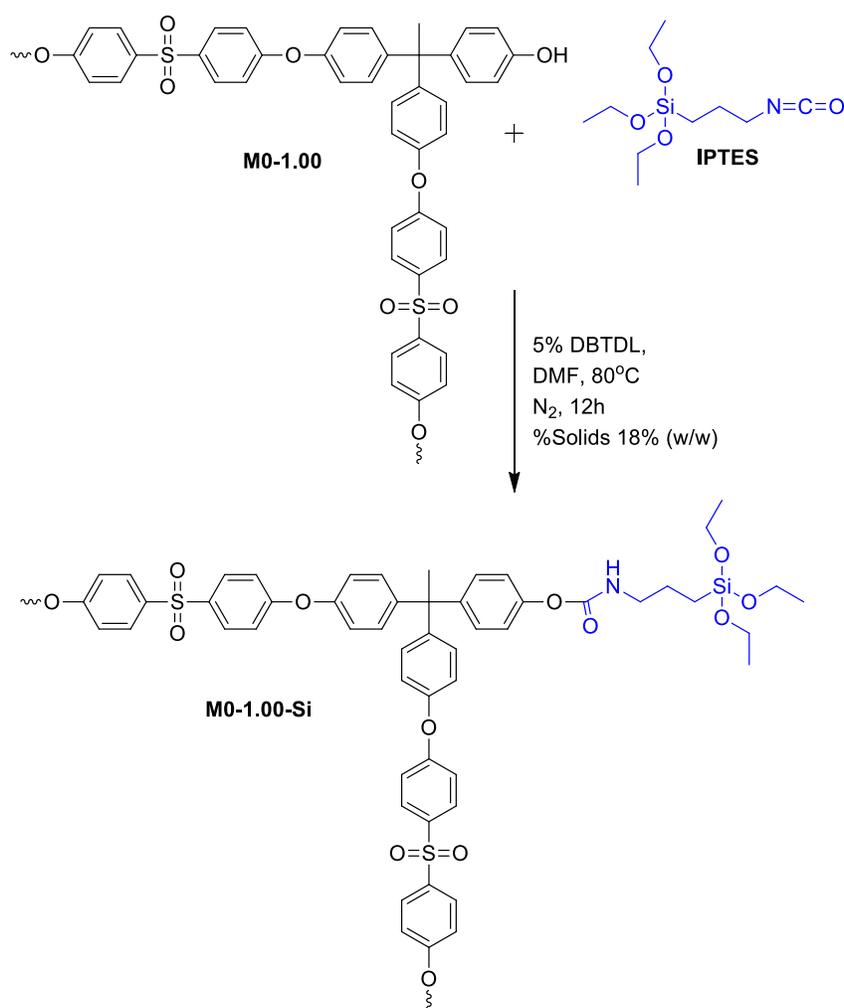
Figure 42 The alkoxysilane functionalization of HBPAES

In order to verify the successful functionalization of HBPAES with IPTES, HBPAES-Si product was dried and cured by heating, as a result of which, an asymmetric stretching band of Si-O-Si appeared at 1070 cm^{-1} as a result of the hydrolysis and condensation of alkoxysilane end-groups.
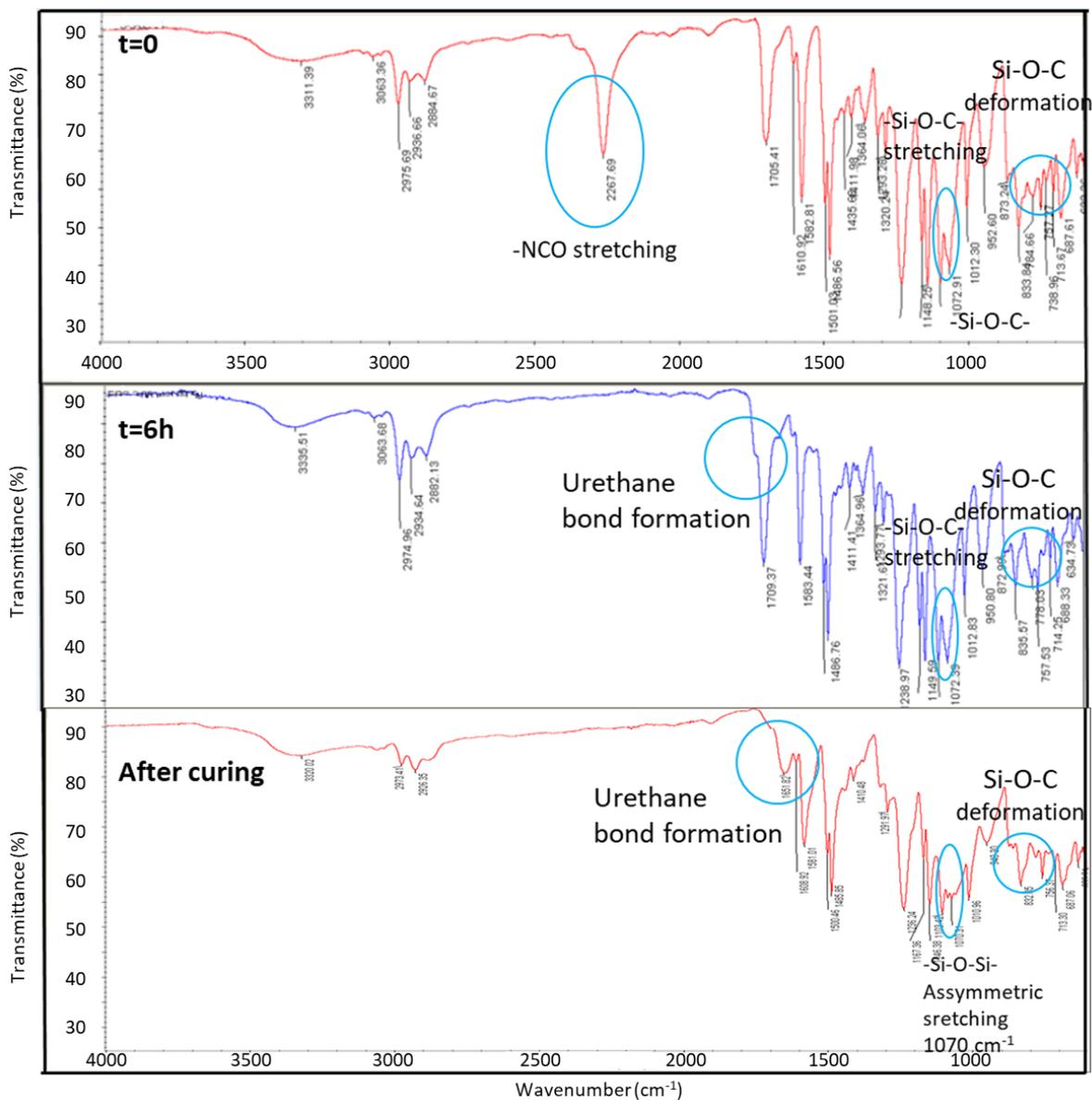
Figure 43 FT-IR spectra of following urethane bridging reaction for M0-0.85

Alkoxysilane end-groups of post-functionalized HBPAES samples with IPTES were prone to hydrolysis in the presence of humidity or acidic media and turn to Si-(OH)$_3$, which are then known to form the Si-O-Si network structure via subsequent condensation reactions, the rate of which accelerated by heating. The overall functionalization strategy with each step is shown in Figure 44.

It was critical to characterize HBPAES-Si samples throughout the self-crosslinking process. Following the reaction between the phenolic end groups of HBPAES and IPTES in the post-functionalization step, the presence of three possible structures such as -SiOEt, -SiOH, -SiOSi were possible for the end groups of HBPAES. For example, for the M0-0.85-Si sample, ethoxysilane end groups could easily hydrolyze in the presence of humidity and acidic environment and form silanol end groups (M0-0.085-SiOH). These structural transformations at HBPAES chain ends were monitored via ^{29}Si NMR spectroscopy by comparing the spectra of IPTES (black), M0-0.85-Si (blue), and M0-0.85-SiOH (dark red) in Figure 45.

The Si atoms of ethoxysilane groups on IPTES was detected at -46.94 ppm. After the post-functionalization reaction, Si atoms of the ethoxysilane end groups of M0-0.85-Si was observed at -45.44 ppm with a slight shift to the lower energy region on the spectrum compared to IPTES. Following the hydrolysis reaction, the condensation reaction of silane groups was expected to take place, therefore, in addition to the main hydrolysis product, -SiOH peak, the peaks originating from the condensation reaction could be seen in ^{29}Si NMR spectrum of M0-0.85-SiOH. The principal -SiOH peak was detected at -45.09 ppm, and the broadened peak at -50.03 ppm was assigned to ...SiOSi(R)(OEt)(OH) and ...SiOSi(R)(OH)$_2$, furthermore, the low-intensity peak at -58.45 ppm was presumed to arise from...SiO)$_2$Si(R)(OH) structures that are expected to form as a result of self-condensation reactions of -SiOH end groups following the hydrolysis. Hence, it can be concluded that the condensation mechanism could start at room temperature for post-functionalized HBPAES samples [250]. As the condensation reactions continued, self-crosslinked HBPAES became insoluble in solvents, therefore, the structural analysis of M0-0.85-SiOSi by ^{29}Si NMR spectroscopy was possible by solid NMR.
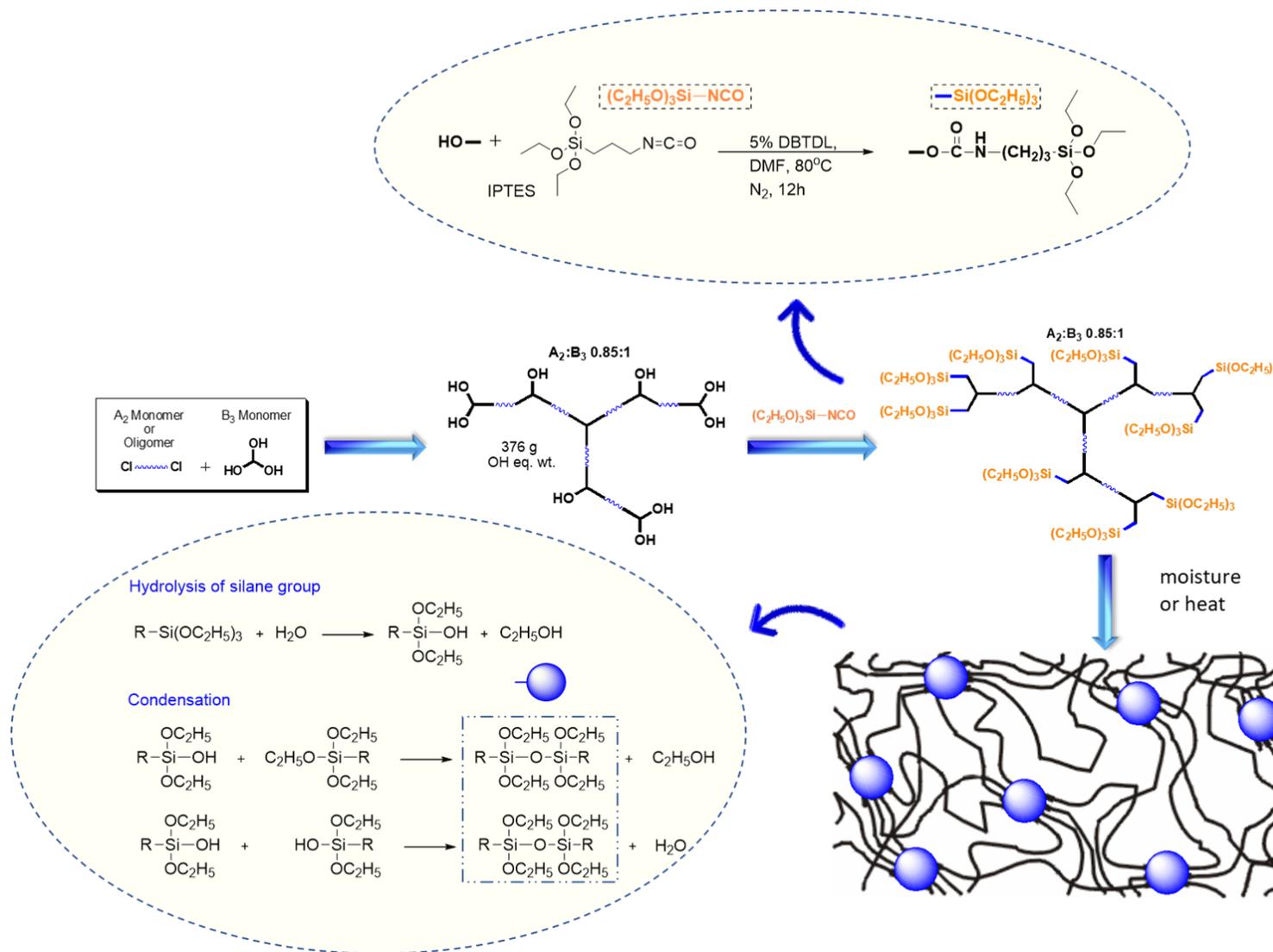
Figure 44 Schematic representation of post-functionalization of HBPAESs by alkoxysilane end groups
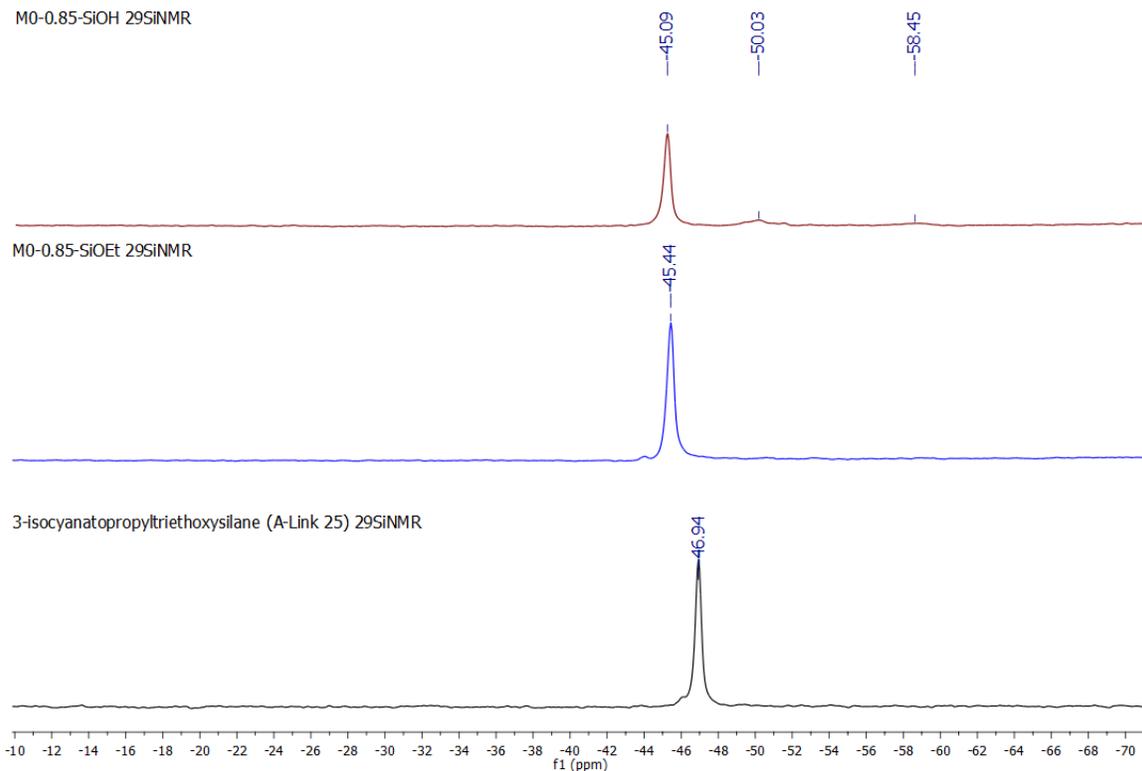
Figure 45 ^{29}Si NMR spectra of IPTES, M0-0.85-Si and M0-0.85-SiOH in DMSO-d^6

The equivalent weights HBPAES samples per phenolic end groups were calculated for each A$_2$: B$_3$ ratio and the branching density, which could change with the distance between branch points. According to the results given in Table 14, the functionality of HB polymer per unit weights reduced with an increase in the distance between branch points in a controlled manner. With the same trend, the degree of crosslinking is also expected to decline upon the self-crosslinking of each HBPAES sample as the A$_2$ oligomer length is increased, which was confirmed by the gel content (wt%) of each self-crosslinked HBPAES sample as shown in Table 15.

The self-crosslinking ability of HBPAES-Si was analyzed by measuring the gel content of each crosslinked HBPAES-SiOSi. This measurement was performed via Soxhlet extraction in DCM for 24 h, and the residue was dried in a vacuum oven at 120 °C for 24 h. Each dried,

solid HBPAES-SiOSi were weighed before and after the Soxhlet extraction. Then, the percentage of gel content (%) was calculated using Equation 32.

$$gel\ content\ (\%) = \frac{w_e}{w_i} \times 100$$

Equation 32

where w_i is the initial weight of the dry polymer and, w_e is the weight of the dry polymer after the Soxhlet extraction process. As the distance between the branched points increased, the crosslink density, thus the gel content of HBPAES-Si decreased as given Table 15 and Figure 46.

Thermal properties of self-crosslinked HBPAES samples were compared with non-crosslinked, phenol terminated HBPAES to elucidate the effect of crosslinking and the incorporation of inorganic moieties in the polymer network. For this purpose, as shown in Figure 46, DSC analysis of all HBPAES samples with phenol (green curves), ethoxysilane (blue curves) and silanol end groups (red curves) were conducted along with final, self-crosslinked HBPAES samples (black curves) synthesized with different A_2:B_3 ratios or A_2 oligomer lengths. To prepare DSC samples of ethoxysilane terminated HBPAESs the reaction mixtures from the post-functionalization step were poured into a Teflon mold and dried under vacuum at 40 °C for 48 hours. Silanol functional HBPAES samples were prepared by pouring the post-functionalization reaction mixtures into water for the hydrolyzation of ethoxysilane end groups and precipitating the reaction product, flowed by drying overnight at 40 °C, under vacuum. Finally, the DSC sample of crosslinked HBPAES samples were prepared by treating each silanol functional HBPAES sample at 120 °C for self-crosslinking. As listed in Table 15 and shown in Figure 46, a significant increase was observed in the T_g of HBPAES samples upon crosslinking. The amount increase in T_g values upon crosslinking of HBPAES samples was lessened as the distance between branch points increased.

Table 15 Gel content (%) and T_g results of HBPAESs and post-functionalized HBPAES state

HBPAES code	T_g(ºC) (HBPAES)	T_g(ºC) (HBPAES-SiOSi)	% Gel content
M0-1.00/-SiOSi	171.06	186.81	96.00
M0-0.85/-SiOSi	157.00	-	96.90
O3-0.85/-SiOSi	146.90	183.36	92.70
O7-0.85/-SiOSi	178.30	191.66	73.20
O19-0.85/-SiOSi	183.60	193.76	10.00
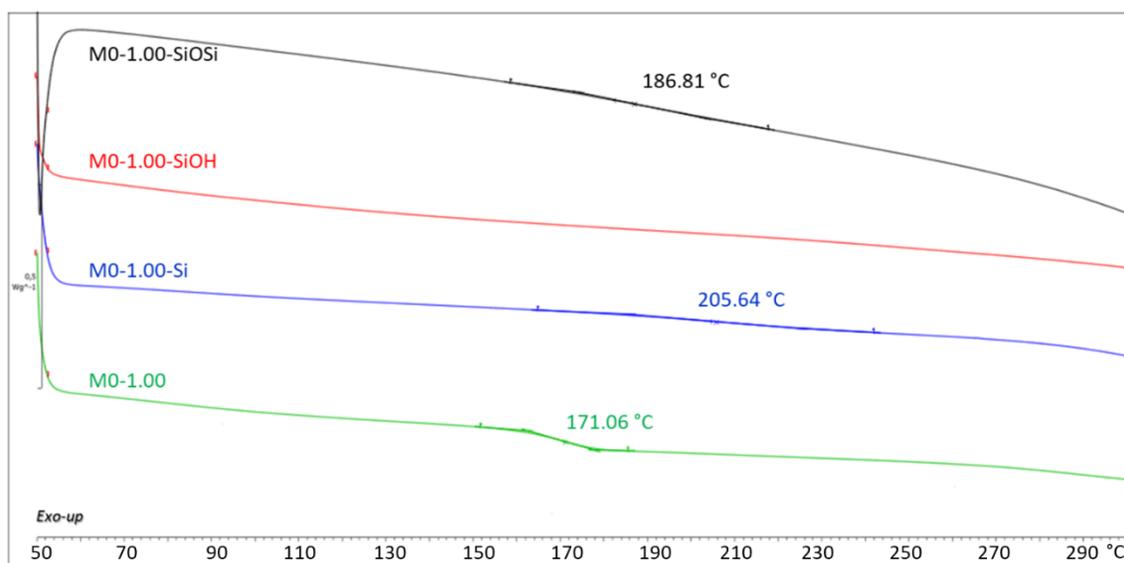
a. DSC curves of M0-1.00 & M0-1.00-Si & M0-1.00-SiOH & M0-1.00-SiOSi
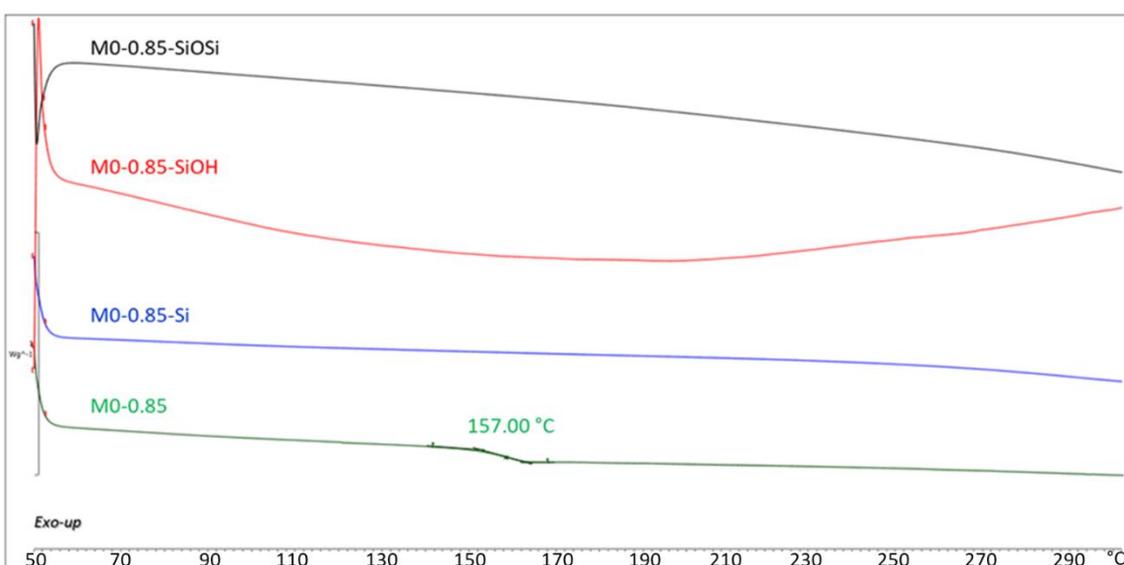
b. DSC curves of M0-0.85 & M0-0.85-Si & M0-0.85-SiOH & M0-0.85-SiOSi
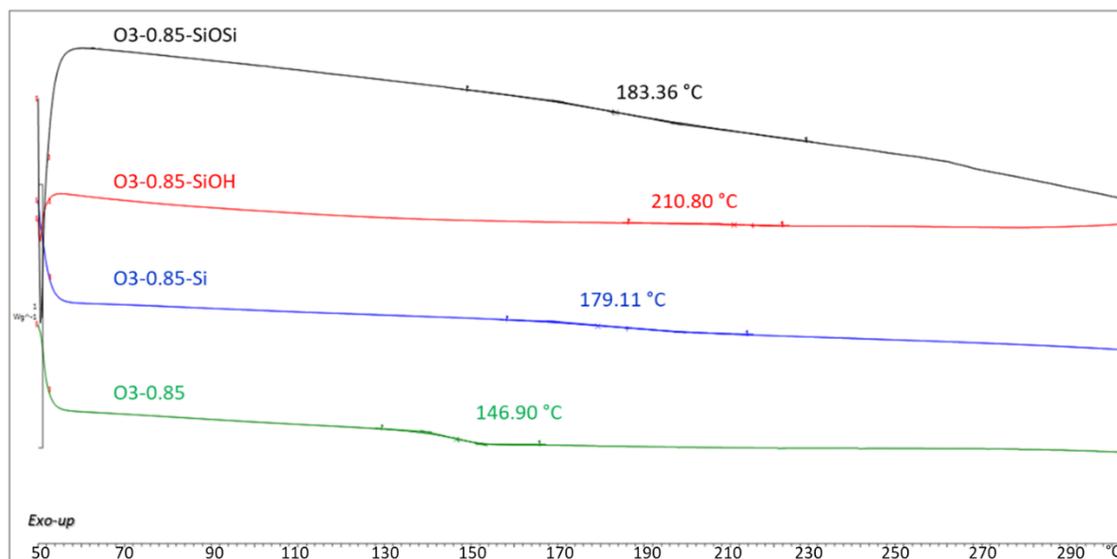
c. DSC curves of O3-0.85 & O3-0.85-Si & O3-0.85-SiOH & O3-0.85-SiOSi
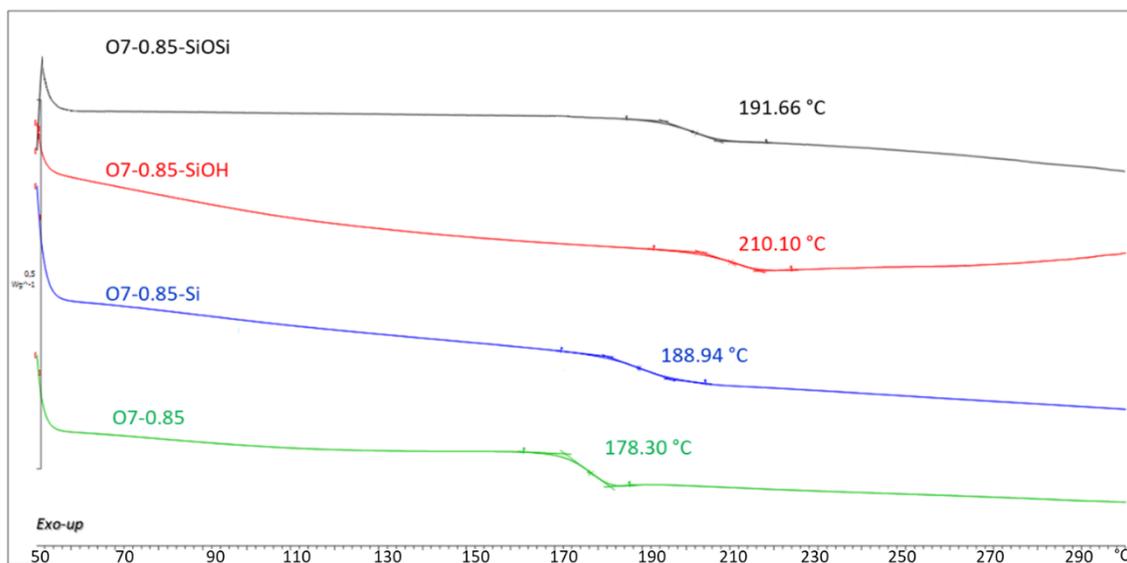
d. DSC curves of O7-0.85 & O7-0.85-Si & O7-0.85-SiOH & O7-0.85-SiOSi
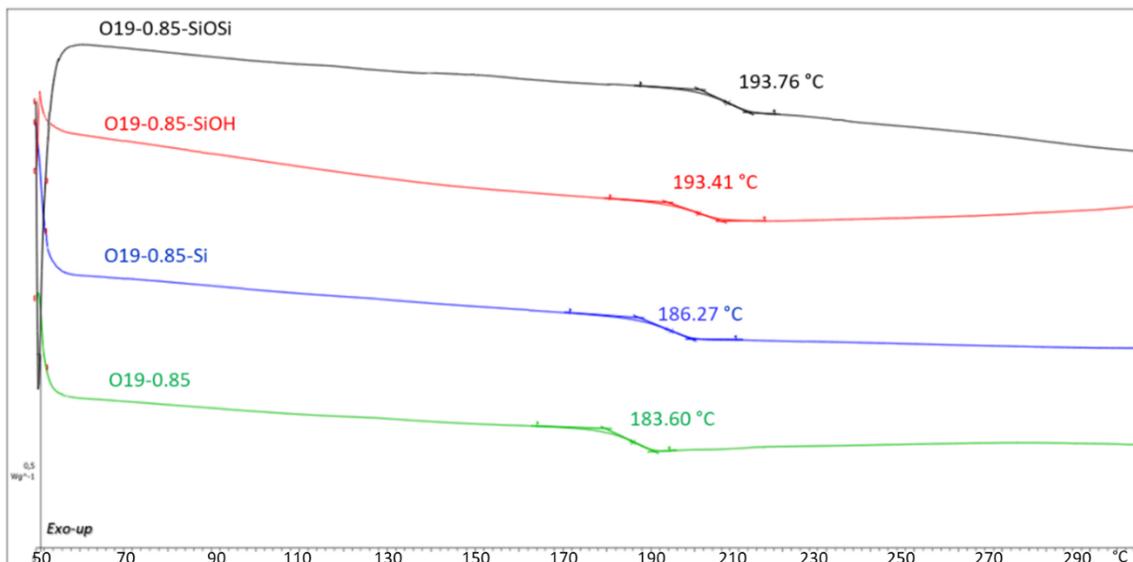
e. DSC curves of O19-0.85 & O19-0.85-Si & O19-0.85-SiOH & O19-0.85-SiOSi

Figure 46 The DSC thermograms showing the effects of different end groups stages on the thermal properties of HBPAES samples with varying oligomeric A_2 length or A_2:B_3 ratio (control HBPAES (green), ethoxysilane functional HBPAES (HBPAES-SiOEt) (blue), silanol functional HBPAES (HBPAES-SiOH) (red), and self-crosslinked HBPAES (HBPAES-SiOSi) (black) for a)M0-1.00, b) M0-0.85 c) O3-0.85, d) O7-0.85, and e) O19-0.85 samples).

4.2.4. Characterization of LPAES/HBPAES blend films

Thermo-mechanical behavior of LPAES and its blends with HBPAESs were investigated by DMA measurements. The onset of the storage modulus (E') is associated with large-scale intermolecular motions (α relaxation) which correspond to T_g value for amorphous polymers. As shown in Figure 47, the pure LPAES film and blend films containing 10% (w/w) HBPAES samples had single T_g values, indicating the formation of homogenous and miscible blends. T_g values that were measured by DSC and DMA are given in Table 16 along with calculated T_g values using the Fox equation [251] for blend films. Experimentally determined T_g values by DMA and DSC measurements were found to be in good agreement and show the same trend with theoretically calculated values from the Fox equation.

The miscibility of HBPAES and LPAES was further investigated at various blend compositions: 5, 10, 25, 40, and 50% (w/w) O3-0.85 HBPAES in LPAES. LPAES/HBPAES

97

blends containing various fractions of O3-0.85 showed single T_g values according to DMA and DSC analyses, and they were very close to the T_g values calculated using the Fox equation. The DMA curves of LPAES and LPAES/HBPAES blend films with various HBPAES fractions cast from DMAc are shown in Figure 48 and T_g values determined by DSC, DMA and Fox equation as a function of HBPAES content are plotted in Figure 49 showing a good agreement.

All blend films containing 10% (w/w) HBPAES showed enhanced thermo-mechanical behaviors compared to neat LPAES (Figure 47). Specifically, O3-0.85-BF was found to show a significantly increased storage modulus value up 2405 MPa at 30 °C, which was approximately 20% greater than the LPAES sample (1998 MPa).

Thermo-mechanical analysis of the blends of LPAES with various fractions of HBPAES O3-0.85 from 5 to 50% (w/w) was also carried out, which showed a systematic increase in the storage modulus value below the T_g as a function of increasing HBPAES O3-0.85 content as presented in Figure 48.
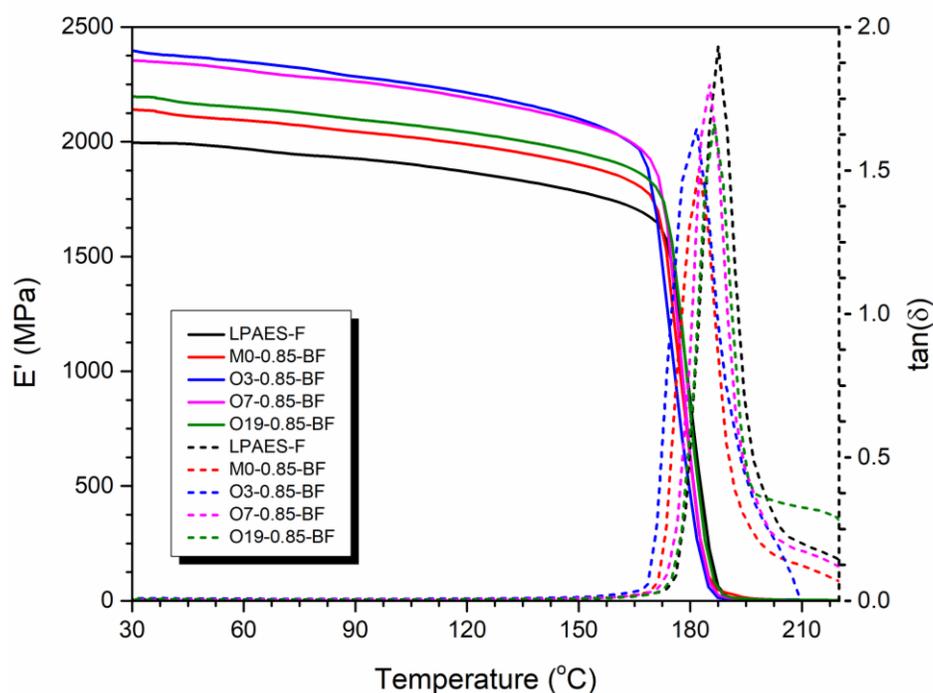
Figure 47 DMA curves of LPAES and LPAES/HBPAES blend films (90/10 w/w) cast from DMAc [180]

Table 16 T_g values of LPAES/HBPAES blend films (90/10 w/w) [180]

Polymer	$T_{g(Fox\ equation)}$* (°C)	$T_{g(DSC)}$ (°C)	$T_{g(DMA)}$** (°C)
LPAES-F	-	189.7	187.5
M0-0.85-BF	185.8	185.4	182.4
O3-0.85-BF	184.3	183.6	181.7
O7-0.85-BF	188.5	188.6	185.2
O19-0.85-BF	189.1	188.9	186.5

*calculated from the Fox equation ($\frac{1}{T_g} = \frac{w_1}{T_{g_1}} + \frac{w_2}{T_{g_2}}$); w: weight fraction, T_{g_1} or T_{g_2}: T_g of each component

** determined from the peak of tan(δ)
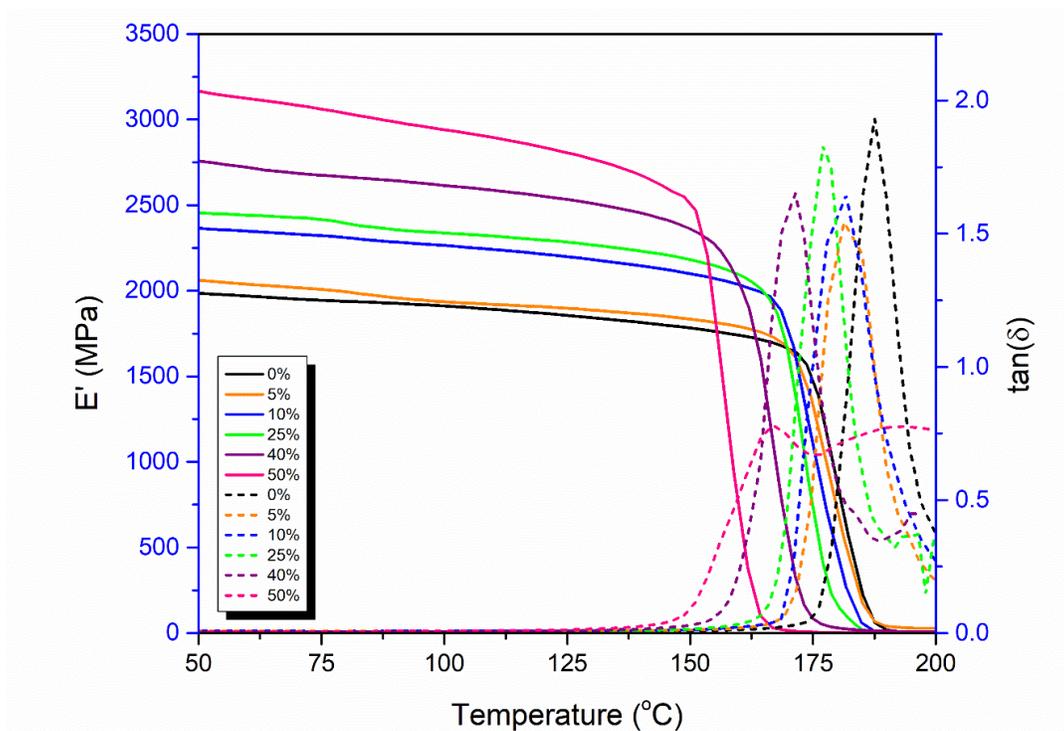
Figure 48 DMA curves of blend films containing various fractions of HBPAES O3-0.85 in LPAES [180]
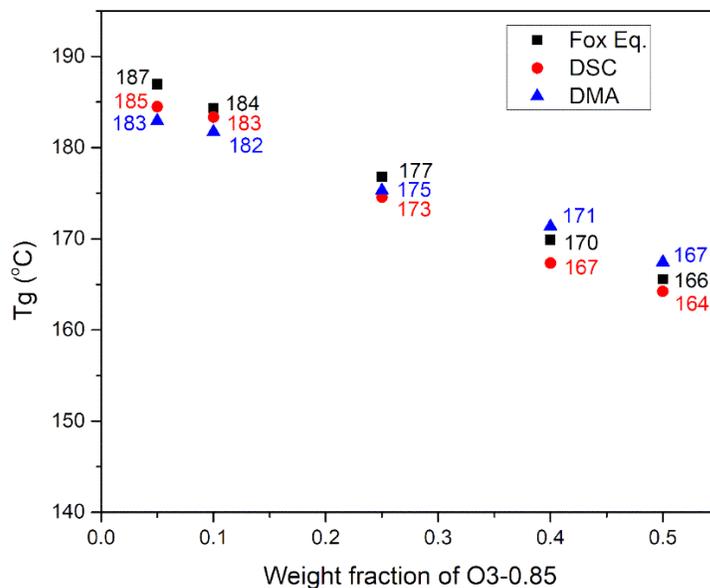
Figure 49 T_g values of LPAES/O3-0.85 blend films with various HBPAES contents from the of DMA and DSC measurements, and Fox-Equation [180]

Tensile stress-strain curves of LPAES/HBPAES blend films cast from DMAc solution are illustrated in Figure 50. It should be noted that all blend films had a composition of 90/10 (w/w) LPAES/HBPAES with different HBPAES samples synthesized with varying distance between branch points. As the distance between the branch points of the HBPAES component shortened, the stress-strain curves showed an increase in the embrittlement character of the final blend film. In other words, as the branching density decreased, the mechanical behavior of blend films became similar to those of LPAES.
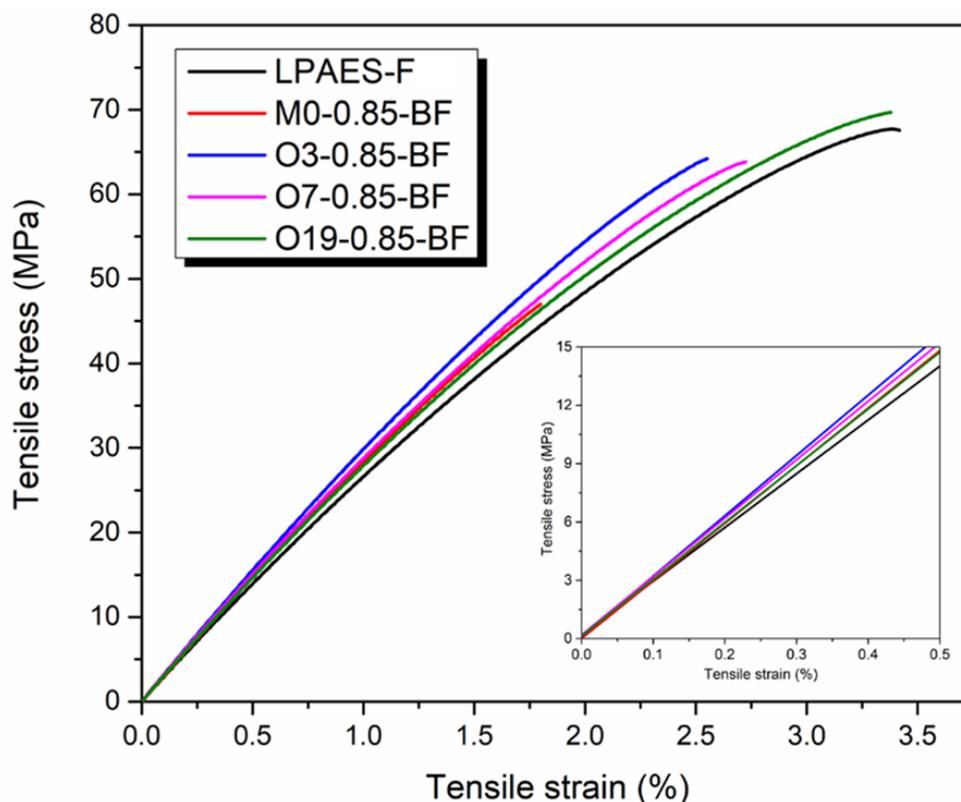
Figure 50 Tensile stress-strain curve of LPAES/HBPAES blend films (90/10 w/w) [180]

Mechanical properties of all blend films are summarized in Table 17. At a ratio of 90/10 LPAES/HBPAES, the Young's modulus values of all samples were almost the same and close to the reference LPAES sample. However, the degree of branching of the HBPAES component had a considerable effect on the strength (σ) and strain at break (ε) values of blend films that were more sensitive to micro-structure related transformations and interactions. In the case of M0-0.85-BF, a significant decrease in both strain and strength was observed, which may be attributed to the small aspect ratio of M0-0.85 (like a nano-scale additive) inside LPAES. As a result, LPAES was presumed to lose its strength due to its large and loosely packed globular conformations disturbed by blending with M0-0.85. From a mechanical point of view, an increase in the aspect ratio was expected to cause smaller interfacial shear stress in the matrix of LPAES [252], which would allow higher deformability. Eventually, strain at break values converged to that of neat LPAES' for the O19-0.85-BF case where linearity is the highest.

101

Table 17 Mechanical properties of LPAES/HBPAES blend films (90/10 w/w) [180]

Polymer	Young's Modulus (MPa)	ε at break (%)	σ at break (MPa)
LPAES-F	2655 ± 43	3.41 ± 0.30	67.58 ± 1.87
M0-0.85-BF	2936 ± 36	1.80 ±0.27	47.00 ± 1.62
O3-0.85-BF	3033 ± 46	2.55 ± 0.10	64.19 ± 0.34
O7-0.85-BF	2983 ± 34	2.72 ± 0.28	63.82 ± 1.18
O19-0.85-BF	2913 ± 26	3.38 ± 0.19	69.71 ± 0.16

The cohesive energy that can be determined by dissipative particle dynamics (DPD) simulations is a useful parameter for the understanding of thermo-physical properties such as heat capacity, shear modulus and T_g for polymer blends [253]. The linear correlation between the normalized cohesive energy and T_g is well-known for systems lacking strong or specific intermolecular interactions and side groups . Since the cohesive energy is a measure of the energy needed to arrange molecules in the gas state into the solid state, it will manifest itself in the DPD simulations via the non-bonded energy values. According to the findings of DPD analysis for HBPAES-LPAES blends [180], the non-bonded energy value of HBPAES-LPAES blends showed a complex relationship with the distance between branch points of the HB component (Figure 51-a). The non-bonded energy value for the neat LPAES system was significantly higher than its highly branched derivatives. This finding was clarified in the study as follows: LPAES chains are only composed of two types of regions such as 2,2-diphenylpropane (came from BisA) and diphenyl sulfone (with etheric linkage). These two regions are smaller than the region of 1,1,1-triphenylethane (came from THPE), where occupies in HBPAES skeleton. As a consequence, the DPD interaction parameters between regions in LPAES chains were found as the smallest when compared with the parameters between the regions in HBPAES chains. In the study, a slight drop in non-bonded energy value observed in O3-0.85-BF blend system revealed that the secondary interactions between polymer chains were less likely to occur as the free volume defined the empty lattice sites according to Locally Correlated Lattice (LCL) model [254]. This provided an insight into the slight decrease in the experimentally measured free volume of these blend films shown in Figure 51-b.

Structure factor (SF) is another key indicator for the understanding of long-range structural events and conformation of macromolecules. For this purpose, experimental SANS and SAXS models are gathered and fit to predefined models using *SANS & USANS analysis method* [255]. SF plots of LPAES in neat and blend systems with respect to wave vector (q) give critical insights on different LPAES conformations (Figure 51-c, d, e). In an SF plot, the distance between the nearest neighbors is related to the position of the first $S(q)$ maximum [256]. For the neat LPAES system, the first $S(q)$ maximum observed at $q>1$ indicates the presence of large, loosely packed globular LPAES conformations (Figure 51-c). On the other hand, in the case of M0.085-LPAES blend system a spherically averaged SF is pronounced [257] with beads of linear and HB polymers that are in close contact with each other (Figure 51-d). For blend systems with increasing distance between branch points (Figure 51-e), the position and type of $S(q)$ peak approaches to randomly oriented monodisperse rods, in which the height and slope of SF peak relates to rod's length and radius, respectively [258]. These findings support the experimental findings that HB polymers with varying distance between branch points as additives show different effects on the mechanical and thermo-mechanical properties when added into linear polymers. In blend systems, M0-0.85 was found to be organized to form spherical formations and acts as a nano-scale additive considering the relatively short, one monomer unit distance between branch points of M0-0.85. On the other hand, HB polymers with longer distance between branch points were organized to form rod-like structures where the rod size increased with respect to increasing distance between branch points, and the non-bonded interactions increased with increasing rod length. This idea supports the findings from SEM analysis of fracture surfaces, which indicates that the incorporation of different HBPAESs has caused different failure behavior depending on the distance between branch points. In addition, combining DPD simulations with mechanical and thermo-mechanical characterization results for LPAES and O3-0.85 blend films (O3-0.85-BF), it can be concluded that this rod size was optimum in O3-0.85-BF system.
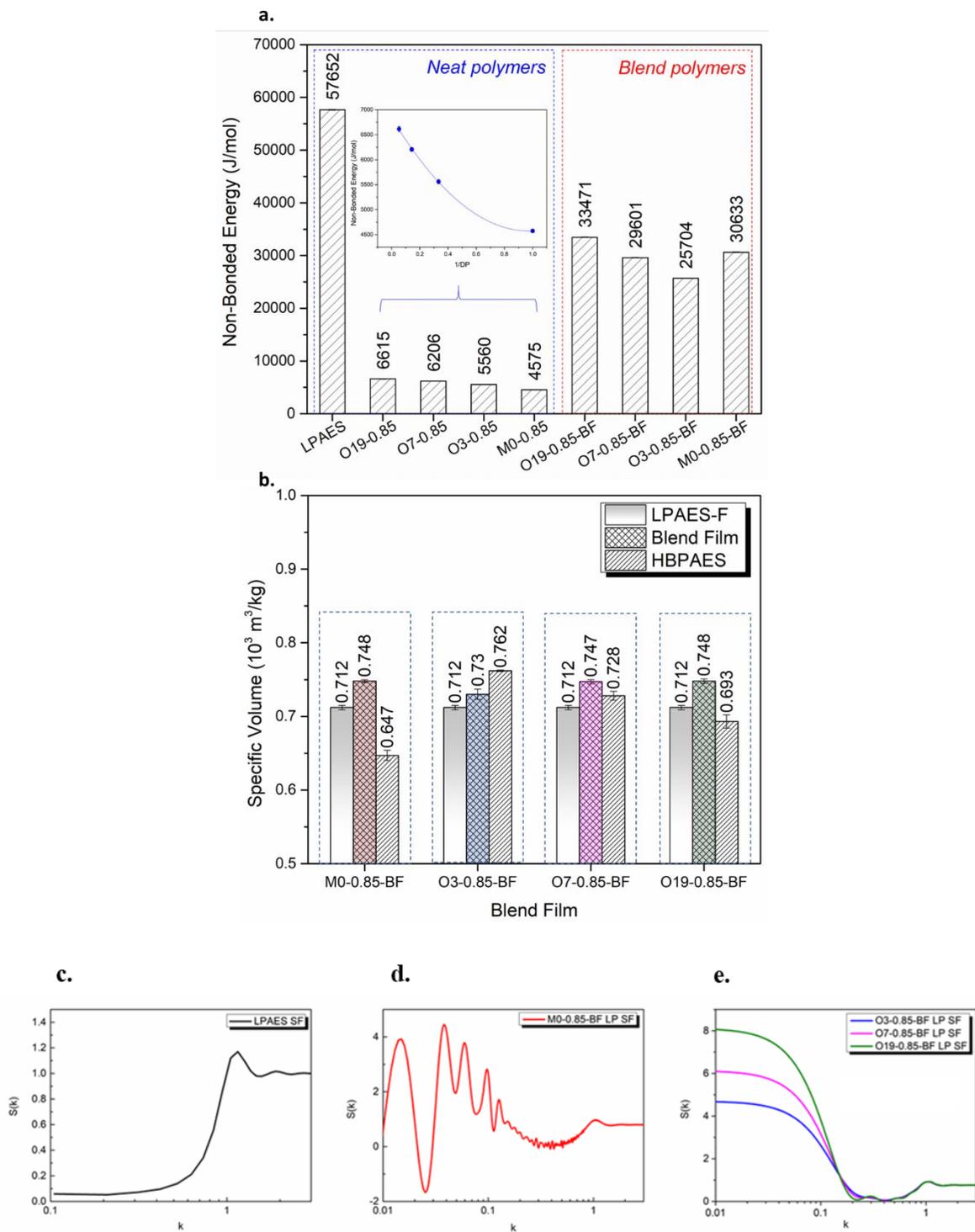
Figure 51 a. Non-bonded energy diagram; b. Specific volume diagram of LPAES, HBPAESs and their blend films; c. The structure factor diagram of LPAES; d. The structure factor diagram of M0-0.85-BF; e. The structure factor diagram of O3-085-BF, O7-0.85-BF, and O19-0.85-BF [180]

Detailed SEM analyses were performed on the fracture surfaces of tensile test specimens to reveal existing multi-scale interactions of LPAES samples with HBPAESs as additives in the blend. Pure LPAES specimens primarily had a smooth fracture surface as shown in Figure 52-a_1, locally altering with different failure morphologies. The smoothness of the fracture surface of LPAES indicated that a brittle failure mechanism was dominant. The smooth failure pattern was disturbed (Figure 52-a_2) with rather wavy fracture signs perpendicular to the loading direction, which suggested that a minor polymeric orientation was present in the sample that would cause through-thickness crack deflection and increase the plasticity of the sample.

M0-0.85-BF sample represented the incorporation of a relatively small HB polymeric structure (M_w=13.5 kDa and the distance between branch points ≈ 7.54 Å) into LPAES, hence promoted smaller scale interactions. A major difference of M0-0.85-BF specimens with respect to LPAES specimens was the lack of smoothness which was replaced with a stepped fracture surface due to multiple crack appearance and propagation during failure (Figure 52-b_1), suggesting that the failure was due to the combination of smaller cracks and their propagation in the polymer bulk (Figure 52-b_2). Multiple crack propagation pathways revealed that formed cracks were forced to propagate in a stiffer medium with more resistance to crack propagation. Due to the presence of multiple stress concentration regions (i.e crack tips), samples were prone to early failure at relatively low strain values.

As the distance between branch points increased for the HBPAES additive in the case of O3-0.85-BF (contained HBPAES O3-0.85 with M_w= 46.8 kDa and the distance between branch points ≈ 28.1 Å), the fracture surface was clearly divided into two sections which indicated that two types of crack propagation mechanisms were present (Figure 52-c_1). At the top edge of the specimen, repeating patterns of ridges were available due to the crack propagating from the edge of the specimen towards the bulk. This formation disappeared in the middle of the sample where a stepped region with a significant through-thickness damage was available. At the bottom edge, a rather smooth fracture surface was present presumably due to a fast propagating crack. When compared with M0-0.85-BF, O3-0.85-BF samples were less prone to cracking (except for edge effects) that resulted in higher tensile strength and ability to deform.

In the case of O7-0.85-BF (contained HBPAES O7-0.85 with M_w= 130.2 kDa, the distance between branch points = 64.2 Å), morphological differences at the edge and the bulk of the specimen were much clearer. The fracture surface became much more similar to LPAES specimens but consisted of three separate regions (Figure 52-d_1). On the left-hand side of the SEM image of the failure surface, a smooth surface was observed similar to LPAES specimens, whereas on the right-hand side a large hole was observed corresponding to a separate interlaminar formation. These two regions were joined together by a rather rough fracture surface (Figure 52-d_2) with signs of plastic deformation, which suggested that observed interlaminar formation heavily contributed to tensile load-bearing. When compared with O3-0.85-BF, it might be concluded that larger distance between branch points caused a laminar formation in polymer blends without causing significant losses in the tensile strength and maximum strain, and therefore observed interlaminar formations were perfectly compatible with the bulk of the polymer.

The interlaminar deformation was more evident in the fracture surfaces of O19-0.85-BF (contained HBPAES O19-0.85 with M_w= 137.8 kDa, the distance between branch points = 172.7 Å) where overall specimen surface was dominated by interlaminar separation (Figure 52-e_1) as was in the case of O7-0.85-BF. Encircling top and bottom surfaces around the interlaminar structure showed a perfect resemblance to LPAES failure surface (Figure 52-e_2) whereas mechanical performance was slightly enhanced.

As a result, the incorporation of HBPAESs into LPAES resulted in different failure behaviors depending on the distance between branch points of the HBPAES. While a total disturbance of pristine LPAES's failure behavior was observed with the smallest HB polymer (M0-0.85) utilized as an additive, as the size of the HB polymer additive and the distance between branch points increased, as a consequence, the failure pattern converged back to pristine LPAES' behavior. In the context of analyzed samples, O3-0.85-BF sample was shown to be morphologically optimum for a compatible blending strategy with a moderate strength improvement and macroscopically homogeneous structure.
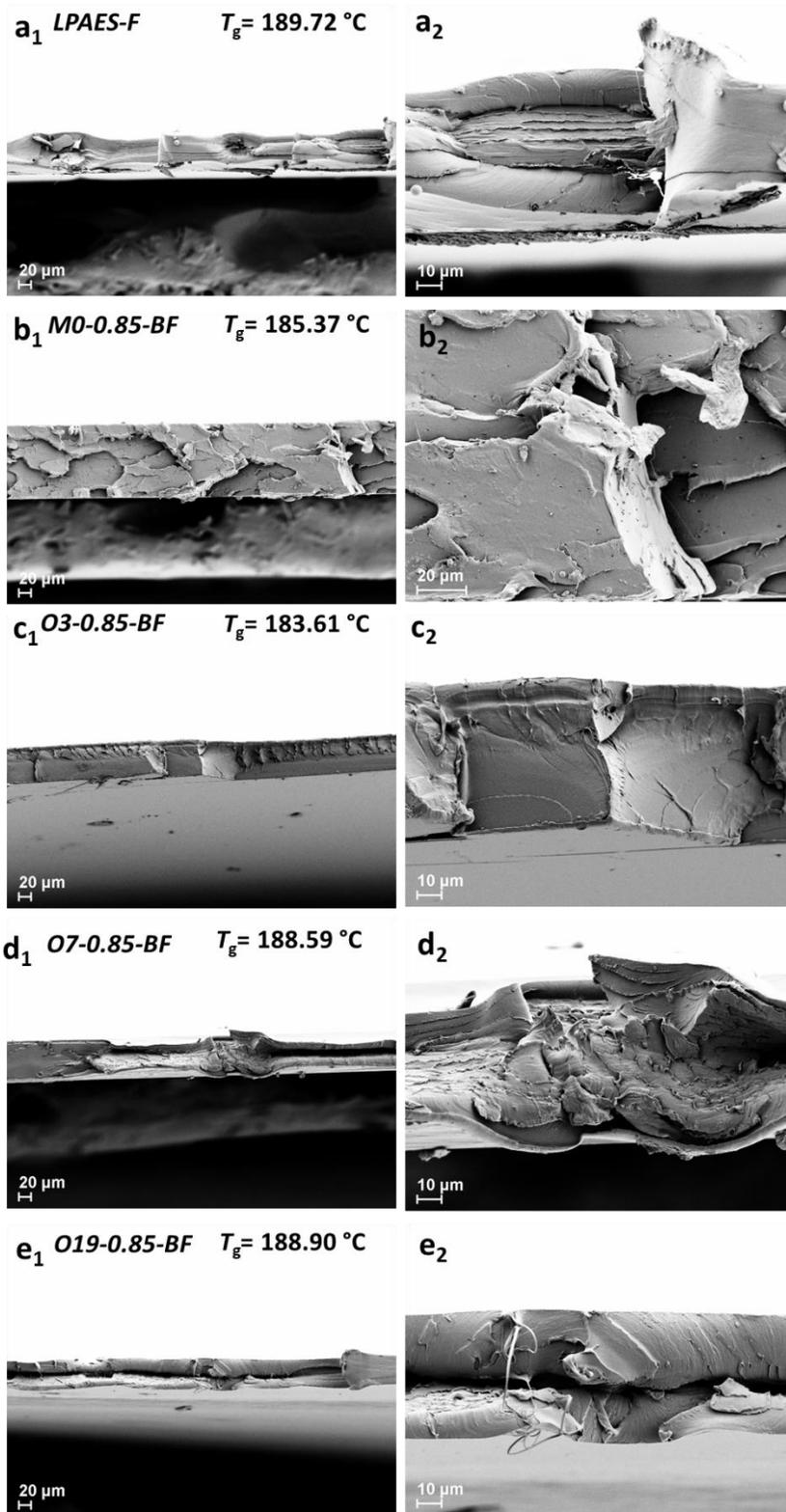
Figure 52 SEM images of fractured surface **a** LPAES-F **b.** M0-085-BF **c.** O3-0.85-BF **d.** O7-0.85-BF **e.** O19-0.85-BF [180]

4.2.5. Characterization of HBPAES-Si/LPAES blend films

The blend film preparation and analyses were discussed under Section 4.2.5. The FT-IR spectra of LPAES film as well blend films of HBPAES-Si samples (O3-0.85-Si-BF, O7-0.85-Si-BF, and O19-0.85-Si-BF) and LPAES are shown from 1800 cm^{-1} to 800 cm^{-1} in a stacked form in Figure 53. The main difference that was observed in the FT-IR spectra arose from the asymmetric stretching peak of urethane-carbonyl groups in the vicinity of 1710 cm^{-1}.that were introduced during the post-functionalization of HBPAES samples via the reaction between phenolic end groups and isocyanate groups of IPTES. It should be noted that while LPAES was presumed to have no functionality due to its high molecular weight, linear structure, whereas phenolic functionality of HBPAES samples with A_2: B_3 0.85:1.00 was 8.7 as calculated earlier above. The intensity of the urethane-carbonyl peak gradually decreased as the DP value of A_2 oligomers increased in each HBPAES sample as seen in the FT-IR spectra.
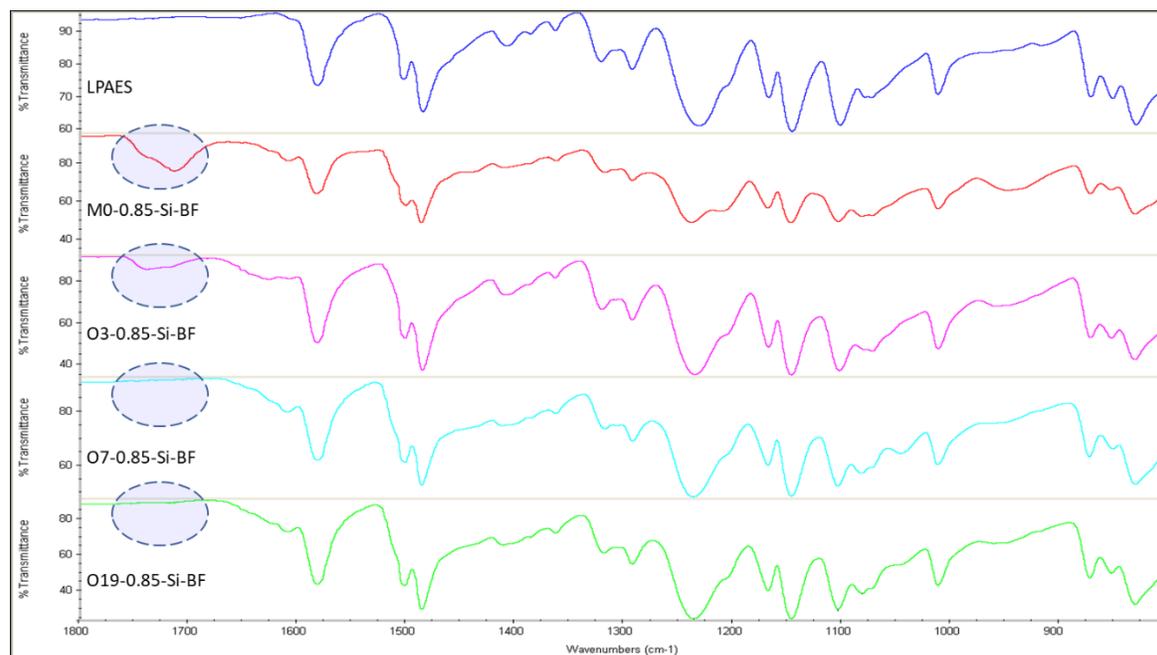
Figure 53 FT-IR spectra of HBPAES-Si-BF and LPAES film from 1800 cm^{-1} to 800 cm^{-1}.

In order to understand their thermo-mechanical behavior, LPAES and its of annealed blend films (195 °C, 120 min, 2.5 tons) containing 10% (w/w) HBPAES-Si samples were investigated using DMA and compared with LPAES/ HBPAES blend films. As shown in Figure 54, pure LPAES film and blend films had single T_g values, which indicated the formation of homogenous and miscible blends. T_g values measured by DSC and DMA, and calculated from the Fox equation [251] for blend films are given in Table 18. In general, silane functional HBPAES containing blend films with LPAES showed slightly higher T_g values compared to the phenol functional HBPAES containing blend films. The most significant increase was observed in the T_g value of O3-0.85-Si-BF compared to the O3-0.85-BF sample, whereas O7-0.85-Si-BF film showed a slightly decreased T_g value compared to the fully crosslinked, neat O7-0.85/-SiOSi sample (Table 15) and similar T_g values to the O7-0.85-BF.
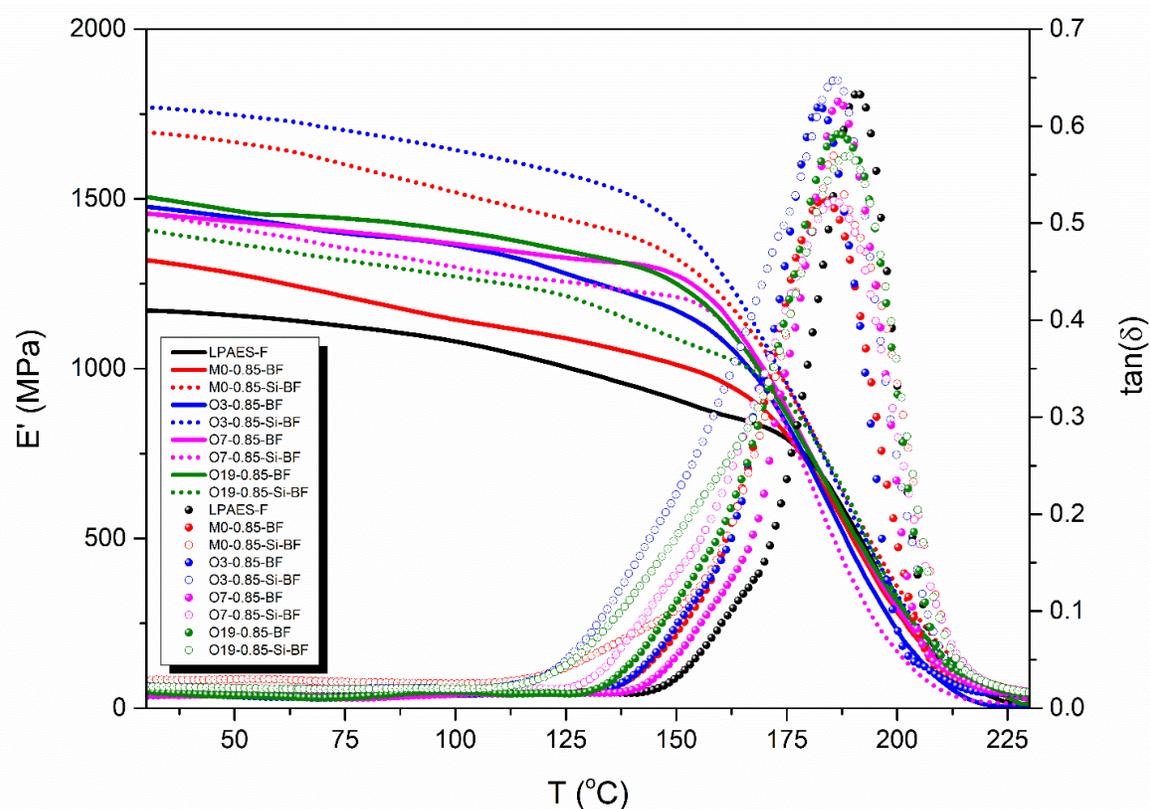
Figure 54 Comparison of the thermo-mechanical behavior of LPAES neat film with LPAES/ HBPAES (90/10 w/w) and annealed LPAES/HBPAES-Si (90/10 w/w) blend films by their DMA thermograms

Table 18 T_g values of LPAES/HBPAES (90/10 w/w) and annealed LPAES/ HBPAES-Si (90/10 w/w) blend films

Material code	$T_{g(Fox\ equation)}$* (°C)	$T_{g(DMA)}$** (°C)	$T_{g(DSC)}$ (°C)	Material code	$T_{g(Fox\ equation)}$* (°C)	$T_{g(DMA)}$** (°C)	$T_{g(DSC)}$ (°C)
LPAES	-	191.6	188.5	-	-	-	-
M0-0.85-BF	185.8	184.5	182.9	M0-0.85-Si-BF	-	185.5	185.4
O3-0.85-BF	184.3	181.8	182.8	O3-0.85-Si-BF	189.3	186.6	185.1
O7-0.85-BF	188.5	186.5	183.6	O7-0.85-Si-BF	190.2	185.6	183.0
O19-0.85-BF	189.1	187.6	184.9	O19-0.85-Si-BF	190.4	188.1	188.0

*calculated from the Fox equation ($\frac{1}{T_g} = \frac{w_1}{T_{g_1}} + \frac{w_2}{T_{g_2}}$); w: weight fraction, T_{g_1} or T_{g_2}: T_g of each component

** determined from the peak of tan(δ)

Tensile stress-strain curves of HBPAES-Si/LPAES annealed blend films cast from DMAc solution are illustrated in Figure 55 and the values are given in Table 19 in comparison with LPAES/ HBPAES blend films. It should be noted that all blend films had a composition of 90/10 (w/w) LPAES/HBPAES or LPAES/HBPAES-Si. As observed in the case of LPAES/ HBPAES blend films, the stress-strain curves of LPAES/HBPAES-Si blends showed an increase in the embrittlement character as the distance between the branch points of the HBPAES-Si component shortened. When HBPAESs were functionalized by the incorporation of an inorganic group such as a silane end group into the polymer backbone, and the mechanical and thermo-mechanical behavior of the corresponding blend films with LPAES were expected to change as well. In general, the effect of the silane functionality of HPAES component on mechanical properties of its blends with LPAES declined with increasing distance between branch points. A similar trend had been observed in gel content (Table 15) and FT-IR (Figure 53) analysis.

Table 19 Stress-strain curves of the annealed blend films of HBPAES-Si/LPAES (10/90 w/w)

Material code	E (MPa)	σ_{break} (MPa)	ε_{break} (%)
LPAES-F	2555±102	63.47±3.00	3.84±0.15
M0-0.85-BF	2738±110	59.48±3.40	2.91±0.21
O3-0.85-BF	2781±147	69.83±3.84	3.29±0.15
O7-0.85-BF	2807±210	57.59±4.30	2.46±0.13
O19-0.85-BF	2558±127	57.37±5.09	3.50±0.17
M0-0.85-Si-BF	2593±206	58.95±5.05	2.84±0.14
O3-0.85-Si-BF	2744±184	63.40±5.62	2.99±0.06
O7-0.85-Si-BF	2700±120	52.71±3.33	2.49±0.11
O19-0.85-Si-BF	2711± 73	65.21±1.90	3.83±0.11
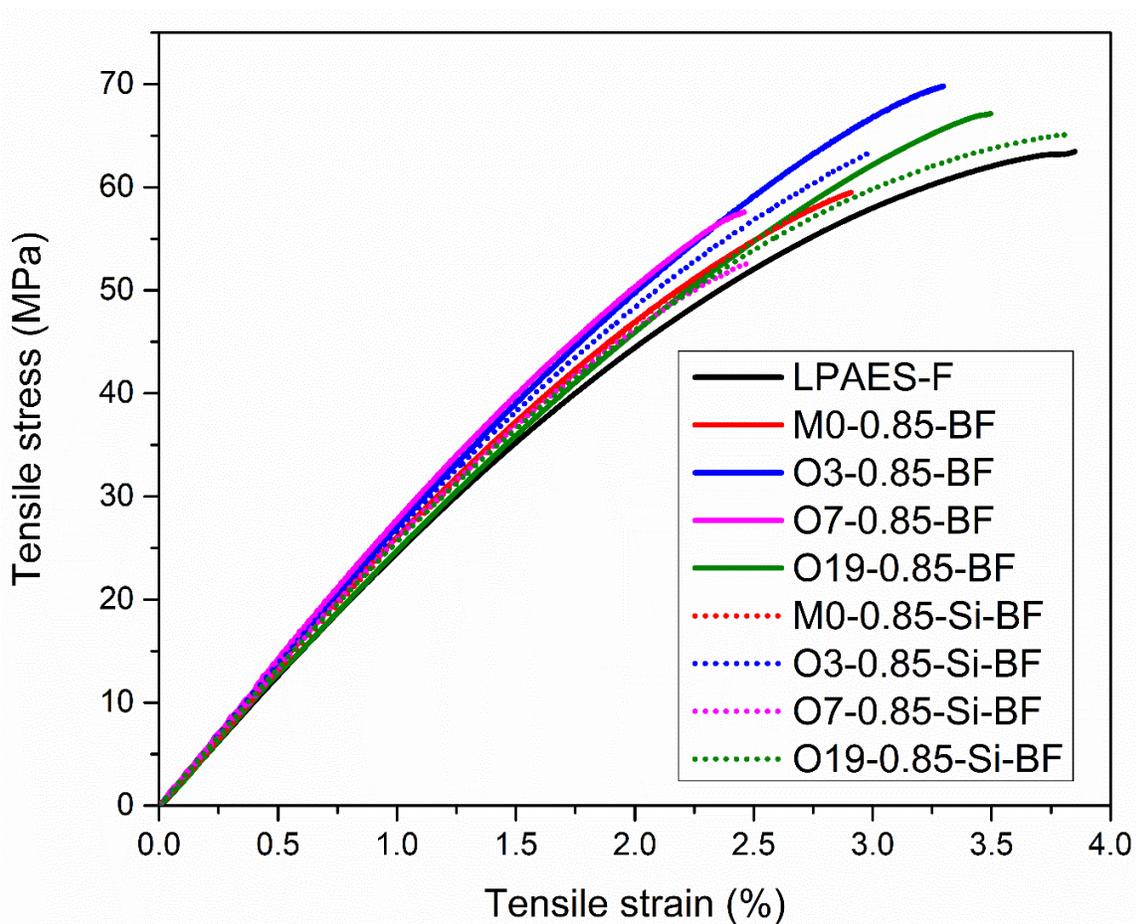
Figure 55 Stress-strain curves of annealed blend films: LPAES, M0-0.85-BF, M0-0.85-Si-BF, O3-0.85-BF, O3-0.85-Si-BF, O7-0.85-BF, O7-0.85-Si-BF, O19-0.85-BF, and O19-0.85-Si-BF; blend films containing 90% (w/w) LPAES.

The fracture surfaces of annealed neat LPAES and HBPAES-Si/LPAES blend films were analyzed by SEM imaging in detail. As a basis or control, the fracture surface of annealed LPAES-F specimens (Figure 56-a_1) showed that a lamellar and periodic alignment was present where the fracture was due to a transverse crack growth propagating in the lamellar structure. Crack propagation in the periodic lamellar microstructure was revealed by a zig-zag morphology as seen in Figure 56-a_2.

As discussed earlier, the annealed M0-0.85-BF represented the addition of a relatively small (M_w=13.5 kDa and the distance between branch points ≈ 7.54 Å) HBPAES samples into polymeric structure, hence resembled the nano-scale additives [180]. When compared to LPAES-F sample, the lamellar structure had entirely disappeared and replaced by local fibrillar regions dispersed in a slightly soft and un-oriented LPAES-F matrix (Figure 56-b_1). By the incorporation of silane functional groups into the M0-0.85 backbone, the fibril regions transformed into spherical regions in the fracture surfaces of corresponding M0-0.85-Si-BF samples. Local voids corresponding to the de-bonded fibril or spherical regions in both M0-0.85-BF and M0-0.85-Si-BF signal that the fibril and spherical regions, respectively, had poorer interactions with the surrounding matrix phase (Figure 56-b_2 & b_4) that supported the observed slight decrease in tensile strength.

As the distance between branch points increased, as per in the case of O3-0.85-BF (M_w = 46.8 kDa and the distance ≈ 28.1 Å), the fracture surface (Figure 56-c_1 & c_3) became much more homogenous. The branched O3-0.85 HB polymers were organized in LPAES to form rod-like structures [180]. Therefore, the fracture surfaces O3-0.85-BF and O3-0.85-Si-BF were different than the cases of LPAES-F (lamellar formation), M0-0.85-BF, and M0-0.85-Si-BF (nano-scale additives). The failure in this case was brittle and due to rapidly propagating transverse crack, a rather smooth fracture surface remained. The crack deflection towards the thickness (loading direction) of the specimens caused a rather block-like failure leaving steps and ridges towards the edge of the example in the fracture surface (Figure 56-

c_2 & c_4). A more homogeneous microstructure resulted in no change or an increase in tensile strength compared to the LPAES film.

When HBPAES additive became a bit larger as in the case of O7-0.85-BF (M_w = 130.2 kDa, branch distance= 64.2 Å), failure marks associated with the transverse failure reappeared (Figure 56-d_1), however different from LPAES-F crack propagation, which resulted in a similar block failure as appeared in O3-0.85-BF case (rod-like additive). However, the interaction domain for the branching additive was larger hence the orientation present in the control specimens still existed (not in lamellar form but similar to the morphology of O3-0.85-BF). The fracture surface of O7-0.85-Si-BF (Figure 56-d_3 & d_4) was quite similar to O3-0.85-Si-BF (Figure 56-c_2) as well.

The morphological transformation from LPAES-F by blending with HBPAES with increasing molecular weight and distance between branched points further continued with the O19-0.85-BF (M_w = 137.8 kDA branch distance= 172.7 Å) specimens, where two separate morphologies (lamellar formation in the middle and un-oriented plastic phase on top and bottom) were distinguishable (Figure 56-e_1 & e_2). The fracture surface homogeneity was disturbed, as the distance between branch points increased. Although the molecular weight was significantly higher than previous cases, T_g was relatively lower than LPAES-F, signaling the fact that middle oriented phase was a transition region between fibril phases appearing on M0-0.85-BF and lamellar LPAES. In contrast, the top and bottom morphologies were similar to O3-0.85-BF and O7-0.85-BF. Silane functionalization of O19-0.85 changed the fracture behavior of the corresponding annealed blend film, and the final appearance of the fracture surface (Figure 56-e_3 & e_4) resembled LPAES-F's zig-zag morphology.
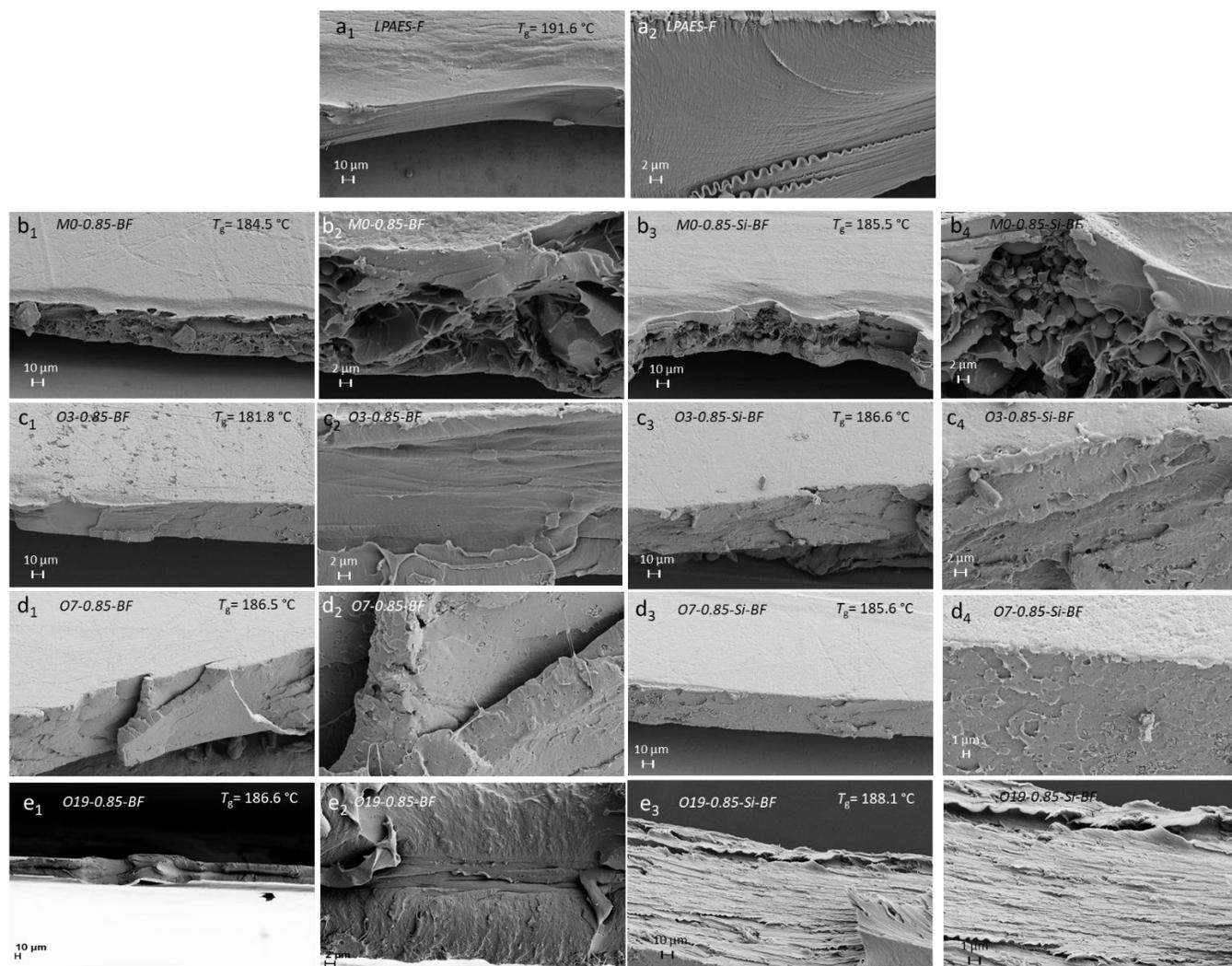
Figure 56 SEM images of fracture surface of annealed films a_{1-2}: LPAES-F; b_{1-2}: M0-0.85-BF; b_{3-4}: M0-0.85-Si-BF; c_{1-2}: O3-0.85-BF; c_{3-4} O3-0.85-Si-BF; d_{1-2}: O7-0.85-BF; d_{3-4} O7-0.85-Si-BF; e_{1-2}: O19-0.85-BF; e_{3-4} O19-0.85-Si-BF.

4.3. Conclusions

A set of HBPAESs was synthesized with varying distance between branch points via the A_2+B_3 polymerization at a A_2:B_3 ratio of 0.85 as potential additives for commercial LPAESs. Polymer blends were prepared in DMAc with a ratio of 10% (w/w) of HBPAES as an additive and 90% (w/w) of LPAES. The characterization of cast blend films by DSC and DMA indicated that linear and HB polymers were miscible with each other with a single T_g value, independent of the distance between branch points. Mechanical characterization of blend films showed that the incorporation of HBPAES affected the strength and strain at break values, and changed the fracture behavior of LPAES, and the distance between branch points played a critical role. O3-0.85-BF system had the highest Young's Modulus improvement, and the fracture surface analysis by SEM showed a morphology less prone to cracking, indicating that the use of an A_2 oligomer with a DP of 3, M_w of 46.8 kDa and approximate distance of 28.1 Å between branch points resulted in a HBPAES with optimum structural features for use as an additive to enhance mechanical properties of LPAESs. It was evident from the experimental R_h measurements using SEC analysis that as the distance between branch points was further increased as in O7.0.85-BF and O19-0.85-BF blends, HBPAESs acted more linear-like and their size converged to that of LPAES. On the other hand, when the distance between branch points of the HBPAES was as short as a monomeric unit, it acted as a nano-scale spherical additive in M0-0.85-BF system. Interestingly, it was not the strength of the non-bonded interactions provided by the rod-like formations in the blend, but rather their physical actions as anchoring regions that contributed to the increased strain at break values as a function of the degree of branching of the HB component.

All HBPAES were functionalized with IPTES to obtain ethoxysilane functional, self-crosslinking HBPAES samples with varying distance between branch points . The effect of the incorporation of inorganic, self-crosslinkable silane group into the HBPAES backbone became less significant on the final properties of corresponding blend films with LPAES as the distance between branch points of the HBPAES-Si sample increased. This finding was supported by FT-IR analysis and gel content measurements. Lastly, significant changes were observed in the mechanical, thermo-mechanical and morphological behavior of blend films

of silane functional HBPAESs with LPAES compared to neat LPAES and LPAES/HBPAES blend films.

This study reports pioneering results for further studies regarding the enhancement of the mechanical and thermo-mechanical properties of linear polymers by blending with their highly branched analogues with various functionalities to form thermoplastic or thermoset like structures for the fabrication of structural parts, membranes and films for high performance applications.

CHAPTER 5: Fabrication and characterization of UF membranes from highly branched and linear poly(arylene ether sulfone) blends

5.1. Introduction

Highly branched polymers can be used as additives for linear polymers because of their low solution viscosity and excellent solubility, as well as a multitude of functional end groups in the backbone, which can be easily converted to custom functionalities [66, 67]. While the use of highly branched polymers as additives have not been reported in water purification membranes, a few studies have reported the use of highly branched polymers to improve membrane properties and performance of proton-exchange membranes for fuel cells. For example, Zou and co-workers [68] developed new proton exchange membranes that were prepared with a mixture of sulfonated highly branched poly(arylene ether sulfone) and linear sulfonated polyether sulfone (SPES), which showed better water uptake, temperature dependence of the proton conductivity, and mechanical properties compared to the membranes consisting of linear SPES only. In another study, blend films were prepared and cured in DMAc by a Friedel–Craft acylation reaction between sulfonic acid end groups of hyperbranched polyether sulfone (HBPES) and electron-rich aromatic rings of linear poly(ether ether ether sulfone) in the presence of FeCl$_3$ [69]. While the mechanical properties of blend films were similar to that of the linear one, the proton conductivity in crosslinked blend films was improved. Spinodal decomposition into bicontinuous phases was observed in the blend films [69].

In this study, a series of HBPAESs with varying degree of branching and multifunctional or crosslinkable silane end groups was synthesized and used as additives to prepare polysulfone based UF membranes. Two sets of blend UF membranes were prepared using LPAES/ HBPAES (90/10 w/w) and LPAES/HBPAES-Si (90/10 w/w) in DMAc as described in Section 3. 4. The effect of the branching density and functional end groups of the HB

branched polymer on blend UF membranes was systematically investigated by morphological, performance, thermal, viscoelastic and mechanical analyses using SEM (Section 3.6.9), UF membrane performance tests (Section 3.6.14), zeta potential measurements (3.6.13), DMA (Section 3.6.7), DSC analysis (Section 3.6.6) and stress-strain test (Section 3.6.8).

5.2. Result and discussion

5.2.1. Membrane morphology

LPAES-UF membrane, which was prepared as the control specimen by the phase inversion technique from DMAc using LPAES only exhibited a sponge-like structure according to the surface and cross-section SEM images (Table 20). On the other hand, the addition of HBPAES and HBPAES-Si mainly changed the morphology of UF membrane from the sponge-like to finger-shaped (Table 21). Moreover, spherical particulates were observed in the surface and cross-section SEM images of HBPAES-Si-UF membranes. The pore sizes given in Figure 57 were calculated from the surface SEM images of UF membranes. All the control and blend membranes are observed to have pore sizes in the range of the UF scale. The spherical particulates were considered to be silica particles that likely originated by the self-condensation reaction of SiOEt end groups of HBPAES-Si. The size of spherical particulates on the membrane surface was in the range between 130 and 160 nm (Figure 58).

Table 20 SEM images from the surface (A1) and cross-section (A2) of the control UF membrane LPAES-UF

Surface of LPAES-UF	Cross-section of LPAES-UF
A1	A2
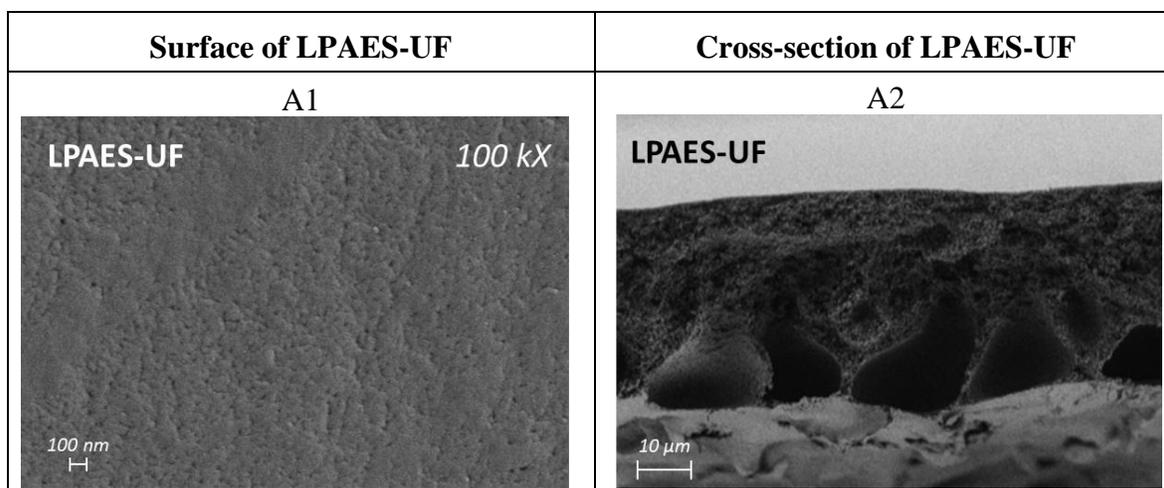
Table 21 SEM images from the surface and cross-section of the blend UF membranes B1&B2: M0-0.85-UF; B3&B4: M0-0.85-Si-UF; C1&C2: O3-0.85-UF; C3&C4: O3-0.85-Si-UF; D1&D2: O7-0.85-UF; D3&D4: O7-0.85-Si-UF; E1&E2: O19-0.85-UF; E3&E4: O19-0.85-Si-UF.

Surface of HBPAES-UF	Cross-section of HBPAES-UF	Surface of HBPAES-Si-UF	Cross-section of HBPAES-Si-UF
B1	B2	B3	B4
C1	C2	C3	C4
D1	D2	D3	D4
E1	E2	E3	E4
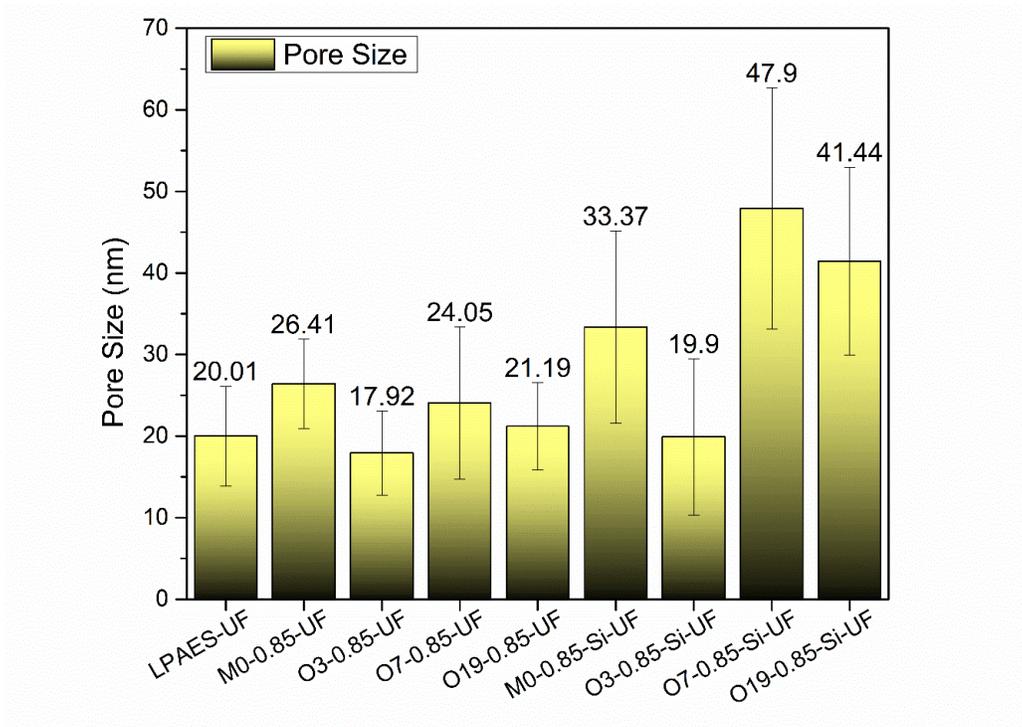
Figure 57 Pore sizes of the control and blend UF membranes determined from SEM images
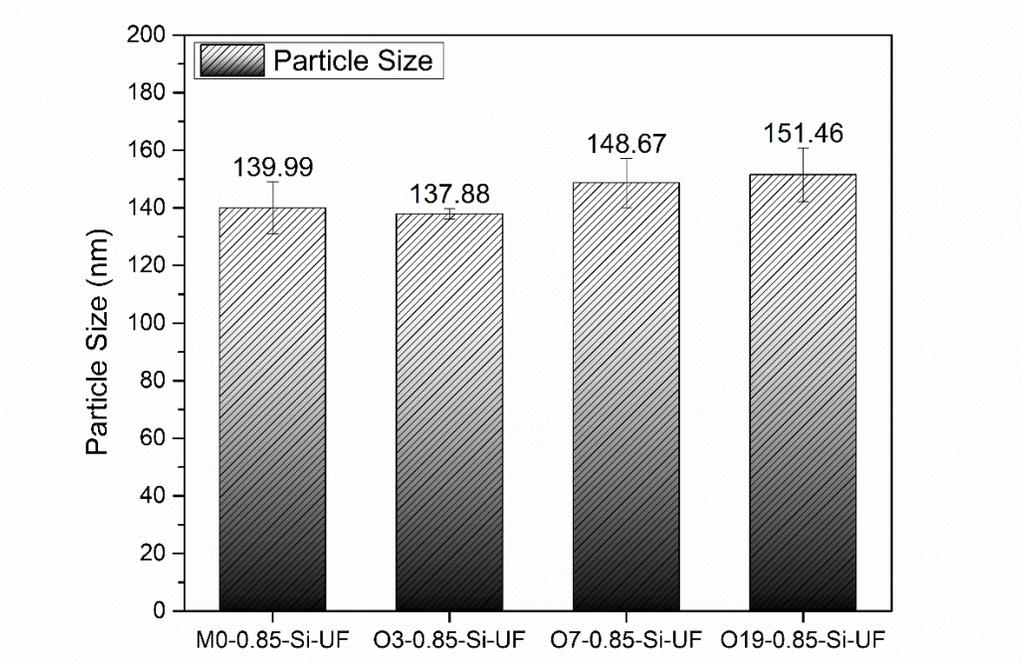
Figure 58 Size distribution of spherical particles on the HBPAES-Si containing blend UF membrane surfaces

5.2.2. Membrane performance

An indicative characteristic of UF membranes is the distilled water flux range and permeability. Thereby, all the control and blend membranes have been analyzed in the scope of flux and permeability performance, results of which are given in Figure 59 and Figure 60, respectively. Except for M0-, O7-, and O19-0.85-Si-UF, the membranes performed as UF membranes. The increases in the distilled water fluxes of M0-, O7-, and O19-0.85-Si-UF membranes were likely due to their larger pore sizes compared to their phenolic analogues and also the control membrane. Furthermore, the permeability measurements showed similar trends with pore sizes. In HBPAES containing blend UF membranes, the increasing distance between the branch points of the HPAES components was found to dictate the flux value, which could be a useful tool to tune the properties of UF membranes. A similar trend was observed in the case of oligomeric A_2-based HBPAES-Si containing blend UF membranes beginning with 2-3 fold higher flux values compared to their phenolic analogues.
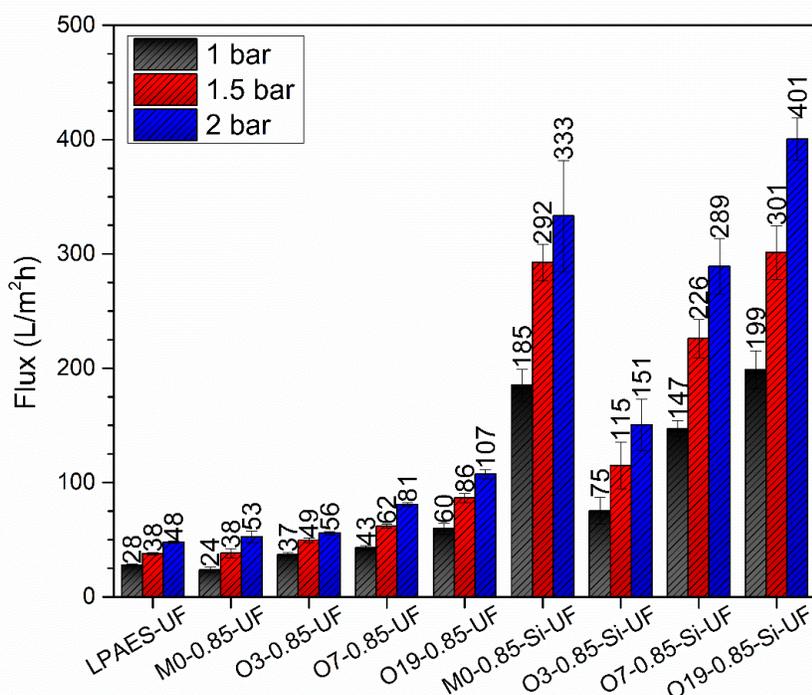
Figure 59 Distilled water fluxes of the control and blend UF membranes under 1.0, 1.5 and 2.0 bars
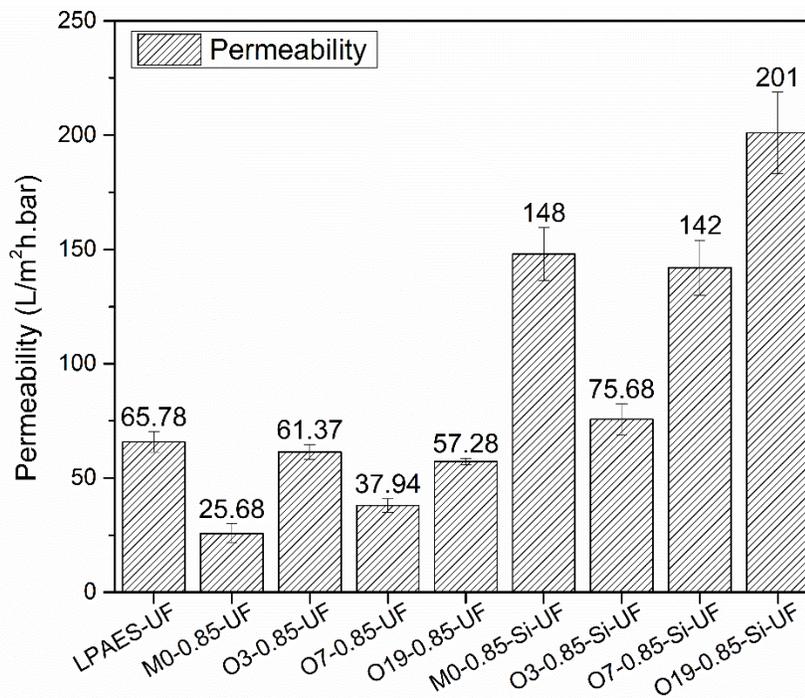
Figure 60 Distilled water permeability of the control and blend UF membranes

The zeta potential arises from the accumulation of electrical charges at the interface between a solid stationary layer and a mobile dispersed medium. Thus, an electrical double layer develops at the interface. Hence, the features of the surface of the stationary phase and the surrounding medium affect the zeta potential; moreover, that as an interfacial parameter brings understanding in the charge and adsorption properties of membrane surfaces.

The zeta potential of a membrane surface naturally responds when the pH of the mobile medium changes. Hence, measuring the liquid flow potential difference on the membrane surface in different pH ranges allows measuring the isoelectric point of the membrane surface.

The determination of the electrokinetic properties of the membranes allows the evaluation of operation conditions and chemical cleaning of the system. Zeta potential of the membrane surface is measured as a response to the changes in the pH of the mobile medium. The control and all blend membranes had negative zeta potentials on the membrane surface when the pH of the mobile medium was greater than 4. The zeta potential values are given in Figure 61.

Sulfone groups in the polymer backbone intrinsically possess negative charges which are expected to prevent the fouling of the membrane surface during the filtration of pollutants with negative charges. It is known that the membrane fouling creates resistance to filtration and adversely affects the operating performance of the membrane. Reactive dyes utilized in the textile industry are negatively charged. Therefore, the negatively charged membrane surface is expected to repel these dyes and facilitates the passage of purified water. The addition of HBPAES or HBPAES-Si increased the zeta potential values of the blend membrane surfaces above pH values of 4. O3-0.85-UF was observed to be more stable against changing pH values. In general, HBPAES-Si containing blend UF membranes seemed to have higher surface negativity at increased pH values compared to the HBPAES containing membranes.
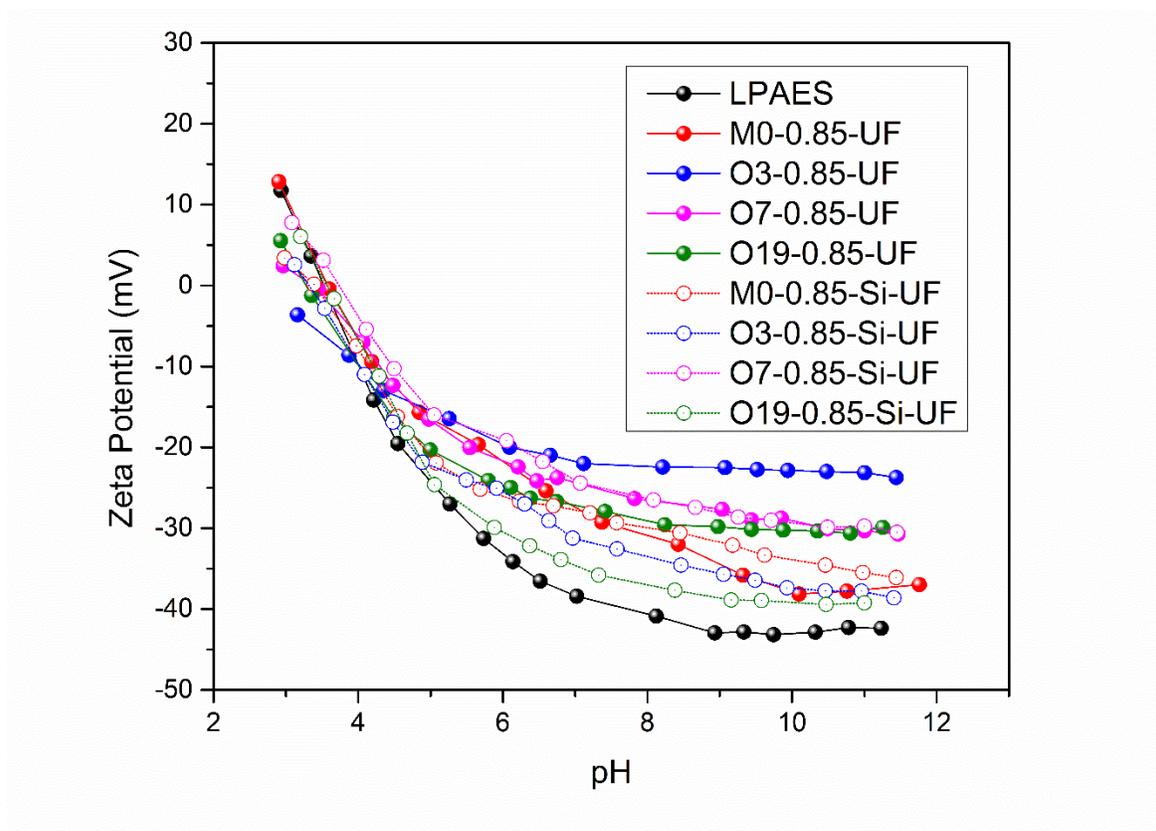
Figure 61 Zeta potential measurements of the control and blend UF membranes

To understand the role of blend UF membranes for the removal of dyes, 100 ppm solutions of Reactive Red 120 (Setazol Red) and Reactive Orange 16 dyes in distilled water were filtrated under 2 bar at RT (Figure 62). The molar masses of dyes are 1463 g/mol and 617.54 g/mol, respectively. Flux values of the control and blend UF membranes for dye solutions were lower compared to the pure water flux, yet they were slightly higher than the LPAES-UF control membrane. Blend UF membranes prepared with O3-, O7-, and O19-0.85 HBPAES samples, which had phenolic end groups, demonstrated an enhanced rejection performance when compared to the control specimen and M0-0.85-UF membrane. While the rejections of Setazol by O3-, O7-, O19-0.85-UF membranes were about 9-10%, the rejection of Reactive Orange 16 gradually decreased with the increase in the distance between branch points from 34.59% for the O3-0.85-UF membrane to 8.9% for the O19-0.85-UF membrane. Dye rejections of all membranes are given in Figure 63. On the other hand, blend membranes containing HBPAES-Si did not show any recovery or water treatment performance likely due to their larger pore sizes also evidenced by significantly higher flux values (Figure 62).
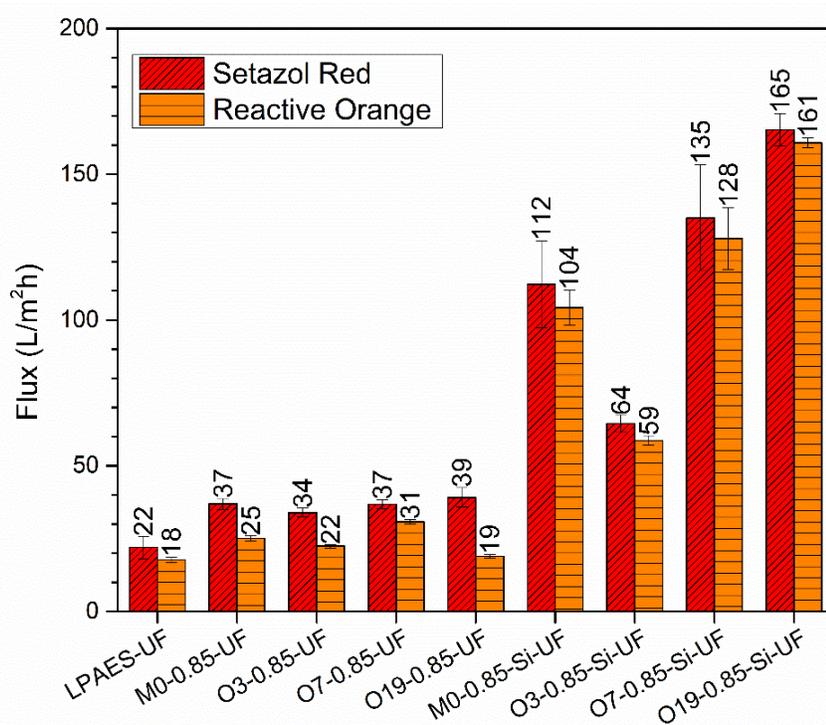
Figure 62 Setazol Red and Reactive Orange 16 flux values of the control and blend UF membranes at 2 bars
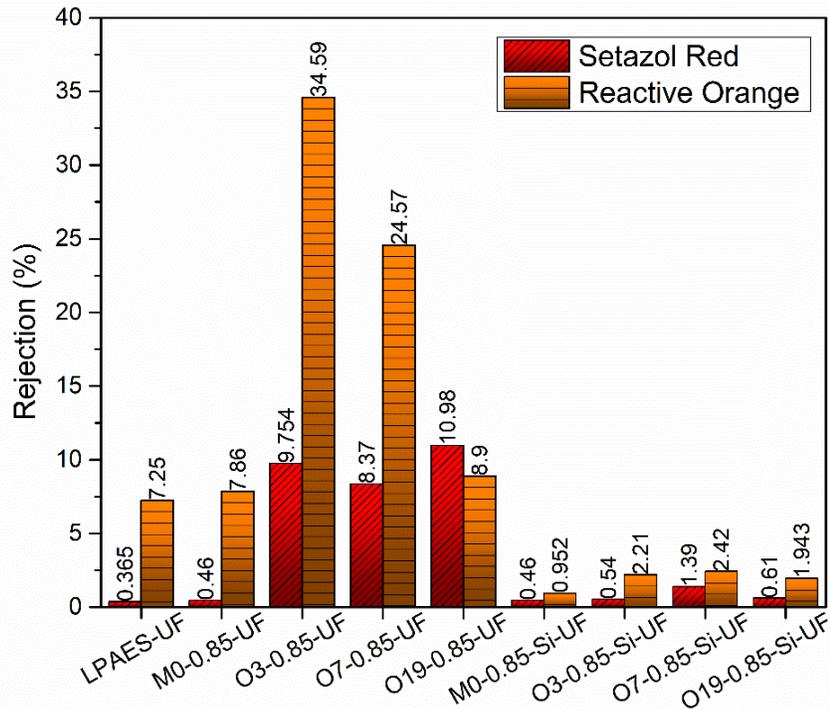
Figure 63 Setazol Red and Reactive Orange 16 dye rejections of the control and blend UF membranes at 2 bars

5.2.3. Thermomechanical analysis

In order to analyze the thermo-mechanical behavior of blend UF membranes, LPAES and its blends with HBPAES or HBPAES-Si (LPAES/HBPAES, 90/10 w/w) were characterized using DMA, and the thermograms are given in Figure 64. The storage modulus values of all of the blend UF membranes demonstrated significant improvements when compared with the control sample (LPAES-UF). Notably, the storage modulus of the silane functionalized O3-0.85-Si-UF membrane increased by almost 70%, despite higher porosity, showing the effect of the crosslinking. A decrease was observed in the thermo-mechanical behavior of O7-0.85-Si-UF presumed to be due to increased distance between crosslink points and thus decreased crosslink density as well as a lack of chain entanglement. O19-0.85-Si-UF exhibited higher storage modulus than O7-0.85-Si-UF, which can be ascribed to its higher chain length between crosslink points that could have enabled entanglement [238, 259]. All

UF membranes displayed single T_g values (Table 22 and Table 23), which showed that the phase inversion process didn't affect the blending of LPAES and HBPAES or HBPAES-Si, and they were all miscible.
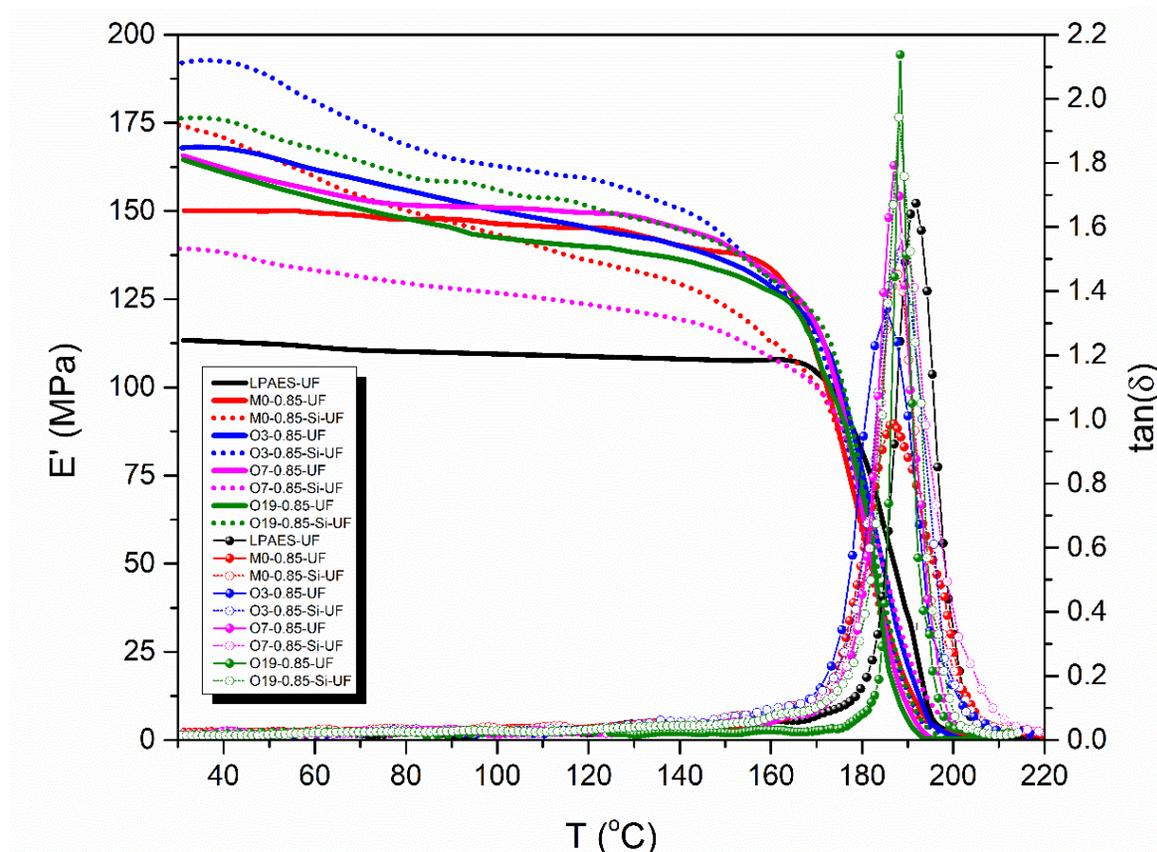
Figure 64 DMA thermograms of the control and blend UF membranes (LPAES/HBPAES, 90/10 w/w)

Table 22 DMA results of blend UF membranes: The storage modulus values at 30 °C and the T_g values from the peak points of tan(δ) curves

Material	E' (MPa) at 30 °C	tanδ T_g (°C)	Material	E' (MPa) at 30 °C	tanδ T_g (°C)
LPAES-UF	113.3	192.0	-	-	-
M0-0.85-UF	150.0	186.9	M0-0.85-Si-UF	174.4	187.9
O3-0.85-UF	167.9	185.4	O3-0.85-Si-UF	192.1	188.4
O7-0.85-UF	165.7	187.1	O7-0.85-Si-UF	139.2	189.1
O19-0.85-UF	164.6	188.4	O19-0.85-Si-UF	176.3	188.1

126

Table 23 Comparison of T_g values obtained by different methods

Material	T_g (°C) Fox Equation	T_g (°C) DMA tanδ curve	T_g (°C) DSC
LPAES-UF	-	192.0	187.5
M0-0.85-UF	187.8	186.9	185.4
O3-0.85-UF	186.2	185.4	183.4
O7-0.85-UF	190.5	187.1	183.1
O19-0.85-UF	191.1	188.4	187.2
M0-0.85-Si-UF	-	187.9	187.2
O3-0.85-Si-UF	191.1	188.4	185.1
O7-0.85-Si-UF	191.9	189.1	183.3
O19-0.85-Si-UF	192.1	188.1	184.8

5.2.4. Mechanical properties

Tensile stress-strain curves of LPAES/HBPAES blend UF membranes cast from DMAc solution and prepared by phase-inversion in distilled water are illustrated in Figure 65. The UF membranes with phenolic end groups exhibited a more ductile character than the control specimen (LPAES-UF), except for O19-0.85-UF. While most of the HBPAES-Si/LPAES membranes displayed lower mechanical performance than the control specimen, mechanical properties of O3-0.85-Si-UF was superior than others. As explained in Section 4.2.4, both O3-0.85-BF and O3-0.85-Si-BF blend films displayed the best mechanical performance, as also observed for the blend membrane systems of O3-0.85 and O3-0.85-Si, which could indicated that 03-0.85 HBPAES sample had an optimum composition for HB/linear PAES blends and their UF membranes.
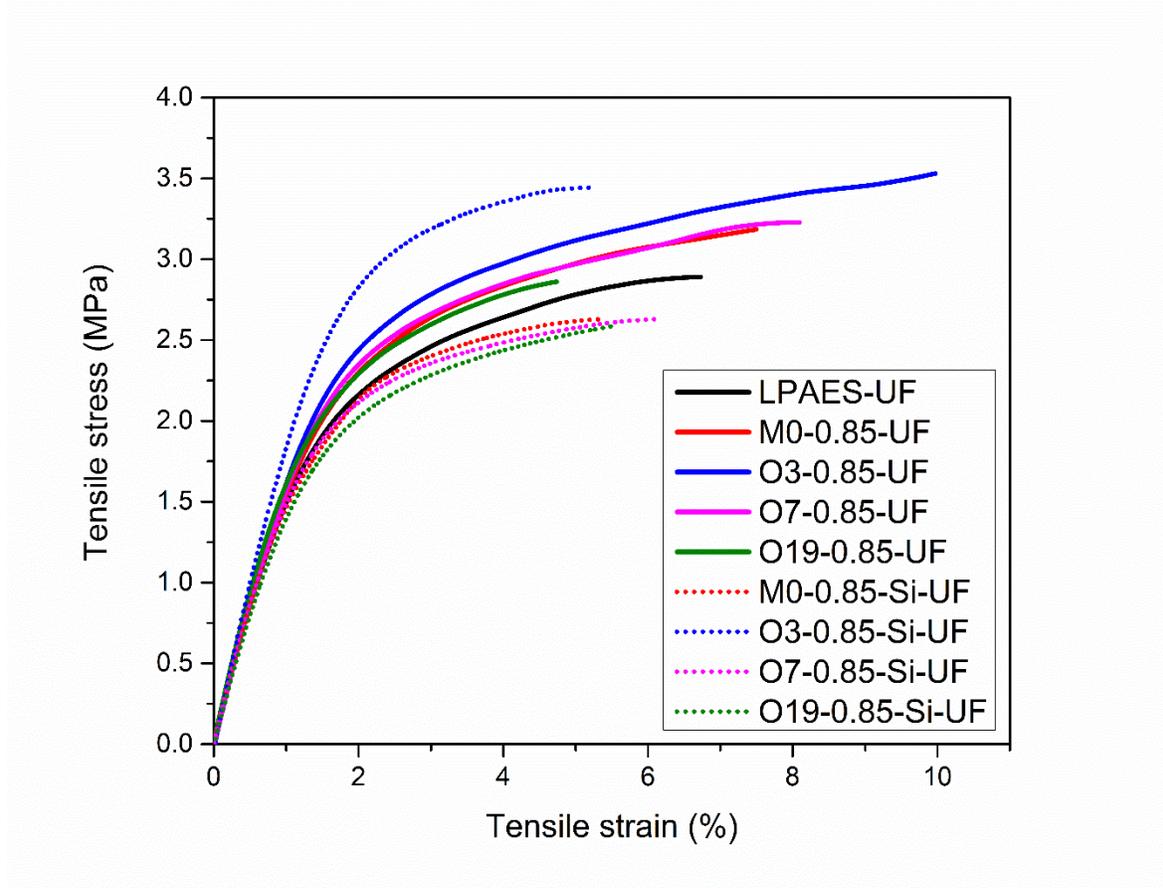
Figure 65 The stress-strain curves of UF membranes of LPAES and its blends with HBPAES and HBPAES-Si (LPAES/HBPAES or HBPAES-Si, 90/10 w/w)

Table 24 Tensile test results of blend UF membranes (ASTM D1708)

Material	Tensile Modulus (MPa)	Tensile Stress at break (MPa)	Tensile Strain at break (%)
LPAES-UF	197.40 ± 8.35	2.89 ± 0.12	6.73 ± 0.28
M0-0.85-UF	199.63 ± 6.43	3.18 ± 0.10	7.48 ± 0.24
O3-0.85-UF	206.99 ± 4.62	3.53 ± 0.08	9.97 ± 0.22
O7-0.85-UF	206.81 ± 7.91	3.23 ± 0.12	8.09 ± 0.31
O19-0.85-UF	207.67 ± 8.78	2.86 ± 0.11	4.73 ± 0.20
M0-0.85-Si-UF	161.59 ± 6.83	2.63 ± 0.12	5.31 ± 0.22
O3-0.85-Si-UF	239.23 ± 5.33	3.44 ± 0.08	5.23± 0.11
O7-0.85-Si-UF	191.73 ± 5.60	2.63 ± 0.08	6.12 ± 0.18
O19-0.85-Si-UF	190.28 ± 4.61	2.58 ± 0.06	5.48 ± 0.13

5.3. Conclusions

A series of HBPAESs with varying degrees of branching and a multitude of phenol functional or crosslinkable silane end groups were synthesized and used as additives in polysulfone based UF membranes. The membrane morphology and performance were affected by the incorporation of HBPAES or HBPAES-Si components, and also by their degree of branching. While LPAES-based UF membranes exhibited a sponge-like structure, blend UF membranes containing HBPAES and HBPAES-Si were finger-like. As a result of the addition of HBPAES or HBPAES-Si into LPAES, homogenous blend UF membranes with single T_g values were obtained. DMA results showed that the thermomechanical properties of the LPAES-UF membranes were improved by the addition of HBPAES or HBPAES-Si. All HBPAES-UF and O3-0.85-Si-UF membranes showed higher tensile strength compared to the control membrane. However, the mechanical properties of blend membranes were adversely affected by the incorporation of silane functional of M0-, O7-, and O19-0.85. O3-0.85 sample was demonstrated to have an optimum distance between branch points that was presumed to enable a homogenous blending with its linear analogue, and improve thermo-mechanical, mechanical and morphological properties of resulting blend films and UF membranes. The controlled distance between the branch points of the phenol functional HBPAES component was demonstrated as a useful tool to tune the water permeability and dye rejection of resulting blend UF membranes. On the other hand, the incorporation of HBPAES-Si samples into UF membranes resulted in larger pore sizes and significantly higher water permeability with insignificant dye rejection. Yet, O3-0.85-Si-UF sample showed promising results as a support layer for TFC membranes with its enhanced mechanical, thermo-mechanical and water permeation performance.

CHAPTER 6: Fabrication and characterization of TFC NF membranes from highly branched, sulfonated, functional poly(arylene ether sulfone)s

6.1. Introduction

NF is a pressure-driven separation technique like MF, UF, and RO. The separation efficiency of NF membranes is between UF and RO membranes; UF membranes can reject dissolved macromolecules higher than 5000 Da, and RO membranes can retain almost all kinds of salts and small molecules greater than 100 Da with a high rejection ratio [80].

The active layer of NF membranes is usually fabricated via the interfacial polymerization occurred between monomer solutions, which are immiscible to each other. The interfacial polymerization reaction occurs mostly in the organic phase because of the low solubility of the organic reagent in the aqueous phase [82, 260]. The main reason for choosing the interfacial polymerization technique is the fact that an extremely thin active layer can be formed on a porous support layer. Also, although the reaction rate is high between the TMC in the organic phase and a nucleophilic monomer in the aqueous phase, the reaction occurs at the interface as the formation of the active layer continues, while the monomer transportation to the interface is limited. Thus, the reaction is diffusion controlled, and the formation of the active layer is self-limited. In summary, a very thin and uniform active layer can be produced on a porous support layer via the interfacial polymerization technique, and as a consequence, NF membranes with this kind of active layer have high rejection yields for polyvalent ions and small organic compounds at moderate pressures.

This study reports the use of hydrophilic, phenol functional SHBPAES in the aqueous phase for the fabrication of TFC NF membranes on PAES-based sponge-like porous support membranes by interfacial polymerization in the presence of TMC in the organic phase. The effect of the degree of branching of sulfonated HB polymer on the performance of fabricated NF membranes was systematically investigated by permeability and rejection measurements

using water, textile dyes, and both monovalent and divalent salts. This pioneering study reports the importance of a structure-morphology relationship on the arylate sulfone-based TFC membranes for the first time in the literature.

Using SDCDPS as the A_2 monomer enabled the attainment of hydrophilicity in the HBPAES polymer synthesized by A_2+B_3 polymerization. This hydrophilicity enabled the ability to disperse resulting branched polymers in water. With this method, two sets of SHBPAESs were synthesized as described in Section 3.2.4. In the first set, ionic and non-ionic A_2 monomers, SDCDPS and DCDPS, respectively, were used in combination with a 50/50 (n/n) ratio and the synthesized SHBPAESs were denoted as SMM0. In the second set, SDCDPS was used as the only A_2 monomer and the synthesized SHBPAESs were denoted as SM0. All branched polymers were characterized via NMR spectroscopy (Section 3.6.1), SEC (Section 3.6.3), TGA (Section 3.6.5), and DSC (Section 3.6.6).

Prior to the fabrication of TFC NF active layer comprised of TMC and SHBPAES network, in order to understand the behavior and reactivity of phenol end groups with TMC, a series TFC membranes were prepared by the interfacial polymerization of TMC in the organic phase and a combination of PIP and THPE (B_3 monomer of the SHBPAES) to obtain hybrid poly(amide-arylate) active layers. These TFC membranes were characterized by zeta potential, FT-IR spectroscopy (Section 3.6.2), contact angle measurements (Section 3.6.11) and filtration performance tests (Section 3.6.15). Next, TFC NF membranes were prepared via the interfacial polymerization reaction between phenol functional SHBPAES in an aqueous phase and TMC in the organic phase (hexane) (Section 3. 5). These TFC membranes are a first attempt in the literature to produce poly(arylate sulfone)-based active layers. The effect of the ionic character of SHBPAES on the morphology, membrane performance was investigated with SEM (Section 3.6.9) and NF membrane performance tests (Section 3.6.15).

6.2.   Results & Discussion

6.2.1. Hybrid poly(amide-arylate) TFC membranes from THPE, PIP and TMC

Seven different TFC membranes were produced using THPE and PIP as nucleophilic monomers to react with TMC to obtain hybrid poly(amide-arylate) networks via interfacial polymerization on polysulfone-based support membranes. PIP and THPE were bifunctional

and trifunctional monomers in the aqueous phase, respectively; and also, TMC was a trifunctional monomer in hexane used as the organic phase. THPE and PIP in the aqueous phase were presumed to migrate to the interphase between water and hexane in order to react with TMC to form a very thin, active layer with a thickness of hundreds of nanometers. Fabricated TFC membranes were named as THPE-X, where x designated the mol percentage of THPE in the THPE/PIP mixture in the aqueous phase. TFC membranes containing 10 to 90 mol% THPE composed of hybrid poly(amide-arylate) networks. THPE-0 sample composed of solely a polyamide-based active layer, whereas THPE-100 sample composed of solely a polyarylate network. Key parameters for the fabrication of polyamide, polyarylate and hybrid poly(amide-arylate) TFC membranes are given in Table 25.

Distilled water fluxes of fabricated TFC membranes were determined under four different pressures of 6, 9, 12, and 15 bar as shown in Figure 69. THPE-0 sample was prepared as a control membrane since polyamide-based TFC membranes are the most common commercial NF membrane. THPE-10, -30, and -100 did not demonstrate a TFC membrane performance. However, their distilled water flux values fall in the range of a tight UF membrane [261]. On the other hand, the TFC membranes of THPE-70 and -90 have higher distilled water fluxes than the control membrane, whereas THPE-50 has a lower flux value. Overall, the flux values of all TFC membranes increase as applied pressures increase as expected.

Table 25 Parameters of TFC membrane fabrication with an interpenetrating network by PIP and THPE

TFC Membrane	Monomer	Monomer % in medium (w/w)	Monomer weight (g)	Monomer moles (mmol)	Monomer mol fractions in aqueous phase (%)	Solvent	Solvent weight (g)	mol% of THPE in THPE+PIP monomers (n/n)	Duration (s)	Oven Curing Temperature (°C)	Oven Curing Time (min)
THPE-0	PIP	2.00	0.50	11.61	100	Water	24.50	0	120	70	5
	THPE	0.00	0.00	0.00	0						
	TMC	0.20	0.05	0.57	-	Hexane	24.95		60		
THPE-10	PIP	1.80	0.45	10.45	90	Water	24.43	10	120	70	5
	THPE	0.47	0.12	1.16	10						
	TMC	0.20	0.05	0.57	-	Hexane	24.95		60		
THPE-30	PIP	1.40	0.35	8.13	70	Water	24.29	30	120	70	5
	THPE	1.42	0.36	3.48	30						
	TMC	0.20	0.05	0.57	-	Hexane	24.95		60		
THPE-50	PIP	1.00	0.25	5.80	50	Water	24.16	50	120	70	5
	THPE	2.37	0.59	5.80	50						
	TMC	0.20	0.05	0.57	-	Hexane	24.95		60		
THPE-70	PIP	0.60	0.15	3.48	30	Water	24.02	70	120	70	5
	THPE	3.32	0.83	8.13	70						
	TMC	0.20	0.05	0.57	-	Hexane	24.95		60		
THPE-90	PIP	0.42	0.36	1.16	10	Water	23.58	90	120	70	5
	THPE	4.27	1.07	10.45	90						
	TMC	0.20	0.05	0.57		Hexane	24.95		60		
THPE-100	PIP	0.00	0.00	0.00	0	Water	21.44	100	120	70	5
	THPE	14.23	3.56	11.61	100						
	TMC	0.20	0.05	0.57		Hexane	24.95		60		

The zeta potentials of the control (from PIP + TMC) and hybrid (from PIP/THPE + TMC) TFC membranes were measured as a function of pH in 1.0 mM KCl electrolyte solution from pH values 4 to 11 by addition of 0.05 M HCl or NaOH via the automatic titration. As can be seen in Figure 66, the control membrane showed the lowest zeta potential in the pH range from 4 to 11, whereas the poly(arylate) THPE-100 membrane showed the highest zeta potential values in the same range. When focused on the pH range of 7 to 11, the zeta potential values of the membrane surfaces gradually increased with increasing mole fraction of THPE in the THPE/PIP aqueous phase, which could be ascribed to the increasing content of more hydrophobic arylate groups compared to hydrophilic amide linkages formed with aliphatic PIP. As a result, the surface hydrophobicity of hybrid membranes systematically increased as a function of the THPE content as evidenced by surface contact angle measurements in Figure 67.
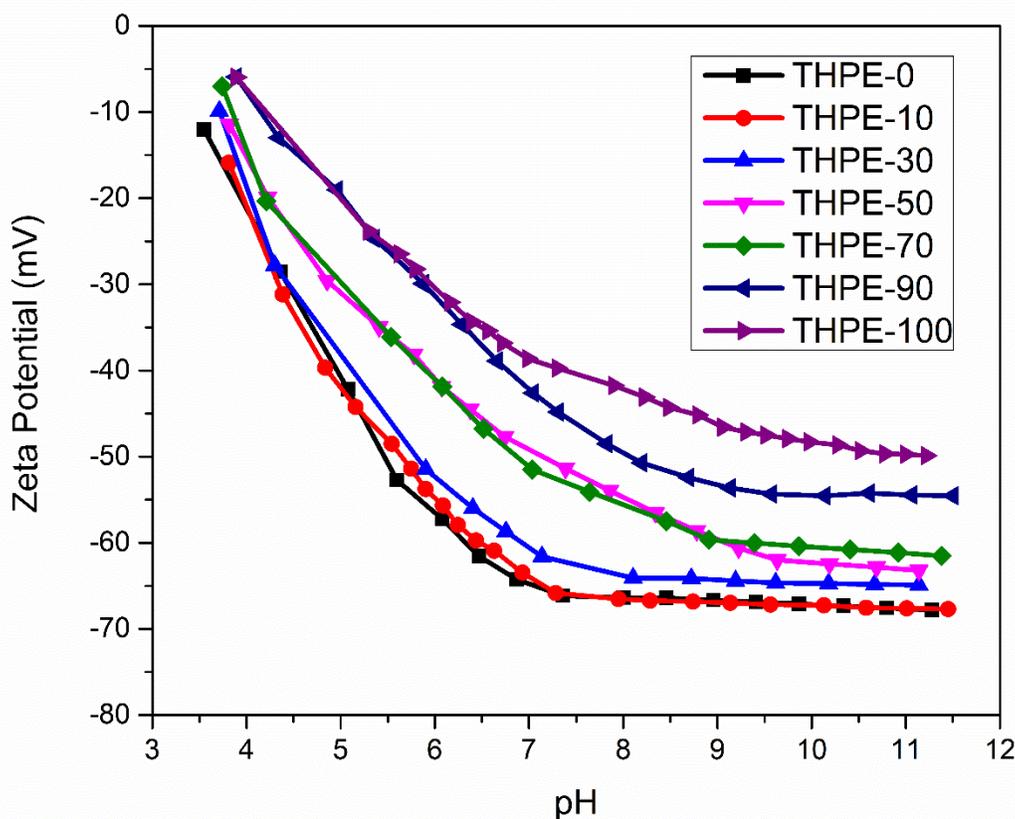
Figure 66 Zeta potential plot of TFC membranes: THPE-0, 30, 50, 70, 90, and 100.
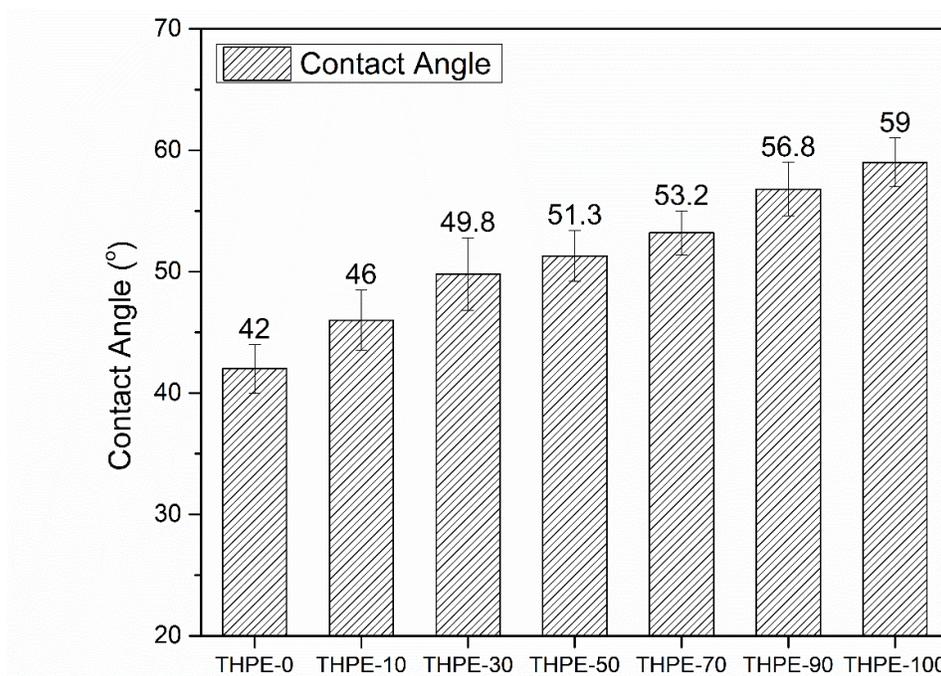
Figure 67 Contact angle measurements of TFC membranes: THPE-0, 30, 50, 70, 90, and 100.

The FT-IR spectra of all TFC membranes prepared from a reaction of TMC with a series of THPE:PIP mole fractions at pH 13 are illustrated in Figure 68. In the FT-IR spectrum of the control membrane (THPE-0), a medium broad band at $1611 – 1632$ cm^{-1} corresponding to the C=O band of amide groups confirmed the polyamide active layer. In the spectrum of THPE-100, which had a pure polyarylate active layer, the C=O band of arylate was found at a higher energy region (1624 cm^{-1}) when compared to polyamide (1611 cm^{-1}), whereas hybrid poly(amide-arylate) membranes showed had carbonyl peaks proportional to the THPE:PIP molar ratio. Furthermore, a broad band at $3418 – 3460$ cm^{-1} corresponding to O–H stretching indicated not only the formation of carboxylic acids by the partial hydrolysis of the acyl chloride of TMC but also unreacted phenol groups of THPE. From the FT-IR spectra, it could be deduced that the intensity of the O–H peak increased as the mole fraction of THPE increased.
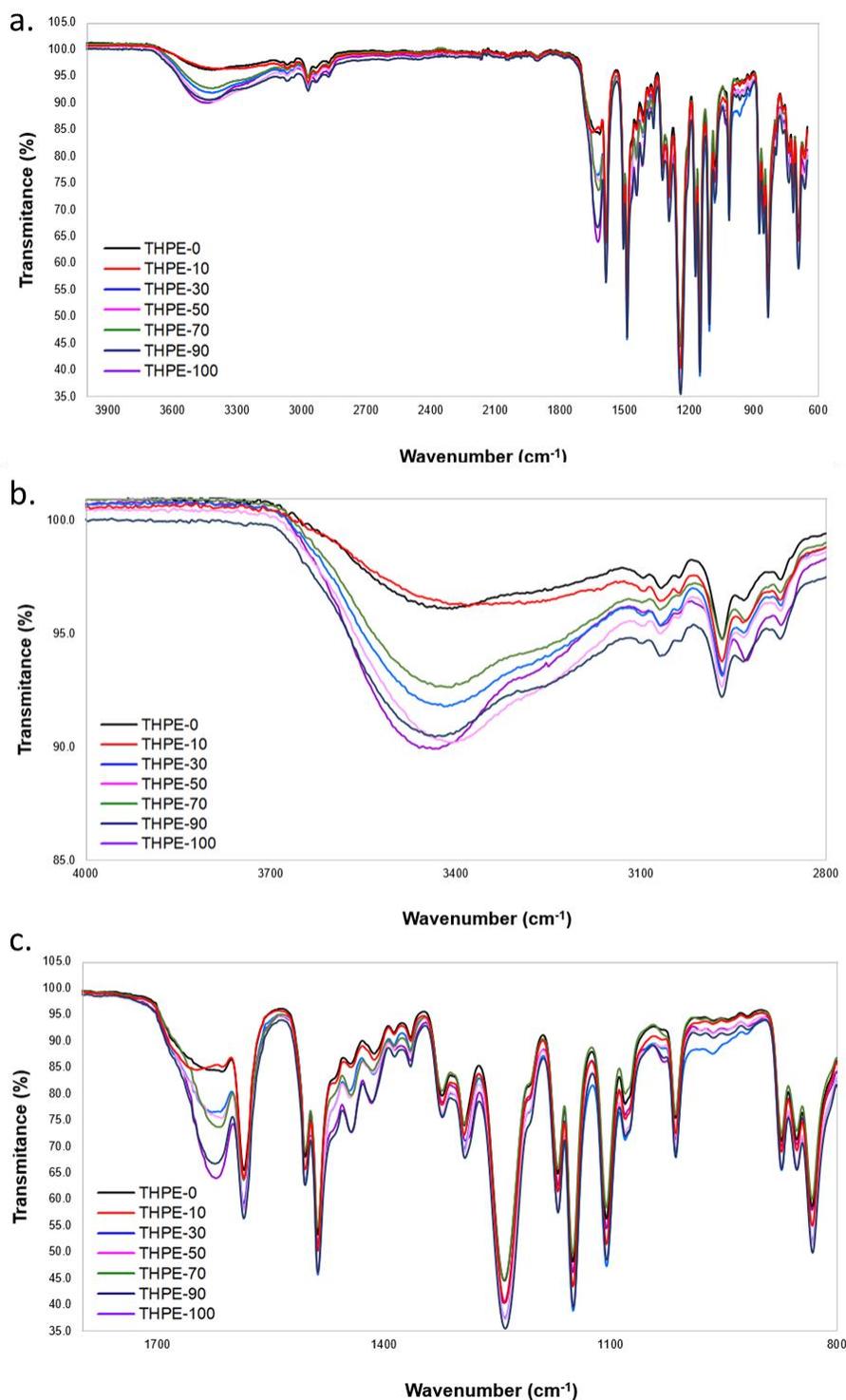
Figure 68 FT-IR transmittance spectra of the active layers of TFC membranes: THPE-0, 30, 50, 70, 90, and 100; a. between 4000 and 600 cm^{-1}, b. between 4000 and 2800 cm^{-1}, c. between 1800 and 800 cm^{-1}

Lastly, as shown in Table 26, the incorporation of arylate groups into the polyamide network was not found to have an effect on the T_g of the TFC active layer. The pure polyamide-based, pure polyarylate-based, and the hybrid poly(amide-arylate) TFC active layer all showed T_g values around 90 °C.

Table 26 T_g of TFC membranes; THPE-0, THPE-50, and THPE-100

TFC Active layer	T_g (°C) from DSC analysis
THPE-0	90.18
THPE-50	89.42
THPE-100	89.47
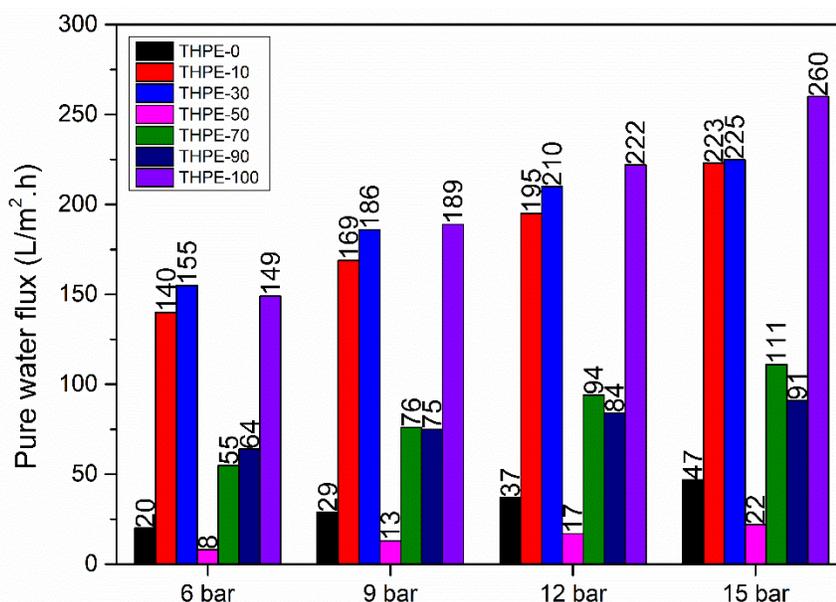
Figure 69 Results of pure water flux of TFC membranes: THPE-0, 30, 50, 70, 90, and 100.

$MgSO_4$ solution flux and rejection results of fabricated TFC membranes, which were obtained by using 2000 ppm $MgSO_4$ in aqueous solution, are given in Figure 70 and Figure 71, respectively. A decline was observed in the $MgSO_4$ flux values of all membranes compared to the distilled water flux, which might be originating from the interaction between the membrane surface and the $MgSO_4$ salt molecules. $MgSO_4$ rejection performance of hybrid poly(amide-arylate) TFC membranes was lower compared to the pure polyamide-based THPE-0 membrane. However, THPE-50 and THPE-90 membranes exhibited $MgSO_4$ rejection in the orders of 60%.
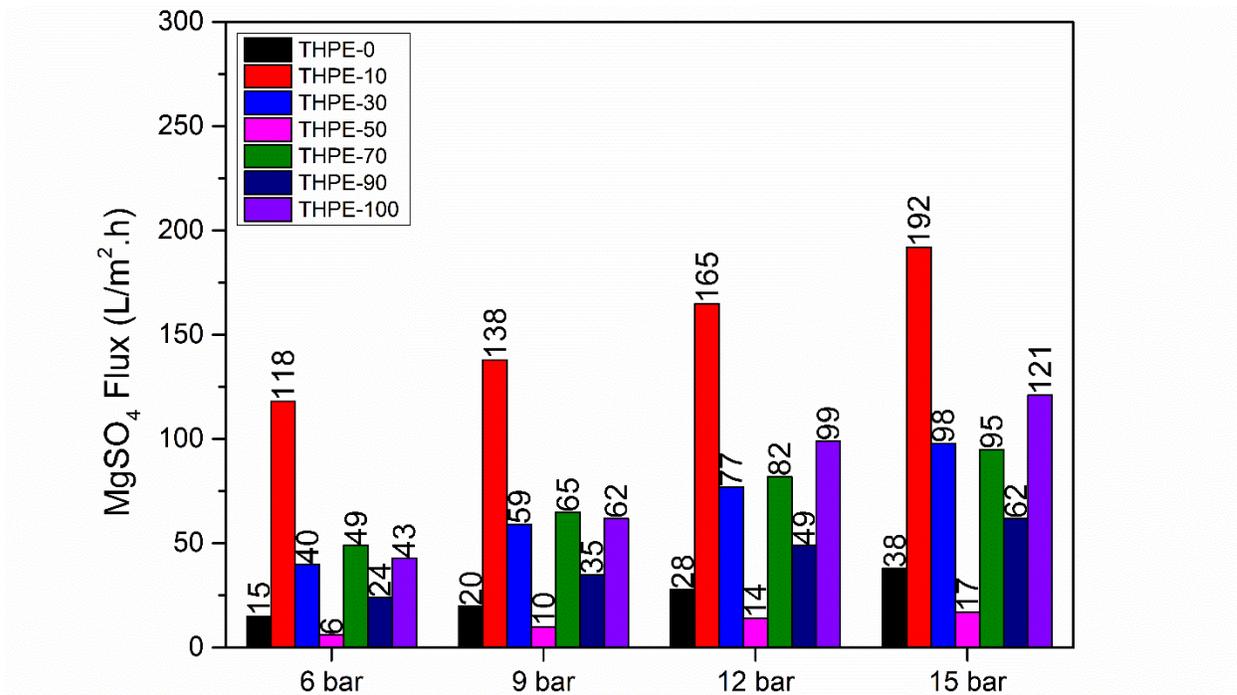
Figure 70 Results of 2000 ppm MgSO₄ aqueous solution flux of TFC membranes: THPE-0, 30, 50, 70, 90, and 100.
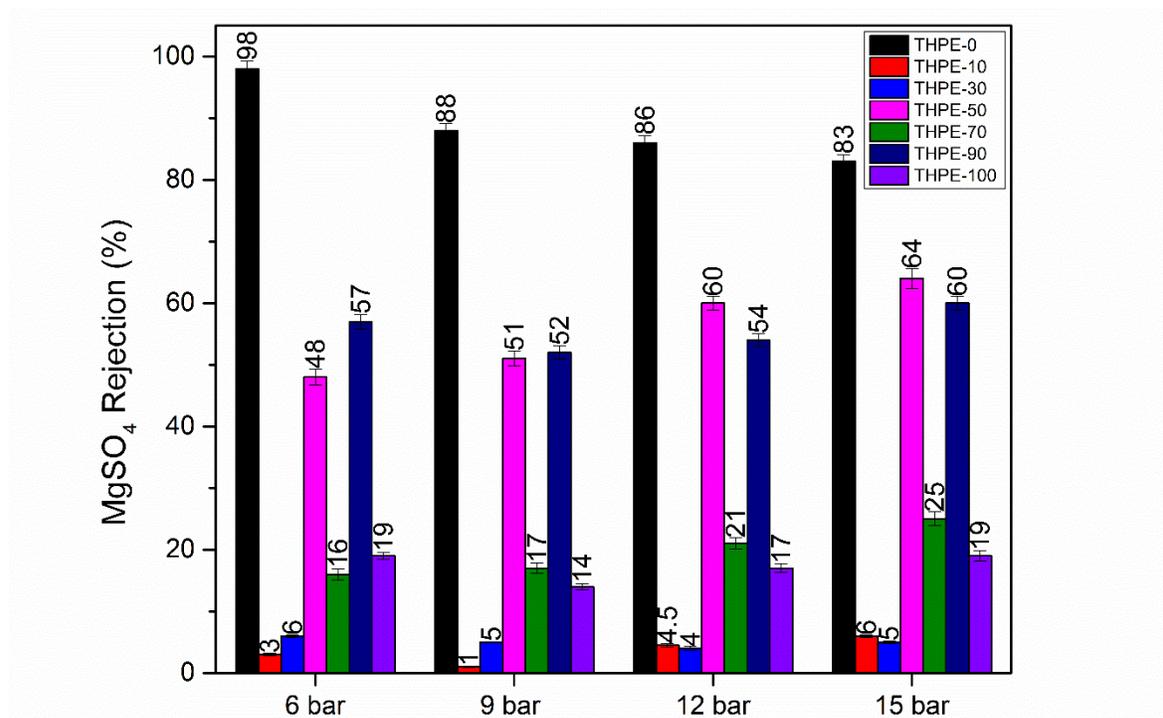
Figure 71 MgSO₄ rejection results of TFC membranes: THPE-0, 30, 50, 70, 90, and 100.

Flux and rejection performances of the TFC membranes were also investigated under four different pressures with 2000 ppm NaCl solution. The NaCl flux and NaCl rejection results are given in Figure 72 and Figure 73. The flux values were slightly higher compared to the flux values of $MgSO_4$ solution and pure water. While NaCl rejections of the TFC membranes except for THPE-50 were drastically less than the control membrane, THPE-50 exhibited an average 96% rejection, which was significantly superior than the control membrane, although it showed a low flux value. This high selectivity towards monovalent ions was presumed to be related to the charge balance on the membrane surface of this specific composition.
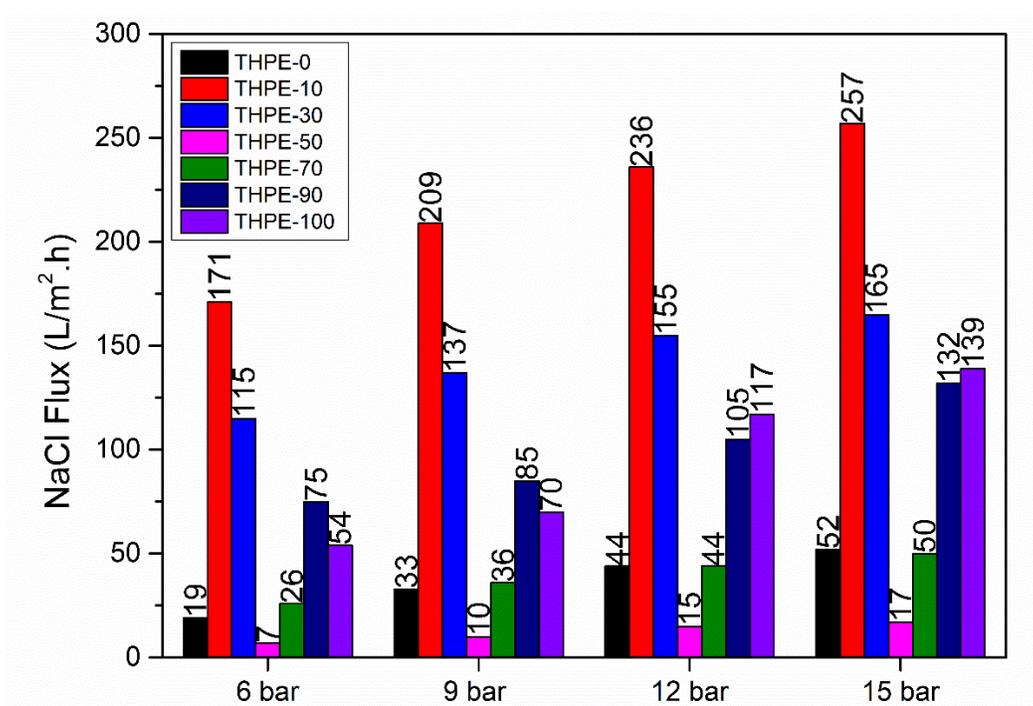
Figure 72 Results of 2000 ppm NaCl aqueous solution flux of TFC membranes: THPE-0, 30, 50, 70, 90, and 100.
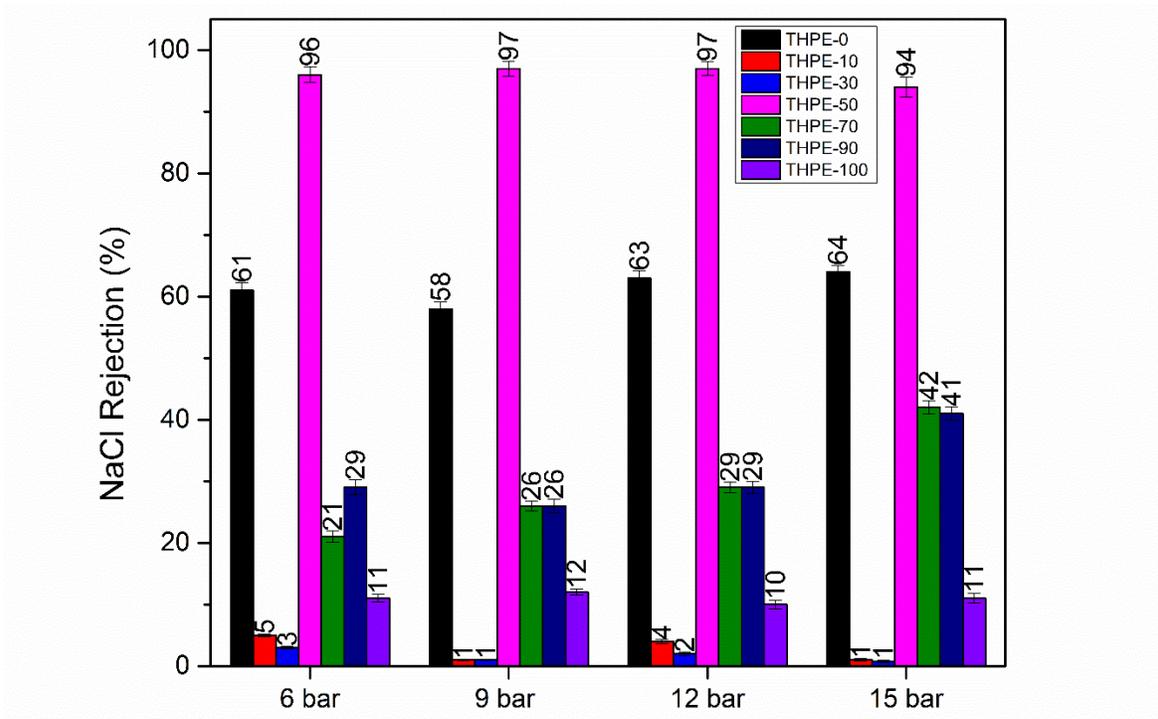
Figure 73 NaCl rejection results of TFC membranes: THPE-0, 30, 50, 70, 90, and 100.

The filtration performance of fabricated hybrid TFC membranes was also evaluated under four different pressures using a 100 ppm aqueous solution of Setazol Red synthetic dye. The flux and rejection results are given with Figure 74 and Figure 75, respectively. Except for the THPE-50 membrane, it could be concluded that the Setazol Red removal efficiencies of hybrid poly(amide-arylate) TFC membranes were lower compared to the THPE-0 membrane.
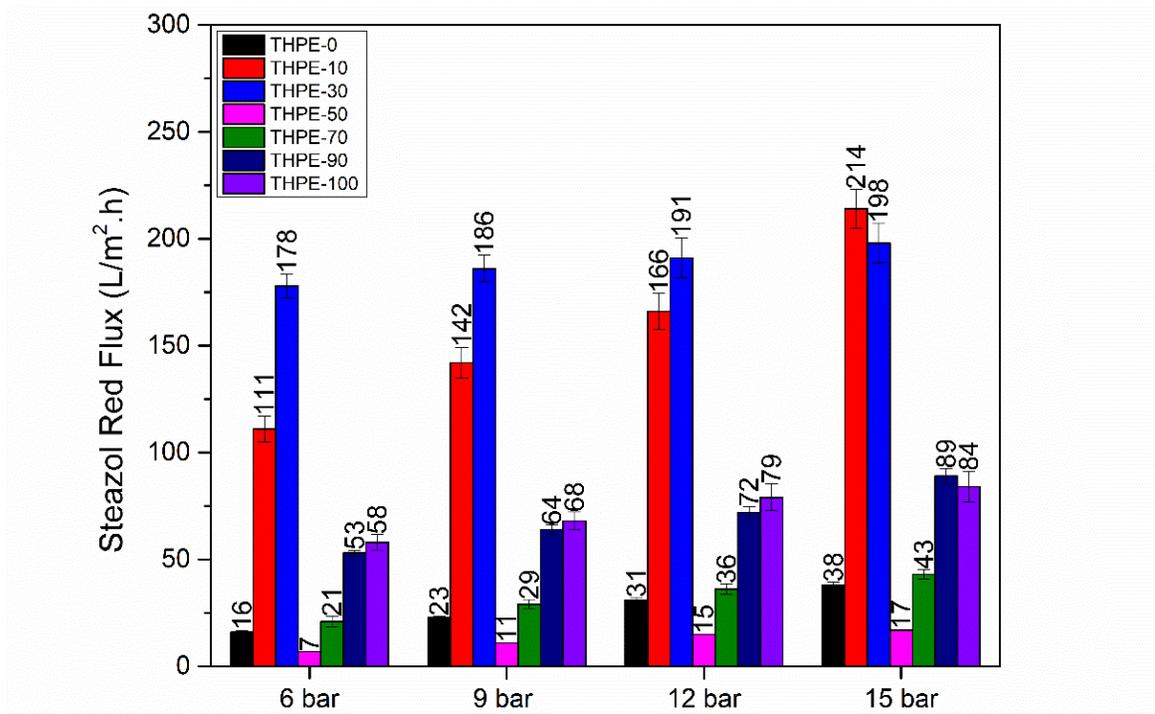
Figure 74 Results of 100 ppm Setazol Red aqueous solution flux of TFC membranes: THPE-0, 30, 50, 70, 90, and 100.
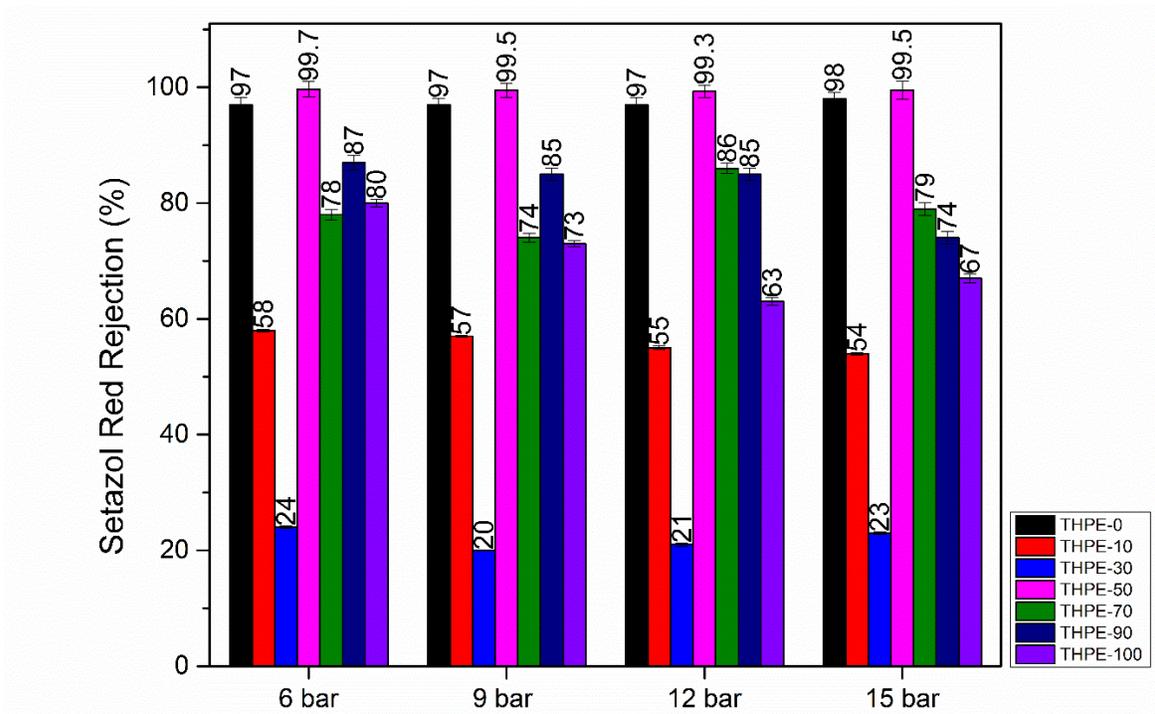
Figure 75 Setazol Red rejection results of TFC membranes: THPE-0, 30, 50, 70, 90, and 100.

Filtration tests were also carried out using a 100 ppm aqueous solution of Reactive Orange 120, which had a lower molecular weight than Setazol Red dye. The flux and rejection results are given in Figure 76 and Figure 77, respectively. Similarly, except for the THPE-50 membrane, hybrid TFC membranes showed lower rejection performance when compared to the THPE-0 membrane. The photographs of filtrates of both Setazol Red and Reactive Orange 120 solutions obtained from each membrane under four different pressures are illustrated in Table 27. Obviously, THPE-50 showed the highest dye rejections compared to both the control membrane and the other TFC membranes.
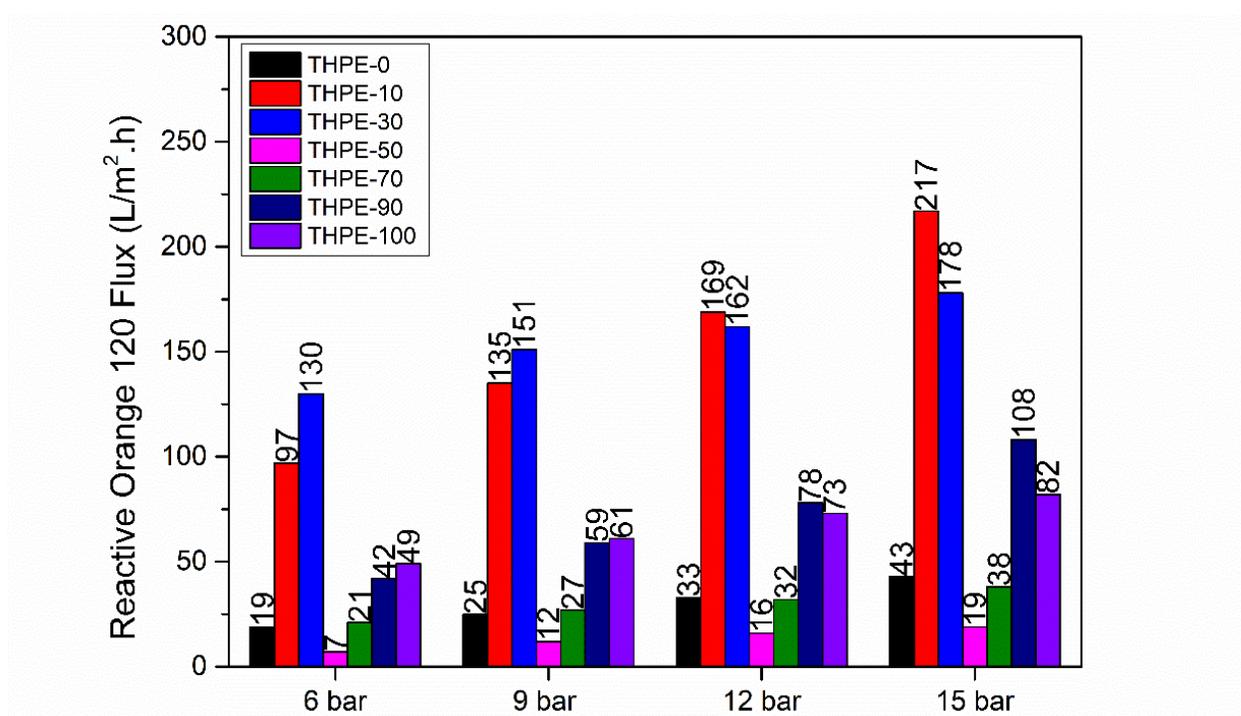
Figure 76 Results of 100 ppm Reactive Orange 120 aqueous solution flux of TFC membranes: THPE-0, 30, 50, 70, 90, and 100.
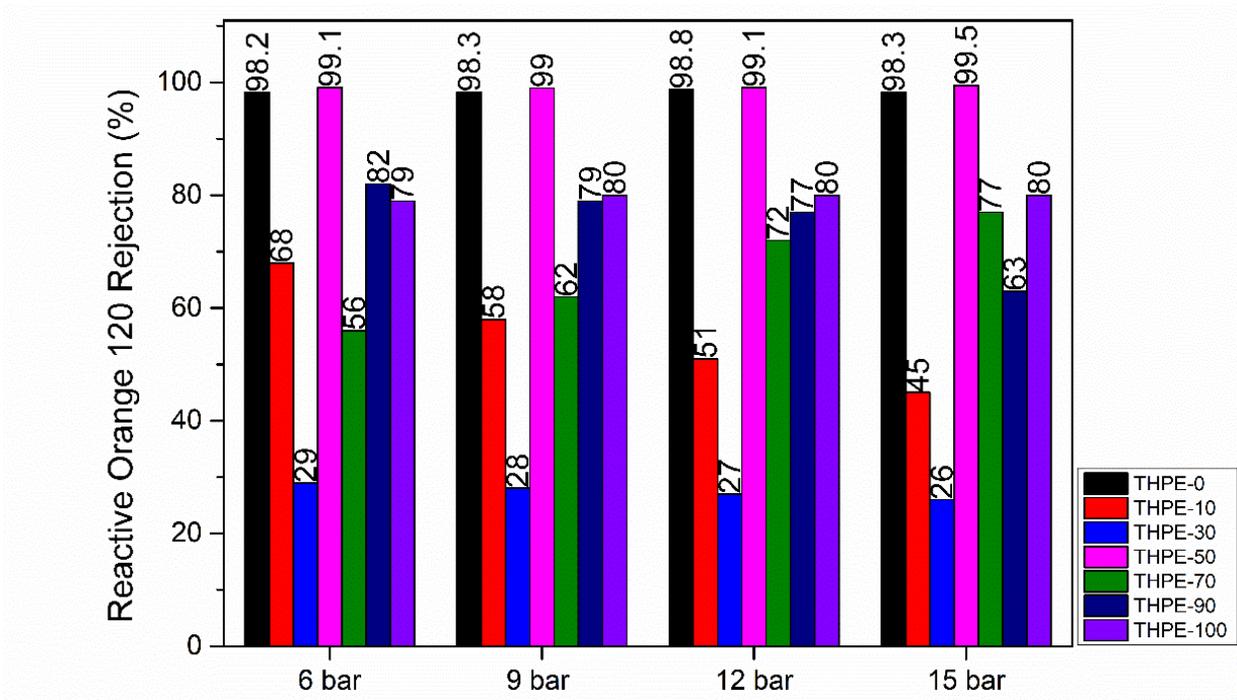
Figure 77 Reactive Orange 120 rejection results of TFC membranes: THPE-0, 30, 50, 70, 90, and 100.

Table 27 Input and Output Photographs of TFC membranes for Setazol Red and Reactive orange 120 dyes: THPE-0, 30, 50, 70, 90, and 100

6.2.1. Characterization of SHBPAES polymers

In this part of the study, two sets of SHBPAES polymers with varying degrees of branching and ionic contents were synthesized by the A_2+B_3 copolymerization approach (Figure 28). In one set, SDCDPS was used as the only A_2 monomer, which was polymerized with B_3 THPE monomer, whereas SDCDPS and DCDPS were used in 50:50 molar ratio in the second sent, both of which were synthesized with varying $A_2:B_3$ ratios as summarized in Table 28 as SM0- and SMM0- series, respectively. In both series, molecular weights of SHBPAESs gradually increased with increasing $A_2:B_3$ ratio. Also, the values of degree of branching and g_h have been calculated according to non-sulfonated analogues (M0- series). In addition to the synthesis of SHBPAES from monomeric SDCDPS and DCDPS, a sulfonated oligomeric A_2 with a DP of three was synthesized from SDCDPS and BisA, which was then used for the synthesis of SHBPAES at an $A_2:B_3$ ratio of 0.75, named SO3-0.75 (Figure 28). 3D schematic models of SHBPAES are represented along with non-sulfonated analogues in Table 29.

Table 28 SEC analysis of SHBPESs

Polymer:	$A_2:B_3$	M_n (kDa)[a]	M_w (kDa)[a]	$[\eta]$ (dL/g)[a]	R_h (nm)[a]	DB (%)	g_h
M0-0.55	0.55	1.90	6.20	0.029	1.30	79.70	0.22
M0-0.75	0.75	4.70	8.80	0.032	1.16	71.10	0.26
M0-0.85	0.85	3.50	13.50	0.050	2.00	54.50	0.33
M0-1.00	1.00	8.90	34.9	0.057	2.80	48.30	0.46
SMM0-0.55	0.55	6.59	10.20	0.036	2.60	79.70	0.22
SMM0-0.75	0.75	21.96	28.82	0.063	3.00	71.10	0.26
SMM0-0.85	0.85	38.85	44.21	0.053	3.30	54.50	0.33
SMM0-1.00	1.00	11.60	19.44	0.076	3.87	48.30	0.46
SM0-0.55	0.55	3.39	5.56	0.011	3.80	79.70	0.22
SM0-0.75	0.75	20.87	46.25	0.070	3.50	71.10	0.26
SM0-0.85	0.85	42.54	68.77	0.016	1.10	54.50	0.33
SM0-1.00	1.00	18.80	45.44	0.060	3.30	48.30	0.46

Table 29 3D schematic representation of the topologies HBPAESs synthesized with four different functionality and three different hydrophilicity.

A$_2$:B$_3$ 0.55	A$_2$:B$_3$ 0.75	A$_2$:B$_3$ 0.85	A$_2$:B$_3$ 1.00	Monomer Combinations
M0-0.55 M$_w$: 6.2 kDa PDI: 3.26	M0-0.75 M$_w$: 8.8 kDa PDI: 1.87	M0-0.85 M$_w$: 13.5 kDa PDI: 3.86	M0-1.00 M$_w$: 34.9 kDa PDI: 3.92	B$_3$ A$_2$ M0
SMM0-0.55 M$_w$: 10.2 kDa PDI: 1.55	SMM0-0.75 M$_w$: 13.5 kDa PDI: 1.47	SMM0-0.85 M$_w$: 44.2 kDa PDI: 1.14	SMM0-1.00 M$_w$: 50.7 kDa PDI: 1.28	50% 50% SMM0
SM0-0.55 M$_w$: 5.7 kDa PDI: 1.67	SM0-0.75 M$_w$: 15.2 kDa PDI: 1.57	SM0-0.85 M$_w$: 45.4 kDa PDI: 2.41	SM0-1.00 M$_w$: 68.7 kDa PDI: 1.61	B$_3$ A$_2$ SM0
	SO3-0.75			SO3
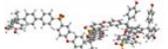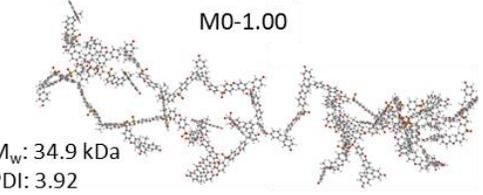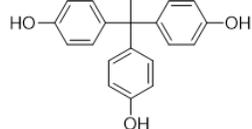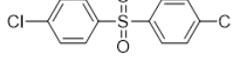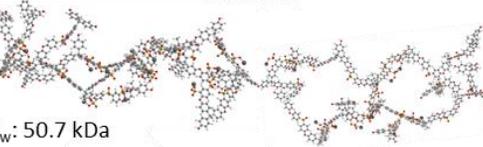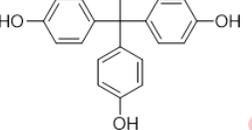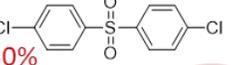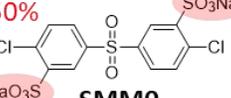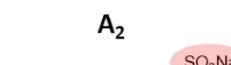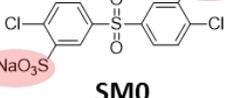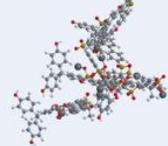
The phenolic end groups of all SHBPAESs (Table 29) were converted to phenolate ions at pH 13 prior to the fabrication of TFC membranes on the support membrane by interfacial polymerization. As discussed in more detail in Section 6.2.2, only SHBPAESs with A_2:B_3 ratios of 0.55 and 0.75 formed an active layer by interfacial polymerization with TMC (remarked as a blue background in Table 29), while the others failed due to their large size and high molecular weight (SM0-0.85, SMM0-0.85, SM0-1.00 and SMM0-1.00) as indicated in Table 29, which might have prevented their diffusion to the interface where the reaction occurs. M0 series of highly branched polymers were also failed to form a network by interfacial polymerization because they have hydrophobic nature and could not dissolve and disperse in water.

SHBPAES sample that were synthesized with the A_2:B_3 ratio of 0.75 were analyzed via ^{1}H-NMR spectroscopy in DMSO-d_6 and the spectra of M0-0.75, SMM0-0.75, SM0-0.75, and SO3-0.75 were given in Figure 78. The most specific peak identified for the SDCDPS monomer was observed between 8.26-8.16 ppm highlighted in all spectra (Figure 78-b-d.) except for the control non-sulfonated HBPAES M0-0.75 (Figure 78-a.). SO3-0.75 sample possessed BisA groups arising from the linear A_2 oligomer species, which were not present in M0-0.75, SM0-0.75 and SMM0-0.75. Aliphatic and aromatic C-H peaks were observed at 1.64-1.42 ppm and 7.26-7.20 ppm, respectively, for SO3-0.75 sample as highlighted in yellow in Figure 78-d.
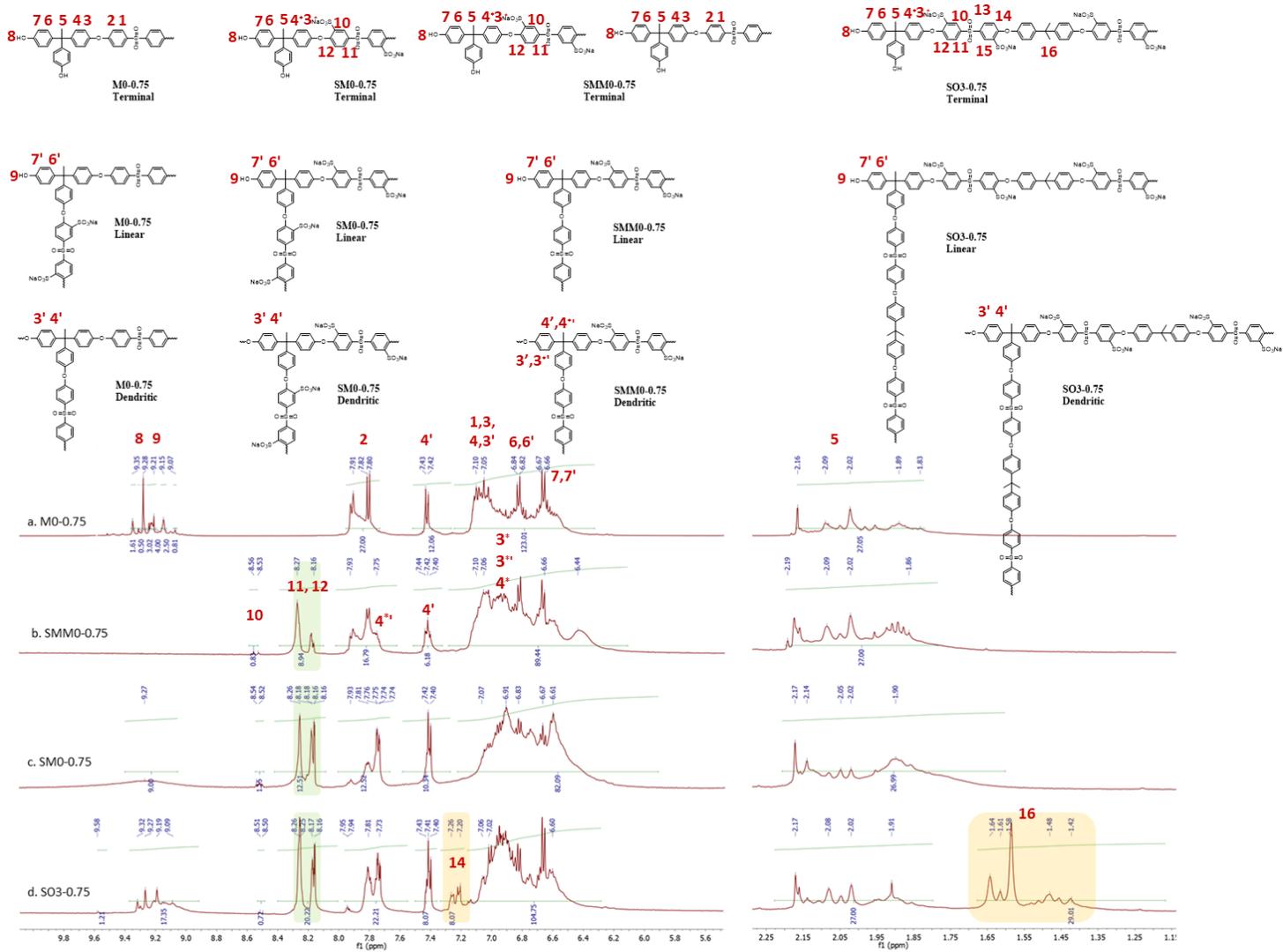
Figure 78 ^{1}H-NMR spectra of SHBPAES with $A_2:B_3$ 0.75

The thermal stability of SHBPAES and their HBPAES analogues were assessed using TGA (Figure 79). The thermal decomposition peak points of M0-0.55, -0.75, -0.85 and -1.00 based on the 1st derivative of the decomposition peaks were observed at relatively higher temperatures compared to with sulfonated analogs due to the elimination of sulfonate moieties from SMM0 and SM0 branched polymers. However, the branched polymers were stable up to 240 °C and showed a significantly higher char yield compared to the non-sulfonated analogues due to the presence of ionic moieties.
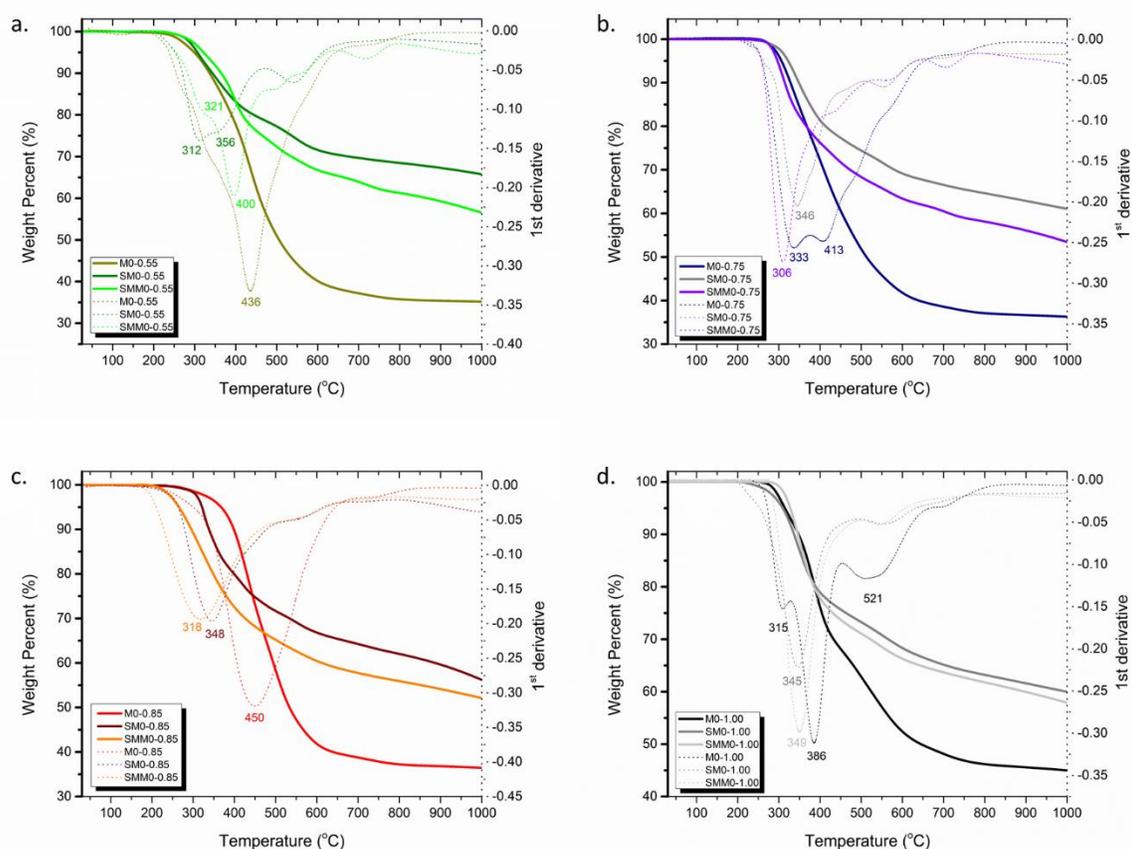
Figure 79 Thermo-gravimetric analyses of the branched polymers a. M0-0.55, SM0-0.55, SMM0-0.55; b. M0-0.75, SM0-0.75, SMM0-0.75; c. M0-0.85, SM0-0.85, SMM0-0.85; d. M0-1.00, SM0-1.00, SMM0-1.00

In order to produce TFC membranes, phenolic end groups of the functional SHBPAES were converted to sodium phenolate groups at pH 13 to achieve higher nucleophilicity at these end

groups, which, not only allowed them to react with acyl chloride groups of TMC at a faster rate but also helped enhance the water solubility/dispersibility of corresponding SHBPAES polymers. Hydrodynamic radii of SHBPAESs samples at pH 7, pH 9, and pH 13 were analyzed via DLS Spectrometry at 532 nm and the particle size distributions were plotted as log size vs number% in Figure 80, Figure 81, and Figure 82, respectively. Moreover, values of UV absorbance at 532 nm and refractive index (RI) were given in Table 30, which were used as input for DLS measurements of SHBPAES samples. SM0-0.85 and SMM0-0.85 samples had relatively larger hydrodynamic radii than others, which explains why a TFC active layer was not able to be formed on the top of the support membrane.

Table 30 Refractive index and absorbance results of SHBPAESs for DLS measurements

SHBPAES	Absorbance at 532 nm	Refractive Index
SM0-0.55	0.060	1.401
SM0-0.75	0.107	1.121
SM0-0.85	0.250	0.810
SMM0-0.55	0.061	1.400
SMM0-0.75	0.122	1.328
SMM0-0.85	0.062	1.176
SO3-0.75	0.085	1.077
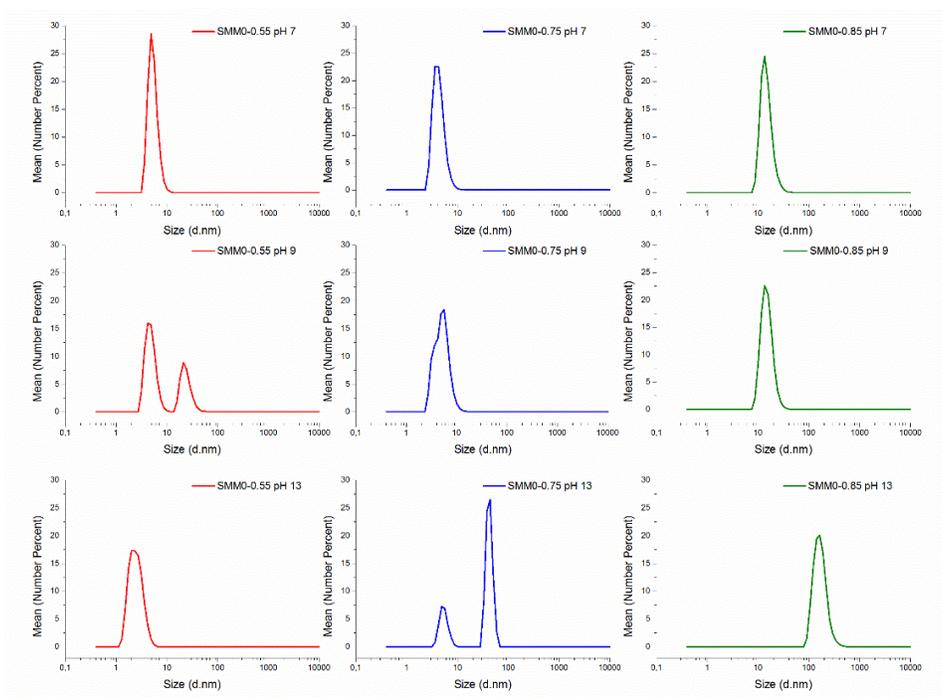
Figure 80 DLS spectra of SMM0-based SHBPAES samples; SMM0-0.55, SMM0-0.75, and SMM0-0.85 at pH 7, pH 9, and pH 13.
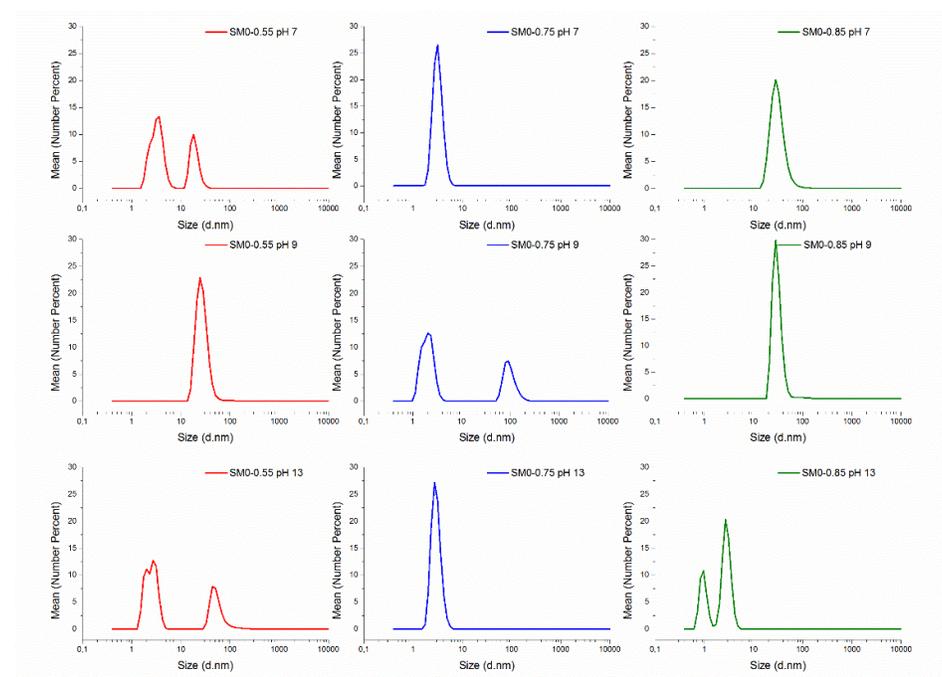
Figure 81 DLS spectra of SM0-based SHBPAES samples; SM0-0.55, SM0-0.75, and SM0-0.85 of A_2:B_3 ratio at pH 7, 9, and 13
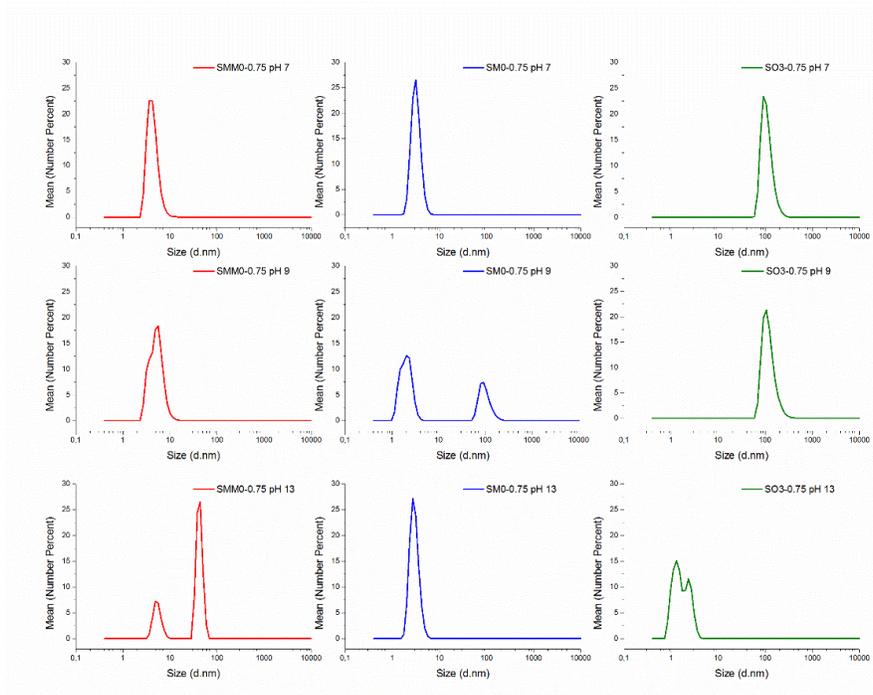
Figure 82 DLS spectra of SMM0, SM and SO3-based SHBPAES samples with a ratio 0.85 of A_2:B_3 ratio at pH 7, 9, and 13

6.2.2. Poly(arylate sulfone)-based TFC membranes from SHBPAESs

The poly(arylate sulfone)-based TFC membranes were prepared according to Section 3. 5. At first, the effect of the SMM0-0.75 concentration in the aqueous phase on the TFC morphology was investigated. Then, performance results of TFC membranes, which were fabricated from two different concentrations of SMM0-0.75 and SO3-0.75 in aqueous media, were compared in respect of fluxes and Mg^{+2} and Setazol red rejection. Lastly, four different TFC membranes, which were produced via using SMM0-0.55, SMM0-0.75, SM0-0.55, and SM0-0.75 with their 2% aqueous solutions, were investigated with regards to fluxes, salt, and dye rejections.

The feasibility of the interfacial polymerization reaction between the phenolate functional SMM0-0.75 in the aqueous phase (bottom layer) and TMC in the organic phase (top layer), and the formation of the resulting poly(arylate sulfone) film at the interface was verified in a beaker as shown in Figure 83-a. In addition, two different TFC membranes were produced from 1 wt% and 2 wt% aqueous solutions of SMM0-0.75 with 0.1% TMC in hexane on LPAES-based support membranes to understand the effect of the SHBPAES concentration. These two TFC membranes were cryo-fractured for cross-sectional SEM analysis as shown in Figure 83-b. With an increasing concentration of SMM0-0.75 in water, the TFC membrane had a smoother surface and thicker active layer.

a. SMM0-0.75

(2wt% in Aq. sol.)

b. SEM images of TFC-NF membranes of SMM0-0.75
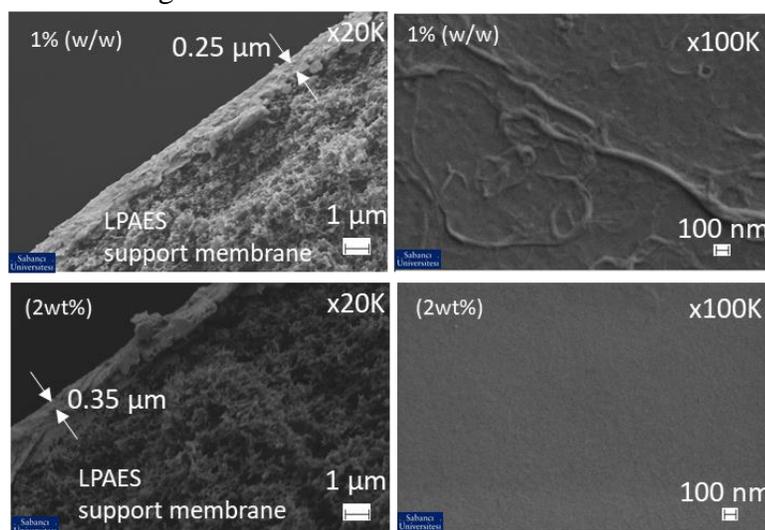
Figure 83 A. Poly(arylate sulfone) film formation at the interface between SMM0-0.75 in aqueous phase and TMC in hexane; B. Surface (right) and cross-sectional (left) SEM images of TFC membranes formed by using 0.1% TMC with 1% (top) and 2% (bottom) aqueous solutions of SMM0-0.75

Lastly, the filtration performance of TFC membranes fabricated from 1 wt% and 2 wt% aqueous solutions of SMM0-0.75 was compared with TFC membranes fabricated from 1 wt% and 2 wt% aqueous solutions of SO3-0.75 with 0.1 wt% TMC in the organic phase as shown in Figure 84. Filtration performance evaluations involved distilled water flux, $MgSO_4$ flux/rejection, and Setazol Red dye flux/rejection tests. It was important to note that the concentration of the SHBPAES reagent in the aqueous phase was critically important for the membrane performance, especially in rejection results. It could be deduced that the TFC active layer formed from 1% aqueous solution of SO3-0.75 resulted in very high flux and low rejection values. TFC membranes of SMM0-0.75 had quite high Setazol Red dye rejections and moderate $MgSO_4$ rejections compared to those fabricated from SO3-0.75 in 2% aqueous solution.
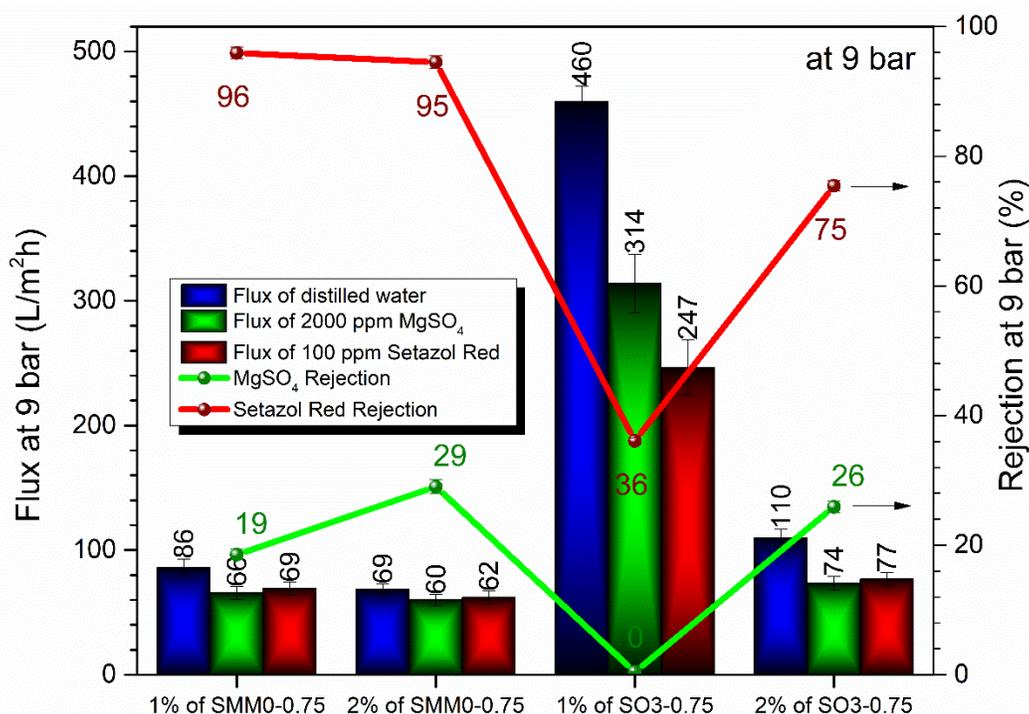
Figure 84 The comparison of the filtration performance of TFC membranes fabricated from 0.1% of TMC in hexane with 1 wt% and 2wt% aqueous solution of two different SHBPAES reagents, SMM0-0.75 and O3-0.75.

Poly(arylate sulfone)-based TFC membranes using SMM0-0.55, SM0-0.55, SMM0-0.75, and SM0-0.75 in the aqueous phase were produced using TMC in hexane via the interfacial polymerization technique defined in detail in Section 3. 5. Thus, all TFC membranes were fabricated using 2 wt% SHBPAES aqueous solutions during the interfacial polymerization process with 0.1 wt% TMC in hexane.

Distilled water fluxes of fabricated TFC membranes are illustrated in Figure 85. Flux values of all TFC membranes increased with increasing pressure. In addition, TFC membranes fabricated from SM0-0.55 and SM0-0.75 samples that were synthesized using SDCDPS only as the A_2 monomer showed slightly higher flux values than their analogues in SMM0 series that had lower amount of sodium sulfonate moieties. The presence of higher sodium sulfonate contents in TFC active layers resulted in slightly higher water flux values.
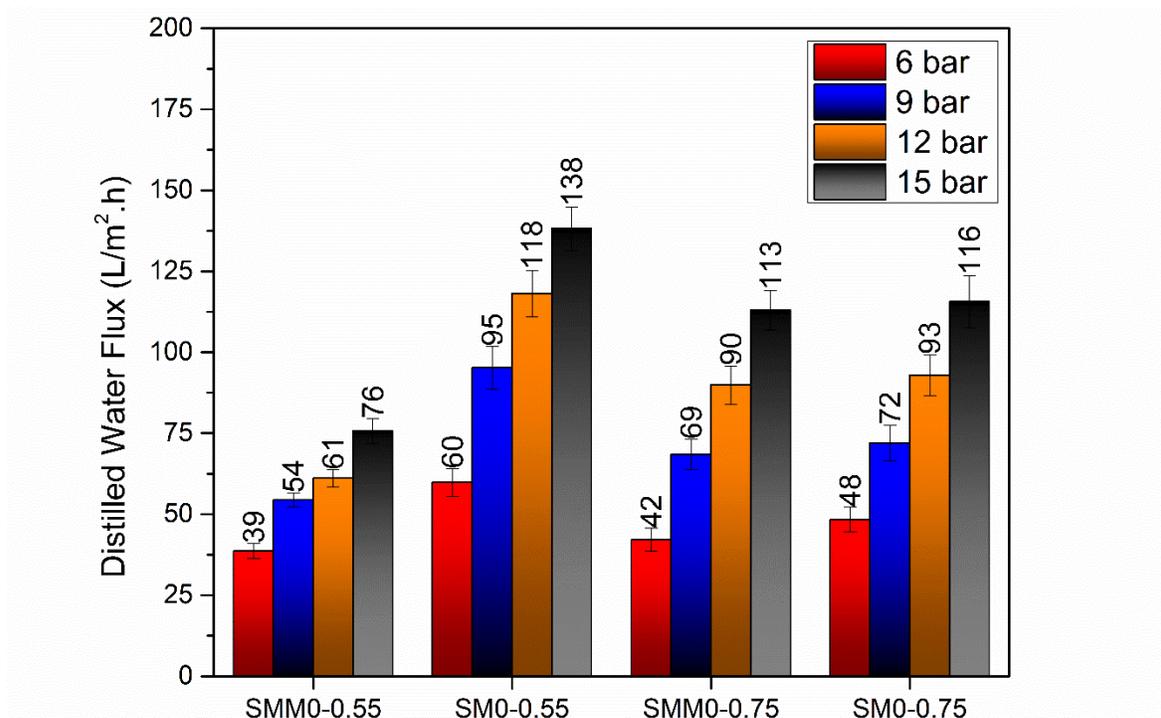
Figure 85 Distilled water fluxes of TFC membranes fabricated by the interfacial polymerization reaction of TMC with SMM0-0.55, SM0-0.55, SMM0-0.75, and SM0-0.75

The salt rejection performance of sulfonated polyarylate-based TFC membranes was examined using 2000 ppm $MgSO_4$ and 2000 ppm NaCl solutions under various pressures such as 6, 9, 12, and 15 bar. The obtained flux and salt rejection values were given in Figure 86, Figure 87, Figure 88, and Figure 89. $MgSO_4$ and NaCl flux values for all membranes were similar to that of distilled water. The highest $MgSO_4$ rejection performance was achieved up to 40% with the TFC membrane obtained fabricated from SMM0-0.55 polymer as the interfacial polymerization reagent in the aqueous phase. The same TFC membrane also showed relatively high NaCl salt rejection, that had monovalent ions, compared to the control membrane (THPE-0). An average of 60% monovalent ion rejection was observed for TFC membranes fabricated from SMM0-0.55 and SMM0-0.75. It was important to note that presence of a mixture of SDCDPS and DCDPS monomers in the synthesis of SHBPAES polymers resulted in TFC membranes with better salt rejection performance than TFC analogues fabricated purely from SDCDPS-based SHBPAES reagents.
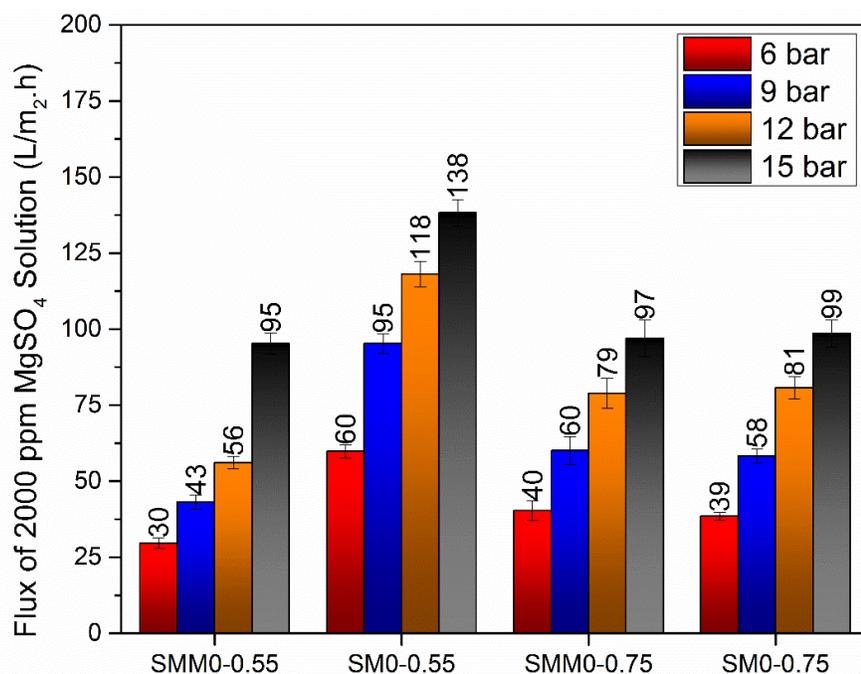
Figure 86 2000 ppm $MgSO_4$ solution fluxes of TFC membranes made by the interfacial reaction of TMC with SMM0-0.55, SM0-0.55, SMM0-0.75, and SM0-0.75
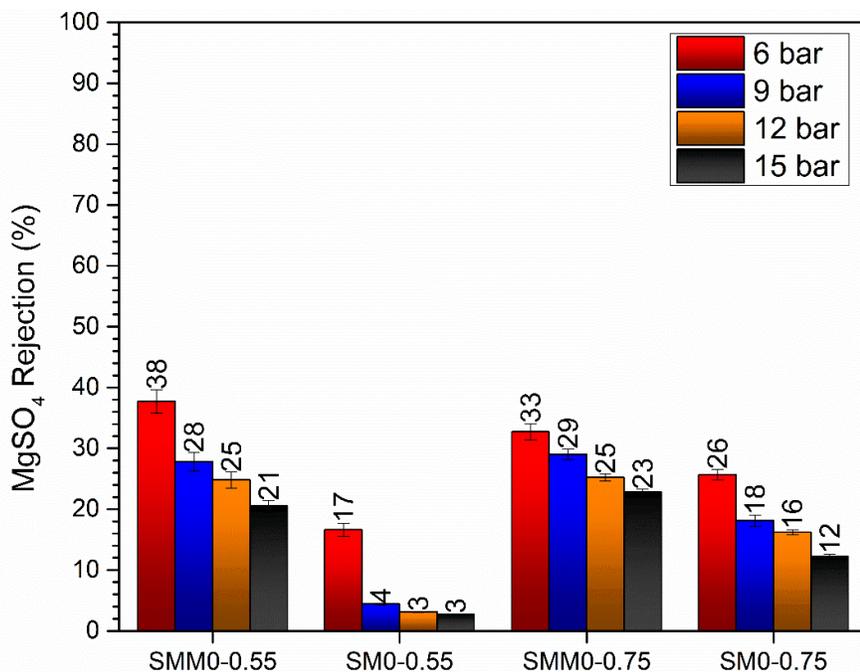
Figure 87 MgSO₄ rejections of TFC membranes made by the interfacial reaction of TMC with SMM0-0.55, SM0-0.55, SMM0-0.75, and SM0-0.75
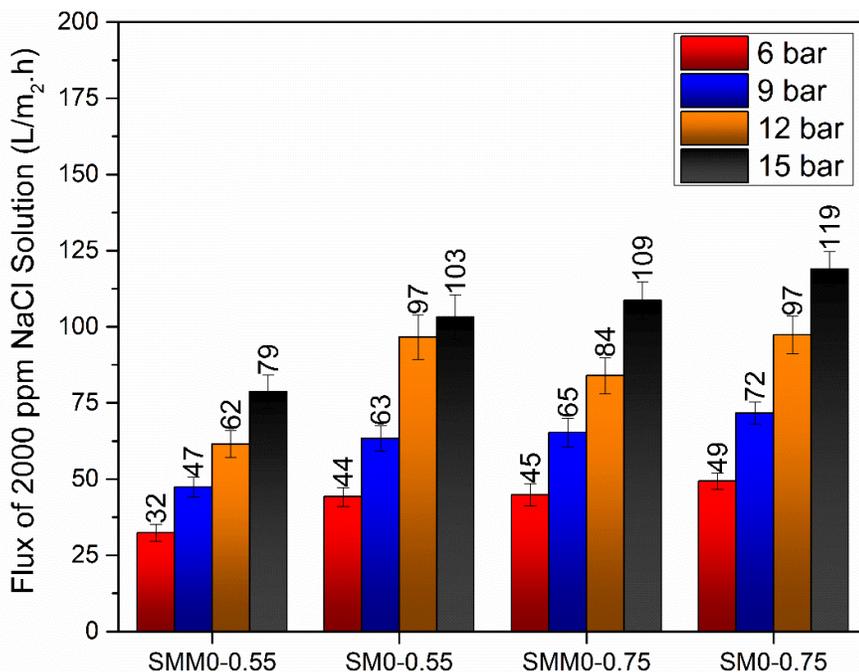
Figure 88 2000 ppm NaCl solution fluxes of TFC membranes made by the interfacial reaction of TMC with SMM0-0.55, SM0-0.55, SMM0-0.75, and SM0-0.75

157
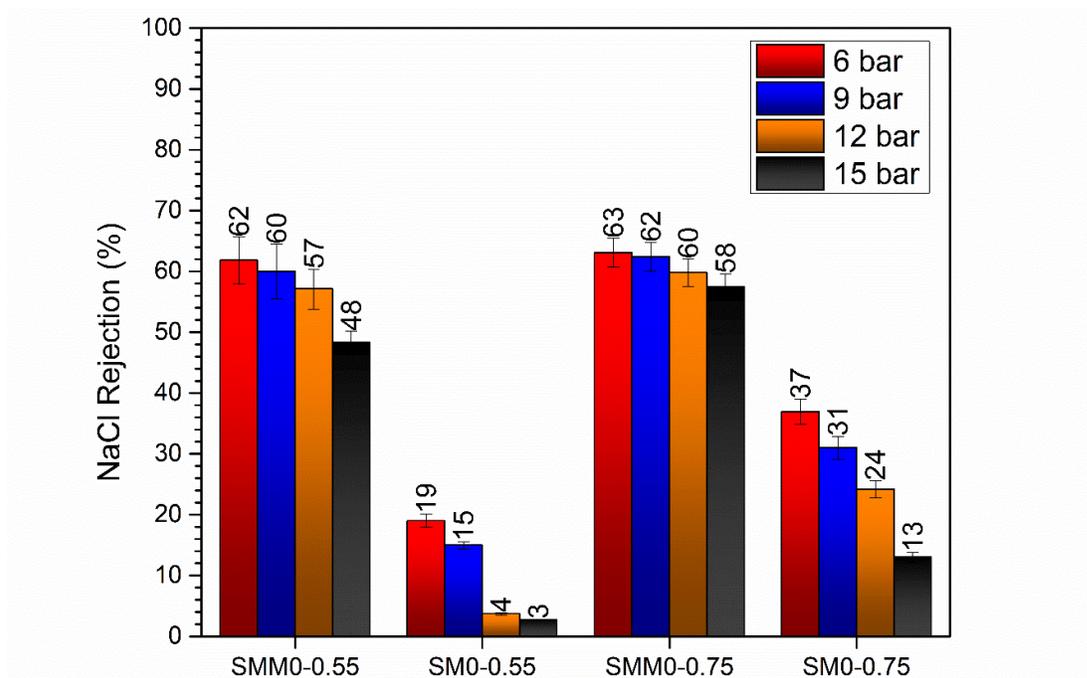
Figure 89 NaCl rejections of TFC membranes made by the interfacial reaction of TMC with SMM0-0.55, SM0-0.55, SMM0-0.75, and SM0-0.75

The poly(arylate sulfone) and hybrid poly(amide arylate) active layers exhibited higher Na^+ ion rejection than Mg^{+2} ions. The rejection performance of a membrane can be changed with surface force interactions and steric exclusions [262, 263]. The higher Na^+ ion rejection may originate from the presence of a TFC layer containing a multitude of phenolic end groups. It is well-known that phenols have stronger acidic nature than water [264]. Thus, a phenol end group can exchange its proton with Na^+ ion and form sodium phenolate groups, which can generate an electrostatic layer on the active layer. It is a well-known phenomenon in the ion transport mechanism that similar charges repel each other, while opposite charges attract each other. As a result of the formation of an electrostatic layer arising from the multitude of sodium phenolate end groups in the active layer, Na^+ ions can be selectively rejected [265]. The proposed Na^+ ion rejection mechanism is depicted in Figure 90.
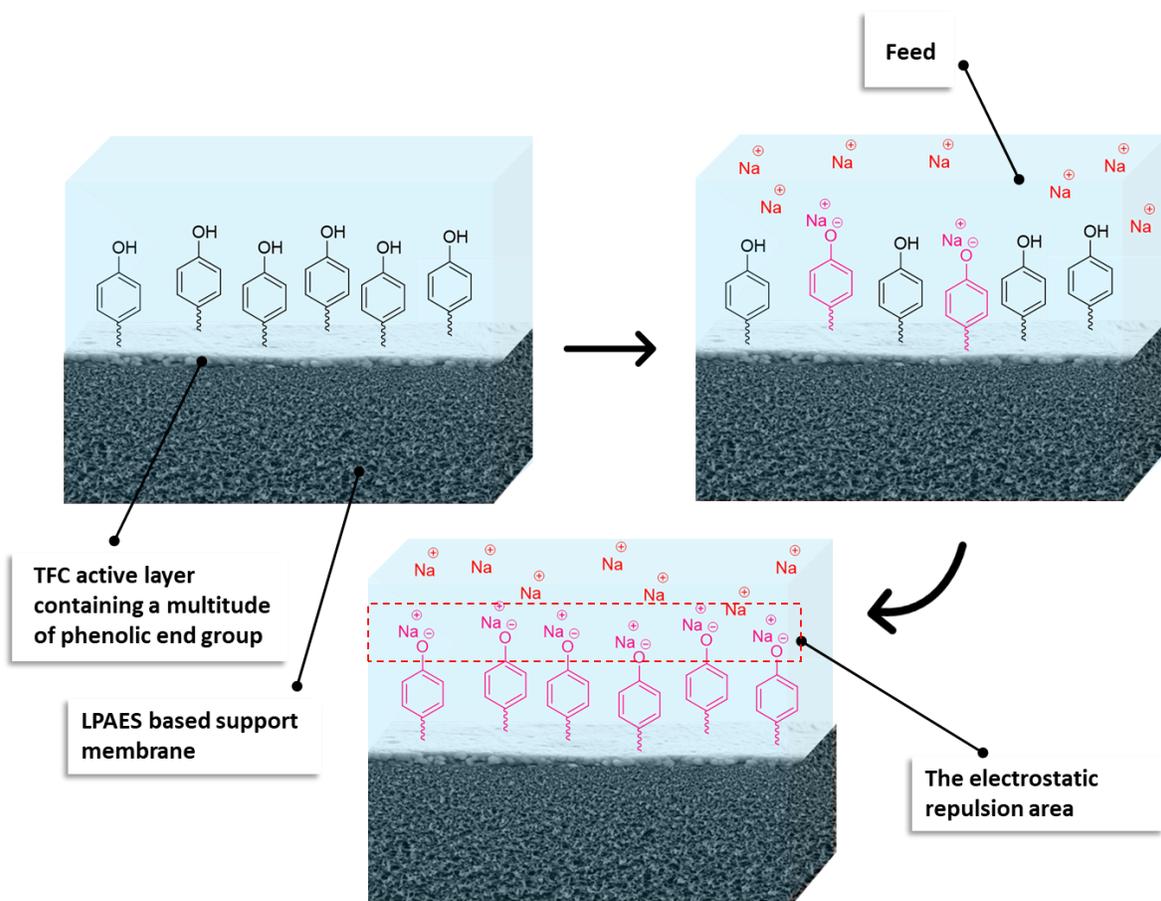
Figure 90 A proposed Na+ rejection mechanism for TFC active layers containing a multitude of phenolic end groups

6.3.   Conclusions

Three series of functional HBPAESs with varying degrees of branching and hydrophilicities were synthesized via the A_2+B_3 polymerization approach as soluble or dispersible reagents in water to prepare poly(arylate sulfone)-based active layers of TFC NF membranes. The reactivity of phenol end groups with acyl chloride groups was investigated for the interfacial reaction between the THPE and TMC. The conversion of phenol end groups to phenolate ions was found to effectively increase the interfacial reaction rate as evidenced by the film formation at the interface between an aqueous layer containing the SHBPAES and organic layer containing TMC. Thus, at first, a series of hybrid poly(amide arylate)-based TFC membranes were fabricated on PAES-based sponge-like support membranes using TMC in hexane with various mole ratios of THPE and PIP monomers at pH 13 in the aqueous phase.

PIP was chosen since it was an amino-functional monomer commonly utilized in the production of commercial TFC NF membranes, and also, to understand the differences in membrane performances of TFC active layers composed of poly(amide), poly(arylate) or their hybrid networks. THPE-0 membrane showed lower flux and higher rejection values than THPE-100 and all hybrid TFC active layers except for THPE-50 membrane. On the other hand, NaCl rejection of THPE-50 membrane significantly reached up to 97%, while the NaCl rejection of THPE-0 control membrane was measured as 64%.

The three sets of HBPAES with tunable hydrophilicity could be categorized as non-ionic, semi-ionic, and ionic branched polymers depending on the nature of the A2 monomer, namely, DCDPS, SDCDPS/DCDPS mixture and SDCDPS, respectively. Furthermore, these HBPAESs were synthesized with A_2:B_3 ratios of 0.55, 0.75, 0.85 and 1.00 to control the degree of branching. Ionic, non-ionic, and semi-ionic branched macromolecules with the A_2:B_3 ratio as 0.85 and 1.00 were useful for the formation of TFC active layer by interfacial polymerization due to their high molecular weight, which might limit their diffusion to the interface. Also, active layers from non-ionic HBPAES such as M0-0.55 and M0-0.75 could not be fabricated due to their non-dispersibility in water even if at pH 13. Semi-ionic poly(arylate sulfone) samples, SMM0-0.55 and SMM0-0.75 were successfully utilized in the interfacial polymerization to obtain poly(arylate sulfone)-based TFC membranes, which interestingly showed higher NaCl rejections than $MgSO_4$. The reason for higher NaCl rejection was presumed to originate from an optimum balance of porosity and sodium sulfonate content in the membrane, which could enable NaCl retention on the membrane surface more than $MgSO_4$. The concentration of the SHBPAES reagent in the aqueous phase was also found to be critical on the membrane morphology and performance. $MgSO_4$ and Setazol Red dye rejections of the TFC membrane fabricated from a sulfonated A_2 oligomer-based SHBPAES, SO3-075, were lower than that of semi-ionic TFC membranes fabricated from SMM0-0.75 reagents. The larger linear distance between branch points was presumed to increase the microporosity of the resulting NF membrane.

Poly(arylate sulfone)-based NF membranes were successfully fabricated and reported for the first time in the literature as pioneering materials for the enhancement of TFC membranes' filtration performance by using reactive HBPAES reagents with tunable hydrophilicity and degrees of branching in the aqueous phase.

CHAPTER 7: Overall conclusions and future work

7. 1. Overall conclusions

In this dissertation, a series of macromolecular structures with poly(arylene ether sulfone) backbones having various degrees of branching and functionalities were designed and synthesized via typical monomeric or oligomeric A_2+B_3 polymerization strategies. For the synthesis of these branched polymers, four different approaches were applied:

i.   controlling the degree of branching by $A_2:B_3$ ratio

ii. controlling the degree of branching, as well as the distance between branch points by using monomeric A_2 or oligomeric A_2 precursors with varying degrees of polymerization

iii. tailoring of branched polymer's end-groups via post-functionalization and the incorporation of inorganic moieties such as silane end-groups into the branched polymers' chain ends

iv. tuning the hydrophobicity/hydrophilicity balance of branched polymers using a combination of anionic and non-ionic A_2 monomers

Within this scope, twenty different HBPAESs, listed in Table 31, were synthesized as components in blend thermoplastic films and water purification UF and TFC NF membranes fabricated by phase-inversion technique and interfacial polymerization, respectively.

The first part of the study focused on the variation of the degree of branching, adjusted by monomeric $A_2:B_3$ ratios, which influenced the topology, molecular weight, as well as physical properties of resulting branched macromolecules. As the $A_2:B_3$ ratio increased, the molecular weight, functionality, and hydrodynamic radius of branched polymers dramatically increased. Moreover, the values of T_g and intrinsic viscosities of these branched polymers increased too.

HBPAES with varying distance between branch points were successfully synthesized using an A_2:B_3 ratio of 0.85. With the increasing distance between branched points, the molecular weight, hydrodynamic radius, OH equivalent weight, and intrinsic viscosity increased, and the degree of branching decreased. This approach was applied to overcome the lack of entanglements and low mechanical properties of HBPAES synthesized monomeric A_2. The branched polymer with oligomeric A_2 was more compatible and appeared to entangle with linear analogues when A_2 oligomers with DP of seven or higher was used.

Studies on LPAES/HBPAES blends revealed that a HBPAES component with an optimum degree of branching and distance between branch points could act as a reinforcing agent in LPAES. Mechanical characterization of blend films showed that the incorporation of HBPAES affected the stress-strain behavior that is more sensitive to micro-structure related transformations and interactions, and changed the fracture behavior of LPAES, in which the distance between branch points played a critical role.

O3-0.85-BF blend film had the highest Young's Modulus with 14% improvement by the addition of 10 wt% O3-0.85 HBPAES into LPAES when compared with the LPAES control film. The fracture surface analysis by SEM showed a morphology less prone to cracking, indicating that the use of HBPAES containing an A_2 oligomer with a DP of three had optimum structural features for use as an additive to enhance mechanical properties of LPAESs.

The same set of HBPAESs with a multitude of phenol functional or cross-linkable silane end-groups were synthesized and incorporated into UF membranes. While LPAES-based UF membranes exhibited a sponge-like structure, blend UF membranes containing HBPAES and HBPAES-Si were a finger-like shape. An oligomeric A_2 for HBPAESs with a DP of three was found to be optimum in improving thermo-mechanical, mechanical, and morphological properties of resulting blend films and UF membranes. The controlled distance between the branch points of the phenol functional HBPAES component was demonstrated as a useful tool to tune the water permeability and dye rejection of resulting blend UF membranes.

With the third approach, inorganic silane moieties were incorporated into branched polymer backbones via post-functionalization in an effort to enhance thermal, mechanical, and morphological behavior of resulting UF membranes. It could be stated that for both blend

film and UF membrane applications, O3-0.85 HBPAES had a unique architecture with an optimum distance between branch points, which resulted in improved material properties thermo-mechanically, mechanically, and morphologically. For example, the UF membrane prepared by10 wt% addition of O3-0.85 in LPAES exhibited thermo-mechanical improvements up to 48% in storage modulus when compared with the control specimen, and silane functionalization provided an additional 14% improvement.

To sum up, mechanical and thermo-mechanical properties LPAES-based films and UF membranes were enhanced by blending with HBPAES analogues. All films and UF membranes prepared from the blends of LPAES and HBPAESs exhibited single T_gs with no phase separation. The distance between branch points of the HBPAES component in the blend UF membrane was demonstrated as a useful tool to tune the water flux, which increased with increasing distance between branch points. To determine the best UF membrane performance, a multi-criteria decision statistical analysis called TOPSIS methodology was carried out according to the order of preferences such as flux, dye rejection, mechanical, and thermomechanical properties of membranes. According to the results of this analysis, HBPAESs synthesized from A_2 oligomers with DPs of three and seven (O3-0.85 and O7-0.85) were found to be promising candidates for UF type support membranes with enhanced flux. Particularly, the O3-0.85-UF membrane exhibited a 59% enhancement in membrane performance when compared with the control membrane. The analysis results of UF membranes are illustrated in Figure 91-a. UF membranes containing silane terminated HBPAES exhibited enhanced thermal and thermo-mechanical properties compared to UF membranes based on pure LPAES and LPAES/phenol terminated HBPAES blends; however, according to the TOPSIS analysis, only O7-0.85-Si-UF and O19-0.85-Si-UF showed higher membrane performances than the control membrane. Also, it can be stated that the membrane performances of these blend membranes were close to that of the blend UF membranes with phenolic end groups. From this similarity, we can deduce that as the degree of branching decreases, the final functionality of branched polymers decreases, which decreases the impact of the functional end-groups on the whole system.

Additionally, fully ionic and semi-ionic HBPAESs were synthesized using SDCDPS or a mixture of SDCDPS and DCDPS as A_2 reagents and THPE as the B_3 monomer at various A_2:B_3 ratios in an effort to use resulting, water-soluble or dispersible SHBPAESs as reagents

in interfacial polymerization for the fabrication of poly(arylate sulfone)-based TFC membranes for the first time. When the A_2: B_3 ratio of the SHBPAES was higher than 0.75, the branched polymer had a relatively high molecular weight, which made it impossible to form an active layer of the TFC NF membrane. On the other hand, poly(arylate sulfone) active layers were successfully fabricated using semi-ionic and ionic HBPAESs with the A_2:B_3 ratios of 0.55 and 0.75. The TOPSIS analysis of these TFC membranes, which is given in Figure 91-b, demonstrated that SHBPAESs synthesized with 1:1 n_{SDCDPS} : n_{DCDPS} had better membrane performance than fully ionic HBPAESs when incorporated into TFC NF membranes. SHBPAESs (SMO series) with fully ionic character may have difficulties migrating to the interface between in aqueous and hexane phase, where the interfacial reaction takes place, because of the high hydrophilic nature. This problem may be overcome by using higher polymer concentration in the aqueous medium or increasing the reaction time of the TFC network formation. Another critical conclusion of this study was the fact that the poly(arylate sulfone) TFC membranes were more selective towards Na^+ ion rejection than Mg^{+2} ions. Also, they had up to 194% enhanced flux values than the control polyamide active layer (THPE-0). It can be deduced that these poly(arylate sulfone) active layers have higher flux values than NF membranes, yet, they can reject Na^+ due to the presence of a multitude of phenolic end groups. Moreover, with the consideration of these results, the poly(arylate sulfone)-based TFC structures can be evaluated as tight UF membranes.

Lastly, a series of hybrid poly(amide arylate)-based TFC membranes were fabricated on PAES-based sponge-like support membranes using TMC in an organic medium with various molar fractions of THPE and PIP monomers at pH 13 in the aqueous phase. PIP was chosen since it was an amino-functional monomer commonly utilized in the production of commercial TFC NF membranes, and also, to understand the differences in membrane performances of TFC active layers composed of poly(amide), poly(arylate) or their hybrid networks. According to the TOPSIS analysis of these TFC membranes, THPE-50 showed the best membrane performance in TFC membranes containing poly(amide arylate) networks. Moreover, THPE-50 and THPE-90 showed similar membrane performances when compared to THPE-0, which had only poly(amide network). THPE-0 membrane showed lower flux and higher rejection values than THPE-100 and all hybrid TFC active layers except for THPE-50 membrane. On the other hand, NaCl rejection of THPE-50 membrane

significantly reached up to 97%, while the NaCl rejection of THPE-0 control membrane was measured as 64%. These hybrid membranes may be good candidates for tight UF membranes because of their higher flux values than NF membranes. Furthermore, it should be stated that these TFC membranes have higher rejection capabilities than UF membranes. For example, the membranes with hybrid poly(amide arylate) active layer exhibited up to 80% dye rejection, as well as, 60% Mg^{+2} and 40% Na^+ rejection performances. On the other hand, the LPAES based control UF membrane only showed up to 22% dye rejection.

Finally, Table 31 summarizes the composition, properties and applications of 20 different branched polymers synthesized throughout this study. As the degree of branching decreases, the effect of functional end groups on the blend system also decreases. When the degree of polymerization of A_2 species was three in the HBPAES, the corresponding LPAES/HBPAES blend system showed optimum features in terms of mechanical, thermomechanical, and membrane performance. Moreover, when the hydrophilicity of an HB polymer is very high, its migration to the interface between aqueous and organic media is restricted, which limits its reaction with TMC. Therefore, controlling the hydrophilicity is very critical to achieve the optimum performance from poly(arylate sulfone)-based active layers fabricated from phenol functional HBPAESs.
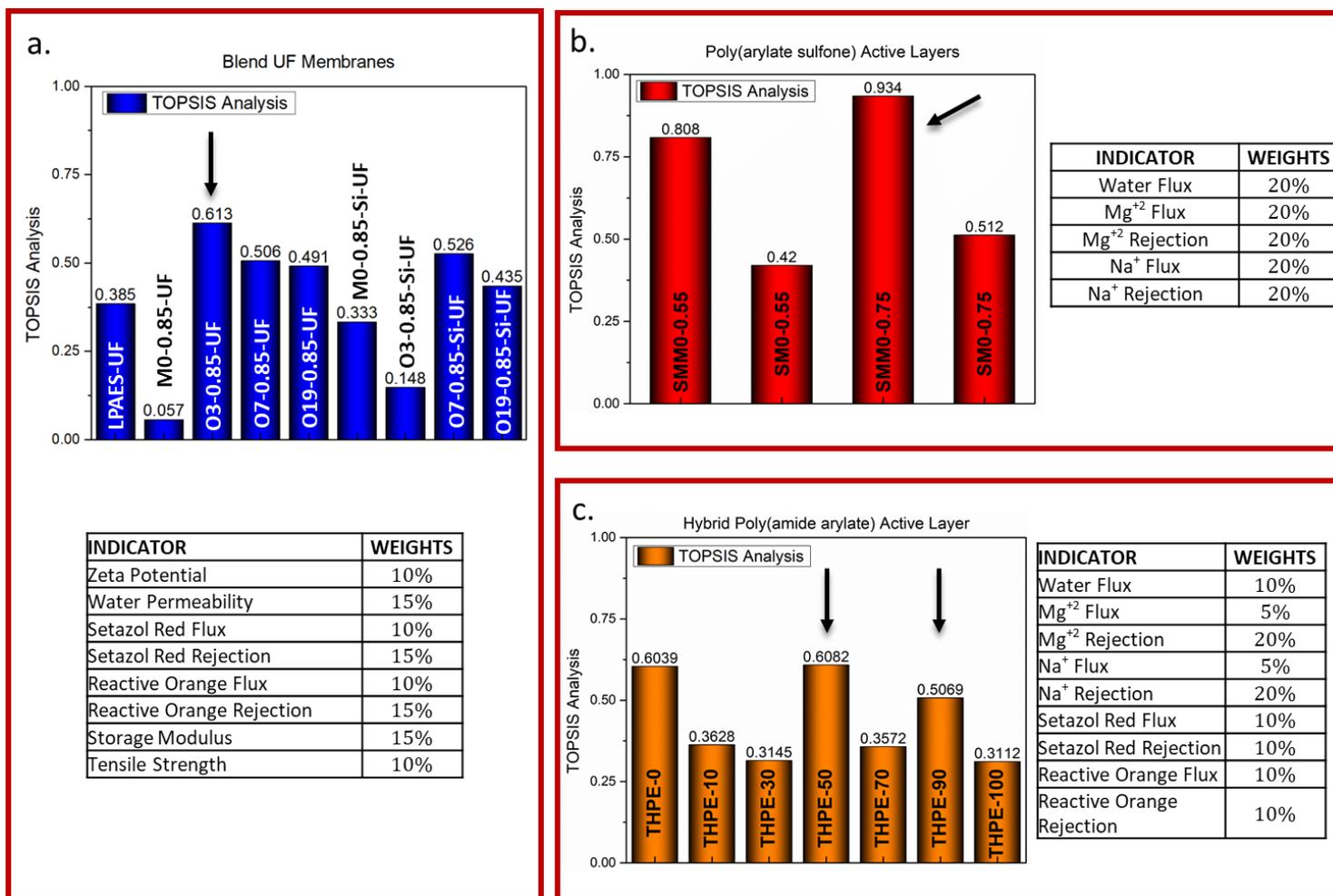
Figure 91 Statistical analysis of fabricated membranes via the TOPSIS method to determine optimum membranes for a given set of properties: a. blend UF membranes; b. TFC membranes containing poly(arylate sulfone) active layers; c. TFC membranes containing hybrid poly(amide active) layers.

Table 31 List of all synthesized HBPAES samples with their A₂:B₃ ratio, DP of A₂ species, and remarks on their blend film and membrane applications

#	HBPAES	$A_2:B_3$ ratio	The degree of polymerization of A_2 species	f_{final} (Equation 29)	Degree of branching (%)	Application type	Remarks
1	M0-0.55	0.55	0	4.22	79.7	TFC NF membrane	These HB polymers were not appropriate to use for the fabrication of a TFC membrane because of its high hydrophobic nature that prevented their dissolutions or dispersion in the aqueous medium.
2	M0-0.75	0.75	0	6.00	71.1	TFC NF membrane	
3	M0-0.85	0.85	0	8.67	54.5	BF, UF and TFC NF membranes	<u>BF and UF membrane application:</u> 10 wt% addition of this HB polymer into linear analogous enhanced thermomechanical properties of blend films and UF membranes. However, the final blend system showed a brittle behavior when compared with the control specimen due to the lack of entanglements in HB polymer synthesized via monomeric A_2. <u>TFC NF membrane application:</u> This HB polymer was not proper to use the fabrication of a TFC membrane because of its high hydrophobic nature that prevented its dissolution or dispersion in the aqueous medium. Also, even if dissolved, it could not migrate to the interface in the interfacial polymerization due to its high M_w.
4	M0-1.00	1.00	0	-	48.3	TFC NF membrane	This HB polymer was not appropriate to use for the fabrication of a TFC membrane, because its high hydrophobic nature prevented its dissolution in the aqueous medium. Also, even if dissolved, it could not migrate to the interface in the interfacial polymerization due to its high M_w.
5	O3-0.85	0.85	3	8.67	27.2	BF, UF membrane	Thermoplastic films and UF membranes were prepared by blends of HB and linear analogous. Both blend film and UF membrane showed the highest mechanical (+14% in Young's modulus) and thermomechanical (+48% in storage modulus) properties. O3-0.85 HBPAES was shown to have an optimum distance between branch points and act as an anchor point in the linear polymer, which enhances these features. The UF

#	HBPAES	$A_2:B_3$ ratio	The degree of polymerization of A_2 species	f_{final} (Equation 29)	Degree of branching (%)	Application type	Remarks
							membrane containing O3-0.85 HBPAES also exhibited the best membrane performance in the UF membrane series.
6	O7-0.85	0.85	7	8.67	13.6	BF, UF membrane	Thermoplastic films and UF membranes were prepared by blends of HB and linear analogous. Both blend film and UF membrane showed higher mechanical and thermomechanical properties when compared with the control specimen. Its water flux value was higher than the UF membrane containing O3-0.85. The UF membrane containing O7-0.85 exhibited the second-best membrane performance in the UF membrane series.
7	O19-0.85	0.85	19	8.67	5.6	BF, UF membrane	Thermoplastic films and UF membranes were prepared by blends of HB and linear analogous. The degree of branching is lower compared to O3- and O7-based HB polymers. The mechanical properties of their blends were closer to linear analogous.
8	M0-0.85-Si	0.85	0	8.67	54.5	BF, UF membrane	Silane functionality improved the thermomechanical properties; however, final blends were not appropriate to use in BF and UF membrane applications.
9	O3-0.85-Si	0.85	3	8.67	27.2	BF, UF membrane	Silane functionality improved the thermal, mechanical, and thermomechanical properties; however, the final blends were not appropriate to use UF membrane applications.
10	O7-0.85-Si	0.85	7	8.67	13.6	BF, UF membrane	For these HB polymers, silane functionality improved thermal properties slightly, however mechanical and thermomechanical properties did not change significantly.
11	O19-0.85-Si	0.85	19	8.67	5.6	BF, UF membrane	
12	SMM0-0.55	0.55	0	4.22	79.7	TFC NF membrane	This sulfonated HB polymer can form a poly(arylate sulfone) network with TMC on a support membrane. The resulting TFC membrane had higher Na^+ ion rejection than Mg^{+2}, and it can be considered as a good candidate for tight UF membrane applications because of its relatively high flux than NF membranes.
13	SMM0-0.75	0.75	0	6.00	71.1	TFC NF membrane	This sulfonated HB polymer can form a poly(arylate sulfone) network with TMC on a support membrane. The resulting TFC membrane had higher Na+ ion rejection than Mg+2. It can be considered as a good

#	HBPAES	A_2:B_3 ratio	The degree of polymerization of A_2 species	f_{final} (Equation 29)	Degree of branching (%)	Application type	Remarks
							candidate for tight UF membrane applications because of its relatively high flux than NF membranes. This TFC membrane was determined to have the best membrane performance in its own series.
14	SMM0-0.85	0.85	0	8.67	54.5	TFC NF membrane	These sulfonated HB polymers were not appropriate to use for the fabrication of a TFC membrane, because they could not migrate to the interface in order to form poly(arylate sulfone) active layers by the interfacial polymerization due to their high M_ws.
15	SMM0-1.00	1.00	0	-	48.3	TFC NF membrane	
16	SM0-0.55	0.55	0	4.22	79.7	TFC NF membrane	This sulfonated HB polymer can form a poly(arylate sulfone) network with TMC on a support membrane. This TFC membrane had slightly higher flux performances than the TFC membranes prepared using SMM0-0.55, and also, it can be considered as a good candidate for tight UF membrane applications because of its relatively high flux than NF membranes.
17	SM0-0.75	0.75	0	6.00	71.1	TFC NF membrane	This sulfonated HB polymer can form a poly(arylate sulfone) network with TMC on a support membrane. This TFC membrane had slightly higher flux performances than the TFC membrane prepared by using SMM0-0.75, and also, it can be considered as a good candidate for tight UF membrane applications because of its relatively high flux than NF membranes.
18	SM0-0.85	0.85	0	8.67	54.5	TFC NF membrane	These sulfonated HB polymers were not appropriate to use for the fabrication of a TFC membrane, because they could not migrate to the interface in order to form poly(arylate sulfone) active layers by the interfacial polymerization due to their high M_ws.
19	SM0-1.00	1.00	0	-	48.3	TFC NF membrane	
20	SO3-0.75	0.75	3	6.00	27.2	TFC NF membrane	This sulfonated oligomeric HB polymer can form a poly(arylate sulfone) network with TMC on a support membrane. This TFC membrane had higher flux performance and lower dye or salt rejection than the TFC membrane prepared by using SMM0-0.75. It can be a good candidate as a tight UF membrane because of its relatively high flux than NF membranes.

7. 2.   Future work

The LPAES/HBPAES blend film study in this dissertation reports pioneering results for further studies for the enhancement of the mechanical and thermo-mechanical properties of linear polymers by blending with their highly branched analogues. These blends can be used for the fabrication of structural parts, gas membranes, and films for high-performance applications.

In the case of poly(arylate sulfone)-based TFC membranes, these systems can be further examined more comprehensively for selectivity and fouling performance. Understanding and verifying the proposed mechanism for Na^+ selectivity of these membranes over Mg^{2+} would be critical as well. Lastly, their performance can be investigated in tight UF membrane applications.

The sulfonated HB polymers containing monomeric A_2 with high $A_2:B_3$ ratios can be evaluated in proton exchange membranes to enhance proton conductivity.

On the other hand, SM0-0.55/-0.75 and SMM0-0.55/-0.75 based HBPAESs can be used to fabricate TFC membranes on different types of support membranes in order to fully examine their membrane performances.

REFERENCES

[1]   E. Shah, J. Liebrand, J. Vos, G. J. Veldwisch, and R. Boelens, The UN Water and Development Report 2016 "Water and Jobs": A critical review, Development and Change, 2018, 49 (2), p. 678-691.

[2]   UNESCO The United Nations World Water Development Report 2019: Leaving no one behind, 2019, Paris.

[3]   I. OECD, Energy and Air Pollution: World Energy Outlook Special Report 2016, 2016.

[4]   The Reuse Opportunity: Cities Seizing the Reuse Opportunity in a Circular Economy, 2018, IWA website.

[5]   S. Judd and B. Jefferson, Membranes for industrial wastewater recovery and re-use 2003, Elsevier.

[6]   J. A. Nollet, X. Part of a letter from Abbè Nollet, of the Royal Academy of Science at Paris, and FRS to Martin Folkes Esq; President of the same, concerning electricity, Philosophical Transactions of the Royal Society of London, 1748, 45 (486), p. 187-194.

[7]   J. Glater, The early history of reverse osmosis membrane development, Desalination, 1998, 117 (1-3), p. 297-309.

[8]   M. Traube, Physiologie und wissenschaftliche Medizin, Arch. An. Physiol, 1867, 87.

[9]   A. Fick, Ueber diffusion, Annalen der Physik, 1855, 170 (1), p. 59-86.

[10]   T. Graham, X. Liquid diffusion applied to analysis, Philosophical Transactions of the Royal Society of London, 1861 (151), p. 183-224.

[11]   T. Graham, On the absorption and dialytic separation of gases by colloid septa, American Journal of Pharmacy (1835-1907), 1866, p. 510.

[12]   W. Pfeffer, Osmotische untersuchungen: studien zur zellmechanik 1877, W. Engelmann.

[13]   J. H. van't Hoff, Die Rolle des osmotischen Druckes in der Analogie zwischen Lösungen und Gasen, Zeitschrift für physikalische Chemie, 1887, 1 (1), p. 481-508.

[14]   W. Nernst, Zur kinetik der in lösung befindlichen körper, Zeitschrift für physikalische Chemie, 1888, 2 (1), p. 613-637.

[15]   M. Planck, Über die Dampfspannung von verdünnten Lösungen flüchtiger Stoffe, Zeitschrift für physikalische Chemie, 1888, 2 (1), p. 405-414.

[16]   F. G. Donnan, Theorie der Membrangleichgewichte und Membranpotentiale bei Vorhandensein von nicht dialysierenden Elektrolyten. Ein Beitrag zur physikalisch-chemischen Physiologie, Zeitschrift für Elektrochemie und angewandte physikalische Chemie, 1911, 17 (14), p. 572-581.

[17]   H. Bechhold, Kolloidstudien mit der Filtrationsmethode, Zeitschrift für physikalische Chemie, 1907, 60 (1), p. 257-318.

[18]   R. Zsigmondy, Über einige Fundamentalbegriffe der Kolloidchemie. II, Zeitschrift für physikalische Chemie, 1922, 101 (1), p. 292-322.

[19]   W. H. Carothers, Linear condensation polymers, 1937, Google Patents.

[20]   T. Teorell, An attempt to formulate a quantitative theory of membrane permeability, Proceedings of the Society for Experimental Biology and Medicine, 1935, 33 (2), p. 282-285.

[21]   K. H. Meyer and J. F. Sievers, La perméabilité des membranes I. Théorie de la perméabilité ionique, Helvetica Chimica Acta, 1936, 19 (1), p. 649-664.

[22]   W. Kolff, H. T. J. Berk, N. M. WELLE, A. Van Der Ley, E. Van Dijk, and J. Van Noordwijk, The artificial kidney: a dialyser with a great area, Acta Medica Scandinavica, 1944, 117 (2), p. 121-134.

[23]   H. Lonsdale, The growth of membrane technology, Journal of membrane science, 1982, 10 (2-3), p. 81-181.

[24]   C. Reid and E. Breton, Water and ion flow across cellulosic membranes, Journal of Applied Polymer Science, 1959, 1 (2), p. 133-143.

[25]   S. Loeb and S. Sourirajan, Saline water conversion-II, Advances in chemistry series, 1963, 38, p. 117.

[26]   M. Padaki, R. S. Murali, M. S. Abdullah, N. Misdan, A. Moslehyani, M. Kassim, N. Hilal, and A. Ismail, Membrane technology enhancement in oil–water separation. A review, Desalination, 2015, 357, p. 197-207.

[27]   C. Gadipelly, A. Pérez-González, G. D. Yadav, I. Ortiz, R. Ibáñez, V. K. Rathod, and K. V. Marathe, Pharmaceutical industry wastewater: review of the technologies for water treatment and reuse, Industrial & Engineering Chemistry Research, 2014, 53 (29), p. 11571-11592.

[28]   Z. Cui and H. Muralidhara, Membrane technology: a practical guide to membrane technology and applications in food and bioprocessing 2010, Elsevier.

[29]   B. Smitha, S. Sridhar, and A. Khan, Solid polymer electrolyte membranes for fuel cell applications—a review, Journal of membrane science, 2005, 259 (1-2), p. 10-26.

[30]   S. J. Peighambardoust, S. Rowshanzamir, and M. Amjadi, Review of the proton exchange membranes for fuel cell applications, International journal of hydrogen energy, 2010, 35 (17), p. 9349-9384.

[31]   W. Lu, Z. Yuan, Y. Zhao, H. Zhang, H. Zhang, and X. Li, Porous membranes in secondary battery technologies, Chemical Society Reviews, 2017, 46 (8), p. 2199-2236.

[32] D. M. Warsinger, S. Chakraborty, E. W. Tow, M. H. Plumlee, C. Bellona, S. Loutatidou, L. Karimi, A. M. Mikelonis, A. Achilli, and A. Ghassemi, A review of polymeric membranes and processes for potable water reuse, Progress in Polymer Science, 2018, 81, p. 209-237.

[33] C. Y. Tang, Z. Yang, H. Guo, J. J. Wen, L. D. Nghiem, and E. Cornelissen, Potable water reuse through advanced membrane technology, 2018, ACS Publications.

[34] M. Marcucci, G. Nosenzo, G. Capannelli, I. Ciabatti, D. Corrieri, and G. Ciardelli, Treatment and reuse of textile effluents based on new ultrafiltration and other membrane technologies, Desalination, 2001, 138 (1-3), p. 75-82.

[35] S. A. Deowan, F. Galiano, J. Hoinkis, D. Johnson, S. A. Altinkaya, B. Gabriele, N. Hilal, E. Drioli, and A. Figoli, Novel low-fouling membrane bioreactor (MBR) for industrial wastewater treatment, Journal of membrane science, 2016, 510, p. 524-532.

[36] X. Tan and D. Rodrigue, A Review on Porous Polymeric Membrane Preparation. Part I: Production Techniques with Polysulfone and Poly (Vinylidene Fluoride), Polymers, 2019, 11 (7), p. 1160.

[37] A. Figoli and A. Criscuoli, Sustainable Membrane Technology for Water and Wastewater Treatment 2017, Springer.

[38] N. Hilal, M. Al-Abri, and H. Al-Hinai, Enhanced membrane pre-treatment processes using macromolecular adsorption and coagulation in desalination plants: a review, Separation science and technology, 2006, 41 (3), p. 403-453.

[39] D. Vial and G. Doussau, The use of microfiltration membranes for seawater pre-treatment prior to reverse osmosis membranes, Desalination, 2003, 153 (1-3), p. 141-147.

[40] A. W. W. Association, Microfiltration and Ultrafiltration Membranes for Drinking Water: M53 Vol. 53, 2005, American Water Works Association.

[41] A. T. Fane, R. Wang, and Y. Jia, Membrane technology: Past, present and future, in Membrane and Desalination Technologies, 2011, Springer, p. 1-45.

[42] A. Mehta and A. L. Zydney, Permeability and selectivity analysis for ultrafiltration membranes, Journal of membrane science, 2005, 249 (1-2), p. 245-249.

[43] S. Lee and R. M. Lueptow, Reverse osmosis filtration for space mission wastewater: membrane properties and operating conditions, Journal of membrane science, 2001, 182 (1-2), p. 77-90.

[44] T. A. Saleh and V. K. Gupta, Nanomaterial and polymer membranes: synthesis, characterization, and applications 2016, Elsevier.

[45] E. Reverchon, R. Adami, S. Cardea, and G. Della Porta, Supercritical fluids processing of polymers for pharmaceutical and medical applications, The Journal of Supercritical Fluids, 2009, 47 (3), p. 484-492.

[46] H. Zhang, H. Zhang, F. Zhang, X. Li, Y. Li, and I. Vankelecom, Advanced charged membranes with highly symmetric spongy structures for vanadium flow battery application, Energy & Environmental Science, 2013, 6 (3), p. 776-781.

[47]   E. Drioli and E. Fontananova, Smart Materials for Smart Membrane Operations, Rende, Italy.

[48]   M. F. Jimenez-Solomon, Q. Song, K. E. Jelfs, M. Munoz-Ibanez, and A. G. Livingston, Polymer nanofilms with enhanced microporosity by interfacial polymerization, Nature materials, 2016, 15 (7), p. 760.

[49]   I. Pinnau, Recent advances in the formation of ultrathin polymeric membranes for gas separations, Polymers for Advanced Technologies, 1994, 5 (11), p. 733-744.

[50]   R. W. Baker, Membrane technology and applications 2012, John Wiley & Sons.

[51]   N. Vasileva and T. Godjevargova, Study on the behaviour of glucose oxidase immobilized on microfiltration polyamide membrane, Journal of membrane science, 2004, 239 (2), p. 157-161.

[52]   J.-K. Pi, H.-C. Yang, L.-S. Wan, J. Wu, and Z.-K. Xu, Polypropylene microfiltration membranes modified with TiO2 nanoparticles for surface wettability and antifouling property, Journal of membrane science, 2016, 500, p. 8-15.

[53]   S. F. Anis, R. Hashaikeh, and N. Hilal, Microfiltration membrane processes: A review of research trends over the past decade, Journal of Water Process Engineering, 2019, 32, p. 100941.

[54]   W. Gao, H. Liang, J. Ma, M. Han, Z.-l. Chen, Z.-s. Han, and G.-b. Li, Membrane fouling control in ultrafiltration technology for drinking water production: a review, Desalination, 2011, 272 (1-3), p. 1-8.

[55]   A. R. Cooper, Ultrafiltration membranes and applications Vol. 13, 1981, Springer Science & Business Media.

[56]   L. J. Zeman and A. L. Zydney, Microfiltration and ultrafiltration: principles and applications 2017, CRC Press.

[57]   A. W. Mohammad, Y. Teow, W. Ang, Y. Chung, D. Oatley-Radcliffe, and N. Hilal, Nanofiltration membranes review: Recent advances and future prospects, Desalination, 2015, 356, p. 226-254.

[58]   Z. Yang, Y. Zhou, Z. Feng, X. Rui, T. Zhang, and Z. Zhang, A review on reverse osmosis and nanofiltration membranes for water purification, Polymers, 2019, 11 (8), p. 1252.

[59]   K. P. Lee, T. C. Arnot, and D. Mattia, A review of reverse osmosis membrane materials for desalination—development to date and future potential, Journal of membrane science, 2011, 370 (1-2), p. 1-22.

[60]   D. R. Paul, Polymeric Gas Separation Membranes: 0 2018, CRC press.

[61]   Q. Zhao, Q. F. An, Y. Ji, J. Qian, and C. Gao, Polyelectrolyte complex membranes for pervaporation, nanofiltration and fuel cell applications, Journal of membrane science, 2011, 379 (1-2), p. 19-45.

[62]   G. Jyoti, A. Keshav, and J. Anandkumar, Review on pervaporation: theory, membrane performance, and application to intensification of esterification reaction, Journal of Engineering, 2015, 2015.

[63] N. N. Li, A. G. Fane, W. W. Ho, and T. Matsuura, Advanced membrane technology and applications 2011, John Wiley & Sons.

[64] A. Moslehyani, A. F. Ismail, T. Matsuura, M. A. Rahman, and P. S. Goh, Recent Progresses of Ultrafiltration (UF) Membranes and Processes in Water Treatment, in Membrane Separation Principles and Applications, 2019, Elsevier, p. 85-110.

[65] B. Van der Bruggen, C. Vandecasteele, T. Van Gestel, W. Doyen, and R. Leysen, A review of pressure-driven membrane processes in wastewater treatment and drinking water production, Environmental progress, 2003, 22 (1), p. 46-56.

[66] N. Pérignon, J.-D. Marty, A.-F. Mingotaud, M. Dumont, I. Rico-Lattes, and C. Mingotaud, Hyperbranched polymers analogous to PAMAM dendrimers for the formation and stabilization of gold nanoparticles, Macromolecules, 2007, 40 (9), p. 3034-3041.

[67] D. Konkolewicz, M. J. Monteiro, and S. Perrier, Dendritic and hyperbranched polymers from macromolecular units: elegant approaches to the synthesis of functional polymers, Macromolecules, 2011, 44 (18), p. 7067-7087.

[68] M. Zou, J. Fang, J. Liu, C. Li, and R. Guan, Synthesis and preparation of sulfonated hyperbranched poly (arylene ether sulfone)/poly (ether sulfone) blend membranes for proton exchange membranes, Solid State Ionics, 2012, 220, p. 23-31.

[69] M.-a. Kakimoto, S. J. Grunzinger, and T. Hayakawa, Hyperbranched poly (ether sulfone) s: Preparation and application to ion-exchange membranes, Polymer journal, 2010, 42 (9), p. 697.

[70] I. Pinnau and B. D. Freeman, Formation and modification of polymeric membranes: overview, 2000, ACS Publications.

[71] S. S. Alias, Z. Harun, and M. F. Shohur, Effect of monovalent and divalent ions in non-solvent coagulation bath-induced phase inversion on the characterization of a porous polysulfone membrane, Polymer Bulletin, 2019, p. 1-23.

[72] F. W. Altena and C. Smolders, Calculation of liquid-liquid phase separation in a ternary system of a polymer in a mixture of a solvent and a nonsolvent, Macromolecules, 1982, 15 (6), p. 1491-1497.

[73] A. Reuvers, F. Altena, and C. Smolders, Demixing and gelation behavior of ternary cellulose acetate solutions, Journal of polymer science part B: Polymer physics, 1986, 24 (4), p. 793-804.

[74] G. Gaides and A. McHugh, Gelation in an amorphous polymer: a discussion of its relation to membrane formation, Polymer, 1989, 30 (11), p. 2118-2123.

[75] G. Gaides and A. McHugh, Measurement and analysis of bath-side interfacial concentration gradients during phase inversion, Journal of membrane science, 1992, 74 (1-2), p. 83-94.

[76] R. Boom, I. Wienk, T. Van den Boomgaard, and C. Smolders, Microstructures in phase inversion membranes. Part 2. The role of a polymeric additive, Journal of membrane science, 1992, 73 (2-3), p. 277-292.

[77] I. Cabasso, E. Klein, and J. K. Smith, Polysulfone hollow fibers. I. Spinning and properties, Journal of Applied Polymer Science, 1976, 20 (9), p. 2377-2394.

[78] C. M. Tam, M. Dal-Cin, and M. D. Guiver, Polysulfone membranes. IV. Performance evaluation of Radel A/PVP membranes, Journal of membrane science, 1993, 78 (1-2), p. 123-134.

[79] G. R. Guillen, Y. Pan, M. Li, and E. M. Hoek, Preparation and characterization of membranes formed by nonsolvent induced phase separation: a review, Industrial & Engineering Chemistry Research, 2011, 50 (7), p. 3798-3817.

[80] M. Paul and S. D. Jons, Chemistry and fabrication of polymeric nanofiltration membranes: A review, Polymer, 2016, 103, p. 417-456.

[81] A. Schaefer, A. G. Fane, and T. D. Waite, Nanofiltration: principles and applications 2005, Elsevier.

[82] V. Freger, Kinetics of film formation by interfacial polycondensation, Langmuir, 2005, 21 (5), p. 1884-1894.

[83] I. C. Kim, J. Jegal, and K. H. Lee, Effect of aqueous and organic solutions on the performance of polyamide thin-film-composite nanofiltration membranes, Journal of polymer science part B: Polymer physics, 2002, 40 (19), p. 2151-2163.

[84] Z. Zhai, C. Jiang, N. Zhao, W. Dong, P. Li, H. Sun, and Q. J. Niu, Polyarylate membrane constructed from porous organic cage for high-performance organic solvent nanofiltration, Journal of membrane science, 2020, 595, p. 117505.

[85] N. Du, H. B. Park, M. M. Dal-Cin, and M. D. Guiver, Advances in high permeability polymeric membrane materials for CO 2 separations, Energy & Environmental Science, 2012, 5 (6), p. 7306-7322.

[86] L. E. Black, Interfacially polymerized membranes for the reverse osmosis separation of organic solvent solutions, 1992, Google Patents.

[87] J. Cadotte and L. Rozelle, In-situ formed condensation polymers for reverse osmosis membranes, 1972.

[88] L. T. Rozelle, J. Cadotte, K. Cobian, and C. Kopp Jr, Nonpolysaccharide membranes for reverse osmosis: NS-100 membranes, in Reverse osmosis and synthetic membranes, 1977, National Research Council of Canada Ottawa, p. 249-261.

[89] J. E. Cadotte, Reverse osmosis membrane, 1977, Google Patents.

[90] T. d. Naylor, Polymer Membranes: Materials, Structures and Separation Performance Vol. 8, 1996, iSmithers Rapra Publishing.

[91] H. C. Buys, A. J. Naaktgeboren, A. Van Elven, and D. A. Noordegraaf, Semipermeable composite membrane, 1988, Google Patents.

[92] W. J. Wrasidlo, Semipermeable membranes and the method for the preparation thereof, 1977, Google Patents.

[93] R. Riley, R. Fox, C. R. Lyons, C. Milstead, M. Seroy, and M. Tagami, Spiral-wound poly (ether/amide) thin-film composite membrane systems, Desalination, 1976, 19 (1-3), p. 113-126.

[94]   M. Hurndall, E. Jacobs, and R. Sanderson, Chemical composition of thin-film composite reverse osmosis membranes made from poly-2-vinylimidazoline, Journal of membrane science, 1993, 78 (3), p. 283-298.

[95]   M. Hurndall, R. Sanderson, E. Jacobs, and A. Van Reenen, Poly (2-vinylimidazoline) composite reverse osmosis membranes, Desalination, 1993, 90 (1-3), p. 41-54.

[96]   A. K. Ghosh, B.-H. Jeong, X. Huang, and E. M. Hoek, Impacts of reaction and curing conditions on polyamide composite reverse osmosis membrane properties, Journal of membrane science, 2008, 311 (1-2), p. 34-45.

[97]   X.-Z. Wei, L.-P. Zhu, H.-Y. Deng, Y.-Y. Xu, B.-K. Zhu, and Z.-M. Huang, New type of nanofiltration membrane based on crosslinked hyperbranched polymers, Journal of membrane science, 2008, 323 (2), p. 278-287.

[98]   X.-Z. Wei, J. Yang, and G.-L. Zhang, Preparation and characterization of nanofiltration membranes synthesized by hyperbranched polyester and terephthaloyl chloride (TPC), Polymers and Polymer Composites, 2012, 20 (3), p. 261-270.

[99]   X. Wei, X. Kong, J. Yang, G. Zhang, J. Chen, and J. Wang, Structure influence of hyperbranched polyester on structure and properties of synthesized nanofiltration membranes, Journal of membrane science, 2013, 440, p. 67-76.

[100] M. H. D. A. Farahani, S. M. Borghei, and V. Vatanpour, Recovery of cooling tower blowdown water for reuse: The investigation of different types of pretreatment prior nanofiltration and reverse osmosis, Journal of Water Process Engineering, 2016, 10, p. 188-199.

[101] A. S. Colburn, N. Meeks, S. T. Weinman, and D. Bhattacharyya, High Total Dissolved Solids Water Treatment by Charged Nanofiltration Membranes Relating to Power Plant Applications, Ind Eng Chem Res, 2016, 55 (14), p. 4089-4097.

[102] S. Heimel, R. D. Hobbs, and F.-S. T. Tao, Methods and systems for treating produced water, 2019, Google Patents.

[103] M. Galiana-Aleixandre, A. Iborra-Clar, B. Bes-Piá, J. Mendoza-Roca, B. Cuartas-Uribe, and M. Iborra-Clar, Nanofiltration for sulfate removal and water reuse of the pickling and tanning processes in a tannery, Desalination, 2005, 179 (1-3), p. 307-313.

[104] F. M. Sukma and P. Çulfaz-Emecen, Cellulose membranes for organic solvent nanofiltration, Journal of membrane science, 2018, 545, p. 329-336.

[105] L. Pérez-Manríquez, P. Neelakanda, and K.-V. Peinemann, Tannin-based thin-film composite membranes for solvent nanofiltration, Journal of membrane science, 2017, 541, p. 137-142.

[106] S. Lashkari, F. Mok, G. Ramasubbu, and A. Mumba, Hydrometallurgical process using multi-stage nanofiltration, 2019, Google Patents.

[107] A. Aguiar, L. Andrade, L. Grossi, W. Pires, and M. Amaral, Acid mine drainage treatment by nanofiltration: A study of membrane fouling, chemical cleaning, and membrane ageing, Separation and Purification Technology, 2018, 192, p. 185-195.

[108] C. Conidi, A. Cassano, F. Caiazzo, and E. Drioli, Separation and purification of phenolic compounds from pomegranate juice by ultrafiltration and nanofiltration membranes, Journal of Food Engineering, 2017, 195, p. 1-13.

[109] A. Cassano, W. Cabri, G. Mombelli, F. Peterlongo, and L. Giorno, Recovery of bioactive compounds from artichoke brines by nanofiltration, Food and bioproducts processing, 2016, 98, p. 257-265.

[110] R. Atra, G. Vatai, E. Bekassy-Molnar, and A. Balint, Investigation of ultra-and nanofiltration for utilization of whey protein and lactose, Journal of Food Engineering, 2005, 67 (3), p. 325-332.

[111] G. Han, T.-S. Chung, M. Weber, and C. Maletzko, Low-pressure nanofiltration hollow fiber membranes for effective fractionation of dyes and inorganic salts in textile wastewater, Environmental science & technology, 2018, 52 (6), p. 3676-3684.

[112] E. Ellouze, N. Tahri, and R. B. Amar, Enhancement of textile wastewater treatment process using nanofiltration, Desalination, 2012, 286, p. 16-23.

[113] E. Sahinkaya, N. Uzal, U. Yetis, and F. B. Dilek, Biological treatment and nanofiltration of denim textile wastewater for reuse, Journal of hazardous materials, 2008, 153 (3), p. 1142-1148.

[114] G. Zeng, Y. He, Y. Zhan, L. Zhang, Y. Pan, C. Zhang, and Z. Yu, Novel polyvinylidene fluoride nanofiltration membrane blended with functionalized halloysite nanotubes for dye and heavy metal ions removal, Journal of hazardous materials, 2016, 317, p. 60-72.

[115] T.-Z. Jia, J.-P. Lu, X.-Y. Cheng, Q.-C. Xia, X.-L. Cao, Y. Wang, W. Xing, and S.-P. Sun, Surface enriched sulfonated polyarylene ether benzonitrile (SPEB) that enhances heavy metal removal from polyacrylonitrile (PAN) thin-film composite nanofiltration membranes, Journal of membrane science, 2019, 580, p. 214-223.

[116] C.-C. Ye, Q.-F. An, J.-K. Wu, F.-Y. Zhao, P.-Y. Zheng, and N.-X. Wang, Nanofiltration membranes consisting of quaternized polyelectrolyte complex nanoparticles for heavy metal removal, Chemical Engineering Journal, 2019, 359, p. 994-1005.

[117] D. Olmos, S. Prolongo, and J. González-Benito, Thermo-mechanical properties of polysulfone based nanocomposites with well dispersed silica nanoparticles, Composites Part B: Engineering, 2014, 61, p. 307-314.

[118] W. Harrison, M. Hickner, Y. Kim, and J. McGrath, Poly (arylene ether sulfone) copolymers and related systems from disulfonated monomer building blocks: synthesis, characterization, and performance–a topical review, Fuel cells, 2005, 5 (2), p. 201-212.

[119] T. Tweddle, O. Kutowy, W. Thayer, and S. Sourirajan, Polysulfone ultrafiltration membranes, Industrial & Engineering Chemistry Product Research and Development, 1983, 22 (2), p. 320-326.

[120] S. S. Lane, R. L. Lindstrom, P. A. Williams, and C. W. Lindstrom, Polysulfone intracorneal lenses, Journal of Refractive Surgery, 1985, 1 (5), p. 207-216.

[121] C. Zhao, J. Xue, F. Ran, and S. Sun, Modification of polyethersulfone membranes–a review of methods, Progress in Materials Science, 2013, 58 (1), p. 76-150.

[122] P. Saxena, M. Gaur, P. Shukla, and P. Khare, Relaxation investigations in polysulfone: thermally stimulated discharge current and dielectric spectroscopy, Journal of Electrostatics, 2008, 66 (11-12), p. 584-588.

[123] A. Linares and R. Benavente, Effect of sulfonation on thermal, mechanical, and electrical properties of blends based on polysulfones, Polymer journal, 2009, 41 (5), p. 407.

[124] J. Robertson, T. Ward, and A. Hill, Thermal, mechanical, physical, and transport properties of blends of novel oligomer and thermoplastic polysulfone, Polymer, 2000, 41 (16), p. 6251-6262.

[125] Y. Yang, T. L. Ramos, J. Heo, and M. D. Green, Zwitterionic poly (arylene ether sulfone) copolymer/poly (arylene ether sulfone) blends for fouling-resistant desalination membranes, Journal of membrane science, 2018, 561, p. 69-78.

[126] J. E. Harris and L. M. Robeson, Miscible blends of poly (aryl ether sulfones), 1989, Google Patents.

[127] B. Motealleh, F. Huang, T. D. Largier, W. Khan, and C. J. Cornelius, Solution-blended sulfonated polyphenylene and branched poly (arylene ether sulfone): Synthesis, state of water, surface energy, proton transport, and fuel cell performance, Polymer, 2019, 160, p. 148-161.

[128] M. Sauers, L. McKenna, and C. Merriam, Polysulfone-Early Market Development Activities, in High Performance Polymers: Their Origin and Development, 1986, Springer, p. 159-168.

[129] J. Y. Park, M. H. Acar, A. Akthakul, W. Kuhlman, and A. M. Mayes, Polysulfone-graft-poly (ethylene glycol) graft copolymers for surface modification of polysulfone membranes, Biomaterials, 2006, 27 (6), p. 856-865.

[130] K. Zodrow, L. Brunet, S. Mahendra, D. Li, A. Zhang, Q. Li, and P. J. Alvarez, Polysulfone ultrafiltration membranes impregnated with silver nanoparticles show improved biofouling resistance and virus removal, Water research, 2009, 43 (3), p. 715-723.

[131] O. Monticelli, A. Bottino, I. Scandale, G. Capannelli, and S. Russo, Preparation and properties of polysulfone–clay composite membranes, Journal of Applied Polymer Science, 2007, 103 (6), p. 3637-3644.

[132] M. Kunita, A. Rinaldi, E. Girotto, E. Radovanovic, E. Muniz, and A. Rubira, Copper sulfide coated polysulfone films, Applied surface science, 2006, 252 (10), p. 3707-3713.

[133] D. Labahn, R. Mix, and A. Schönhals, Dielectric relaxation of ultrathin films of supported polysulfone, Physical Review E, 2009, 79 (1), p. 011801.

[134] H. Sun and J. E. Mark, Preparation, characterization, and mechanical properties of some microcellular polysulfone foams, Journal of Applied Polymer Science, 2002, 86 (7), p. 1692-1701.

[135] A. Filimon, R. M. Albu, I. Stoica, and E. Avram, Blends based on ionic polysulfones with improved conformational and microstructural characteristics: Perspectives for biomedical applications, Composites Part B: Engineering, 2016, 93, p. 1-11.

[136] D. C. Fuccella, The Evolution of Engineering Thermoplastics in Automotive Applications, 1983, SAE Technical Paper.

[137] M. Ciobanu, L. Marin, V. Cozan, and M. Bruma, Aromatic polysulfones used in sensor applications, Rev. Adv. Mater. Sci, 2009, 22, p. 89-96.

[138] J. W. Labadie, J. Hedrick, M. Ueda, J. Hedrick, and J. Labadie, Step-growth polymers for high-performance materials, in ACS Symp. Ser, 1996 ACS Publications.

[139] R. N. Johnson, A. G. Farnham, R. A. Clendinning, W. F. Hale, and C. N. Merriam, Poly (aryl ethers) by nucleophilic aromatic substitution. I. Synthesis and properties, Journal of Polymer Science Part A-1: Polymer Chemistry, 1967, 5 (9), p. 2375-2398.

[140] R. Viswanathan, B. Johnson, and J. McGrath, Synthesis, kinetic observations and characteristics of polyarylene ether sulphones prepared via a potassium carbonate DMAC process, Polymer, 1984, 25 (12), p. 1827-1836.

[141] J. Rose, Preparation and properties of poly (arylene ether sulphones), Polymer, 1974, 15 (7), p. 456-465.

[142] F. A. Carey and R. J. Sundberg, Advanced organic chemistry: part A: structure and mechanisms 2007, Springer Science & Business Media.

[143] J. F. Bunnett and R. E. Zahler, Aromatic Nucleophilic Substitution Reactions, Chemical reviews, 1951, 49 (2), p. 273-412.

[144] T. F. Magnera, G. Caldwell, J. Sunner, S. Ikuta, and P. Kebarle, Solvation of the halide anions in dimethyl sulfoxide. Factors involved in enhanced reactivity of negative ions in dipolar aprotic solvents, Journal of the American Chemical Society, 1984, 106 (21), p. 6140-6146.

[145] R. Alexander, E. Ko, A. Parker, and T. Broxton, Solvation of ions. XIV. Protic-dipolar aprotic solvent effects on rates of bimolecular reactions. Solvent activity coefficients of reactants and transition states at 25°, Journal of the American Chemical Society, 1968, 90 (19), p. 5049-5069.

[146] Y. Zheng, S. Li, Z. Weng, and C. Gao, Hyperbranched polymers: advances from synthesis to applications, Chemical Society Reviews, 2015, 44 (12), p. 4091-4130.

[147] B. I. Voit and A. Lederer, Hyperbranched and Highly Branched Polymer Architectures- Synthetic Strategies and Major Characterization Aspects, Chemical reviews, 2009, 109 (11), p. 5924-5973.

[148] S. J. Grunzinger, M. Watanabe, K. Fukagawa, R. Kikuchi, Y. Tominaga, T. Hayakawa, and M.-a. Kakimoto, Hyperbranched-linear poly (ether sulfone) blend films for proton exchange membranes, Journal of Power Sources, 2008, 175 (1), p. 120-126.

[149] S. Unal and T. E. Long, Highly branched poly (ether ester) s via cyclization-free melt condensation of A2 oligomers and B3 monomers, Macromolecules, 2006, 39 (8), p. 2788-2793.

[150] T. Emrick, H. T. Chang, and J. M. Fréchet, The preparation of hyperbranched aromatic and aliphatic polyether epoxies by chloride-catalyzed proton transfer polymerization from ABn and A2+ B3 monomers, Journal of Polymer Science Part A: Polymer Chemistry, 2000, 38 (S1), p. 4850-4869.

[151] D. Yan, C. Gao, and H. Frey, Hyperbranched polymers: synthesis, properties, and applications Vol. 8, 2011, John Wiley & Sons, 462.

[152] M. G. McKee, S. Unal, G. L. Wilkes, and T. E. Long, Branched polyesters: recent advances in synthesis and performance, Progress in Polymer Science, 2005, 30 (5), p. 507-539.

[153] C. Oguz, S. Unal, T. Long, and M. Gallivan, Interpretation of molecular structure and kinetics in melt condensation of A2 oligomers, B3 monomers, and monofunctional reagents, Macromolecules, 2007, 40 (18), p. 6529-6534.

[154] Q. Lin and T. E. Long, Polymerization of A2 with B3 monomers: a facile approach to hyperbranched poly (aryl ester) s, Macromolecules, 2003, 36 (26), p. 9809-9816.

[155] Q. Lin, S. Unal, A. R. Fornof, I. Yilgor, and T. E. Long, Highly branched poly (arylene ether) s via oligomeric A2+ B3 strategies, Macromolecular Chemistry and Physics, 2006, 207 (6), p. 576-586.

[156] T. E. Long, B. Voit, and O. Okay, Porous Carbons–Hyperbranched Polymers–Polymer Solvation Vol. 266, 2014, Springer, 216.

[157] D. Massa, K. Shriner, S. Turner, and B. Voit, Novel blends of hyperbranched polyesters and linear polymers, Macromolecules, 1995, 28 (9), p. 3214-3220.

[158] J. M. Frechet, Functional polymers and dendrimers: reactivity, molecular architecture, and interfacial energy, Science, 1994, 263 (5154), p. 1710-1715.

[159] D. Schmaljohann, B. Voit, J. Jansen, P. Hendriks, and J. Loontjens, New coating systems based on vinyl ether-and oxetane-modified hyperbranched polyesters, Macromolecular Materials and Engineering, 2000, 275 (1), p. 31-41.

[160] R. Vicari, O. S. Fruchey, K. N. Juneau, S. F. Thames, and J. W. Rawlins, Reactive hyperbranched polymers for powder coatings, 2000, Google Patents.

[161] S. Unal, Q. Lin, T. H. Mourey, and T. E. Long, Tailoring the Degree of Branching: Preparation of Poly (ether ester) s via Copolymerization of Poly (ethylene glycol) Oligomers (A2) and 1, 3, 5-Benzenetricarbonyl Trichloride (B3), Macromolecules, 2005, 38 (8), p. 3246-3254.

[162] M. Johansson and A. Hult, Synthesis, characterization, and UV curing of acrylate functional hyperbranched polyester resins, JCT: Journal of Coatings Technology, 1995, 67, p. 35-39.

[163] J. R. Bury and T. M. Vickers Jr, Use of HyperBranched polyether surfactant in cementitious systems, 2015, Google Patents.

[164] X. Zheng, I. Oviedo, and L. J. Twyman, Pseudo-generational effects observed for a series of hyperbranched polymers when applied as epoxidation catalysts, Macromolecules, 2008, 41 (21), p. 7776-7779.

[165] R. Mezzenga, L. Boogh, and J.-A. E. Månson, A review of dendritic hyperbranched polymer as modifiers in epoxy composites, Composites Science and Technology, 2001, 61 (5), p. 787-795.

[166] M. Sangermano, A. Priola, G. Malucelli, R. Bongiovanni, A. Quaglia, B. Voit, and A. Ziemer, Phenolic hyperbranched polymers as additives in cationic photopolymerization of epoxy systems, Macromolecular Materials and Engineering, 2004, 289 (5), p. 442-446.

[167] J. M. Misasi, Q. Jin, K. M. Knauer, S. E. Morgan, and J. S. Wiggins, Hybrid POSS-Hyperbranched polymer additives for simultaneous reinforcement and toughness improvements in epoxy networks, Polymer, 2017, 117, p. 54-63.

[168] P. J. Flory, Principles of polymer chemistry 1953, Cornell University Press.

[169] P. J. Flory, Molecular size distribution in three dimensional polymers. VI. Branched polymers containing A—R—Bf-1 type units, Journal of the American Chemical Society, 1952, 74 (11), p. 2718-2723.

[170] S. Unal, G. I. Ozturk, and T. E. Long, Synthesis of hyperbranched polymers via polymerization of functionally symmetric monomer Pairs, Hyperbranched Polymers: Synthesis, Properties, and Applications, 2011, p. 79-106.

[171] J. Hao, M. Jikei, and M.-a. Kakimoto, Preparation of hyperbranched aromatic polyimides via A2+ B3 approach, Macromolecules, 2002, 35 (14), p. 5372-5381.

[172] J. Hao, M. Jikei, and M.-a. Kakimoto, Synthesis and comparison of hyperbranched aromatic polyimides having the same repeating unit by AB2 self-polymerization and A2+ B3 polymerization, Macromolecules, 2003, 36 (10), p. 3519-3528.

[173] D. Schmaljohann and B. Voit, Kinetic evaluation of hyperbranched A2+ B3 polycondensation reactions, Macromolecular theory and simulations, 2003, 12 (9), p. 679-689.

[174] H. Komber, B. Voit, O. Monticelli, and S. Russo, H and 13C NMR Spectra of a Hyperbranched Aromatic Polyamide from p-Phenylenediamine and Trimesic Acid, Macromolecules, 2001, 34 (16), p. 5487-5493.

[175] C. Hawker, R. Lee, and J. Fréchet, One-step synthesis of hyperbranched dendritic polyesters, Journal of the American Chemical Society, 1991, 113 (12), p. 4583-4588.

[176] D. Hölter, A. Burgath, and H. Frey, Degree of branching in hyperbranched polymers, Acta Polymerica, 1997, 48 (1-2), p. 30-35.

[177] M. Jikei and M. a. Kakimoto, Dendritic aromatic polyamides and polyimides, Journal of Polymer Science Part A: Polymer Chemistry, 2004, 42 (6), p. 1293-1309.

[178] M. Jikei, S.-H. Chon, M.-a. Kakimoto, S. Kawauchi, T. Imase, and J. Watanebe, Synthesis of hyperbranched aromatic polyamide from aromatic diamines and trimesic acid, Macromolecules, 1999, 32 (6), p. 2061-2064.

[179] S. Russo, A. Boulares, A. Da Rin, A. Mariani, and M. E. Cosulich, Hyperbranched aramids by direct polyamidation of two reactant systems: synthesis and properties, in Macromolecular Symposia, 1999 Wiley Online Library.

[180] E. B. S. Ozbulut, S. Seven, K. Bilge, T. Akkas, C. E. Tas, B. Yildiz, C. Atilgan, Y. Z. Menceloglu, and S. Unal, Blends of highly branched and linear poly (arylene ether sulfone) s: Multiscale effect of the degree of branching on the morphology and mechanical properties, Polymer, 2019, p. 122114.

[181] T. Emrick, H.-T. Chang, and J. M. Frechet, An A2+ B3 approach to hyperbranched aliphatic polyethers containing chain end epoxy substituents, Macromolecules, 1999, 32 (19), p. 6380-6382.

[182] S. P. Rannard and N. J. Davis, A highly selective, one-pot multiple-addition convergent synthesis of polycarbonate dendrimers, Journal of the American Chemical Society, 2000, 122 (47), p. 11729-11730.

[183] C. Gao, D. Yan, and W. Tang, Hyperbranched Polymers Made from A2-and BB′ 2-Type Monomers, 3. Polyaddition of N-Methyl-1, 3-propanediamine to Divinyl Sulfone, Macromolecular Chemistry and Physics, 2001, 202 (12), p. 2623-2629.

[184] P. Kubisa, Hyperbranched polyethers by ring-opening polymerization: Contribution of activated monomer mechanism, Journal of Polymer Science Part A: Polymer Chemistry, 2003, 41 (4), p. 457-468.

[185] H.-T. Chang and J. M. Fréchet, Proton-transfer polymerization: a new approach to hyperbranched polymers, Journal of the American Chemical Society, 1999, 121 (10), p. 2313-2314.

[186] A. Sunder, R. Hanselmann, H. Frey, and R. Mülhaupt, Controlled synthesis of hyperbranched polyglycerols by ring-opening multibranching polymerization, Macromolecules, 1999, 32 (13), p. 4240-4246.

[187] H. Magnusson, E. Malmström, and A. Hult, Synthesis of hyperbranched aliphatic polyethers via cationic ring-opening polymerization of 3-ethyl-3-(hydroxymethyl) oxetane, Macromolecular rapid communications, 1999, 20 (8), p. 453-457.

[188] M. Bednarek, T. Biedron, J. Helinski, K. Kaluzynski, P. Kubisa, and S. Penczek, Branched polyether with multiple primary hydroxyl groups: polymerization of 3-ethyl-3-hydroxymethyloxetane, Macromolecular rapid communications, 1999, 20 (7), p. 369-372.

[189] Z. Guan, Control of polymer topology through late-transition-metal catalysis, Journal of Polymer Science Part A: Polymer Chemistry, 2003, 41 (22), p. 3680-3692.

[190] S. Graham, P. A. Cormack, and D. C. Sherrington, One-pot synthesis of branched poly (methacrylic acid) s and suppression of the rheological "polyelectrolyte effect", Macromolecules, 2005, 38 (1), p. 86-90.

[191] F. Isaure, P. A. Cormack, and D. C. Sherrington, Synthesis of branched poly (methyl methacrylate) s: effect of the branching comonomer structure, Macromolecules, 2004, 37 (6), p. 2096-2105.

[192] T. Sato, N. Sato, M. Seno, and T. Hirano, Initiator-fragment incorporation radical polymerization of divinylbenzene in the presence of glyoxylic oxime ether: Formation of soluble hyperbranched polymer, Journal of Polymer Science Part A: Polymer Chemistry, 2003, 41 (19), p. 3038-3047.

[193] H. R. Kricheldorf, L. Vakhtangishvili, and D. Fritsch, Synthesis and functionalization of poly (ether sulfone) s based on 1, 1, 1-tris (4-hydroxyphenyl) ethane, Journal of Polymer Science Part A: Polymer Chemistry, 2002, 40 (17), p. 2967-2978.

[194] Q. Lin and T. E. Long, Synthesis and characterization of a novel AB2 monomer and corresponding hyperbranched poly (arylene ether phosphine oxide) s, Journal of Polymer Science Part A: Polymer Chemistry, 2000, 38 (20), p. 3736-3741.

[195] J.-Y. Choi, L.-S. Tan, and J.-B. Baek, Self-controlled synthesis of hyperbranched poly (ether ketone) s from A3+ B2 approach via different solubilities of monomers in the reaction medium, Macromolecules, 2006, 39 (26), p. 9057-9063.

[196] H. Cao, Y. Zheng, J. Zhou, W. Wang, and A. Pandit, A novel hyperbranched polyester made from aconitic acid (B3) and di (ethylene glycol)(A2), Polymer International, 2011, 60 (4), p. 630-634.

[197] S. Unal, G. Ozturk, K. Sisson, and T. E. Long, Poly (caprolactone) containing highly branched segmented poly (ester urethane) s via A2 with oligomeric B3 polymerization, Journal of Polymer Science Part A: Polymer Chemistry, 2008, 46 (18), p. 6285-6295.

[198] A. R. Fornof, T. E. Glass, and T. E. Long, Degree of branching of highly branched polyurethanes synthesized via the oligomeric A2 plus B3 methodology, Macromolecular Chemistry and Physics, 2006, 207 (14), p. 1197-1206.

[199] S. Unal, I. Yilgor, E. Yilgor, J. Sheth, G. Wilkes, and T. Long, A new generation of highly branched polymers: hyperbranched, segmented poly (urethane urea) elastomers, Macromolecules, 2004, 37 (19), p. 7081-7084.

[200] H. Liu, X. Gao, B. Deng, and G. Huang, Simultaneously reinforcing and toughening epoxy network with a novel hyperbranched polysiloxane modifier, Journal of Applied Polymer Science, 2018, 135 (23), p. 46340.

[201] M. Czupik and E. Fossum, Manipulation of the molecular weight and branching structure of hyperbranched poly (arylene ether phosphine oxide) s prepared via an A2+ B3 approach, Journal of Polymer Science Part A: Polymer Chemistry, 2003, 41 (24), p. 3871-3881.

[202] S. Banerjee, H. Komber, L. Häußler, and B. Voit, Synthesis and characterization of hyperbranched poly (arylene ether) s from a new activated trifluoro B3 monomer adopting an A2+ B3 approach, Macromolecular Chemistry and Physics, 2009, 210 (16), p. 1272-1282.

[203] G. Kickelbick, Concepts for the incorporation of inorganic building blocks into organic polymers on a nanoscale, Progress in Polymer Science, 2003, 28 (1), p. 83-114.

[204] B. P. Tripathi and V. K. Shahi, Organic–inorganic nanocomposite polymer electrolyte membranes for fuel cell applications, Progress in Polymer Science, 2011, 36 (7), p. 945-979.

[205] V. K. Shahi, Highly charged proton-exchange membrane: sulfonated poly (ether sulfone)-silica polyelectrolyte composite membranes for fuel cells, Solid State Ionics, 2007, 177 (39-40), p. 3395-3404.

[206] O. Vandenabeele-Trambouze, L. Mion, L. Garrelly, and A. Commeyras, Reactivity of organic isocyanates with nucleophilic compounds: amines; alcohols; thiols; oximes; and phenols in dilute organic solutions, Advances in Environmental Research, 2001, 6 (1), p. 45-55.

[207] A. I. Isayev and S. Palsule, Encyclopedia of polymer blends, Volume 2: Processing Vol. 2, 2011, John Wiley & Sons, 404.

[208] X. Li, S. Zhang, H. Wang, C. Zhang, J. Pang, J. Mu, G. Ma, G. Wang, and Z. Jiang, Study of blends of linear poly (ether ether ketone) of high melt viscosity and hyperbranched poly (ether ether ketone), Polymer International, 2011, 60 (4), p. 607-612.

[209] M. F. Jimenez-Solomon, Q. Song, K. E. Jelfs, M. Munoz-Ibanez, and A. G. Livingston, Polymer nanofilms with enhanced microporosity by interfacial polymerization, Nat Mater, 2016, 15 (7), p. 760-767.

[210] H. Bukšek, T. Luxbacher, and I. Petrinić, Zeta potential determination of polymeric materials using two differently designed measuring cells of an electrokinetic analyzer, Acta chimica slovenica, 2010, 57 (3), p. 700-706.

[211] Y. Yang, H. Zhang, P. Wang, Q. Zheng, and J. Li, The influence of nano-sized TiO2 fillers on the morphologies and properties of PSF UF membrane, Journal of membrane science, 2007, 288 (1-2), p. 231-238.

[212] C.-L. Hwang and K. Yoon, Methods for multiple attribute decision making, in Multiple attribute decision making, 1981, Springer, p. 58-191.

[213] G. R. Jahanshahloo, F. H. Lotfi, and M. Izadikhah, An algorithmic method to extend TOPSIS for decision-making problems with interval data, Applied mathematics and computation, 2006, 175 (2), p. 1375-1384.

[214] S.-J. Chen and C.-L. Hwang, Fuzzy multiple attribute decision making methods, in Fuzzy multiple attribute decision making, 1992, Springer, p. 289-486.

[215] H.-S. Shih, H.-J. Shyur, and E. S. Lee, An extension of TOPSIS for group decision making, Mathematical and computer modelling, 2007, 45 (7-8), p. 801-813.

[216] Z. Hellwig, Zastosowanie metody taksonomicznej do typologicznego podziału krajów ze względu na poziom ich rozwoju oraz zasoby i strukturę wykwalifikowanych kadr, Przegląd statystyczny, 1968, 4 (1968), p. 307-326.

[217] B. Roy, Classement et choix en présence de points de vue multiples, Revue française d'informatique et de recherche opérationnelle, 1968, 2 (8), p. 57-75.

[218] C. Kwong and S. Tam, Case-based reasoning approach to concurrent design of low power transformers, Journal of Materials Processing Technology, 2002, 128 (1-3), p. 136-141.

[219] T. Yang and P. Chou, Solving a multiresponse simulation-optimization problem with discrete variables using a multiple-attribute decision-making method, Mathematics and Computers in simulation, 2005, 68 (1), p. 9-21.

[220] A. Milani, A. Shanian, R. Madoliat, and J. Nemes, The effect of normalization norms in multiple attribute decision making models: a case study in gear material selection, Structural and multidisciplinary optimization, 2005, 29 (4), p. 312-318.

[221] K. Yoon and C.-L. Hwang, Manufacturing plant location analysis by multiple attribute decision making: Part I—single-plant strategy, International Journal of Production Research, 1985, 23 (2), p. 345-359.

[222] M. Janic, Multicriteria evaluation of high-speed rail, transrapid maglev and air passenger transport in Europe, Transportation Planning and Technology, 2003, 26 (6), p. 491-512.

[223] M.-F. Chen and G.-H. Tzeng, Combining grey relation and TOPSIS concepts for selecting an expatriate host country, Mathematical and computer modelling, 2004, 40 (13), p. 1473-1490.

[224] B. Srdjevic, Y. Medeiros, and A. Faria, An objective multi-criteria evaluation of water management scenarios, Water resources management, 2004, 18 (1), p. 35-54.

[225] Y.-J. Lai, T.-Y. Liu, and C.-L. Hwang, Topsis for MODM, European journal of operational research, 1994, 76 (3), p. 486-500.

[226] H.-S. Shih, W.-Y. Lin, and E. Lee, Group decision making for TOPSIS, in Proceedings Joint 9th IFSA World Congress and 20th NAFIPS International Conference (Cat. No. 01TH8569), 2001 IEEE.

[227] J. I. Padrón-Páez, S. D.-L. Almaraz, and A. Román-Martínez, Sustainable Wastewater Treatment Plants Design through Multiobjective Optimization, Computers & Chemical Engineering, 2020, p. 106850.

[228] S. Sudhakaran, S. Lattemann, and G. L. Amy, Appropriate drinking water treatment processes for organic micropollutants removal based on experimental and model studies—A multi-criteria analysis study, Science of the total environment, 2013, 442, p. 478-488.

[229] S. Sadr, D. Saroj, S. Kouchaki, A. Ilemobade, and S. Ouki, A group decision-making tool for the application of membrane technologies in different water reuse scenarios, Journal of environmental management, 2015, 156, p. 97-108.

[230] A. Kolios, M. Collu, A. Chahardehi, F. Brennan, and M. Patel, A multi-criteria decision making method to compare support structures for offshore wind turbines, in European Wind Energy Conference, Warsaw, 2010.

[231] E. Roszkowska, Multi-criteria decision making models by applying the TOPSIS method to crisp and interval data, Multiple Criteria Decision Making/University of Economics in Katowice, 2011, 6, p. 200-230.

[232] A. Nebipasagil, B. J. Sundell, O. R. Lane, S. J. Mecham, J. S. Riffle, and J. E. McGrath, Synthesis and photocrosslinking of disulfonated poly (arylene ether

sulfone) copolymers for potential reverse osmosis membrane materials, Polymer, 2016, 93, p. 14-22.

[233] J. Hedrick, I. Yilgor, M. Jurek, J. Hedrick, G. Wilkes, and J. McGrath, Chemical modification of matrix resin networks with engineering thermoplastics: 1. Synthesis, morphology, physical behaviour and toughening mechanisms of poly (arylene ether sulphone) modified epoxy networks, Polymer, 1991, 32 (11), p. 2020-2032.

[234] W. H. Carothers, Polymers and polyfunctionality, Transactions of the Faraday Society, 1936, 32, p. 39-49.

[235] A. Rudin and P. Choi, The elements of polymer science and engineering 2012, Academic Press, 529.

[236] J. Brandrup, E. H. Immergut, E. A. Grulke, A. Abe, and D. R. Bloch, Polymer handbook Vol. 89, 1999, Wiley New York, 2366.

[237] P. J. Flory, Principles of Polymer Chemistry Vol. 1, 1953, Ithaca, New York, Cornell University Press.

[238] B. Bersted, Entanglement network model relating tensile impact strength and the ductile-brittle transition to molecular structure in amorphous polymers, Journal of Applied Polymer Science, 1979, 24 (1), p. 37-50.

[239] H. K. Jeon, C. W. Macosko, B. Moon, T. R. Hoye, and Z. Yin, Coupling reactions of end-vs mid-functional polymers, Macromolecules, 2004, 37 (7), p. 2563-2571.

[240] A. Okamoto, Y. Shimanuki, and I. Mita, Kinetic study on reactions between polymer chain-ends. Coupling reactions of living polystyrene with chloro-ended polystyrene, European Polymer Journal, 1982, 18 (6), p. 545-548.

[241] M. Murayama, M. Okada, T. Fukutomi, and T. Nose, Radius of gyration and hydrodynamic radius of branched polystyrenes in cyclohexane and toluene measured by static and dynamic light scattering, Die Makromolekulare Chemie: Macromolecular Chemistry and Physics, 1987, 188 (4), p. 829-843.

[242] A. Chardin, C. Laurence, M. Berthelot, and D. G. Morris, Hydrogen-bond basicity of the sulfonyl group. The case of strongly basic sulfonamidates RSO 2 NNMe 3, Journal of the Chemical Society, Perkin Transactions 2, 1996 (6), p. 1047-1051.

[243] R. S. Drago, B. Wayland, and R. L. Carlson, Donor properties of sulfoxides, alkyl sulfites, and sulfones, Journal of the American Chemical Society, 1963, 85 (20), p. 3125-3128.

[244] C. A. Kingsbury, Why are the Nitro and Sulfone Groups Poor Hydrogen Bonders?, 2015.

[245] S. Scheiner, Hydrogen bonding: a theoretical perspective 1997, Oxford University Press on Demand.

[246] H. Mori, A. Müller, and P. Simon, Macromolecular Engineering, Matyjaszewski, K, 2007.

[247] L. J. Markoski, J. S. Moore, I. Sendijarevic, and A. J. McHugh, Effect of linear sequence length on the properties of branched aromatic etherimide copolymers, Macromolecules, 2001, 34 (8), p. 2695-2701.

[248] J. Dumais, A. Cholli, L. Jelinski, J. Hedrick, and J. McGrath, Molecular basis of the β-transition in poly (arylene ether sulfones), Macromolecules, 1986, 19 (7), p. 1884-1889.

[249] G. C. Behera, A. Saha, and S. Ramakrishnan, Hyperbranched copolymers versus linear copolymers: A comparative study of thermal properties, Macromolecules, 2005, 38 (18), p. 7695-7701.

[250] S. A. Myers, R. A. Assink, D. A. Loy, and K. J. Shea, Investigation of the transmission of substituent effects by 29Si NMR, Journal of the Chemical Society, Perkin Transactions 2, 2000 (3), p. 545-549.

[251] W. Brostow, R. Chiu, I. M. Kalogeras, and A. Vassilikou-Dova, Prediction of glass transition temperatures: Binary blends and copolymers, Materials Letters, 2008, 62 (17-18), p. 3152-3155.

[252] X.-L. Gao and K. Li, A shear-lag model for carbon nanotube-reinforced polymer composites, International Journal of Solids and Structures, 2005, 42 (5-6), p. 1649-1667.

[253] D. Porter, Group interaction modelling of polymer properties 1995, CRC Press.

[254] R. P. White and J. E. Lipson, Polymer free volume and its connection to the glass transition, Macromolecules, 2016, 49 (11), p. 3987-4007.

[255] H. D. Mertens and D. I. Svergun, Structural characterization of proteins and complexes using small-angle X-ray solution scattering, Journal of structural biology, 2010, 172 (1), p. 128-141.

[256] A. Agrawal, B. M. Wenning, S. Choudhury, and L. A. Archer, Interactions, structure, and dynamics of polymer-tethered nanoparticle blends, Langmuir, 2016, 32 (34), p. 8698-8708.

[257] M. Doi and S. F. Edwards, The theory of polymer dynamics Vol. 73, 1988, oxford university press.

[258] J. S. Pedersen, Form and Structure Factors: Modeling and Interactions, Adv. Colloid Interface Sci, 1997, 70, p. 171-210.

[259] Y. H. Zang and P. J. Carreau, A correlation between critical end-to-end distance for entanglements and molecular chain diameter of polymers, Journal of Applied Polymer Science, 1991, 42 (7), p. 1965-1968.

[260] B.-H. Jeong, E. M. Hoek, Y. Yan, A. Subramani, X. Huang, G. Hurwitz, A. K. Ghosh, and A. Jawor, Interfacial polymerization of thin film nanocomposites: a new concept for reverse osmosis membranes, Journal of membrane science, 2007, 294 (1-2), p. 1-7.

[261] J. Lin, W. Ye, M.-C. Baltaru, Y. P. Tang, N. J. Bernstein, P. Gao, S. Balta, M. Vlad, A. Volodin, and A. Sotto, Tight ultrafiltration membranes for enhanced separation of

dyes and Na2SO4 during textile wastewater treatment, Journal of membrane science, 2016, 514, p. 217-228.

[262] M. Zhang, K. Guan, Y. Ji, G. Liu, W. Jin, and N. Xu, Controllable ion transport by surface-charged graphene oxide membrane, Nature communications, 2019, 10 (1), p. 1-8.

[263] P.-Y. Pontalier, A. Ismail, and M. Ghoul, Mechanisms for the selective rejection of solutes in nanofiltration membranes, Separation and Purification Technology, 1997, 12 (2), p. 175-181.

[264] J. Clayden, N. Greeves, S. Warren, and P. Wothers, Organic Chemistry, OxfordUniv. Press, Oxford, 2001, p. 585.

[265] Z. Wang, K. Xiao, and X.-m. Wang, Role of coexistence of negative and positive membrane surface charges in electrostatic effect for salt rejection by nanofiltration, Desalination, 2018, 444, p. 75-83.

VITA of EMINE BILLUR SEVINIS OZBULUT

Emine Billur Sevinis Ozbulut was born on March 16, 1988, in Yalova, Turkey. She graduated from Cagaloglu Anatolian High School (CAL) in June 2006 and began her undergraduate studies at Istanbul Technical University (ITU), Istanbul, Turkey. She graduated both from ITU with B.Sc. and M.Sc. degrees in Chemistry Department in June 2012 and January 2014, respectively. For one semester in 2011, she had studied Technical Chemistry Program at Vienna University of Technology (TU Wien) as an Erasmus exchange student. Before she began her Ph.D. studies in Material Science and Engineering Program at Sabanci University in Istanbul, she worked as Project Engineer at Sabanci University Nanotechnology Research and Application Center (SUNUM) between April and September 2014. During her Ph.D., she served as a teaching assistant in the lectures: Science of Nature 101 (NS101, one semester), Polymer Synthesis (MAT302, four semesters), and Organic Chemistry (NS207, four semesters). She has been employed with Kordsa as a Project Leader at Composite Technologies Center of Excellence since May 2019.